UNIVERSITAT POLITÈCNICA DE VALÈNCIA

DEPARTAMENTO DE COMUNICACIONES

Doctoral Thesis

Spin-Dependent Optical Phenomena: Fundamentals and Applications

J. Enrique Vázquez-Lozano

Supervised by Prof. Alejandro Martínez

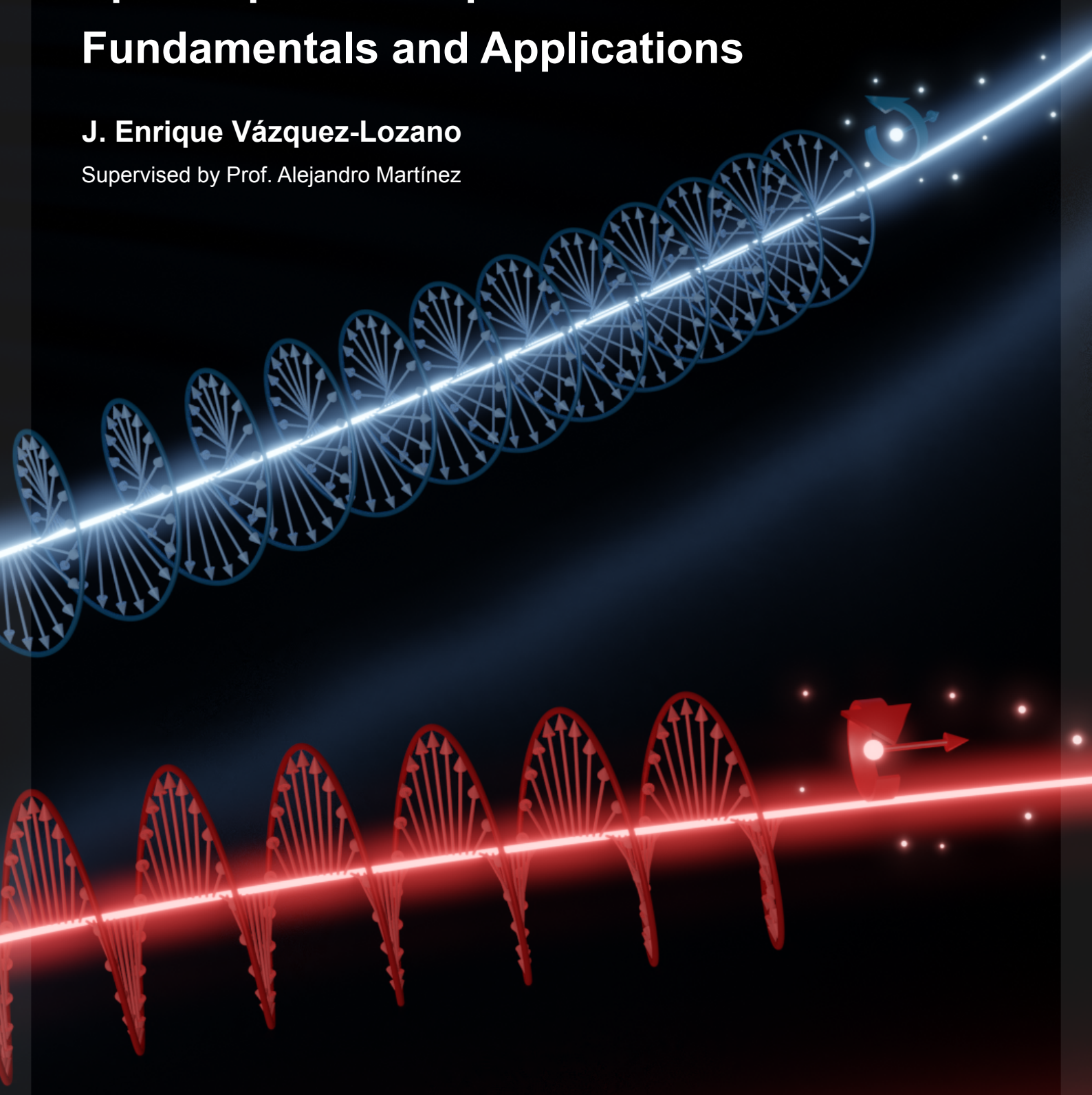

April 2021, Valencia (Spain)

UNIVERSITAT POLITÈCNICA DE VALÈNCIA

DEPARTAMENTO DE COMUNICACIONES

Spin-Dependent Optical Phenomena: Fundamentals and Applications

Juan Enrique Vázquez Lozano

Supervisor: Prof. Alejandro José Martínez Abiétar

Doctoral Thesis

submitted for the degree of

Doctor of Philosophy in Telecommunications Engineering

Valencia, April 2021

juavazlo@ntc.upv.es
Ph.D. Thesis, Valencia Nanophotonics Technology Center
Universitat Politècnica de València

First printing: February 2021 (deposit of draft version)
Second printing: March 2021 (deposit of final version)
Third printing: April 2021 (thesis defense)

A mis padres,
a Inma;
mis maestros.

Acknowledgements

No hay nada como una buena sombra
para mirar a la creación de tú a tú.

J. Losada (Delirio en tres actos)

Llevo tanto tiempo deseando poder escribir estos renglones, por lo que significan, que me apoca el hecho de no estar a la altura. Realmente, este tipo de sensaciones han sido persistentes y han estado fluctuando y pululando por mi mente durante gran parte del desarrollo de este trabajo, en su conjunto, y más aún (o será porque lo tengo más reciente) durante esta última fase de escritura. En ese sentido, tengo el orgullo de poder decir que, durante todos estos años, he estado siempre y en todo lugar bien rodeado, bien aconsejado, y en general bien respaldado, tanto en los buenos como en los malos momentos. Estas líneas están dirigidas a todas esas personas que, tanto en lo personal como en lo profesional, han contribuido, consciente o incluso inconscientemente, a que esto haya sido posible. A tod@s ell@s, sinceramente y de todo corazón, os doy las gracias. En lo que sigue, me gustaría expresar mi gratitud y dedicar unas breves palabras a algunas personas que, de un modo u otro, han sido fundamentales para mí en esta etapa.

El primer agradecimiento va dirigido a mi supervisor de tesis, Prof. Alejandro Martínez. Gracias sinceramente por darme la oportunidad de investigar y de poder hacer el doctorado en el *Nanophotonics Technology Center* (NTC-UPV), por tu apoyo, y sobre todo, por tu confianza, dejándome volar libremente para desarrollar mis ideas y haber contribuido a hacer de mí la persona que ahora soy. Gracias a Dr. Francisco J. Rodríguez-Fortuño (Pak), por acogerme en tu grupo y permitirme cumplir el sueño de poder pisar los pasillos del *King's College London* (KCL), por el tiempo que compartimos juntos, por todo lo que he podido aprender de tí, y por tu ayuda durante mi estancia en Londres. Por último, este primer párrafo quedaría incompleto si dejo sin mencionar a los profesores Diego Frustaglia y José Pablo Baltanás (US), con quienes empecé mis andaduras en este maravilloso mundo de la investigación científica. Un afectuoso agradecimiento a vosotros por el tiempo que pudimos compartir, por enseñarme a dar los primeros pasos, por vuestra dedicación, y porque pese a todo este tiempo y la distancia, seguís estando ahí.

Gracias a mis compañeros y amigos del grupo de *Plasmonics and Optomechanics* (anteriormente *Plasmonic Metamaterials*), a los que están y a los que estuvieron; gracias a

Laura, Evelyn, Javi (Redolat), Elena, Víctor, Alba, Ángela, Pablo, Leo, y Javi (Losada). Ha sido un verdadero placer haber podido compartir con vosotr@s todos estos años.

Gracias, en general, a todas las personas que forman parte del NTC, los que hacéis posible que todo siga adelante, a nivel administrativo, técnico, científico, y sobre todo, a nivel humano. Gracias a tod@s vosotr@s que habéis hecho que venir cada día a hacer ciencia sea un gusto aún mayor, y muy especialmente a mis compañeros y colegas de la 'sala diáfana' (los que están y los que, desgraciadamente, hace tiempo que se fueron), con quienes los años se han pasado volando: Luis, Álvaro, Andrés, Julio, Dani, Manel, Gustavo, Miguel, Elena, Carles, Paula, Irene, Cristina, Maribel,..., gracias porque con vosotr@s todo ha sido mucho más fácil y divertido. Y por supuesto, una mención muy muy especial a Sergio, Angie, y a Carlos G. Meca, por vuestro cariño, vuestra amistad, y vuestra ayuda (tanto en lo personal como en los asuntos científicos), con la que siempre he sentido (porque así me lo habéis demostrado) que podía contar, muchísimas gracias.

Más allá de los éxitos, de los resultados, de los papers, ... mucho más allá de todo eso, el mayor logro que me llevo de València, de todos estos años, es un grupo de personas que quedarán para siempre en mi memoria y en mi corazón. Por todo lo vivido, por los buenos momentos, por los no tan buenos, por saber que puedo contar con vosotros, por vuestra calidad como personas, por vuestra forma de ser, de compartir, de hacer las cosas, de disfrutar, y porque espero y deseo que todo esto no sea pasajero, os quiero agradecer enormemente todo este tiempo, porque nada hubiera sido igual sin vosotros; Javi, Fran, Luis, Seppo, Jad, sinceramente, gracias.

Esto es lo que me llevo, pero para eso, antes de todo, había necesitado llegar hasta aquí, lo cual habría sido imposible sin contar con el cariño y el respaldo incondicional de mucha gente a la que, aunque a veces pueda no parecerlo (porque siempre ando trabajando...), guardo muy dentro de mí. Estas líneas son para vosotros: Juampa, Ezequiel, Cristian, Carolina, María Cala, Fran, Niff, María José, Santi, Jezú (Sevilla), Rafa, María Gil, Laura, Migue, Pablo, Raúl (Facultad de Física), Víctor, Gabi, Ismael, Loli (Huelva), a tod@s vosotr@s, y a much@s otr@s, muchas gracias por formar parte de mi vida.

Las últimas líneas las he reservado para mis pilares más básicos, mi familia. Por un lado estáis vosotros, mis padres, Javier y Charo. Gracias por enseñarme a tratar de la misma manera al éxito que al fracaso, por haberme guiado hasta aquí, mostrándome las jerarquías de las cosas que más importan frente a las que son intrascendentes, por los valores que me habéis transmitido y en general porque sin vosotros no estaría aquí ni sería el que hoy soy. Y finalmente, estás TÚ, Inma. Gracias por enseñarme cada día a ser mejor persona, por tu cariño, por tu amor, por tu alegría y tu dulzura. Gracias por comprenderme siempre, por enseñarme el lado bueno de la vida, por haber querido compartir conmigo todo este tiempo y por darme la felicidad.

J. Enrique Vázquez-Lozano
València, Marzo 2021

Resumen

Al igual que la masa o la carga, el espín es una propiedad física fundamental que, típicamente, aparece en la descripción de los sistemas cuánticos. Más allá de sus importantes implicaciones teóricas, el creciente avance de la tecnología y el desarrollo de los dispositivos hacia escalas cada vez más pequeñas ha favorecido el surgimiento de multitud de aplicaciones que involucran al espín, entre las cuales se destaca la *espintrónica*; una nueva forma de electrónica en la que, además de la carga, también se explotan los grados de libertad otorgados por el espín del electrón. Por supuesto, el espín no es exclusivo de los electrones, está presente en todas las partículas elementales, y por ende, en los fotones. En este caso, y a diferencia de lo que ocurre con los electrones, existe una correspondencia clásica que relaciona el espín del fotón con los estados de polarización circular de la luz. Por lo tanto, en nano-óptica y en fotónica, los fenómenos basados en el espín se refieren, *grosso modo*, a aquellos que son fuertemente dependientes de la polarización circular de la luz.

En este marco general, uno de los ejemplos más preponderantes se halla en la *interacción espín-órbita*. En su versión óptica establece que, bajo ciertas condiciones, es posible que exista una influencia mutua entre el estado de polarización (*espín*) y la propagación (*órbita*) de la luz. A pesar de su carácter ubicuo en todos los procesos ópticos básicos, sus efectos son muy débiles, y su manifestación se restringe a la nanoescala, lo cual dificulta su observación e identificación. En este mismo contexto, otro concepto heredado del formalismo cuántico que tiene análogo fotónico directo es la *quiralidad óptica*; una propiedad dinámica local que, de alguna manera, permite cuantificar escalarmente el espín de un campo óptico. Aparte de su controvertido significado físico y su estrecho vínculo con los sistemas plasmónicos y los metamateriales, como amplificadores de sus efectos, su principal característica fundamental es que, para los campos ópticos en el vacío, es una cantidad conservada.

En esta tesis se ahonda teóricamente en los fundamentos básicos de estas características fotónicas. Específicamente, se demuestra analíticamente que la interacción espín-órbita es un fenómeno que surge natural y necesariamente en la nanoescala. Sobre esta base se expone un formalismo para extender la excitación unidireccional de campo cercano más allá de la aproximación dipolar, lo cual facilita su observación y mejora las propiedades de acoplo. Por otra parte, se analiza el concepto de la quiralidad óptica, originalmente definida en el vacío, y se generaliza a cualquier tipo de medio, incluyendo sistemas altamente dispersivos. Asimismo, se exploran diferentes configuraciones que permitan implementar las principales funcionalidades quirópticas (sensado y espectroscopía) en plataformas de fotónica integrada. Además de su potencial para aplicaciones, este estudio tiende un puente para abordar clásicamente propiedades y efectos que tradicionalmente son de tipo cuántico.

Resum

Igual que la massa o la càrrega, l'espín és una propietat física fonamental que, típicament, apareix en la descripció dels sistemes quàntics. Més enllà de les seves importants implicacions teòriques, el creixent avanç de la tecnologia i el desenvolupament dels dispositius cap a escales cada vegada més petites ha afavorit el sorgiment de multitud d'aplicacions que involucren l'espín, entre les quals es destaca l'*espintrònica*; una nova forma d'electrònica en què, a més de la càrrega, també s'exploten els graus de llibertat atorgats per l'espín de l'electró. Per descomptat, l'espín no és exclusiu dels electrons, és present en totes les partícules elementals, i per tant, en els fotons. En aquest cas, i a diferència del que passa amb els electrons, hi ha una correspondència clàssica que relaciona l'espín del fotó amb els estats de polarització circular de la llum. Per tant, en nano-òptica i en fotònica, els fenòmens basats en l'espín es refereixen, *grosso modo*, a aquells que són fortament dependents de la polarització circular de la llum.

En aquest marc general, un dels exemples més preponderants es troba en la *interacció espín-òrbita*. En la seva versió òptica estableix que, sota certes condicions, és possible que hi hagi una influència mútua entre l'estat de polarització (*espín*) i la propagació (*òrbita*) de la llum. Malgrat el seu caràcter ubic en tots els processos òptics bàsics, els seus efectes són molt febles, i la seva manifestació es restringeix a la nanoescala, la qual cosa dificulta la seva observació i identificació. En aquest mateix context, un altre concepte heretat del formalisme quàntic que té anàleg fotònic directe és la *quiralitat òptica*; una propietat dinàmica local que, d'alguna manera, quantifica escalarment l'espín d'un camp òptic. A banda del seu controvertit significat físic i el seu estret vincle amb els sistemes plasmònics i els metamaterials, com amplificadors dels seus efectes, la seva principal característica fonamental és que, per als camps òptics en el buit, és una quantitat conservada.

Des d'un enfocament teòric, aquesta tesi aprofundeix en els fonaments bàsics d'aquestes característiques fotòniques. Específicament, es demostra analíticament que la interacció espín-òrbita és un fenomen que sorgeix natural i necessàriament en la nanoescala. Sobre aquesta base s'exposa un formalisme per estendre l'efecte d'excitació unidireccional de camp pròxim més enllà de l'aproximació dipolar, la qual cosa facilita la seva observació i millora les propietats d'acoblo. D'altra banda, s'analitza el concepte de la quiralitat òptica, originalment definida en el buit, i es generalitza a qualsevol tipus de mitjà, incloent sistemes altament dispersius. Així mateix, s'exploren diferents configuracions que permetin implementar les principals funcionalitats quiròptiques (sensat i espectroscòpia) en plataformes de fotònica integrada. A més del seu potencial per a aplicacions, aquest estudi tendeix un pont per abordar clàssicament propietats i efectes tradicionalment quàntics.

Abstract

Just like mass or charge, spin is a fundamental physical property that, typically, appears in the description of quantum systems. Beyond its important theoretical implications, the rapid advance of technology along with the relentless trend toward the development of devices at increasingly smaller scales have boosted the occurrence of a wide range of applications involving spin, among which is highlighted the *spintronics*; a novel form of electronics which, besides the charge, also exploits the degrees of freedom provided by the electron spin. Of course, the spin is not exclusive to electrons, but is actually present in all the elementary particles, and therefore in photons. In such a case, and unlike what happens with electrons, there exists a direct classical correspondence relating the spin of photons with the circular polarization states of light. Thus, in nano-optics and photonics, spin-dependent phenomena are broadly referred to as those that strongly rely upon the circular polarization of light.

Within this general framework, one of the most preponderant examples is found in the *spin-orbit interaction*. In its optical version, it states that, under certain conditions, it is possible that there exists a mutual influence between the state of polarization (*spin*) and the propagation (*orbit*) of light. Despite its ubiquitous character in all basic optical processes, its effects are very weak, and its manifestation is restricted at the nanoscale, thereby hindering its observation and identification. In this same context, another concept somehow inherited from the quantum formalism with a direct photonic analogue is the *optical chirality*; a local dynamical property that, in a way, allows one to quantifying scalarly the spin of an optical field. Apart from its controversial physical meaning and its close relationship with plasmonic systems and metamaterials, often regarded as chiral enhancers, its main feature is that, for optical fields in the vacuum, it is a conserved quantity.

From a theoretical standpoint, this thesis delves into the basics of these photonic traits. Specifically, it is analytically demonstrated that the spin-orbit interaction is indeed a phenomenon that naturally and necessarily emerges at the nanoscale. Building on this, it is addressed a formalism to extend the effect of near-field unidirectional excitation beyond the dipolar approximation, thus facilitating its observation and improving the coupling performance. On the other side, the optical chirality, originally put forward for electromagnetic fields in vacuum, is thoroughly analyzed and generalized to any arbitrary medium, including highly dispersive systems. Furthermore, different configurations for implementing the main chiroptical functionalities (sensing and spectroscopy) in integrated photonic platforms are explored. Besides its potential for applications, this study lays a bridge to classically approach features and effects which are traditionally quantum-like.

Contents

Introduction and objectives **1**

I Original Contributions on Spin-Orbit Interactions of Light **21**

1 PAPER A: *Classical emergence of intrinsic spin-orbit interaction of light at the nanoscale* **23**

A.I Introduction . . . 25
A.II Overview of Full-Vector Waves . . . 27
A.III Optical Spin-Orbit Interaction . . . 29
A. Intrinsic evolution of the SoP . . . 29
B. Factorizability condition and SOI term . . . 31
C. Definition of the near-field region based on the factorizability condition . . . 34
D. Local dynamical properties of multipole fields: Poynting vector, spin, and orbital momentum . . . 34
A.IV Conclusion . . . 38
References . . . 38

2 PAPER B: *Near-Field Directionality Beyond the Dipole Approximation: Electric Quadrupole and Higher-Order Multipole Angular Spectra* **43**

B.I Introduction . . . 45
B.II Angular Spectrum of Electric Quadrupole . . . 47
B.III Near-Field Directionality Beyond the Dipole . . . 50
B.IV Angular Spectrum of Higher-Order Electromagnetic Multipole Fields . . . 52
B.V Concluding Remarks . . . 56
References . . . 57

3 PAPER B: *Supplemental Material* **63**

B.SM.I Angular Spectrum Representation, Weyl's Identity and Hertz Potentials 65
B.SM.II Angular Spectrum Representation of the Electric Dipole . . . 68
B.SM.III Angular Spectrum Representation of the Electric Quadrupole . . . 69
B.SM.IV Spectral Amplitudes for the Electric and Magnetic Fields of the Electric Dipole and Quadrupole . . . 73

B.SM.V Angular Spectrum Representation of the Electromagnetic Multipole Fields . . . 75
B.SM.VI Verification and Relationship between the Results Obtained via the Hertz's and Standard Vector Potentials for both the Electric Dipole and Quadrupole . . . 85
Appendix: Angular Spectrum Representation of the Magnetic Dipole . . . 88
References . . . 90

II Original Contributions on Optical Chirality 93

4 PAPER C: *Optical Chirality in Dispersive and Lossy Media* 95
C.I Introduction . . . 97
C.II Conservation Law for the Optical Chirality . . . 98
C.III Optical Chirality in Lossless Dispersive Media: Brillouin's Approach . 100
C.IV Optical Chirality in Lossy Dispersive Media: Loudon's Approach . . . 102
C.V Summary . . . 105
References . . . 105

5 PAPER C: *Supplemental Material* 113
C.SM.I Energy Conservation in Dispersive and Lossy Media: Energy Density and Flow . . . 115
C.SM.II Continuity Equation for Optical Chirality in Dispersive and Lossy Media 121
C.SM.III Optical Chirality Density in Linear Dispersive and Lossy Media . . . 124
A. Optical chirality density in dispersive and lossy media: Loudon's approach . . . 124
B. Optical chirality density in dispersive and lossless media: Brillouin's approach . . . 128
C. Brillouin's approach vs Loudon's approach: some additional remarks 129
D. Loss rate of the optical chirality in dispersive and lossy media . . . 131
E. Loss rate of the optical chirality in dispersive and lossless media . 132
Appendix: Values of the Drude-Lorentz model parameters characterizing silver and silicon . . . 132
References . . . 133

6 PAPER D: *Toward Chiral Sensing and Spectroscopy Enabled by All-Dielectric Integrated Photonic Waveguides* 139
D.I Introduction . . . 141
D.II Optical Chirality Density in All-Dielectric Integrated Photonic Waveguides . . . 144
D.III Probing the Chiroptical Response in Dielectric Strip Waveguides: Normal Incidence (in-gap configuration) and Evanescent-Induced Chiral Interaction (on-top configuration) . . . 147

D.IV Further Considerations for a Realistic Approach of Chiroptical Applications in Integrated Platforms . . . 151
A. Beyond the ideal PEC model: Drude–Lorentz materials . . . 151
B. Enhancing the evanescent effect: Slotted configuration . . . 152
C. Breaking the C_4 rotational symmetry: Polarization beat length and its effect on chiroptical applications . . . 153
D.V Conclusion and Outlook . . . 156
D.VI Numerical Methods . . . 157
References . . . 158

III Discussions & Conclusions **165**

7 General Discussion of Results **167**
7.I SOI of Light & Near-Field Directionality . . . 167
PAPER E: *Near-Field Unidirectional Excitation...and Beyond* . . . 181
7.II Optical Chirality & Chiral Light-Matter Interactions . . . 185
PAPER F: *Generalizing Optical Chirality to an Arbitrary Medium* . . . 199

8 Conclusions and Outlook **203**
8.I Main Conclusions . . . 203
8.II Future Work . . . 208
8.III Concluding Remarks . . . 210

Author's Merits **213**

Bibliography **219**

List of Acronyms **237**

List of Figures **239**

List of Tables **243**

Introduction and objectives

There is nothing new to be discovered in physics now.
All that remains is more and more precise measurement.

Willian Thomson (Lord Kelvin) – British Association
for the Advancement of Science (1900)

Although the opening quotation is generally attributed to Lord Kelvin (1824 – 1907), there is not complete certainty about that, and it is indeed often claimed that it was actually paraphrased by Albert A. Michelson* (1852 – 1931). Regardless to whom this statement is credited, what is undeniably true is that it could not be further from reality. Not only at the time in which is supposed it was raised, but, according to our own experience, it still continues being so at present. Needless to say that neither modern science nor the state-of-the-art of current cutting-edge technologies would be as they are nowadays without the advent of quantum mechanics or relativity (in its both flavors), which were yet to come around at that time. As we now know, these revolutionary theories have played an essential role in the overhaul and upgrade of longstanding branches of physics, for instance, turning from classical electrodynamics to its quantum counterpart, befitting it with a relativistic formalism, and in a wider sense, leading to the much celebrated *quantum field theory* — the theoretical framework hosting the fundamental origin of *photons* as the quanta of light. Both, though more particularly quantum mechanics, have been pivotal in the revival of interest in the foundations of condensed matter physics, now becoming one of the most active and prolific areas of fundamental and applied physics [1], and have also been crucial in the development of new emerging technologies [2], especially as the scale of the systems turns increasingly smaller. Of course, these breakthroughs are just some examples of a large list evincing that, contrary to the Kelvin's (or Michelson's) assertion, physics remained (and it does still today) fizzing, and, consequently, the technological advancement.

It is evident that science and technology are closely tied to each other, on their own contents, and in the pathways of research and development. Of course, this is applicable to any of the major scientific disciplines, such as physics, chemistry, biology, and even mathematics. Yet, in the case of physics, and in particular for many of its branches

*American physicist famous for his works on measuring the speed of light and, particularly, for his contribution to the *Michelson-Morley experiment*, aimed at demonstrating the (in)existence of the *ether*.

(thermodynamics, electronics, or optics, just to mention a few), such a link seems to be more straightforward to grasp, since, in a way, it can be regarded as the first hurdle to overcome before to "get in touch" with nature. Be that as it may, this interconnection leads to a continuous and mutual feedback, thereby setting down one the main mechanism that they both, science and technology, often use to push themselves forward. In this manner, the scientific knowledge could be applied to improve the already existing technology (or just to figure out how to do it), and, conversely, one could otherwise use the technology to tackle on basic science (e.g., by getting better resolutions in the observation instruments, or higher performance in the computing devices), or even indirectly, by posing challenging venues that may require new scientific approaches. One of the most illustrative examples showing this involvement is well abridged in the famous 1959 lecture given by Richard P. Feynman (1918 – 1988) [3]: «*There's Plenty of Room at the Bottom*». As pointed out in the subtitle, this talk was envisaged as *An Invitation to Enter a New Field of Physics*, namely, it was a manifesto appealing to undertake a new research direction delving into the possibility of *manipulating and controlling things on a small scale*. With the only constraint of not violating any physical law, Feynman speculated about the prospects and benefits of arranging single atoms or molecules *one by one the way we want them*. In this regard, it should be noted that, already at that time, it was well known that the scientific basis underlying the realm of microscopic things was dictated by the rules of quantum mechanics, with their weirdness and unfamiliar effects — likely as a part of its lure. In this scenario and from a general focus intended to a broad audience beyond physicists, including chemists and biologists, Feynman highlighted joyfully, but insistently, the necessity of deploying a more advanced technology able to carry out and deal with the downscaling procedure and the emerging phenomena occurring at so small scale. A clear example is underlined by the pressing need that there was at the time to improve the electron microscopes, to make them more powerful and with a much higher resolution. Additionally, it was also pondered upon multiple situations and applications that would be triggered by the miniaturization of physical systems, thus showcasing interesting possibilities, e.g., for writing or etching over microscopic structures, storing and processing data within tiny systems, integrating electrical circuitry, or even for performing smart chemical synthesis, biologically inspired self-assembly, or microscopic medical bots for surgery or drug delivery, among others. Astonishingly, many of these outlandish proposal, if not all, have already been realized, and have led to a whole set of novel concepts, and even to new scientific areas in their own right, whose denomination is usually preceded by the prefix *nano*. Nanoelectronics, nanophotonics, nanofabrication, nanoparticles, or nanostructures, are just some of the examples whose usage is becoming increasingly widespread all around the scientific landscape. So much so, that in a broad sense, they all are usually encompassed in a new field of study, now referred to as the *nanoscience*.

Just as a matter of fact, the origin of the nanoscience (and/or the nanotechnology) is often set to the date in which was delivered the above Feynman's lecture [4, 5]. However, this onset event has not been widely accepted, mainly, because it relies upon retroactively awarded successes [6]. Instead, a more conservative and recognized stance sets that such a

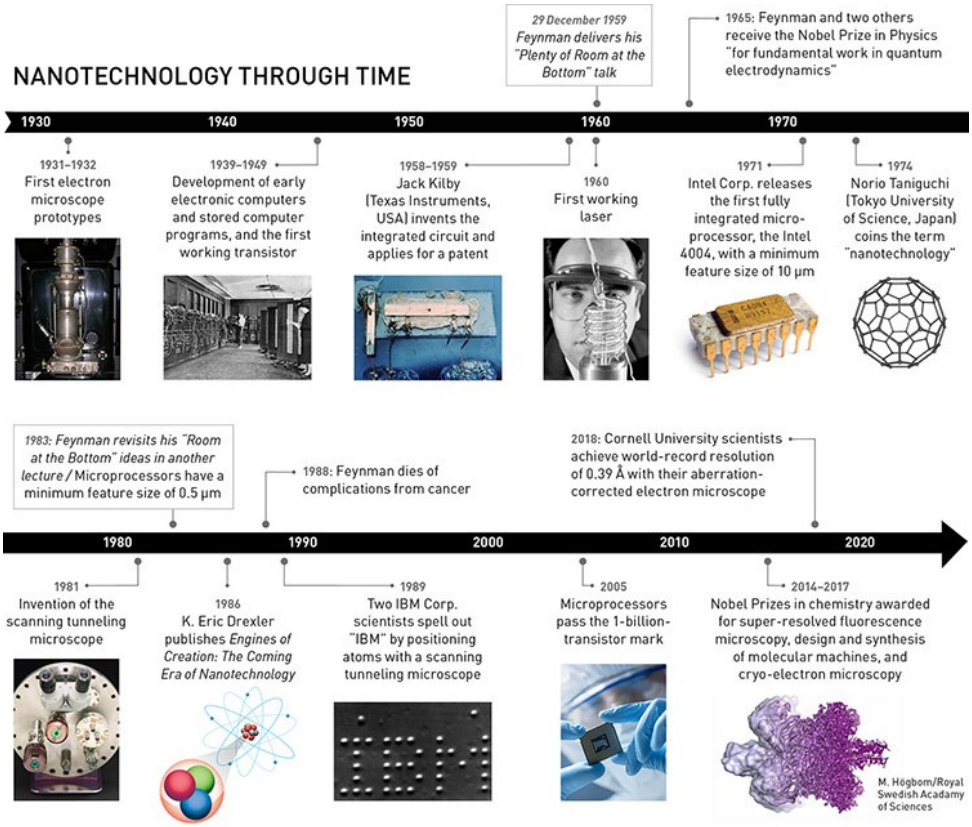

Figure 1: Timeline of major milestones and breakthroughs in nanoscience and nanotechnology [7].

birth took place with the achievement of the following technical landmarks (see Figure 1): the invention of the *scanning tunnelling microscope* (STM) in 1981, the came of the *atomic-force microscope* (AFM) in 1985, and the first *manipulation of individual atoms* by STM spelling out the IBM acronym in 1989 [7]. As it can be appreciated (and expected), since the early stages of this race toward the miniaturization, the branch of (classical) optics already showed out signs that it was meant to play a fundamental role. Nonetheless, still for the moment, its relevance has only been showcased from an instrumental (or passive) standpoint, namely, just as an efficient toolbox that turned out to be very useful for the construction of equipments able to zoom into the micro (or even the nano) scale [8].

Concurrently, in this cascade of accomplishments that did contribute to the development of the nanotechnology, it is a must to mention the *Field-Effect Transistor* (FET) and the *Metal-Oxide-Semiconductor* (MOS) architecture, as well as the confluence of both, giving rise to the well-known *MOSFET transistor*. Owing to its ability to be miniaturized and embedded, MOSFETs have grown into the fundamental building-block of the modern electronics industry, thus driving up the mass production of *integrated circuits*, in which the electronic elements (i.e., the MOSFETs) are monolithically embedded in a single piece of a semiconductor material (typically made of silicon). Noteworthily, these technological breakthroughs have been acknowledged

by the Institute of Electrical and Electronics Engineers (IEEE) to be included in the List of Milestones [9], and, what is even more remarkable, they were, directly or indirectly, involved in the award of various Nobel Prizes — the discovery of the FET and the invention of the integrated circuit were awarded in 1956 and 2000, respectively, and the discovery of the *quantum Hall effect*, which was instigated by the MOSFET [10], got it in 1985. Furthermore, the realization of the MOSFET led in turn to what has come to be called the *Complementary Metal-Oxide-Semiconductor* (CMOS) technology; a whole set of fabrication techniques (lithography, epitaxial growth, chemical depositions, ...) and materials (basically the III-V semiconductors), widely used in the nanofabrication of electrical integrated circuits for a wide range of uses (chips, microprocessors, memories, ...). This standard semiconductor-based technology has become dominant in the fabrication of planar devices, providing with numerous practical benefits: high performance (reducing power consumption and heat generation), high-density integration and scalability (yielding ultra-low footprints), as well as cost-effective and mass-volume production, among others.

The transition from vacuum tubes to solid-state systems relying upon semiconductor physics meant a formidable change in the development of transistors, and its impact has transcended far beyond the scientific-technical ground. Today, electronic devices — and consequently MOSFET transistors — flood practically all over the society, and their use extends to nearly whatever daily activity one can think of, thereby becoming in almost a new limb of the human body. In fact, it is not unreasonable to state that MOSFETs in themselves, along with the enormous commitment to reach integration in chips of increasingly smaller scales, are behind great part of the global economic growth, triggering and shaping what is commonly known as the *digital revolution*, the *silicon age*, and/or the *information age*. In this regard, it should be noted that, since the very first conception of the MOSFET transistor, its integration in electronic circuits have undergone an impressive quantitative leap, passing from a little dozen, to tens of thousand, millions, and even billions of MOSFETs integrated in a single chip. Who could have imagined so high level of progress in so little time (barely in a half of century)? A look back allows us to find a short answer to this question in the so-called *Moore's law* [11], according to which, just by taking into account the shrinkage of the transistors' size, it is forecasted that the number of transistors in the integrated circuits is doubled about every two years — and so the chips' performance. But, if this downscaling pace is kept, next questions would be, until when?, is there any limit, or is it, otherwise, possible to go down indefinitely to scales smaller and smaller? Of course there are limits. Indeed, a first bound might be readily reached on account of the overheating that would appear when transistors are extremely tightly packed and bonded to each other. This classical-like shortcoming could be mitigated, e.g., by capping the clock speed of the device, and hence, cutting down the process yield [12]. Interestingly, this kind of issues, along with other possible ways for facing them, were already alluded in the aforementioned Feynman's lecture [3]:

> «*There is also the problem of heat generation and power consumption [...] so, ultimately, when our computers get faster and faster and more and more elaborate, we will have to make them smaller and smaller*»;

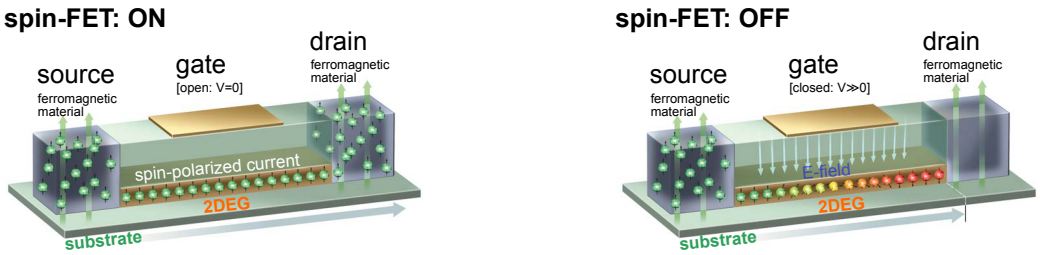

Figure 2: Schematic of the spin Field-Effect Transistor (spin-FET) proposed by Datta and Das [17].

> «*I have thought about some of the problems of building electric circuits on a small scale, and the problem of resistance is serious. [...] Possibly we can beat resistance through the use of superconductivity if the frequency is not too high, or by other tricks*».

However, a more fundamental limitation arises as the transistors' size shrink below a certain dimension (say, below 100 nanometers), from which quantum effects start to emerge. In such a case, quantum features such as the tunneling effect or some others related to the uncertainty principle turn out to be predominant, thus affecting the system's behavior so much that they may even jeopardize its stability and reliability.

In order to face with these limitations, there have been proposed many different road maps. One of them is based on what has been termed as the *More than Moore* strategy. It basically consists in adapting and customizing the chips to the needs of specific applications [12]. Namely, it is based on an inverse approach in which the improvements are undertaken by looking at the *Top* [13] (in resemblance to the Feynman's lecture which, instead, urges to look into de *Bottom*), that is, by working on the hardware architecture, improving the software coding, and optimizing the computation algorithms and protocols. On the other side, another more insightful strategy is aimed to tap positively into the potential advantages brought about by quantum mechanical features. Indeed, in the same way as the quantum tunneling and the uncertainties, at the microscopic regime there appear likewise the so-called *quantum coherence* and the *quantum superpositions*. These features normally weaken and fade out as the scale of the systems goes up, but, for quantum systems, say the spin of electrons, turn out prevailing, and in fact, essentials to deal with them. In this respect, it should be noted that, just like the electric charge, the spin is nothing but another fundamental property of electrons, and hence, is amenable to be considered as a suitable resource for being exploited, for instance, in solid-state devices [14]. This realization gave rise to *spintronics*, a field of study that focuses on the generation, injection, transport, manipulation, and detection of spin-polarized electron currents through semiconductor-based mesoscopic systems [15]. In this vein, early proposals began to become popular in the eighties, with the discovery of the giant magnetoresistance (GMR), whose main application has enabled the miniaturization of the recording heads of hard-disk drives [16]. Afterwards, other more sophisticated spin-dependent electronic applications came up, being the most outstanding the Datta-Das spin-FET (Figure 2) [17].

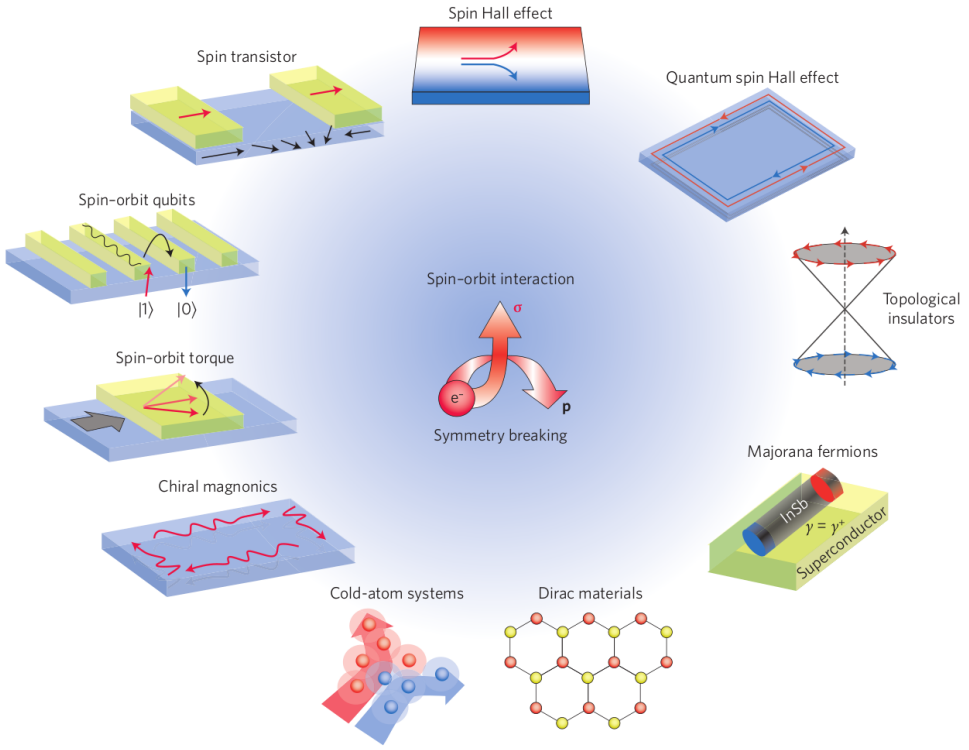

Figure 3: Spin-dependent electron transport phenomena in solid-state systems [21].

This transistor (which, by the way, was originally inspired by optical phenomena [18]) was conceived to be the spin-analog to the conventional MOSFET, in which the information is stored, conveyed, and processed by means of the spin of the carriers (in addition to, or instead of the charge). Besides overcoming the fundamental limitation on chip integration [19], this kind of quantum-based components are being expected to outperform the capabilities of current electronics, e.g., in terms of non-volatility, higher processing speed, lower power consumption, and, of course, by taking advantage of the quantum superposition of the electronic spin states [20]. Notwithstanding, the ensuing researches aiming to accomplish its practical implementation have encountered several and serious challenges, mainly concerning the efficient injection of spin-polarized currents into the conducting channel — owing to the impedance mismatch between the transistor's components — as well as on the active control of the spin dynamics and its transport across semiconductor materials, particularly at or above room temperatures. At any rate, what should be stressed out here is that this field of *spin-dependent electron transport phenomena* has become a burgeoning research topic that has put the spin — so far mostly regarded just as a theoretical concept — on the ground of solid-state applications, and thus, has paved the way for a wealth of fundamental effects, including the *spin Hall effect*, the *quantum spin Hall effect*, or the *topological insulators*, among many others. In this regard, it is also worth pointing out that, as depicted in Figure 3, within this palette of spin-dependent (and/or chiral) effects, the *spin-orbit interaction* (SOI), occurring in low-dimensional semiconductor structures with inversion asymmetry, lies right at the heart [21].

Heretofore we have seen how the transition from the macro to the nanoscale has brought forth a great variety of new devices (MOSFETs, integrated circuits, spin-FETs, ...), along with a whole technology able to deal with the fabrication process of semiconductor structures in an efficient and effective way (CMOS technology). Apart from the applications, this downscaling process has also enabled the disclosure of a plethora of new physical effects (quantum Hall effect, spin Hall effect, spin-orbit coupling in semiconductor heterostructures, ...), most of them belonging, up to then, to the theoretical realm. All of that has been performed under the framework of electronics in its widest sense (i.e., by including considerations coming from solid-state physics, and more particularly from semiconductor physics, together with some quantum mechanical traits), making emphasis in its evolution toward nanoelectronics, as well as in the efforts put into the exploration of further alternatives such as spintronics. Noticeably, this trend toward the miniaturization has also had a significant impact in the birth and integral development of the photonics and subsequently in nanophotonics. For this, it turned out to be essential the realization of a coherent light source. This was held with the discovery of the *laser*, which has been widely recognized as the fact that marked the onset of photonics. Since then, light began to play a fully active role in the successive technological breakthroughs coming ahead. In this sense, whereas (classical) optics mainly involves passive instruments, such as lenses, polarizers, wave plates, or mirrors, photonics, for its part, apart from lasers, entails the usage of sophisticated equipment, including amplifiers, transmission media, modulators, or photodetectors, among others. Furthermore, there are also significant differences as for the applications, which for the case of photonics ranges from light detection, to imaging, spectroscopy, communications, processing, computing, or even medicine. As it can be noted, some of the main applications of photonics (in particular, those related with communications, processing, and computing) resemble somehow to those of electronics, but considering photons (light) instead of electrons (electric charges) as the information carriers. Thus, akin to electronics as for the transport properties of electrons, the ultimate goal of photonics basically consists in dominating the light properties (i.e., spatial distribution, polarization, dispersion, ...), and its interaction with matter, and this is mainly done in the frequency range that usually goes from infrared (IR) to ultraviolet (UV). Upon this basis, and harnessing the whole machinery deployed for nanoelectronics, there emerge the *nanophotonics* [22].

Besides reducing the size of the structures with which light interacts, nanophotonic systems affords a number of practical benefits, especially if realized onto silicon-based platforms compatible with standard CMOS technology. Cost-effectiveness, mass-volume production, compactness, robustness, reproducibility, high yield, as well as integration with electronics are indeed the main advantages of silicon-nanophotonics [23]. In addition, since silicon is a material with a moderately high refractive index (about 3.5), exhibiting transparency at the optical communication band (roughly ranging from 1300 to 1600 nm) [24], it is well suited to achieve a broadband confinement and guidance of light. In fact, thanks to the high index contrast attainable in *silicon-on-insulator* (SoI) platforms (e.g., between silicon and its oxide, which is the typical insulator material employed as

a substrate in electronic circuits), and the total internal reflection (straightforwardly coming from the *Snell's law*), it is possible to concentrate and propagate optical energy along structures of sub-wavelength dimensions. This constitutes the very basics behind the most common realization of lithographically defined all-dielectric waveguides, which are usually regarded as the (nano)wires of the *photonics integrated circuits* (PICs).

Although *a priori* it may seem that nanophotonics is technologically far superior than nanoelectronics (e.g., in terms of processing performance, communication speed, bandwidth, and power consumption), the catch is that there exists a major limitation as for the minimum dimension attainable in PICs. This is imposed by the *diffraction limit*, according to which, light cannot be neither confined nor guided within structures whose dimensions are smaller than approximately half of its wavelength. Hence, whereas integrated electronics has largely reached nanoscaled circuits, silicon-based photonics components are still compelled to keep on the microscale, in compliance with the diffraction law. This then poses the disjunctive of whether it is actually feasible to get both the high-speed of photonic systems and the miniaturized size of electronic elements in a same chip. A first tentative proposal to face this issue has been based on hybrid designs, that is, a combination of both electronic and photonic technologies so as to gain the best of each world [22, 23]. It should be noted that this synergistic approach, often dubbed the *electronic-photonic convergence*, is possible because of the mutual CMOS compatibility of PICs with their electronic counterparts, and has led to a wide variety of optoelectronic applications such as switches, modulators, filters, or (de)multiplexers, just to mention a few. Yet, for some time now, it has been suggested that a more insightful way to meet these technical demands at once might be accomplished by means of plasmonic systems [25].

Very roughly and shallowly, *plasmonics* can be deemed as the science that lies right in between nanoelectronics and nanophotonics, thereby settling down a direct link between them [26]. Indeed, the main physical ingredients of plasmonics are basically two: high frequency electromagnetic (EM) fields — ranging from the near-infrared (NIR) to visible frequencies — and the free electron gas of metallic structures — typically considered as planar surfaces or metallic nanoparticles, which should be assumed to be surrounded by a dielectric medium. As a result of their mutual interaction, and presuming the adequate resonant conditions (depending on the material properties of both the metal and the surrounding dielectric), an external EM wave impinging at the metal/dielectric interface drives a partially coherent collective oscillation of the conduction electron charges which, in turn, induces a self sustained surface EM wave [27]. Such a mutual coupling between the surface-charge-density oscillations and the surface-EM-wave over the metal interface is what we call the *surface plasmon polariton* (SPP)[†]. Depending on the geometric characteristics of the metallic structure, these surface waves will be propagating

[†]Note that, strictly speaking, surface plasmons (SPs) actually refer to the charge motion (i.e., the excitation of the plasma oscillation), whereas polaritons, on the other side, are associated to the surface EM field induced and self sustained by the SPs (i.e., the excitation resulting from the coupling between plasmons and photons). Therefore, SPPs come up from the joint action of both elementary excitations.

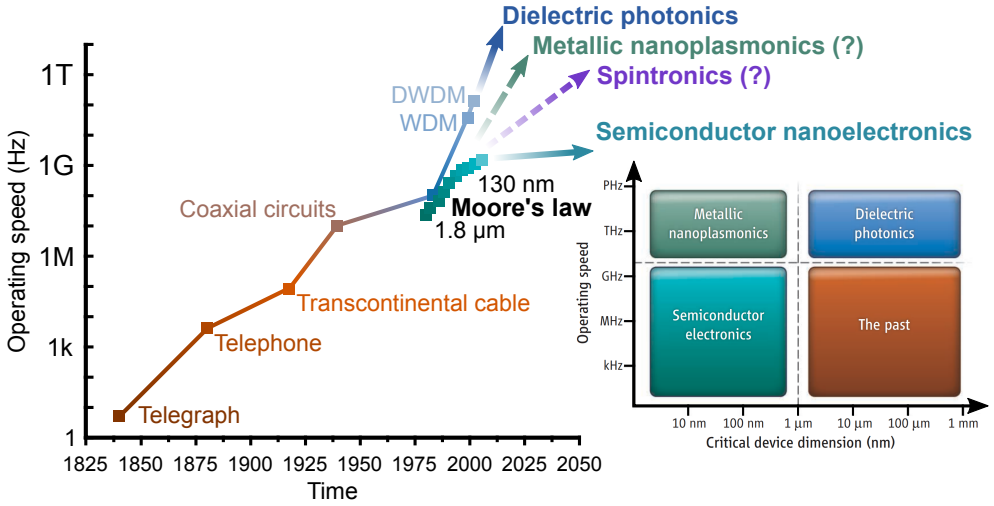

Figure 4: Evolution and future forecast of different technological approaches (electronics, photonics, or plasmonics) and materials (semiconductors, dielectrics, or metals) in terms of working performance (operating speed) along the time and as a function of the critical device size [31].

(in extended metal surfaces) or localized (in the case of finite metallic nanoparticles, yielding localized surface plasmon resonances), either way, exhibiting an unparalleled ability to confine light into deep-subwavelength volumes [28]. In addition to overcoming the diffraction limit, such an extreme light concentration, enabled by plasmonic nanostructures, may eventually lead to an enormous local field enhancement (often referred to as *hot spots*) [29]. These features have proven to be very useful, for instance, to boost non-linear phenomena (e.g., for spectroscopy based on surface-enhanced Raman scattering), as well as for controlling light-matter interactions at the nanoscale (e.g., to manipulate light properties such as the EM field distribution, the propagation, or the state of polarization, or even dynamical properties such as the energy, the spin, or the optical chirality). Furthermore, the possibility of squeezing and guiding light in subwavelength metallic structures has opened new paths toward the realization of surface plasmon-based photonic elements (i.e., waveguides, switches, modulators, couplers, ...) in order to reach the coveted miniaturization of PICs — which is certainly one of the central goals of current research in plasmonics [30]. In this sense, plasmonic circuits would allow gathering together, on a same chip, both the size of nanoelectronics and the high operating speed of conventional dielectric-based photonics, with the additional benefit (though still potential) of conveying electric currents, optical signals, or even both, through the same channel (owing to the hybrid electron-photon nature of SPPs). Plasmonics is then expected to provide the sought convergence between optical communications and electronic computations for data and information processing (Figure 4); or at least the way to interface them in highly integrated circuits [31]. Yet, a major challenge in the accomplishment of all-plasmonic structures is due to the high absorption losses of metals at optical frequencies. This fact limits the maximum distance at which the SPPs can be propagated, and therefore would set an upper bound on the size of the whole circuit.

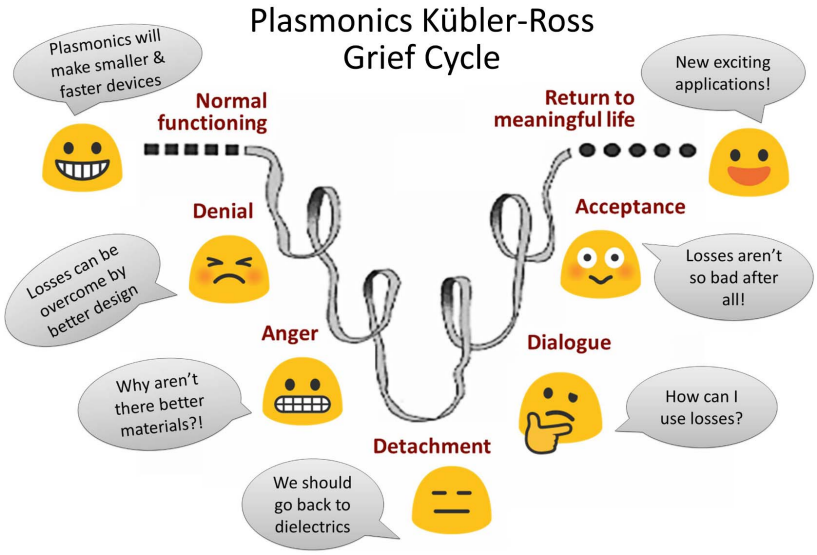

Figure 5: Plasmonics Kübler-Ross Grief Cycle. Lighthearted diagram showing gradually the different attitudes when examining the role played by absorption losses in plasmonic systems [33].

Moreover, the CMOS compatibility severely restricts the number of eligible materials (e.g., aluminum, copper, and even semiconductors such as ITO, are some of the few viable options). As a practical, though provisional approach (or even perhaps for long-term) to address these kind of shortcomings, it has recently been suggested a hybrid architecture integrating both silicon-based platforms and CMOS-compatible plasmonic materials [32]. In such a way, dielectrics would be in charge of guiding and conveying the optical signals and the plasmonic nanostructures of carrying out the corresponding functionalities.

It is worth remarking that, albeit absorption losses — which essentially entail dephasing as well as an exponential and rapid decay of signals — are often considered as a harmful effect in the context of optical communication and data processing (e.g., in many functional circuit elements such as interconnects or waveguides), there are many other applications in which they are not only harmless, but they turn essential, or even advantageous (Figure 5) [33]. In this vein, topical strategies to deal with absorption losses in plasmonic systems (and also in metamaterials) are lately experiencing a change of paradigm; moving from avoidance — either minimizing or compensating the losses, e.g., by improving the fabrication processes, or just by means of optical gain media — to harnessing, namely, considering alternative approaches in which losses may be profitably exploited [34]. This is the case, for example, of light-induced (local) heat generation, which can be very useful in chemical control of reactions (e.g., in thermo-catalysis) or in thermally activated physical processes (such as heat-assisted magnetic recording). All in all, loss-enabled plasmonic functionalities might be useful in a wide variety of scenarios in which an efficient and targeted (even into deep subwavelength regions) delivery of both, light and heat, could be demanded, including nanofabrication, nanomanipulation, spectroscopy, or near-field nanorouting of thermal radiation [33, 34]. On the other side,

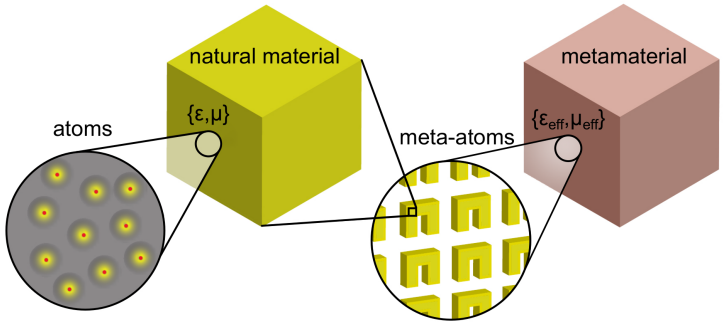

Figure 6: Conceptualization of naturally occurring materials formed by atoms, against metamaterials, built upon meta-atoms that are in turn made of atoms. The effective parameters of metamaterials (ε_{eff} and μ_{eff}) will depend on that of the constituent matter (ε and μ) as well as on the shape, size, orientation, and the arrangement of the meta-atoms.

and regardless of their source (either due to plasmonic materials, or any other kind of dispersive medium), absorption losses, and, in general, any dissipative effect, are of utmost theoretical importance when dealing with physical systems undergoing irreversible processes. Upon this basis, and taking into account an intricate connection between the ideas of *reversibility* and *reciprocity* (certainly well distinct notions [35], although somehow related to each other through the so-called *Onsager-Casimir relations*), it has been possible to demonstrate the existence of insightful relationships as for the role played by the absorption losses into the analysis of complex dynamical properties of light such as the optical chirality [36]. Furthermore, insofar as dissipation and dispersion are necessarily tied to each other (on account of the *Kramers-Kronig relations*, which, in turn, underpin the fundamental *principle of causality*), absorption losses are indirectly, but ultimately, behind a myriad of dispersive phenomena occurring in nano-optics and photonics.

Intimately linked to plasmonics, the ultimate leap forward in this fervent road toward the miniaturization has come with the relatively recent advent of *metamaterials* [37]. As its very name indicates, metamaterials refer to artificial materials whose properties go beyond from those that can be found in nature [38]. Even though at first glance it could be thought that such a realization might affect to any kind of physical property, the term metamaterials traditionally revolves around photonics, thus concerning the optical behavior of matter [39]. The underlying idea basically consists in designing and constructing nanostructures much smaller than the wavelength so that they can behave as nanoscale artificial light scatterers, usually referred to as *meta-atoms* (Figure 6). Then, provided that they are densely arranged in periodic arrays properly engineered, the resulting structure will exhibit a tailor-made optical response with properties on demand [40]. As opposed to *photonic crystals*, whose structure has a periodicity comparable to the wavelength of light (enabling one to perform a sort of *bandgap engineering* via diffraction effects), in metamaterials the lattice constant should be much smaller than the wavelength. In this way, and after carrying out the corresponding homogenization process (ruled by the *Clausius-Mossotti equation*), metamaterials are to be considered as *effective continuous media*.

Just like in any natural medium, the optical response of metamaterials, averaged over many meta-atoms, is characterized in terms of the constitutive effective parameters: the electric permittivity (ε_{eff}) and the magnetic permeability (μ_{eff}). Essentially, these quantities set the relationship between free-space EM fields, and those passing through material systems, which are indeed routinely expressed in terms of the polarization and the magnetization vector fields[‡]. Hence, ε_{eff} and μ_{eff} enclose the overall optical features of the matter, determining its character in terms of (non)linearity, (in)homogeneity, (an)isotropy, and, importantly, its dispersion relation. Likewise, an equivalent characterization of the medium might also be done in terms of the refractive index ($n_{\text{eff}} \equiv \sqrt{\varepsilon_{\text{eff}}\mu_{\text{eff}}}$) and the relative wave impedance ($Z_{\text{eff}} \equiv \sqrt{\mu_{\text{eff}}/\varepsilon_{\text{eff}}}$). In any case, in order to find out the explicit expressions of these parameters one should resort to material models that account for the behavior of matter under the presence of EM fields, so providing with the corresponding *constitutive relations*, relating, respectively, the polarization and the magnetization with the external electric and magnetic field. For the case of natural metals, the most well known example is given by the *Drude model* — or its extension, known as the *Drude-Lorentz model* — which, among other things, affords a classical explanation for the existence of SPs as well as for the negative value of the permittivity at optical frequencies. However, the range of permittivities (and even more that of permeabilities) attainable in nature at a given frequency band (e.g., in the visible spectrum) is considerably narrow, limiting so the possible applications. Metamaterials, then, come to fill this gap, enabling not only to reach extreme values of ε and μ, but also, and more importantly, modeling its character.

Unlike the permittivity in the case of metals, the occurrence of negative permeability at optical frequencies lies out of the range of most natural materials — it is often said that matter is nonmagnetic. This poses a clear limitation in many situations, for example, restricting the excitation of SPPs, or the Brewster effect, only to p-polarized waves (also referred to as TM modes). Furthermore, the difference of sign between ε and μ in a given material (e.g., in electric plasmas yielded by the free electrons of metallic structures, in which $\varepsilon < 0$ and $\mu > 0$) is behind the evanescent character of EM waves in such a medium, even under the assumption that it may be lossless (i.e., presuming that the imaginary part of the permittivity could be equal to zero). Indeed, it is easy to see that such a difference of signs would result in a purely imaginary contribution for the refractive index, and accordingly, for the wave vector, thereby making the complex phase factor to exhibit an exponentially decaying behavior. Musing over these issues, for the very first time in 1968, Viktor G. Veselago (1929 – 2018) put forward theoretically the idea of considering a medium with both the permittivity and the permeability negative [41]. Besides showing the possibility of having propagating waves through media with $\varepsilon < 0$, the most important consequence was that, along such a propagation, the phase evolution (characterized in terms of the phase velocity) and the energy transport (which can be expressed by the group velocity, or more precisely, by means of the Poynting vector) are antiparallel. This feature is usually known as the *backward propagation*, and its explanation raises on the fact

[‡]Physically, polarization and magnetization fields give an account of the density of electric and magnetic dipole moments that result from averaging the motion of the charges and currents induced by an EM field.

that the refractive index is to be negative. Materials displaying this astonishing hallmark are termed as *left-handed metamaterials* (LHM) or *negative-index metamaterials* (NIM), and have enabled a variety of new and surprising optical effects [42]; essentially leading to a reverse behavior with respect to customary phenomena such as the Doppler effect and the Čerenkov radiation, as well as over the more intriguing Goos-Hänchen shift (allowing for stopping and trapping light in LHM-made waveguides) [43], and the Casimir effect (turning attraction into repulsion and then enabling quantum levitation effects) [44]. Yet, though seemingly much simpler, the most remarkable consequence of LHMs is arguably the *anomalous refraction*, which led to the proposal of the so-called *perfect* (or *super*) *lens*, consisting in a planar slab made of a LHM that is able to focus light through it (something physically impossible in conventional right-handed media, as it would require a certain curvature), and, strikingly, get super-resolution (by considering also the evanescent contribution, that in LHMs is amplified). This latter realization was actually demonstrated by John B. Pendry in 2000 [45], and it was the fact that led Richard A. Shelby, David R. Smith, and Sheldon Schultz to carry out in 2001 the first experimental demonstration of LHMs in the microwave range [46]. Since then and up until now, LHMs are being regarded as the cornerstone of metamaterials.

During the last years, the area of metamaterials has been subject of intense and relentless research activity [47,48]. In the first stages, in order to reach the optical regime and improve the overall performance, main efforts were directed, on the one hand, to reduce more and more the size of meta-atoms, and, secondly, to look into other geometries and arrangements beyond the ones originally proposed (mostly based on a combination of thin metal straight wires and split-ring resonators); endeavors for which plasmonic nanostructures have proven to be crucial [49]. As a result, there have arisen (and still keep on emerging) a considerable showcase of promising structures bearing a huge amount of enticing properties and functionalities, some of which have become in hot-topics within the current research landscape of nanophotonics. A good example of this are the fields of extreme (either high or low) refractive index materials [50,51], as well as the transformation optics, this latter providing the ultimate paradigm for controlling the light propagation by means of artificially engineered materials [52,53]. Other current trends in the development of metamaterials are being conducted toward the design and implementation of the so-called *hyperbolic materials* [54], and *stereometamaterials* [55] (customarily referred to as *bianisotropic metamaterials* [56], or simply as *chiral metamaterials*), which, by properly shaping, respectively, the anisotropic and bianisotropic features of artificial materials, are sparking off a number of outstanding possibilities (for instance, allowing to get media with optical gain, greatly enhancing nonlinear effects, or enabling dynamic control over the state of polarization, e.g., so as to perform spin-dependent light-matter interactions). Obviously, and as might be expected, the complete list of effects and applications brought about by metamaterials would go far beyond what it could be outlined here — and surely anywhere else. In fact, at the present time, metamaterials (in conjunction with plasmonic nanostructures) are technologically poised to enable the manipulation and achieve a full control over practically whatever optical property of EM waves, including the intensity wave

profile, the polarization structure, the dispersion relation, and the phase distribution [57]. Still, despite the overwhelming wealth of mainstream structures and configurations that have been proposed for applications that are potentially realizable, taking into account the current technical means, the major challenge of metamaterials lies on the fabrication process, and more specifically, in the way to get cost-efficient and large-scale production, as well as their integration into actual devices [58]. This limitation becomes even greater when aiming to work at optical frequencies. Indeed, in that regime, the meta-atoms should be so extremely small that the distinction between matter and device would turn out to be quite blurred [59]. Hence, and turning back to the first paragraphs of this introduction, such an accomplishment — for now only realizable at laboratory level — might be somehow envisaged as a preliminary (though rather meaningful) materialization before going on to properly address the final questions posited in the aforementioned Feynman's lecture, wondering *as to whether, ultimately, we can arrange the atoms the way we want; the very atoms, all the way down!* [3]:

> «*What could we do with layered structures with just the right layers? What would the properties of materials be if we could really arrange the atoms the way we want them? They would be very interesting to investigate theoretically. I can't see exactly what would happen, but I can hardly doubt that when we have some control of the arrangement of things on a small scale we will get an enormously greater range of possible properties that substances can have, and of different things that we can do*».

In that respect, it is worth noticing that right there, and expressly with the focus put on photonic applications, it was already foreseen a precursory notion of what we now know as an artificial metamaterial, namely, «*a piece of material in which we make little coils and condensers (or their solid state analogs) 1.000 or 10.000 angstroms in a circuit, one right next to the other, over a large area, with little antennas sticking out at the other end [...] for example [...] to beam the light out in a definite direction with very high intensity*».

Finally, and for completeness, we will conclude this survey on the breakthroughs entailed by the miniaturization of the physical systems (and especially as far as photonics is concerned) by highlighting that the final goal foreshadowed by Feynman has actually been surpassed. Even though far from the classical standpoint of metamaterials, the long awaited *atom-by-atom manipulation* for practical applications (beyond the "simple" positioning), and in particular within the context of nano-optics, e.g., for sculpting light waves and controlling its interaction with matter, even at a single-photon level, it is already a reality. Notwithstanding, the fundamental framework to properly deal with these matters and perform accurate assessments, is the *quantum optics* [60,61], an entire field of research that would require further and careful considerations on many specific aspects (involving, e.g., coherent states, light squeezing, or quantum entanglement) [62], which largely exceeds the aims of this work. Be that as it may, nanophotonics, including the branches of plasmonics and metamaterials, might be somehow regarded as the classical anteroom of such a quantum *milieu*, and will indeed be the arena over which this thesis shall be grounded.

Objectives & Structure of the Thesis

Throughout the above pages there has been presented a rather cursory overview setting down the overall impact and benefits that the continuous process of **miniaturization** and integration of physical systems have had on the current development of science and technology, all the way to the present status. Specifically, from the main events that prompted the onset of the nanoscience and nanotechnology, we have underscored the major milestones that have fostered and contributed to their advance, bearing the focus on those related with nanoelectronics and nanophotonics. In this respect, starting with the realization of the FET, regarded as the trigger of this downscaling race toward devices increasingly smaller, we have gone on seeing how, one by one, there have been appearing successive shortcomings and limitations: the shrinkage limit of electronic devices, the diffraction limit for guiding and confining optical fields in dielectric-based photonic structures, and the high absorption losses displayed by plasmonic systems. It has been the research aimed at facing and overcoming each of these hurdles that sparked off the subsequent strides, thus giving rise to new physical effects as well as to the establishment of new scientific areas. In this manner, conventional electronics upgraded to nanoelectronics, and this, in turn, pushed forward the disruptive proposal of spintronics. Each of them brought along, among other things, the deployment of the CMOS technology as the standard of nanofabrication of integrated circuits, the discovery of the quantum analogue to the Hall effect, and the inclusion of spin-based effects on the ground of electron transport phenomena for applications in solid-state devices. At the same time, in another plane, classical optics gave way to photonics, thereby opening a new path for getting an active control over light beams and their properties. Then, and taking advantage of the whole technology already developed for nanoelectronics, came up nanophotonics, which was, in turn, splitted up into dielectric photonics and metal-based plasmonics, thus enabling the proposal of PICs as a promising alternative to the mainstream circuits of nanoelectronics. Finally there emerged the novel area of metamaterials, providing the ultimate paradigm for designing and crafting nanostructures to engineer the optical response at will. Obviously, this story is neither so fast nor so lineal, but described in this way may be helpful to illustrate the **parallelism** that, to some extent, there exists between nanoelectronics and nanophotonics.

Apart from merging different scientific branches, as has thus far been outlined, another insightful strategy for gaining more understanding about the underlying physics of a given system — either in electronics, photonics, or in whatever other area — and so furthering on the development of new technologies, simply consists in the search of **analogies**. In fact, as insistently stressed once and again in *The Feynman Lectures on Physics*: «*The same equations have the same solutions*». In this regard, it is worth pointing out that, lately, nanophotonics is being strongly spurred on account of its potential resemblances with quantum features, in particular on those involving the behavior of local dynamical properties of electrons. Although strictly speaking quantum electronics and nanophotonics deal with matters of well different physical nature, the fact is that they actually share a

similar mathematical framework, essentially relying upon a wave-like analysis[§]. Hence, because of their formal similarities they both can serve as a bridge, in the sense that they are susceptible to feedback into each other, so that the knowledge learned from one side may be directly transferred to the other, and vice versa. Such a relationship has inspired and boosted the burgeoning of new predictions, discoveries, and innovative concepts in photonics, and, at the same time, has opened up the possibility to perform out-of-reach quantum experiments through their corresponding classical analogue in nanophotonics.

Furthermore, enabled by the current technological **capabilities**, we are now, more than ever, ready to explore and exploit properties and physical phenomena, which, up to now, were only accessible from a theoretical approach. Specifically, in regards to nanophotonics, the ability of plasmonic systems for concentrating and enhancing light fields at the nanoscale, along with the feasibility for realizing and engineering metamaterials tailored at will, has brought forth an ideal playground with practically infinite prospects to control the light-matter interactions at the nanoscale. This would include the possibility of manipulating elementary properties of EM waves such as the state of polarization (describing the vector-like amplitude) and the spatial propagation features (which are essentially enclosed within the phase of the wave). Consequently, and more importantly, this allows one to look into the deeper behavior of many of the main local dynamical properties, such as the EM energy density, the linear momentum, the orbital and the spin angular momentum, the EM helicity, or the optical chirality.

Taking into account these basic pillars (highlighted in boldface), namely, the **miniaturization** of physical systems, the **parallelism** between nanoelectronics and nanophotonics, the interest in the search of quantum **analogies**, and the state-of-the-art of current photonic technologies enabling unprecedented experimental **capabilities** to deal with nanoscopic systems, the emergence of **SPIN-DEPENDENT OPTICAL PHENOMENA** come into sight as a natural consequence of the latest research trends in nano-optics and photonics. Within this wide scenario, and building on criteria of novelty and relevance, the *spin-orbit interaction of light* and the *chiroptical light-matter interactions* conform two of the most important families of spin-based optical effects, and shall be the specific topics over which we will delve into throughout the present thesis.

Regarding the novelty of these topics, it is worth remarking that the spin-orbit interaction appeared for the very first time in the context of optics only very recently, in 1992, in a seminal work authored by V. S. Liberman and B. Y. Zel'dovich [63]. The chirality, for its part, was introduced into the optical framework, even more recently, in an original contribution due to Y. Tang and A. E. Cohen in 2010 [64]. From then until

[§]Besides the differences on the character (vector or scalar) of the waves appearing in photonics and quantum physics, the main discrepancy lies on their physical interpretation. In the case of photonics, the waves are real-valued vector fields with a real physical meaning, indicating the EM field density. Conversely, waves in quantum physics, actually dubbed matter waves, are given by complex-like scalar functions representing the state of a quantum system, and whose connection with reality is to be carried out through the modulus squared, that provides the probability density of finding the system in such a state.

now, the research activity on these matters, which, by the way, are closely tied with each other, is currently witnessing a tremendous growth on all the fronts: from theoretical studies to experimental realizations, either from fundamental or applied approaches, all the possible combinations. As a result one can find a vast number of scientific contributions on these topics appearing almost every day in the most renowned journals, thereby providing an evidence sufficiently objective to justify their actual relevance.

After an extensive and thorough review over a large volume of literature related to the spin-orbit interaction (SOI) of light and the optical chirality we found out some fundamental aspects that have often been either assumed or directly disregarded. Specifically, as far as the **optical SOI** is concerned, it can be spotted the following lacks:

- Either implicitly and/or explicitly, it has been widely assumed that SOI of light is a phenomenon that only occurs at the nanoscale. This characteristic feature has been extensively researched numerically, confirmed experimentally, and exploited in a multitude of applications, but always from the viewpoint of the stemming effects. Yet, regarding the fundamental theory we observe an important lack: there is not any *demonstration showing analytically that optical SOI is a phenomenon naturally implicit in Maxwell's equations that necessarily emerges at subwavelength distances.*

- A paramount example among spin-dependent optical phenomena is the *quantum spin Hall effect of light*, which has led to a unified framework to explain the *spin-momentum locking*, and, consequently, the *spin-controlled unidirectional excitation.* According to this latter phenomenon, the propagation direction of EM guided modes can be controlled by the spin of an oscillating optical source put in close proximity to a waveguiding structure. Thus far the focus has only been placed on dipolar sources (either electric or magnetic), so a *general description of the near-field directionality induced by higher-order multipole fields* still remained to be performed.

On the other side, as for the **optical chirality**, one can realize the following points:

- During the last few years, there has been a considerable interest in the optical chirality of EM waves and its relationship with chiral properties of matter. Recent advances in nanofabrication are resulting in plasmonic structures and metamaterials that greatly boost the chiral light-matter interactions, thus enabling enhanced chiroptical applications, such as spectroscopy as well as ultrasensitive detection of enantiomers. Nonetheless, *a full theoretical description of optical chirality in dispersive and lossy media* (as it is the case of metamaterials and plasmonic systems) is still lacking.

- So far, prevailing chiroptical approaches to determine the chirality of either chemical (bio)molecules or artificial nanostructures relies upon free-space excitation and detection schemes. Despite the current trend toward miniaturization and integration of photonic devices, there is an eye-catching gap in the research concerning the *generation and conveyance of chiral modes through lithographically defined photonic waveguides, as well as on the realization of chiroptical applications, such as sensing or spectroscopy, in silicon-based integrated photonic platforms.*

In view of the above considerations, the central goal of this thesis is to fill these gaps. As can be noted, in general, the focus is eminently theoretical and the matters addressed revolve around the most innovative foundations of modern optics. Indeed, as has been pointed out by many authors, spin-dependent optical phenomena (including chiroptical interactions) represent an important and integral part of cutting-edge research in nano-optics, photonics, and plasmonics, including the area of metamaterials, and feature the most distinctive landmarks in optical engineering, namely, the miniaturization of the systems and the outperformance of the communication and processing capabilities, enabled by the additional spin degrees of freedom. Likewise, it should be noted that, as far as possible, in order to yield a treatment as general as possible, particular emphasis will be placed on the search and construction of analytical models[¶]. In this sense, besides providing fresh physical insights, thereby underpinning and upgrading the fundamentals of spin-based photonics, the resulting outcomes hold the promise of being useful for expanding and improving the current palette of polarization-dependent optical functionalities and applications, ranging from communications (particularly as for routing and switching), processing, computing, metrology, polarimetry, sensing, or spectroscopy, among many others. Hence, and ultimately, the end goal of this dissertation is to contribute to lay down the basis for a sound and self-consistent theoretical framework to deal with spin-dependent light-matter interactions in nano-optics and photonics, and, so, pave the way for the development of the emerging field of *spinoptics* (the optical counterpart of spintronics in solid-state systems) [65–69]. Given the generality of the whole approach, the scope of this work would hopefully become relevant to a broad scientific community, from both fundamental and applied perspectives, especially in atomic and molecular physics, electrical engineering, chemistry and biology, and, of course, in nano-optics, photonics, and even quantum optics.

After this introduction aimed at setting down the overall context of the current state-of-the-art of nanophotonics (including its stemming branches; plasmonics and metamaterials), and the motivation to carry out a research on spin-dependent optical phenomena, the thesis is essentially structured as a collection of published papers. To render the text easier to read, the contents have been divided into the following parts:

- Part I: *Original Contributions on Spin-Orbit Interactions of Light*. This part includes three chapters (actually corresponding to two original papers published in international peer-reviewed scientific journals plus a Supplemental Material) related to the optical SOI. PAPER A [Chapter 1] focuses on the fundamentals of the SOI of light, specifically in showing its classical emergence at the nanoscale from an analytical approach. PAPER B [Chapter 2] (and its Supplemental Material [Chapter 3]) generalizes one important application of optical SOI: the spin-controlled unidirectional excitation.

[¶]Here it is worth emphasizing the importance of finding out analytical results (either when solving a given equation or when approaching a physical issue), as they provide an incontrovertible and general demonstration, or description, of a given problem. In contrast to numerical methods, useful for addressing particular cases, or when there is no analytical solutions, analytical models are extensible to any situation.

- Part II: *Original Contributions on Optical Chirality*. This part contains three chapters corresponding to two original contributions (along with a Supplemental Material) concerning the optical chirality and the chiral light-matter interactions. PAPER C [Chapter 4] (and its Supplemental Material [Chapter 5]) is a fundamental work that put forward a generalization of the optical chirality to arbitrary media. PAPER D [Chapter 6] analyzes by numerical means the feasibility for carrying out chiroptical applications (sensing and spectroscopy) in integrated photonic platforms.

- Part III: *Discussions & Conclusion*. This part constitutes the closure of this thesis. Chapter 7 provides with a final discussion, summarizing and highlighting the main results and some important remarks. As a culmination, at the end of each discussion there is included an additional contribution [PAPER E and PAPER F][‖]. Chapter 8 gathers up and summarizes, from an unified perspective, some overall conclusions, sketching out a general outlook for potential future research directions.

All the above papers, conforming the body of this thesis [PAPER A – PAPER F], appear perfectly referenced at the end of this document, in the section of *Author's Merits*. In addition, the whole set of contributions and research activities undertaken during this thesis are also listed, including additional papers (published or ready to be submitted to international journals), a book chapter, a list of the attended conferences (specifying the corresponding contribution, either poster, oral, invited, or other), as well as other activities, such as a research stay, reviewing of papers, and a selection of scientific artwork. Lastly, the complete list of references cited throughout this work appears recapitulated, in order of appearance, in the section of *Bibliography*. Notice that, despite each chapter already includes its own list of references and that many of the them are repeated over different articles, in the final list each citation is included only once, and will be numbered with respect to the order of appearance in this thesis, seen as a whole document.

[‖]Notice that these contributions are actually a research highlight (proposed by ourselves, but peer-reviewed), on two of the above original contributions [PAPER B and PAPER C, respectively]. Despite not being published in a JCR-indexed journal (and so without impact factor associated), the importance of these publications lies on their own character as a special recognition, since they were selected by the Editorial Board of the journal *Optics & Photonics News* (OSA) to be featured in the December Special Issue as among the top 30 most interesting research in optics and photonics conducted both in 2018 and 2019.

Part I

Original Contributions on Spin-Orbit Interactions of Light

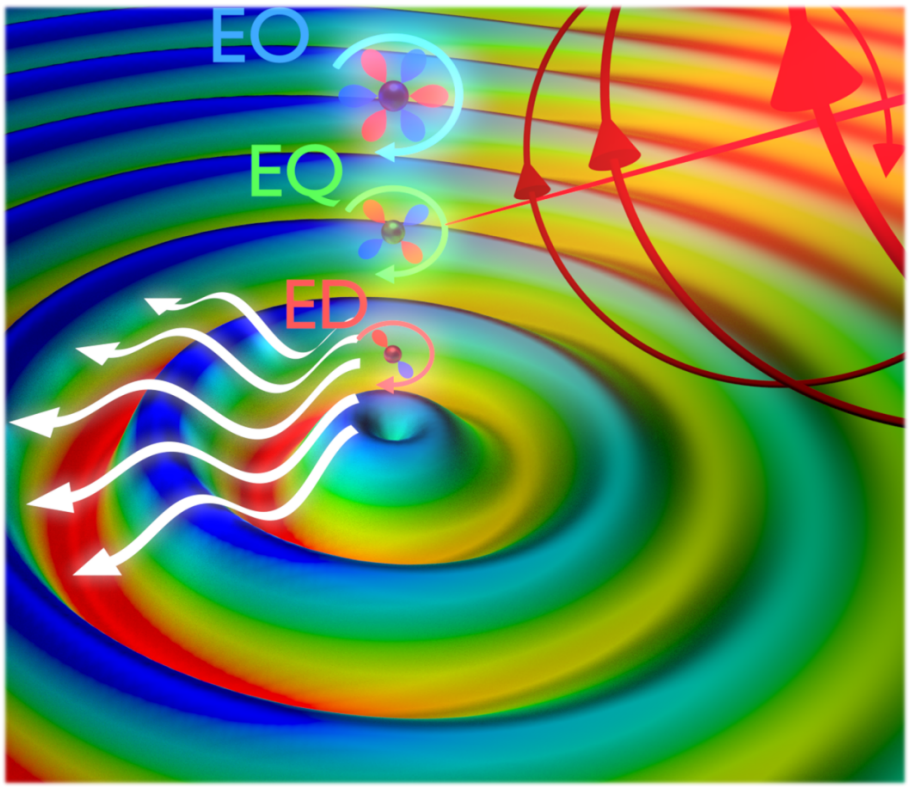

Chapter 1

PAPER A

Classical emergence of intrinsic spin-orbit interaction of light at the nanoscale

---

Phys. Rev. A 97, 033804 (2018)

Classical emergence of intrinsic spin-orbit interaction of light at the nanoscale

J. Enrique Vázquez-Lozano and Alejandro Martínez

Nanophotonics Technology Center, Universitat Politècnica de València, Camino de Vera s/n, 46022 Valencia, Spain

Traditionally, in macroscopic geometrical optics intrinsic polarization and spatial degrees of freedom of light can be treated independently. However, at the subwavelength scale these properties appear to be coupled together, giving rise to the spin-orbit interaction (SOI) of light. In this work we address theoretically the classical emergence of the optical SOI at the nanoscale. By means of a full-vector analysis involving spherical vector waves we show that the spin-orbit factorizability condition, accounting for the mutual influence between the amplitude (spin) and phase (orbit), is fulfilled only in the far-field limit. On the other side, in the near-field region, an additional relative phase introduces an extra term that hinders the factorization and reveals an intricate dynamical behavior according to the SOI regime. As a result, we find a suitable theoretical framework able to capture analytically the main features of intrinsic SOI of light. Besides allowing for a better understanding into the mechanism leading to its classical emergence at the nanoscale, our approach may be useful to design experimental setups that enhance the response of SOI-based effects.

A.I Introduction

Spin-orbit interaction (SOI) comprises a broad class of effects very well-known in the branches of atomic and solid state physics [1,2]. Roughly speaking, such phenomena involve charged particles moving within a region where there is an electric field, e.g., that originated by the atomic nuclei or by the asymmetry in the confinement potential of electrons in heterostructures. In these contexts, SOI can be conceived as an effective phenomenon of a relativistic nature wherein the motion of the particle is coupled with its spin [3]. The importance of this interaction is noteworthy since it has allowed to explain the fine-structure energy corrections of hydrogen-like atoms. Nonetheless, even more important has been the occurrence of SOI in solids, paving the way to the area of spintronics [4].

The extension of SOI to optics is attributed to the seminal work by Liberman and Zel'dovich [5]. Their approach was based on the conservation of the state of polarization

(SoP) when light propagation was subjected to bending and/or twisting in an optically inhomogeneous medium. Under this scheme, they introduced the optical SOI as the mutual interaction between the SoP (spin) and the propagation process (orbit). This coupling can be simply characterized in a mathematical way by means of the so-called *factorizability (or separability) condition*, which accounts for the mutual influence between the amplitude and the phase of light.

Akin to mechanical systems, light possesses a set of dynamical properties such as energy, linear momentum, and angular momentum among others [6]. Due to the vector character of the electromagnetic fields two types of rotations can be distinguished [7,8], giving rise to the corresponding contributions termed as spin angular momentum (SAM) [9] and orbital angular momentum (OAM) [10], respectively. Whereas OAM is related to the spatial distribution and propagation of the optical field, SAM is generally determined by the SoP [11,12]. Notice that, from a quantum approach, the correspondence principle states that each of the two possible spin states of photons can be identified with the corresponding right- and left-handed circular polarization. This rule only holds for the usual longitudinal SAM, closely linked to the plane wave representation. Still, this picture is in sharp contrast to the transverse SAM, which is characteristic of evanescent as well as structured optical fields [13–15]. Taking into account the above dynamical quantities, from a pragmatic point of view, the optical SOI is commonly understood as the interplay and mutual conversion between the different types of angular momenta [16,17]. However, this definition only emphasizes into the effects, neglecting its fundamental appearance and leading to a certain controversy related to the proper way in which must be performed the separation of the total angular momentum into the spin and orbital contributions [8,12,18,19]. In this regard, it is noteworthy to mention that this difficulty may be, in turn, associated with the so-called *Abraham-Minkowski dilemma*, a long-standing problem concerning with an ambiguity that arises from the real definition of the linear and angular momentum for optical radiation in media. Even though there are a number of influential papers claiming to have solved it (see, e.g., Refs. [20,21]), this challenging problem still remains as a subject of current interest and debate [22,23]. Notice also that, in relation to the above example regarding the homonymous phenomenon occurring either in atomic or in solid state physics, the interplay between the different kinds of angular momenta play the same role in this case as the spin-dependent splitting in the electronic energy levels, namely, just as an observable effect but not as the ultimate reason leading to the classical emergence of intrinsic SOI of light.

In the past few years, SOI of light has been the subject of intense research activity. Huge efforts have been devoted to investigate novel photonic applications and functionalities (for a complete overview on this issue see Ref. [24] and references therein), paying little attention to the fundamental theory underlying its origin. In this regard it has only been argued that, since photons are relativistic spin-1 particles, SOI of light is inherent to Maxwell's equations [25], arising from the transversality condition [26] and described in terms of the geometric Berry phase formalism [27].

Furthermore, the close relation between SOI and the intrinsic spin Hall effect of light has been extensively studied, both theoretically and experimentally [28]. The latter manifests itself as a topological spin-dependent transport of photons taking place in inhomogeneous media as well as in free space, thereby ensuring the conservation of the total angular momentum [29]. Additional spin-related optical phenomena such as the aforementioned transverse spin [30], topological insulators [31], or spin-momentum locking [32], leading to the so-called spin-controlled unidirectional excitation [33], have been recently demonstrated as manifestations of the quantum spin Hall effect of light [34]. The vast and unified body of knowledge that exists around SOI is evident. Nonetheless, as already stated, its occurrence is ultimately justified from elementary effects such as the Rytov-Vladimirskii-Berry rotation, the Imbert-Fedorov transverse shift, or the optical Magnus effect [5]. In addition, it is important to stress that the subwavelength character of the optical SOI is a prescription that, although widely assumed and confirmed both experimentally and numerically by means of rather qualitative arguments stemming from its effects, to the best of our knowledge, still remains without any reliable analytical demonstration that supports it.

In this paper we aim to provide further understanding into the classical emergence of optical SOI. From a full-vector description based on the multiple-multipole method [35], we demonstrate analytically that SOI of light is a phenomenon that naturally and necessarily comes into play at the subwavelength scale, even in homogeneous media. Indeed, by using the formalism of vector spherical wave functions (VSWFs) [36] in combination with the above-mentioned factorizability condition, we find an additional relative phase that introduces an extra term enclosing the main features of SOI, i.e., it prevents the amplitude-phase separability, but solely in the near-field region. Although it seems a somewhat trivial standpoint, this is certainly the key point to demonstrate the universal occurrence of optical SOI at the nanoscale. Of course, this approach satisfies the overall prescriptions underlying the SOI of light, i.e., it is implicit in the Maxwell's equations, and is ultimately related to the transversality condition of the electromagnetic fields. Importantly, our results also allow us to identify accurately the region wherein SOI-based phenomena naturally emerge. Therefore, besides providing a more fundamental definition for the near-field region in terms of the factorizability condition, they may be used to facilitate or improve the setups for the experimental observation of SOI-based effects.

A.II Overview of Full-Vector Waves

To start with, let us consider an arbitrary electromagnetic wave which propagates in a homogeneous medium. By means of the angular spectrum representation, this field can be expressed as a superposition of elementary plane waves, each having a well-defined SoP, constant over the whole space

$$\mathbf{E}(\mathbf{r}) = (\alpha \mathbf{e}_1 + \beta \mathbf{e}_2)\, E_0(\mathbf{r}) e^{i\phi(\mathbf{r})}, \tag{A.1}$$

where α and β are arbitrary complex constants describing the normalized SoP ($|\alpha|^2 + |\beta|^2 = 1$), $\mathbf{e}_{1,2}$ are two orthogonal unit vectors, E_0 is the scalar field profile, and ϕ is the phase distribution. As pointed out above, following Ref. [5], SOI of light is envisioned from a fundamental approach as the mutual influence between the SoP and the phase distribution. Hence, owing to the factorized form of the plane wave in Eq. (A.1), the mutual interaction between the SoP and the phase vanishes, avoiding the occurrence of SOI. This is the usual picture in macroscopic geometrical optics [37], wherein light is characterized by means of propagating rays which, in turn, can be described as a field expansion into local plane waves. This scalar-like scheme can also be extended to the zeroth order of the paraxial approximation [5,27]. Nevertheless, at the nanoscale, near or beyond the diffraction limit, this usual treatment based on the plane-like waves seems to be pretty naive. Furthermore, due to the extraordinary properties of the angular momentum associated to evanescent fields [30], the understanding of SOI-based effects for such kinds of fields deserves a special approach (for further details on this issue see Ref. [38]).

Close to the sources, or in the near-field region of the processes wherein light-matter interaction takes place, the spatial field distribution of electromagnetic waves displays complex shapes. Therefore, to deal with nontrivially structured optical fields, it becomes necessary to perform a full-vector wave analysis [35]. Regardless of the spatial distribution, any optical field can be generally expressed as a multipole expansion [36], i.e., as a proper linear combination of the vector spherical harmonics (VSH). In this way, the electromagnetic field can be regarded as that radiated from a point-like source [39], thus providing a suitable tool to deal with phenomena occurring at the subwavelength scale. This includes the SOI of light as well [40], which has been experimentally demonstrated to induce subtle observable effects upon the far-field via imaging systems [41]. Hence, instead of the plane-wave basis, VSWFs seems to be a better choice to accomplish a full description of processes at the nanoscale.

It is well known that in a source-free, homogeneous, isotropic, and linear medium, the time-independent electromagnetic fields can be obtained from the vector Helmholtz wave equation

$$\nabla \times [\nabla \times \mathbf{\Psi}(\mathbf{r})] - k^2 \mathbf{\Psi}(\mathbf{r}) = 0, \tag{A.2}$$

where $\mathbf{\Psi}(\mathbf{r})$ can be either the electric or magnetic field, $k = n\omega/c$ is the wave number, and $n = \sqrt{\varepsilon\mu}$ is the refractive index, with ε and μ being the corresponding relative permittivity and permeability of the medium. Although there exist several conventions to define the VSH, throughout this work we will follow that given in Ref. [42] as follows:

$$\mathbf{R}_{lm}(\Omega) = \mathbf{e}_r Y_{lm}(\Omega), \tag{A.3a}$$

$$\mathbf{\Theta}_{lm}(\Omega) = N_l r \nabla Y_{lm}(\Omega), \tag{A.3b}$$

$$\mathbf{\Phi}_{lm}(\Omega) = N_l r \nabla Y_{lm}(\Omega) \times \mathbf{e}_r, \tag{A.3c}$$

where $N_l = 1/\sqrt{l(l+1)}$ is a normalization constant, $Y_{l,m}(\Omega)$ are the scalar spherical harmonics of order (l, m), and $\Omega \equiv (\theta, \varphi)$ represents the standard angular coordinates

(i.e., polar and azimuthal angles, respectively). Taking into account that the VSH form an orthogonal and complete set of basis vectors, any source-free electric (or magnetic) field can be expanded in terms of the VSWFs as follows:

$$\mathbf{E}(\mathbf{r}) = \sum_{l=1}^{\infty} \sum_{m=-l}^{l} \alpha_{lm} \mathbf{E}_{lm}^{\mathrm{TE}}(\mathbf{r}) + \beta_{lm} \mathbf{E}_{lm}^{\mathrm{TM}}(\mathbf{r}), \tag{A.4}$$

where α_{lm} and β_{lm} are the multipole expansion coefficients (also called beam-shape coefficients), and $\mathbf{E}_{lm}^{\mathrm{TE}} \equiv E_l^{(\Phi)} \mathbf{\Phi}_{lm}$ and $\mathbf{E}_{lm}^{\mathrm{TM}} \equiv E_l^{(\Theta)} \mathbf{\Theta}_{lm} + E_l^{(\mathrm{R})} \mathbf{R}_{lm}$ are, respectively, the mutually perpendicular *transverse electric* (TE) and *transverse magnetic* (TM) multipole fields of (l, m) order [43]. It is important to note that, in each of both subsets of solutions, each element verifies individually the vector Helmholtz equation (A.2). Furthermore, the radial dependence of each VSWF is incorporated into the $E_l^{(\cdot)}$ functional coefficients and appears separately from the angular coordinates, thereby allowing an independent treatment. To determine their specific form we should substitute this last expression (A.4) into the vector Helmholtz equation (A.2). In this manner, it can be demonstrated that the radial distribution is given in terms of the solutions of the spherical Bessel differential equation, which explicitly reads as follows [36,37]:

$$E_l^{(\mathrm{R})}(r) = \frac{f_l(kr)}{N_l kr}, \tag{A.5a}$$

$$E_l^{(\Theta)}(r) = \frac{[kr f_l(kr)]'}{kr}, \tag{A.5b}$$

$$E_l^{(\Phi)}(r) = f_l(kr), \tag{A.5c}$$

where $f_l(kr) \equiv \{j_l(kr), y_l(kr)\}$ are the l-dependent Bessel-like functions, and the prime denotes differentiation with respect to the dimensionless variable kr. Notice that since there are two independent solutions [$j_l(kr)$ and $y_l(kr)$, being the spherical Bessel functions of the first and second kinds, respectively], any linear combination will also be a proper solution. This provides the physical meaning for the radial functions depending on the specific situation. Indeed, if we consider a time-harmonic dependence of the form $e^{-i\omega t}$, to describe propagating spherical waves (purely outgoing or incoming) we will use the spherical Hankel functions $h_l^{(\pm)}(kr) = j_l(kr) \pm i y_l(kr)$. On the other hand, singularity-free spherical Bessel functions $j_l(kr)$ are appropriate functions for representing standing or regular waves.

A.III Optical Spin-Orbit Interaction

A. Intrinsic evolution of the SoP

Unlike the aforementioned plane-wave scheme, where the SoP of each field was conserved over the whole space, it can be readily observed that the SoP of the multipole fields is spatially inhomogeneous. This fact is precisely the first hint into the emergence of intrinsic SOI at the nanoscale, even in homogeneous media. We illustrate this idea in Fig. A.1 by means of the amplitude ratio and the phase-delay profiles between the

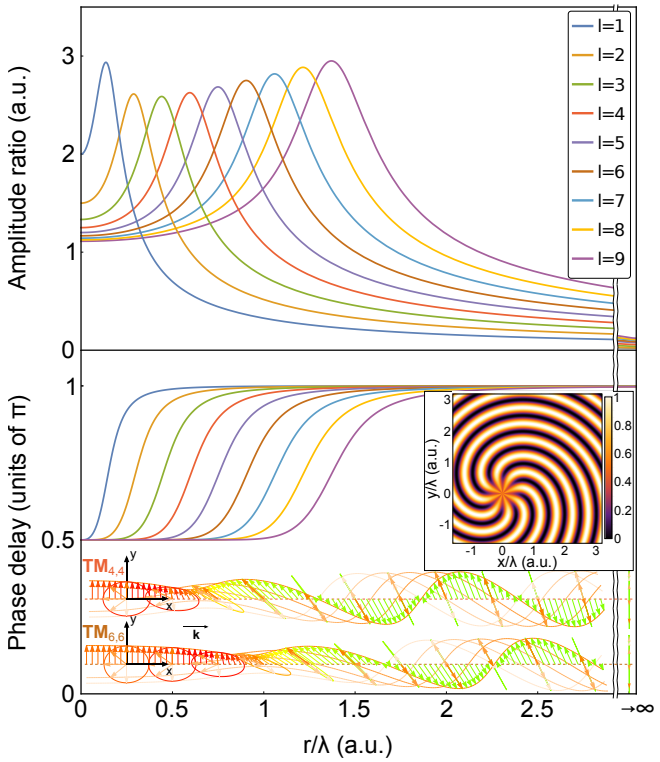

Figure A.1: Amplitude ratio (upper panel) and phase delay (lower panel) between the longitudinal and transverse components for different propagating TM multipole fields of (l, l) order with $l \in [1, 9]$, over the xy plane. The inset shows the locally normalized instantaneous intensity distribution of the $\mathbf{E}^{\mathrm{TM}}_{4,4}$ mode, whose spatially varying polarization ellipse along the x axis is schematically depicted at the bottom. For comparison, the evolution of the SoP for the $\mathbf{E}^{\mathrm{TM}}_{6,6}$ mode is also plotted. The color coding used in the evolution of the ellipses illustrates the transition from the near- to the far-field zone according to the scale represented in Fig. A.3, with the corresponding values for the azimuthal mode order l.

longitudinal ($\propto \mathbf{R}_{lm}$) and transverse ($\propto \mathbf{\Theta}_{lm}$) components of different propagating TM modes of (l, l) order over the xy plane. By considering the electric field contribution, it should be noted that TE modes are purely transverse, and therefore, the SoP manifests essentially a plane-like behavior, except for the attenuation factor $1/kr$ ensuring the energy conservation. Instead, TM modes enclose generally the joint action of the longitudinal field component (with a possible transverse SAM), together with the transverse one, owning the main features of SOI (see more details below). The upper panel of Fig. A.1 shows that, in the near-field zone $|\mathbf{E}^{\mathrm{TM(R)}}_{lm}|/|\mathbf{E}^{\mathrm{TM(\Theta)}}_{lm}| > 1$, namely, the dominant contribution for these individual (l, l) modes is due to the longitudinal component. This crucial remark, according to which the transverse field component is screened by the longitudinal one, agrees with the already predicted difficulty into the experimental observation of optical SOI [24,25]. On the other hand, the phase delay curves reveal the presence of a relative phase between both components, causing an intricate evolution of the polarization ellipse along the trajectory. Remarkably, the most significant variation takes place in the near-field region, i.e., where

the relative phase changes drastically from $\pi/2$ to π, and coincides with the range for which the amplitude ratio is maximum. As expected, in the far-field limit, the relative phase becomes a constant value and the amplitude ratio goes to zero, thus forcing the polarization plane to keep it purely orthogonal to the propagation direction. Still, an additional intriguing property is the presence of a minimum in the envelope curve of the amplitude ratio that occurs only for the $\mathbf{E}_{3,3}^{\mathrm{TM}}$ mode. Indeed, in Fig. A.1 we can see that for each (l, m) order there is an absolute maximum value in the amplitude ratio. Surprisingly, the trend in their magnitudes with respect to the azimuthal mode order l is not trivial, showing a minimum for $l = 3$. Therefore, according to the above arguments, this could enable to set a suitable multipole field distribution to facilitate the observation of SOI-based effects [44]. Finally, it should be noted that the regions which we refer to as the near- and far-field zone are ultimately determined by the azimuthal index l (also called topological charge), which is in turn tied to the intrinsic OAM of the corresponding mode [10]. As it will be shown below, we can find a more accurate definition for these regions via the spin-orbit factorizability condition, thus endowing it with a more fundamental sense and removing the arbitrariness related to the dependence on the distance from the source [36].

B. Factorizability condition and SOI term

In the following, neglecting the angular distribution, we will show how amplitude (leading to the SoP's modulation) and phase are intrinsically coupled together in the near-field region of propagating spherical waves. To elucidate this effect we start by writing the spherical Bessel functions from the recursive Rayleigh's formulas

$$j_l(kr) = (-kr)^l \left[\frac{1}{kr}\frac{d}{dkr}\right]^l \left(\frac{\sin kr}{kr}\right) = \frac{1}{kr}\left[P_l(kr)\cos kr + Q_l(kr)\sin kr\right], \tag{A.6}$$

$$y_l(kr) = -(-kr)^l \left[\frac{1}{kr}\frac{d}{dkr}\right]^l \left(\frac{\cos kr}{kr}\right) = \frac{1}{kr}\left[P_l(kr)\sin kr - Q_l(kr)\cos kr\right], \tag{A.7}$$

where $P_l(kr)$ and $Q_l(kr)$ are real-valued polynomials of degree l-dependent. To simplify the analysis, we define the function $F_l(kr) \equiv P_l(kr) + iQ_l(kr) = R_l(kr)e^{i\phi_l(kr)}$, from which the spherical Hankel functions associated with the propagating waves are given by

$$h_l^{(+)}(kr) = \frac{R_l(kr)}{kr}\exp\left\{i[kr - \phi_l(kr)]\right\} = \left[h_l^{(-)}\right]^*, \tag{A.8}$$

where the asterisk denotes complex conjugation. From the latter expression we can observe that, despite the inhomogeneous spatial distribution stemming from the phase ϕ_l, the spherical Hankel function behaves locally as a plane wave, i.e., is expressible as a product of an amplitude multiplied by a phase factor. Hence, analogously to Eq. (A.1), we can say that the scalar function $h_l^{(\pm)}$ retains the spin-orbit factorizability (or separability) condition. This result applies both to the radial-dependent functional coefficients $E_l^{(\mathrm{R})}$ and $E_l^{(\Phi)}$. However, in Eq. (A.5b) one can readily see that $E_l^{(\Theta)}$ involves the first derivative with respect to kr, thus yielding the appearance of a relative phase. Indeed, since $F_l'(kr) = P_l'(kr) + iQ_l'(kr) = (R_l' + iR_l\phi_l')e^{i\phi_l} = \tilde{R}_l(kr)e^{i\delta_l(kr)}$, Eq. (A.5b) can be rewritten in the

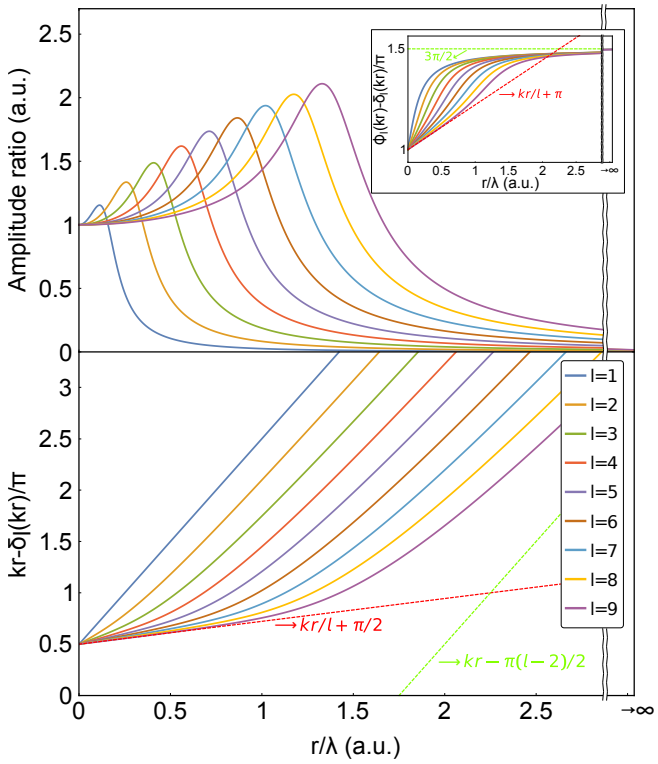

Figure A.2: Main features of the SOI term $\Delta_l^{(\pm)}$ for different values of l. Upper panel displays the amplitude ratio between the SOI term and the whole $E_l^{(\Theta)}$ function, i.e., $|\Delta_l|/|E_l^{(\Theta)}|$. Panel at the bottom shows the phase distribution of the SOI term. Dashed red (dark gray) and green (light gray) lines indicate the asymptotic behavior in the near- and far-field regions, respectively. The inset shows the relative phase $\phi_l(kr) - \delta_l(kr)$.

following form:

$$\frac{\left(krh_l^{(\pm)}(kr)\right)'}{kr} = \pm ih_l^{(\pm)}(kr) + \Delta_l^{(\pm)}(kr), \tag{A.9}$$

where we define

$$\Delta_l^{(\pm)}(kr) \equiv \frac{\tilde{R}_l(kr)}{kr} \exp\left\{\pm i[kr - \delta_l(kr)]\right\}. \tag{A.10}$$

This l-dependent term (hereafter referred to as the SOI term) entails the nonseparability of the spin-orbit degrees of freedom in multipole fields, and therefore provides a suitable benchmark for claiming the fundamental emergence of intrinsic SOI-based effects at the nanoscale (see Fig. A.2). In fact, by a straightforward calculation it can be found that the relative phase $\phi_l - \delta_l$ influences dynamically only in the near-field region, thereby precluding the amplitude-phase separability (see inset of Fig. A.2). Moreover, since the amplitude $\tilde{R}_l$ vanishes in the far-field limit, $\Delta_l^{(\pm)} \to 0$, and the factorizability condition is recovered, leading, as expected, to the separable plane-like wave behavior. As displayed in the upper panel of Fig. A.3, by gathering these features, the near and the far-field regions can be simply and accurately defined via the SOI term as $d\left[\phi_l - \delta_l\right]/dkr$. In this way, we can set the far-field as the region where the relative phase is constant with respect

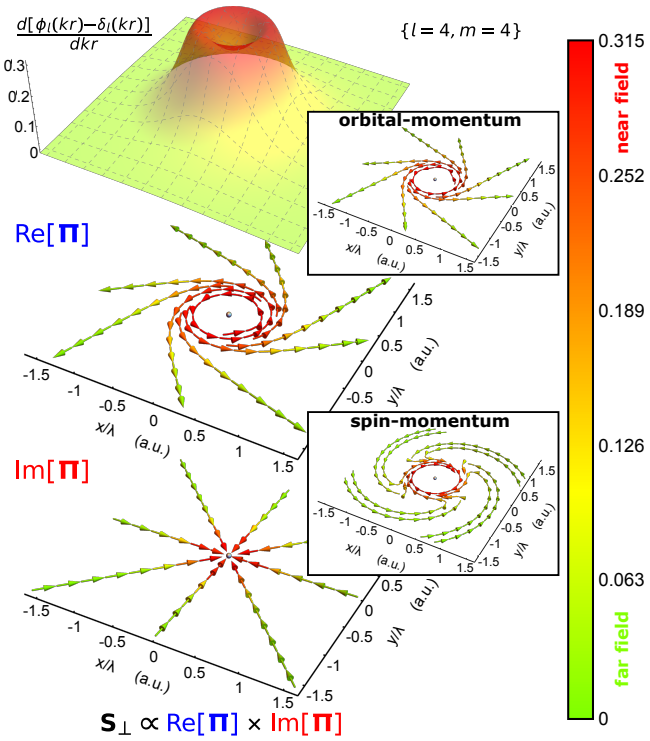

Figure A.3: Schematic representation of the near-field features for the $\mathbf{E}_{4,4}^{\mathrm{TM}}$ mode. From the SOI term, the near- and the far-field region can be characterized in terms of the relative phase as $d\left[\phi_l - \delta_l\right]/dkr$. In the near-field region the spatial distribution of the multipole field exhibits a complex shape. This manifests itself by means of a rich and strikingly interesting structure of the local dynamical properties such as the complex Poynting vector, the orbital and the spin momentum given in Eqs. (A.12)–(A.14) (cf. Ref. [15] for further details on these properties). On the other side, in the far-field limit the field distribution tends to be orthogonal to the direction of propagation.

to the dimensionless variable kr, namely, $[\phi_l - \delta_l]' \to 0$. On the other hand, according to our results, the near-field zone is strongly dependent on the azimuthal mode order l, and is characterized by $[\phi_l - \delta_l]' \to 1/l$. It is important to highlight that, irrespective of the spatial intensity distribution, the SOI term tends to zero as $kr \to \infty$, thus confirming the, up to now assumed, intrinsic subwavelength character of SOI. This would enable the enhancement of SOI-based effects directly by raising the light intensity, still preserving the region wherein they appear.

From the above discussion it is worth noticing that the spin-orbit separability condition resembles the genuine concept of nonlocal quantum entanglement [45]. In fact, this mathematical structure describing the nonseparability between different degrees of freedom in a single physical system (SoP and phase in this case) is often termed as classical entanglement or correlation [46]. These correlations have already allowed to find interesting experimental capabilities for the realization of encoding and processing of polarization-dependent classical information (see Ref. [47] and references therein).

C. Definition of the near-field region based on the factorizability condition

The distinction between the near- and the far-field region is often useful in theories of radiating systems because it provides a significant simplification in the analysis of the fields. Therefore, it would be convenient to have a precise condition to identify them accurately. In the particular case of an oscillating electric dipole

$$\mathbf{E}_{\text{dipole}} = \frac{k^2}{4\pi\varepsilon_0}\left[(\mathbf{e}_r \times \mathbf{p}) \times \mathbf{e}_r + (3\,(\mathbf{e}_r \cdot \mathbf{p})\,\mathbf{e}_r - \mathbf{p})\left(\frac{1}{k^2 r^2} - \frac{i}{kr}\right)\right]\frac{e^{ikr}}{r}, \tag{A.11}$$

the near- and the far-field terms are those proportional to $1/r^3$ and $1/r$, respectively [36]. In addition, the term proportional to $1/r^2$ is associated with the so-called intermediate-field or induction zone. These regions are actually characterized by a reasonable but arbitrary dependence with respect to the distance from the source r, assuming it as a emitter whose characteristic dimension d is much smaller than the wavelength λ and the distance r. This arbitrariness is even more evident for higher-order multipoles. Nonetheless, it can be demonstrated that the transverse component of the near-field term of the electric dipole given in Eq. (A.11) is closely related to the SOI term of the corresponding multipole field. Besides giving a more accurate definition for the above regions in terms of the spin-orbit separability condition, our approach allows us to show that the term preventing the factorization solely influences in the near-field region. Therefore, this example provides a perfect test for demonstrating the agreement with the already existing theory, thus showing the universality of the optical SOI as a phenomenon occurring at the subwavelength scale. Furthermore, following Ref. [48], we can find a subtle relationship between the near-field distribution given in Eq. (A.11) and the cross-polarization of a propagating beam described within the paraxial approximation. This may be the reason why the occurrence of SOI has been mostly identified under these distinct approaches. Indeed, as we have already seen, in the near-field region, the electric dipole cannot be generally expressed in a factorized form, and then the polarization and the propagation are mutually influenced. This behavior is similar to that of a propagating beam in inhomogeneous media [5], and is the ultimate responsible for the appearance of SOI-based effects.

D. Local dynamical properties of multipole fields: Poynting vector, spin, and orbital momentum

Until now, our analysis has been mainly focused into the influence of the SOI term on the evolution of the SoP at the nanoscale. Still, according to the fundamental definition of the optical SOI, the propagation process must also be affected. Below we will address this remaining issue qualitatively by showing the behavior of the local momentum densities in the near-field zone.

It is well known that in the simplest case of homogeneous plane-like waves the electromagnetic propagation is dictated by the real part of the complex Poynting vector [36]

$$\mathbf{\Pi} = \mathbf{E}^* \times \mathbf{H}, \tag{A.12}$$

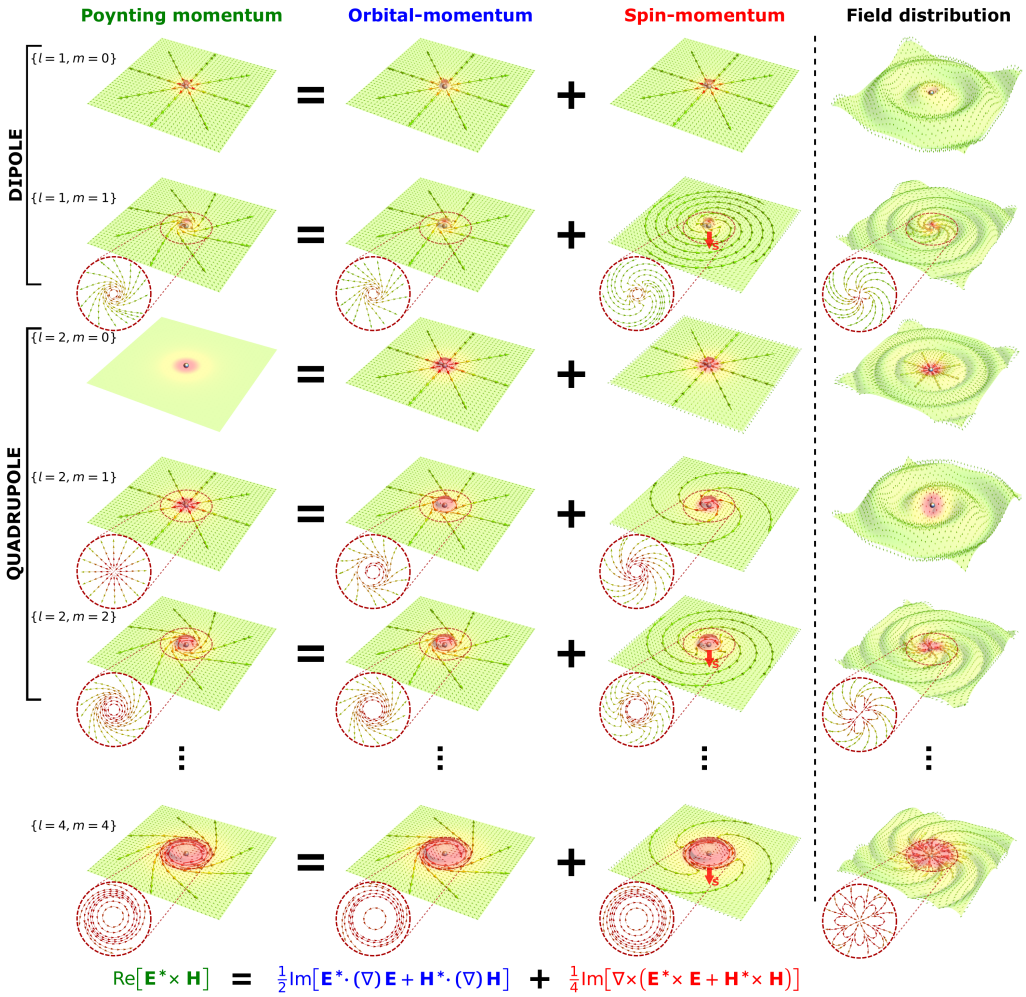

Figure A.4: Densities of the local dynamical properties for different multipole fields of (l, m) order over the xy plane. Columns 1 to 4 show the real part of the Poynting vector [Eq. (A.12)], the orbital and spin momentum [Eqs. (A.13) and (A.14)], and the locally normalized electric field distribution, respectively. The color coding used indicates the transition from the near- to the far-field zone, according to the scale represented in Fig. A.3, for the corresponding value of l. Owing to the complex-shaped spatial field structure of the modes in-plane polarized, the local dynamical properties present streamlines that are sharply twisted in the near-field region. In fact, despite their seemingly planar character, there arises a transverse SAM, which is, in turn, responsible for the occurrence of an abrupt switching on the handedness of the spin-momentum near the source. Insets show a zoom-in view of this feature, underpinned by the nonseparability of the spin-orbit degrees of freedom.

which points in the same direction as the wave vector $\mathbf{k}$. However, in structured optical fields, it is more convenient to decompose the latter quantity into the orbital (or canonical) and the spin contributions, $\mathrm{Re}[\mathbf{\Pi}] = \mathbf{P}^{\mathrm{orbit}} + \mathbf{P}^{\mathrm{spin}}$:

$$\mathbf{P}^{\mathrm{orbit}} = \mathrm{Im}[\mathbf{E}^* \cdot (\nabla)\,\mathbf{E} + \mathbf{H}^* \cdot (\nabla)\,\mathbf{H}]/2, \tag{A.13}$$

$$\mathbf{P}^{\mathrm{spin}} = \mathrm{Im}[\nabla \times (\mathbf{E}^* \times \mathbf{E}) + \nabla \times (\mathbf{H}^* \times \mathbf{H})]/4, \tag{A.14}$$

where we use the notation $\mathbf{A}\cdot(\nabla)\,\mathbf{B}=\sum_i A_i\nabla B_i$, and the proportionality factors are absorbed into the normalization of the fields. Taking into account this separation, it has been recognized that the energy transport, characterizing the wave propagation, is associated with the orbital contribution to the total momentum of light (i.e., with its local phase gradient). On the other hand, the solenoidal-like spin-momentum has often been considered as a virtual divergence-less current. A deeper understanding of the role played by these properties deserves further efforts beyond the scope of this work (cf. Refs. [15,49]). Despite that, by analyzing the influence of the SOI term given in Eq. (A.10), we can show a number of dynamical characteristics underlying the occurrence of intrinsic SOI at the nanoscale. Specifically, as is shown in Fig. A.4, the most complex spatial field distribution arises for the multipole fields of (l,l) order, polarized over the xy plane. For these modes, the streamlines describing the spin and orbital energy flows are sharply twisted in the near-field region, thus showing a vortex-like behavior (see also Fig. A.5). Importantly, as also shown in Fig. A.3, the spin-momentum abruptly switches its handedness. It can be demonstrated that this intriguing feature, together with the appearance of a transverse SAM, relies on the nonseparability of the spin-orbit degrees of freedom, thereby providing a clear signature of the emergence of intrinsic SOI. Notice that the existence of the spin momentum does not depend on the SAM, i.e., there are modes without SAM over the xy plane, still with a spin-momentum contribution. However, the change on the handedness of the spin-momentum only occurs for those modes with transverse SAM. In any case, the overall structure of the complex Poynting vector involves the joint action of the two types of momentum and is strongly dependent on the factorizability condition encompassed by the SOI term. Indeed, we can show its effect on the light propagation by plotting separately the radial and the azimuthal components for both the orbital- and spin-momentum densities (see Fig. A.5). Although, we only consider the $\mathbf{E}^{\mathrm{TM}}_{1,1}$ mode, corresponding to a circularly polarized oscillating electric dipole, the present discussion is extensible to any other higher-order multipole field. In Fig. A.5(a) we first consider the whole VSWF, i.e., including the SOI-term, the azimuthal angular dependence given by the phase $e^{il\varphi}$, and the plane-like part of the wave. For this case, owing to the presence of intrinsic-OAM, we can observe that all the contributions to the orbital-momentum are deviated from the radial direction. Therefore, to isolate the effect of the SOI term we should remove, by hand, the azimuthal dependence. By doing so [see Fig. A.5(b)], we find that the plane-like contribution to the orbital momentum is radially orientated, just as expected. Furthermore, we can observe a variety of anomalous effects such as the backward flow or the superluminal propagation. It has been established that these features are closely related to vortices and evanescent waves [50]. However, our approach is able to demonstrate that these effects are actually characteristics of intrinsic SOI.

As a final remark, it should be noted that spin-momentum locking has been demonstrated to be an inherent property of evanescent waves [32,33]. This behavior, regarded as a manifestation of the quantum spin Hall effect of light [34], is tied to the occurrence of SOI. Indeed, due to the transversality condition of the electromagnetic fields,

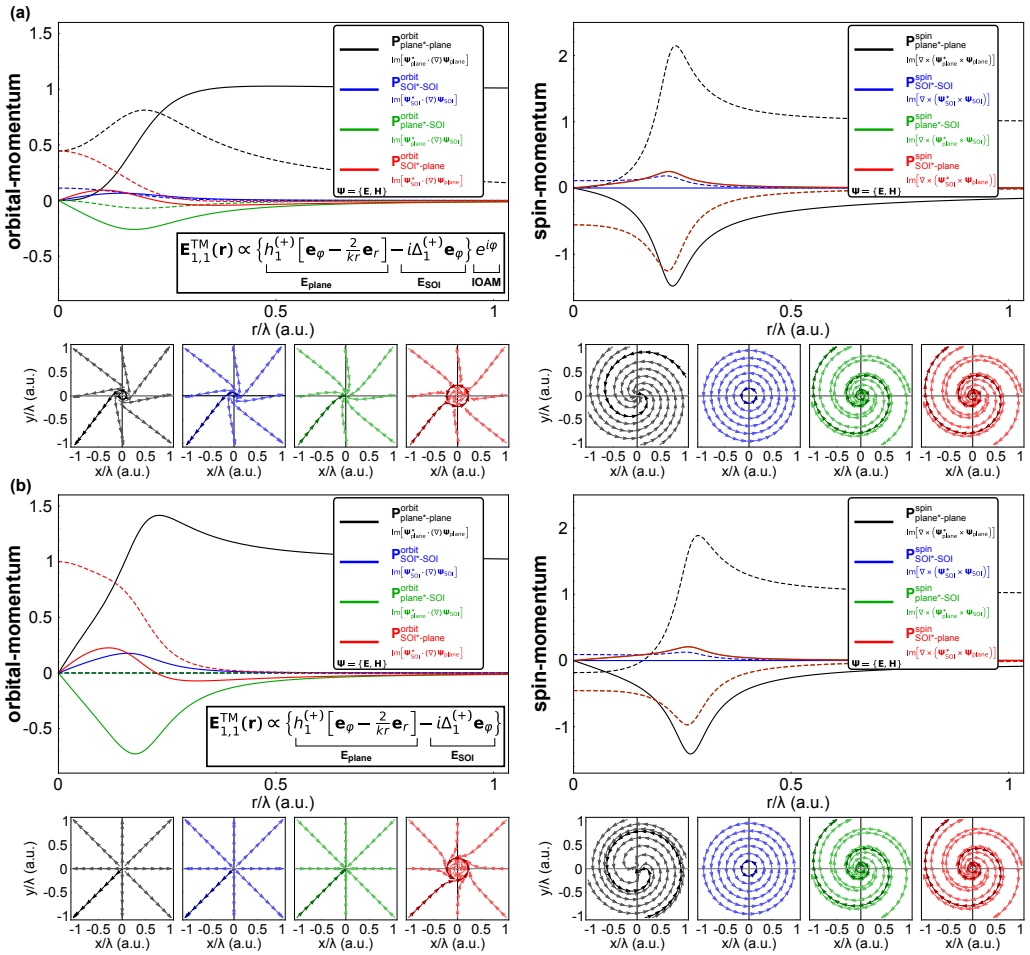

Figure A.5: Separate contributions to the local orbital- and spin-momentum densities for the $\mathbf{E}_{1,1}^{\mathrm{TM}}$ mode. Solid and dashed curves in the graphs show, respectively, the evolution of the radial and the azimuthal components normalized with respect to the corresponding local momentum density. Lower panels below the plots provides a better visual representation displaying the trajectories associated to the corresponding curves. In panel (a) the orbital and spin momentum are calculated by considering the whole VSWF, i.e., including both the SOI term and the azimuthal angular dependence given by the phase term $e^{il\varphi}$. In panel (b) the underlying influence of the SOI term is revealed by removing the azimuthal dependence. In this latter case, the plane-like contribution to the orbital-momentum density shows a purely radial behavior. The deviation from the radial direction is due to the nonseparability of the spin-orbit degrees of freedom.

$\nabla \cdot \mathbf{E} = \mathbf{k} \cdot \mathbf{E} = 0$, it was demonstrated that the transverse SAM and the wave vector are coupled to each other in such a way that $\mathbf{S}_{\perp}^{\mathrm{evan}} = \left(\mathrm{Re}[\mathbf{k}] \times \mathrm{Im}[\mathbf{k}]\right)/\mathrm{Re}[\mathbf{k}]^2$. Remarkably, we can find a similar relationship between the complex Poynting vector and the transverse SAM for propagating waves:

$$\mathbf{S}_{\perp}^{\mathrm{prop}} = \pm \frac{\mathrm{Re}\left[\mathbf{\Pi}_{(\mathrm{TE/TM})}\right] \times \mathrm{Im}\left[\mathbf{\Pi}_{(\mathrm{TE/TM})}\right]}{W_{(\mathrm{E/H})}}, \tag{A.15}$$

where $W_{\Psi} = |\mathbf{\Psi}^* \cdot \mathbf{\Psi}|$. It can be demonstrated that the validity of this result also relies

on the nonseparability of the spin-orbit degrees of freedom, and then, it can be seen as a consequence of intrinsic SOI of light as well.

A.IV Conclusion

In summary, building on the already existing theory around the intrinsic SOI of light, we put forward a suitable theoretical framework able to explain analytically its main features. The use of full-vector analysis involving spherical vector waves, highly appropriate for studying electromagnetic interaction at the nanoscale, allows us to obtain a factorizability condition for the electric (or magnetic) field that is only fulfilled in the far-field limit. In contrast, in the near-field region, both spin and orbit degrees of freedom get inherently coupled. It is important to remark that the nonseparability of the spin-orbit degrees of freedom, together with the transversality condition, are certainly the most important ingredients to unveil the mechanism leading to the classical emergence of the intrinsic SOI of light at the nanoscale. Even though the occurrence of SOI has already been theoretically reported in previous works (see, e.g., Refs. [5] and [27]), there the treatment was based on a perturbative analysis where the nonseparability between the spin-orbit degrees of freedom arose from higher-order terms stemming from the paraxial approximation. Importantly, in those demonstrations light was assumed to propagate as point-like particles, obeying Hamiltonian (or Lagrangian) dynamics and thereby neglecting its wave-like nature. Our finding, however, has the advantage of describing SOI of light from an analytical full-wave approach, providing a fundamental insight into the appearance of SOI-based effects in nano-optics. In spite of the simplicity of our treatment, it meets the overall prescriptions underlying the occurrence of optical SOI, showing that it naturally arises from the fundamental spin properties of Maxwell's equations and that necessarily appears at subwavelength distances. Furthermore, by using the spin-orbit factorizability condition, we can find a more accurate definition for the near-field region, thus removing the arbitrariness related to the dependence on the distance from the source. In view of the growing current interest in the optical SOI, we hope this analysis can be useful for the development of further optimum applications of SOI in classical [51] and quantum nanophotonic devices [52,53].

Acknowledgments

The authors are grateful to F. J. Rodríguez-Fortuño for valuable comments and discussions. This work was supported by fundings from Ministerio de Economía y Competitividad (MINECO) of Spain under Contract No. TEC2014-51902-C2-1-R.

References

[1] H. Mathur, *Thomas precession, spin-orbit interaction, and Berry's phase*, Phys. Rev. Lett. **67**, 3325 (1991).

[2] E. I. Rashba, *Spin-orbit coupling and spin transport*, Physica E **34**, 31 (2006).

[3] A. I. Akhiezer and V. B. Berestetskii, *Quantum Electrodynamics* (Interscience, New York, USA, 1965).

[4] S. A. Wolf, D. D. Awschalom, R. A. Buhrman, J. M. Daughton, S. von Molnár, M. L. Roukes, A. Y. Chtchelkanova, and D. M. Treger, *Spintronics: A spin-based electronics vision for the future*, Science **294**, 1488 (2001).

[5] V. S. Liberman and B. Y. Zel'dovich, *Spin-orbit interaction of a photon in an inhomogeneous medium*, Phys. Rev. A **46**, 5199 (1992).

[6] F. J. Belinfante, *On the current and the density of the electric charge, the energy, the linear momentum and the angular momentum of arbitrary fields*, Physica (Utrecht) **7**, 449 (1940).

[7] D. L. Andrews and M. Babiker, *The Angular Momentum of Light* (Cambridge University Press, Cambridge, England, 2013).

[8] I. Bialynicki-Birula and Z. Bialynicka-Birula, *Canonical separation of angular momentum of light into its orbital and spin parts*, J. Opt. **13**, 064014 (2011).

[9] J. H. Poynting, *The wave motion of a revolving shaft, and a suggestion as to the angular momentum in a beam of circularly polarised light*, Proc. R. Soc. London A **82**, 560 (1909).

[10] L. Allen, M. W. Beijersbergen, R. J. C. Spreeuw, and J. P. Woerdman, *Orbital angular momentum of light and the transformation of Laguerre-Gaussian laser modes*, Phys. Rev. A **45**, 8185 (1992).

[11] K. Y. Bliokh, A. Y. Bekshaev, and F. Nori, *Dual electromagnetism: helicity, spin, momentum and angular momentum*, New J. Phys. **15**, 033026 (2013).

[12] S. M. Barnett, L. Allen, R. P. Cameron, C. R. Gilson, M. J. Padgett, F. C. Speirits, and A. M. Yao, *On the natures of the spin and orbital parts of optical angular momentum*, J. Opt. **18**, 064004 (2016).

[13] A. Aiello, P. Banzer, M. Neugebauer, and G. Leuchs, *From transverse angular momentum to photonic wheels*, Nat. Photonics **9**, 789 (2015).

[14] K. Y. Bliokh and F. Nori, *Transverse spin of a surface polariton*, Phys. Rev. A **85**, 061801 (2012).

[15] A. Y. Bekshaev, K. Y. Bliokh, and F. Nori, *Transverse spin and momentum in two-wave interference*, Phys. Rev. X **5**, 011039 (2015).

[16] M. Nieto-Vesperinas, *Optical torque: Electromagnetic spin and orbital-angular-momentum conservation laws and their significance*, Phys. Rev. A **92**, 043843 (2015).

[17] S. Abdulkareem and N. Kundikova, *Joint effect of polarization and the propagation path of a light beam on its intrinsic structure*, Opt. Express **24**, 19157 (2016).

[18] T. A. Nieminen, A. B. Stilgoe, N. R. Heckenberg, and H. Rubinsztein-Dunlop, *Angular momentum of a strongly focused Gaussian beam*, J. Opt. A **10**, 115005 (2008).

[19] E. Leader and C. Lorcé, *The angular momentum controversy: What's it all about and does it matter?*, Phys. Rep. **541**, 163 (2014).

[20] D. F. Nelson, *Momentum, pseudomomentum, and wave momentum: Toward resolving the Minkowski-Abraham controversy*, Phys. Rev. A **44**, 3985 (1991).

[21] S. M. Barnett, *Resolution of the Abraham-Minkowski dilemma*, Phys. Rev. Lett. **104**, 070401 (2010).

[22] K. Y. Bliokh, A. Y. Bekshaev, and F. Nori, *Optical momentum and angular momentum in complex media: from the Abraham-Minkowski debate to unusual properties of surface plasmon-polaritons*, New J. Phys. **19**, 123014 (2017); *Optical momentum, spin, and angular momentum in dispersive media*, Phys. Rev. Lett. **119**, 073901 (2017).

[23] M. G. Silveirinha, *Reexamination of the Abraham-Minkowski dilemma*, Phys. Rev. A **96**, 033831 (2017).

[24] F. Cardano and L. Marrucci, *Spin-orbit photonics*, Nat. Photonics **9**, 776 (2015).

[25] K. Y. Bliokh, F. J. Rodríguez-Fortuño, F. Nori, and A. V. Zayats, *Spin-orbit interactions of light*, Nat. Photonics **9**, 796 (2015).

[26] K. Y. Bliokh, M. A. Alonso, E. A. Ostrovskaya, and A. Aiello, *Angular momenta and spin-orbit interaction of nonparaxial light in free space*, Phys. Rev. A **82**, 063825 (2010).

[27] K. Y. Bliokh, *Geometrodynamics of polarized light: Berry phase and spin Hall effect in a gradient-index medium*, J. Opt. A **11**, 094009 (2009).

[28] M. Onoda, S. Murakami, and N. Nagaosa, *Hall effect of light*, Phys. Rev. Lett. **93**, 083901 (2004).

[29] D. Haefner, S. Sukhov, and A. Dogariu, *Spin Hall effect of light in spherical geometry*, Phys. Rev. Lett. **102**, 123903 (2009).

[30] K. Y. Bliokh, A. Y. Bekshaev, and F. Nori, *Extraordinary momentum and spin in evanescent waves*, Nat. Commun. **5**, 3300 (2014).

[31] A. B. Khanikaev, S. H. Mousavi, W.-K. Tse, M. Kargarian, A. H. MacDonald, and G. Shvets, *Photonic topological insulators*, Nat. Mater. **12**, 233 (2013).

[32] T. Van Mechelen and Z. Jacob, *Universal spin-momentum locking of evanescent waves*, Optica **3**, 118 (2016).

[33] F. J. Rodríguez-Fortuño, G. Marino, P. Ginzburg, D. O'Connor, A. Martínez, G. A. Wurtz, and A. V. Zayats, *Near-field interference for the unidirectional excitation of electromagnetic guided modes*, Science **340**, 328 (2013).

[34] K. Y. Bliokh, D. Smirnova, and F. Nori, *Quantum spin Hall effect of light*, Science **348**, 1448 (2015).

[35] L. Novotny and B. Hecht, *Principles of Nano-Optics* (Cambridge University Press, Cambridge, England, 2012).

[36] J. D. Jackson, *Classical Electrodynamics* (Wiley, New York, USA, 1998).

[37] M. Born and E. Wolf, *Principles of Optics* (Pergamon, New York, USA, 2005).

[38] I. Fernandez-Corbaton, X. Zambrana-Puyalto, N. Bonod, and C. Rockstuhl, *Transverse multipolar light-matter couplings in evanescent waves*, Phys. Rev. A **94**, 053822 (2016).

[39] Rigorously speaking, a multipole expansion can be performed for electromagnetic fields emanating from an arbitrarily shaped source, regardless of its size [35]. Still, localized oscillating sources whose dimensions are comparable to or smaller than the wavelength of light are often assumed [36]. This is indeed the case for the lowest multipole orders, such as the electric or magnetic dipole fields, or even for the higher multipole orders as well. Furthermore, for simplicity, the electric dipole fields are sometimes treated as point-like sources.

[40] O. G. Rodríguez-Herrera, D. Lara, K. Y. Bliokh, E. A. Ostrovskaya, and C. Dainty, *Optical nanoprobing via spin-orbit interaction of light*, Phys. Rev. Lett. **104**, 253601 (2010).

[41] K. Y. Bliokh, E. A. Ostrovskaya, M. A. Alonso, O. G. Rodríguez-Herrera, D. Lara, and C. Dainty, *Spin-to-orbital angular momentum conversion in focusing, scattering, and imaging systems*, Opt. Express **19**, 26132 (2011).

[42] R. G. Barrera, G. A. Estévez, and J. Giraldo, *Vector spherical harmonics and their application to magnetostatics*, Eur. J. Phys. **6**, 287 (1985).

[43] Notice that the TE and TM multipole fields are also referred to as the *magnetic and electric multipole fields*, respectively (see, e.g., Ref. [36]). This terminology is meaningful since it emphasizes the nature of the source that originates the electromagnetic radiation. In addition, it also indicates which is the contribution that actually exhibits the SOI term discussed in the present work. In fact, from the free-space Maxwell's equations it is straightforward to show that $\mathbf{E}_{lm}^{\mathrm{TE/TM}} \equiv i\mathbf{H}_{lm}^{\mathrm{TM/TE}}$, thus demonstrating the dual symmetry [11,12] (or *electric-magnetic democracy* [M. V. Berry, J. Opt. A **11**, 094001 (2009)]).

[44] A. G. Curto, T. H. Taminiau, G. Volpe, M. P. Kreuzer, R. Quidant, and N. F. van Hulst, *Multipolar radiation of quantum emitters with nanowire optical antennas*, Nat. Commun. **4**, 1750 (2013).

[45] L. J. Pereira, A. Z. Khoury, and K. Dechoum, *Quantum and classical separability of spin-orbit laser modes*, Phys. Rev. A **90**, 053842 (2014).

[46] R. J. C. Spreeuw, *A classical analogy of entanglement*, Found. Phys. **28**, 361 (1998).

[47] A. Aiello, F. Töppel, C. Marquardt, E. Giacobino, and G. Leuchs, *Quantum-like nonseparable structures in optical beams*, New J. Phys. **17**, 043024 (2015).

[48] A. Aiello and M. Ornigotti, *Near field of an oscillating electric dipole and cross-polarization of a collimated beam of light: Two sides of the same coin*, Am. J. Phys. **82**, 860 (2014).

[49] A. Y. Bekshaev, K. Y. Bliokh, and M. Soskin, *Internal flows and energy circulation in light beams*, J. Opt. **13**, 053001 (2011).

[50] K. Y. Bliokh, A. Y. Bekshaev, A. G. Kofman, and F. Nori, *Photon trajectories, anomalous velocities and weak measurements: a classical interpretation*, New J. Phys. **15**, 073022 (2013).

[51] A. Espinosa-Soria, F. J. Rodríguez-Fortuño, A. Griol, and A. Martínez, *On-chip optimal Stokes nanopolarimetry based on spin-orbit interaction of light*, Nano Lett. **17**, 3139 (2017).

[52] B. le Feber, N. Rotenberg, and L. Kuipers, *Nanophotonic control of circular dipole emission*, Nat. Commun. **6**, 6695 (2015).

[53] I. Söllner, S. Mahmoodian, S. L. Hansen, L. Midolo, A. Javadi, G. Kiršanskė, T. Pregnolato, H. El-Ella, E. H. Lee, J. D. Song, S. Stobbe, and P. Lodahl, *Deterministic photon-emitter coupling in chiral photonic circuits*, Nat. Nanotechnol. **10**, 775 (2015).

Chapter 2

PAPER B

Near-Field Directionality Beyond the Dipole Approximation: Electric Quadrupole and Higher-Order Multipole Angular Spectra

---

Phys. Rev. Applied 12, 024065 (2019)

Near-Field Directionality Beyond the Dipole Approximation: Electric Quadrupole and Higher-Order Multipole Angular Spectra

J. Enrique Vázquez-Lozano,[1,2] Alejandro Martínez,[1] and Francisco J. Rodríguez-Fortuño[2]

[1]*Nanophotonics Technology Center, Universitat Politècnica de València, Camino de Vera s/n, 46022 Valencia, Spain*

[2]*Department of Physics, King's College London, Strand, London WC2R 2LS, United Kingdom*

Within the context of spin-related optical phenomena, near-field directionality is generally understood from the viewpoint of the quantum spin Hall effect of light, according to which the transverse spin of surface or guided modes is locked to the propagation direction. Most previous works have been focused on the spin properties of circularly polarized dipolar sources. However, in near-field optics, higher-order multipole sources (e.g., quadrupole, octupole, and so on) might become relevant, so a more in-depth formulation would be highly valuable. Building on the angular-spectrum representation, we provide a general, analytical, and ready-to-use treatment in order to address the near-field directionality of any multipole field, particularizing to the electric quadrupole case. Besides underpinning and upgrading the current framework on spin-dependent directionality, our results may open up interesting perspectives for engineering light-matter coupling at the nanoscale.

B.I Introduction

The current trend toward miniaturization and integration of photonic devices has spurred an unprecedented ability to exploit the spin of light in a multitude of nanophotonic applications based on the so-called spin-orbit interaction (SOI) [1,2]. Essentially, optical SOI comprises a broad class of effects involving the mutual influence between the state of polarization (spin) and the spatial propagation features (orbit) of evanescent as well as nontrivially structured optical fields [3], which naturally and necessarily emerges at the subwavelength scale [4]. In classical and quantum optics, some of the most important evidences of the occurrence of SOI comes from the spin-controlled unidirectional excitation of guided waves [5], which has been successfully demonstrated both theoretically and experimentally in a wide variety of photonic platforms and spectral ranges, including dielectric-based integrated optics [6–8], plasmonic systems [9], hyperbolic metamaterials [10], photonic crystals [11,12], microwave waveguides [13], and optical fibers [14,15]. Within this context, the relatively recent discovery of

the photonic counterpart of the quantum spin Hall effect [16] may be regarded as a major breakthrough in the unified understanding of spin-momentum locking and its incontrovertible relationship with the transverse spin associated with the evanescent waves supported by either surface or guided modes [17–19]. This general framework has provided an insightful explanation for the near-field directionality of electromagnetic (EM) guided modes by circularly polarized electric (and/or magnetic) dipoles [5,20]. Indeed, from the point of view of the local dynamical properties, spin-controlled unidirectional excitation can be simply understood as the coupling between the longitudinal spin components of the dipolar source with the transverse ones of the corresponding guided mode [21–23].

For a more accurate description of near-field coupling, a full-vector wave analysis becomes necessary [24], thereby taking into account both the relative amplitude and the phase between the electric and magnetic field contributions [25,26]. This leads to an approach that strongly resembles Fermi's golden rule, according to which the chiral (or directional) waveguide coupling efficiency is proportional to $|\mathbf{p}\cdot\mathbf{E}^{*}+\mathbf{m}\cdot\mu\mathbf{H}^{*}|^{2}$, i.e., it relies on the similarity between the electric (and/or magnetic) dipole moment, $\mathbf{p}$ (and/or $\mathbf{m}$), and the electric (and/or magnetic) field distribution, $\mathbf{E}$ (and/or $\mathbf{H}$), of the guided mode at the same location of the dipolar sources, where μ is the magnetic permeability of the medium [11,14,21–23]. Nonetheless, in structures exhibiting a translational symmetry along two directions of a given plane, this scheme for the mode coupling can be further simplified [25]. Indeed, in these scenarios, one may also employ an alternative and equivalent approach based on the asymmetric features of the near-field *angular-spectrum representation* together with considerations of structural symmetry and momentum conservation [5,9,27,28]. This formalism has the advantage of only accounting for the matching condition between the wave vector of the electric (and/or magnetic) dipole and that of the corresponding confined mode, thus gaining some physical intuition and simplifying the mathematics.

Regardless of the specific approach, the vast majority of previous works addressing unidirectional near-field scattering have only been focused on dipolar sources. This includes the Janus dipole [26,29], which is side-dependent topologically protected, as well as the directional Huygens' dipole [30]. Yet, higher-order multipole moments (e.g., quadrupole, octupole, and so on) turn out to be relevant at the nanoscale [24,31], and a more in-depth treatment for the spin-dependent directionality beyond the dipole approximation is required. Building upon the angular-spectrum representation, in this work we provide a complete and systematic formulation for the near-field directionality of EM multipole fields of arbitrary order. Special emphasis is placed on the particular case of the electric quadrupole, for which we explicitly show the potential benefits of increasing the available degrees of freedom as well as of broadening the spatial range over which the evanescent modes have a significant contribution [4,32]. Importantly, the end results are elegantly expressed in an easy-to-use form. Indeed, we also include an online tool that directly provides the angular spectra for arbitrary multipole sources [33]. In this way, they can be directly applied to the analytical design of nanoscale optical sources for the purpose of

engineering the directional scattering and coupling of EM fields to both confining structures and waveguiding systems [34–38].

B.II Angular Spectrum of Electric Quadrupole

The angular-spectrum representation, often referred to as the *generalized plane-wave expansion* [39], is a very familiar theoretical concept that allows us to obtain a mode representation of any EM field in terms of elementary plane waves, which can be either propagating or evanescent [24,40]. It has been found to be especially well suited for describing near- and far-field light-matter interaction of optical sources neighboring material structures exhibiting planar geometries, such as slabs, interfaces, or layered media [24,31,40]. Accordingly, this approach has been used extensively in a plethora of fundamental problems in classical optics (see, e.g., Refs. [41–43] and references therein), with special emphasis on the study of reflection and transmission of EM multipole fields by interfaces [44,45] and more recently for the analytical characterization of near-field directionality of dipolar sources [5,25,27,28].

Regarding our main goal toward a complete description of near-field directionality, the aforementioned angular-spectrum formalism is actually used to represent the EM radiation emanating from a localized optical source via the partial Fourier transform [46]:

$$\tilde{\mathbf{\Psi}}(\kappa_x,\kappa_y;z) \equiv \frac{k^2}{4\pi^2}\iint_{-\infty}^{+\infty} \mathbf{\Psi}(\mathbf{r}) e^{-ik(\kappa_x x+\kappa_y y)} dxdy, \tag{B.1}$$

where $\mathbf{\Psi}(\mathbf{r})$ is the complex amplitude of any scalar or vector field satisfying the *Helmholtz wave equation*, so that $\tilde{\mathbf{\Psi}}(\kappa_x,\kappa_y;z) = \tilde{\mathbf{\Psi}}_0(\kappa_x,\kappa_y;0)e^{\pm ik\kappa_z z}$. For the sake of completeness as well as for comparison purposes, we will first sketch the derivation of the angular spectrum (momentum representation) of an electric dipole [40,47]. To this end, it should be noted that, in general, any optical source (i.e., dipole, quadrupole, and so on) can be characterized by either the charge-current density distribution or, alternatively, through the associated vector potential [24]. Then, following Jackson's textbook on classical electrodynamics [48], for the particular case of the electric dipole (ED), the vector potential reads as follows:

$$\mathbf{A}^{\mathrm{ED}} = \frac{\mu}{4\pi}\left[\int_{-\infty}^{+\infty} \mathbf{J}(\mathbf{r}')d\mathbf{r}'\right]\frac{e^{ikr}}{r} = -\frac{i\mu\omega}{4\pi}\mathbf{p}\frac{e^{ikr}}{r}, \tag{B.2}$$

where $\mathbf{p} \equiv \int \mathbf{r}'\rho(\mathbf{r}')d\mathbf{r}'$ is the electric dipole moment, which is in turn tied to the electric current density $\mathbf{J}(\mathbf{r}) = -i\omega\delta^3(\mathbf{r}-\mathbf{r}')\mathbf{p}$, and $\rho(\mathbf{r})$ is the charge density. Note that throughout this work we will assume fields with a harmonic time dependence of the form $e^{-i\omega t}$, where ω is the angular frequency. Making use of *Weyl's identity* [40,49],

$$\frac{e^{ikr}}{r} = \frac{ik}{2\pi}\iint_{-\infty}^{+\infty}\frac{1}{\kappa_z}e^{ik(\kappa_x x+\kappa_y y\pm\kappa_z z)}d\kappa_x d\kappa_y, \tag{B.3}$$

it is straightforward to show that

$$\mathbf{A}^{\mathrm{ED}} = \frac{\mu c k^2}{8\pi^2 n}\mathbf{p}\iint_{-\infty}^{+\infty}\frac{1}{\kappa_z}e^{ik(\kappa_x x+\kappa_y y\pm\kappa_z z)}d\kappa_x d\kappa_y, \tag{B.4}$$

where $\mathbf{k}^{\pm} = k\,(\kappa_x, \kappa_y, \pm\kappa_z)$ is the wave vector and the $+$ and $-$ signs denote wave propagation through the half-spaces $z > 0$ and $z < 0$, respectively. Furthermore, solutions to the Helmholtz wave equation must obey $\mathbf{k}^{\pm} \cdot \mathbf{k}^{\pm} = k^2$, so it follows that

$$\kappa_z = \begin{cases} \sqrt{1 - \kappa_x^2 - \kappa_y^2}, & \text{if} \quad \kappa_x^2 + \kappa_y^2 \leq 1, \\ i\sqrt{\kappa_x^2 + \kappa_y^2 - 1}, & \text{if} \quad \kappa_x^2 + \kappa_y^2 > 1, \end{cases} \tag{B.5}$$

which correspond, respectively, to the propagating and evanescent modes in the partial Fourier (or momentum) space (κ_x, κ_y) [24,40]. Hence, according to the basic properties of the Fourier transform, from Eqs. (B.1) and (B.4), the spectral amplitude of the electric dipole vector potential is $\tilde{\mathbf{A}}^{\mathrm{ED}}(\kappa_x, \kappa_y; z) = \tilde{\mathbf{A}}_0^{\mathrm{ED}}(\kappa_x, \kappa_y; 0) e^{\pm ik\kappa_z z}$, where

$$\tilde{\mathbf{A}}_0^{\mathrm{ED}}(\kappa_x, \kappa_y; 0) = \frac{\mu c k^2}{8\pi^2 n} \frac{1}{\kappa_z} \mathbf{p}. \tag{B.6}$$

Following a similar but slightly trickier procedure, we may also obtain a closed expression for the angular-spectrum amplitude of the electric quadrupole. With this aim in mind, we start again from the vector potential of the electric quadrupole (EQ) as given in Ref. [48]:

$$\mathbf{A}^{\mathrm{EQ}} = \frac{\mu\omega k}{24\pi} \left(\frac{1}{ikr} - 1 \right) [\vec{\mathcal{Q}} \cdot \mathbf{e}_r] \frac{e^{ikr}}{r}, \tag{B.7}$$

where $\vec{\mathcal{Q}} \cdot \mathbf{e}_r$ is the term that conveys the "quadrupolar character" to the vector potential, in which $\mathbf{e}_r$ is the radial unit vector. The quadrupole moment $\vec{\mathcal{Q}}$ is a rank-2 tensor, usually represented by a 3×3 traceless, complex, and symmetric matrix, thus reducing the number of unknowns to five. In this case, the scalar contribution of Eq. (B.7) is no longer a proper solution of the Helmholtz wave equation. Moreover, since $\mathbf{e}_r$ depends on the direction of observation, we cannot take it out of the integral [50]. With these considerations in mind, the spectral amplitude of the electric quadrupole vector potential can be directly obtained by applying a partial Fourier transform as defined in Eq. (B.1) to the corresponding vector potential [Eq. (B.7)]. In this way, after some straightforward but lengthy manipulations that involve a change of variables to cylindrical coordinates (in both real and momentum space), the utilization of some integral identities leading to Bessel functions [51], and a judicious choice of integration by parts (see Sec. III in the Supplemental Material [50] for further details), we finally find that, in the limit as $z \to 0$,

$$\tilde{\mathbf{A}}_0^{\mathrm{EQ}}(\kappa_x, \kappa_y; 0) = \frac{\mu c k^2}{8\pi^2 n} \frac{1}{\kappa_z} \frac{(-i)\,[\vec{\mathcal{Q}} \cdot \mathbf{k}^{\pm}]}{6}. \tag{B.8}$$

When performing the integration, it is important to take into account the divergent behavior at the origin due to the presence of a singularity. This also happens for the electric dipole [40] and it may lead to misleading outcomes. Despite that, as pointed out in the Supplemental Material [50], we can formally obtain the angular spectrum of the electric quadrupole in each of the half-spaces $z > 0$ and $z < 0$ [Eq. (B.8)].

Equation (B.8), expressed analytically in a closed form, constitutes the first main result of this work. In this respect, it is worth pointing out that it has been deliberately

written in such a way that is easy to compare it with the angular-spectrum amplitude of the electric dipole. Indeed, one can directly obtain the spectral amplitude of the electric quadrupole [Eq. (B.8)] from that of the electric dipole [Eq. (B.6)] simply by substituting $\mathbf{p} \to (-i)\left[\vec{\mathcal{Q}} \cdot \mathbf{k}^{\pm}\right]/6$. Furthermore, these results are perfectly consistent with those presented in Refs. [35] and [36] for the multipole decomposition of scattered fields by arbitrary-shaped nanoparticles. According to this, the light-induced polarization vector can be Taylor expanded as follows:

$$\mathbf{P}(\mathbf{r}) \approx \left[\mathbf{p} - \frac{1}{6}\vec{\mathcal{Q}}\nabla + \frac{i}{\omega}\left(\nabla \times \mathbf{m}\right) + \ldots\right]\delta(\mathbf{r}). \tag{B.9}$$

It should be noted that $\mathbf{P}$ is related to the electric current density $\mathbf{J}$, which is in turn tied to the vector potential $\mathbf{A}$ [24,48]. Thus, by means of the substitution $\nabla \to i\mathbf{k}^{\pm}$, it can be readily seen that Eq. (B.9) coincides with Eqs. (B.6) and (B.8), as well as with the magnetic dipole term (see the Appendix in the Supplemental Material [50]):

$$\tilde{\mathbf{A}}_0 = \tilde{\mathbf{A}}_0^{\mathrm{ED}} + \tilde{\mathbf{A}}_0^{\mathrm{EQ}} + \tilde{\mathbf{A}}_0^{\mathrm{MD}} = \frac{\mu c k^2}{8\pi^2 n}\frac{1}{\kappa_z}\left[\mathbf{p} - \frac{i}{6}\left(\vec{\mathcal{Q}} \cdot \mathbf{k}^{\pm}\right) - \frac{1}{\omega}\left(\mathbf{k}^{\pm} \times \mathbf{m}\right)\right]. \tag{B.10}$$

In addition to providing a rapid verification of the above results, this correspondence between $\tilde{\mathbf{A}}_0$ and $\mathbf{P}$ permits us to infer the next higher-order terms through a simple identification of each term in the Taylor expansion of the Dirac delta function around the origin.

So far, we have been focused on the angular spectrum of localized sources (electric dipole and quadrupole) from a characterization based on the standard vector potentials. As we will see below, this perspective will enable us to elaborate a sound and systematic formulation for higher-order multipolar sources. At any rate, we are typically more concerned in dealing with the EM fields themselves [5,25,26]. In fact, this is a major advantage of the angular-spectrum approach, because cumbersome analysis involving the computation of gradients, divergences, curls, and Laplacians is reduced to simple algebra relying upon the product between the wave vector $\mathbf{k}^{\pm}$ and the spectral amplitudes $\tilde{\mathbf{A}}_0$. Specifically, from the relationship between the magnetic field and the vector potential, $\mathbf{B} = \mu\mathbf{H} = \nabla \times \mathbf{A}$, together with the curl-like Maxwell equation $\nabla \times \mathbf{H} = -i\omega\varepsilon\mathbf{E}$, in which ε is the permittivity of the medium, the complex field amplitudes in momentum space (κ_x, κ_y) can be nicely expressed in a compact form:

$$\tilde{\mathbf{E}}(\kappa_x, \kappa_y; 0) = \frac{ik^3}{8\pi^2\varepsilon}\frac{1}{\kappa_z}\left\{[\mathbf{e}_s \cdot \mathbf{p}_{\mathrm{eff}}]\mathbf{e}_s + [\mathbf{e}_p^{\pm} \cdot \mathbf{p}_{\mathrm{eff}}]\mathbf{e}_p^{\pm}\right\}, \tag{B.11}$$

$$\tilde{\mathbf{H}}(\kappa_x, \kappa_y; 0) = \frac{ik^3}{8\pi^2\varepsilon}\frac{1}{Z}\frac{1}{\kappa_z}\left\{[\mathbf{e}_p^{\pm} \cdot \mathbf{p}_{\mathrm{eff}}]\mathbf{e}_s - [\mathbf{e}_s \cdot \mathbf{p}_{\mathrm{eff}}]\mathbf{e}_p^{\pm}\right\}, \tag{B.12}$$

where $\mathbf{p}_{\mathrm{eff}}$ corresponds to the term in square brackets in Eq. (B.10) and $Z = \sqrt{\mu/\varepsilon}$ is the medium impedance. These expressions are readily obtained by introducing the polarization-vector basis, $\mathbf{e}_s = (-\kappa_y, \kappa_x, 0)/\kappa_R$ and $\mathbf{e}_p = \left(\pm\kappa_x\kappa_z, \pm\kappa_y\kappa_z, -\kappa_R^2\right)/\kappa_R$, where the subscripts indicate the s, or transverse electric (TE), and p, or transverse magnetic

(TM), polarizations, and $\kappa_R \equiv (\kappa_x^2 + \kappa_y^2)^{1/2}$. Note that in the lossless propagating case (i.e., when $\mathbf{k}^{\pm}$ is real), they correspond to the usual unit vectors in spherical coordinates, $\mathbf{e}_\varphi$ and $\mathbf{e}_\theta$, respectively [50]. Importantly, the same mathematical structure as given in Eqs. (B.11) and (B.12) can be applied to both the electric dipole and the quadrupole moments; we only have to replace $\mathbf{p}_{\text{eff}}$ by either $\mathbf{p}$ or $(-i)[\vec{\vec{Q}} \cdot \mathbf{k}^{\pm}]/6$, respectively. Likewise, the EM fields related to the magnetic dipole can be obtained either by substituting $\mathbf{p}_{\text{eff}}$ by $[\mathbf{m} \times \mathbf{k}^{\pm}]/\omega$ or directly from the symmetry of Maxwell's equations [52].

B.III Near-Field Directionality Beyond the Dipole

In translationally symmetric nanostructures, such as dielectric slab waveguides or metal-dielectric interfaces supporting surface plasmons, the near-field directional coupling of guided modes can be simply understood either from the matching condition of the local EM fields (underpinning the aforementioned Fermi's golden rule) [11,14,21–23] or, alternatively, from the angular-spectrum representation accounting for the phase-matching condition [25,26]. Whereas the former approach requires prior knowledge of the EM field structure of the guided modes, the angular-spectrum formalism only relies on the source by itself, together with structural symmetry aspects, thereby linked to conservation of momentum [5,9,27,28]. Hence, it can also be applied to nonplanar structures as long as they are translationally invariant along a given direction [25].

The results given in Eqs. (B.11) and (B.12) correspond to the angular spectrum of the source, which are equal to the angular spectrum of the total field in an unbounded homogeneous medium. In the presence of nearby structures with translational invariance in the x and y directions, the reflected and transmitted fields can be easily included. Indeed, their angular spectra are simply given by the angular spectrum of the source with a multiplicative transfer function [40], as shown in Fig. B.1. This allows us to transit from a homogeneous surrounding to the inhomogeneous case in a very simple manner. To do that, we first have to look at the angular spectrum of the total optical field, which consists of a superposition of propagating and evanescent waves. Then, we may consider each wave individually, propagating each one through the slabs, e.g., using the well-known *transfer matrix method*, to finally add them all up together. After that, the EM fields in real space can be straightforwardly retrieved just by using a numerical inverse fast Fourier transform on each plane [see Figs. B.1 and B.2]. For example, in the case of a single planar interface, the total field in the upper half-space is given by the sum $\tilde{\mathbf{E}}_{\text{total}}(\kappa_x, \kappa_y; z) = \tilde{\mathbf{E}}_{\text{s}}(\kappa_x, \kappa_y; z) + \tilde{\mathbf{E}}_{\text{r}}(\kappa_x, \kappa_y; z)$, where $\tilde{\mathbf{E}}_{\text{s}}$ is the angular spectrum of the field radiated by the source and $\tilde{\mathbf{E}}_{\text{r}}$ is that of the field reflected from the interface [25]. The latter can be directly determined from the source's field evaluated at the interface plane, weighted by the corresponding reflection coefficients $r_s(\kappa_x, \kappa_y)$ and $r_p(\kappa_x, \kappa_y)$, associated, respectively, with the s-polarized and p-polarized modes at the surface. The same can be done for the transmitted fields, but using the transmission coefficients $t_s(\kappa_x, \kappa_y)$ and $t_p(\kappa_x, \kappa_y)$. At any rate, the general form of the transfer function simply involves the reflection and transmission Fresnel coefficients, depending on the characteristics of the medium [24]. Therefore, the near-field directional

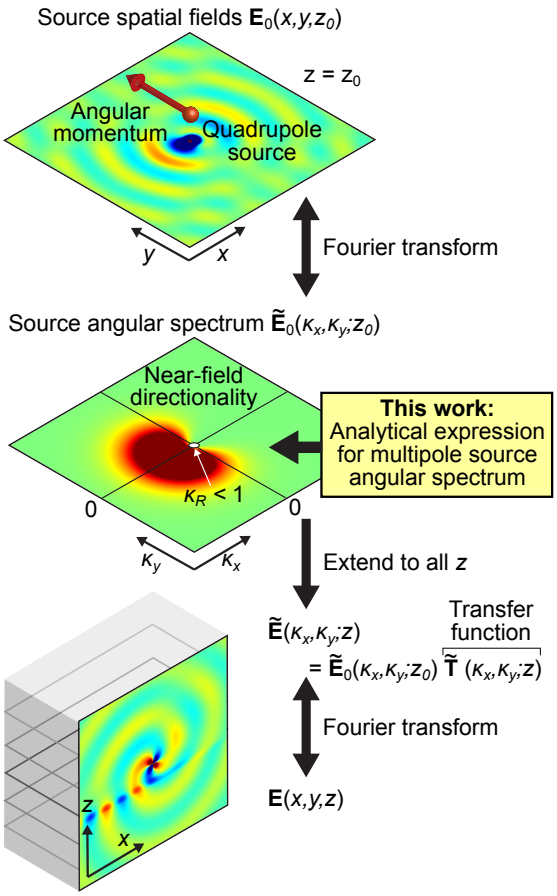

Figure B.1: A schematic description for visualizing the near-field directionality of arbitrary multipole sources. Starting from the space-dependent complex representation for the EM fields, over a given plane, e.g., $z = z_0$, the angular spectrum is directly obtained via the partial Fourier transform [Eq. (B.1)]. Within this representation, the analytical extension to the whole space with a dielectric slab is simply performed by using a transfer function, depending on the Fresnel coefficients.

coupling of the source relies solely on the asymmetry in the evanescent components of the angular spectrum of the optical sources. This fact has been shown for circularly polarized electric and magnetic dipoles [25], as well as for Huygens' and Janus sources [26,29]. The same idea can, of course, be exploited for the electric quadrupole case [see Fig. B.2(b)]. Indeed, as follows from Eqs. (B.10)–(B.12), the electric quadrupole with nonzero elements $\mathcal{Q}_{11} = -\mathcal{Q}_{33} = -1$ and $\mathcal{Q}_{13} = \mathcal{Q}_{31} = i$ shows a strongly asymmetrical p-polarized angular spectrum, with a high amplitude in the near-field region $\kappa_x < -1$ and a negligible amplitude for $\kappa_x > 1$, as shown in Fig. B.1, thus behaving very similarly to a circularly polarized electric dipole source. As a consequence, both sources show a clear unidirectionality when placed near a waveguide or slab [see Figs. B.2(a) and B.2(b)]. It is noteworthy that a quadrupole source has more degrees of freedom than a dipole, due to its tensorial nature, thereby allowing a more versatile engineering of its near field for potential

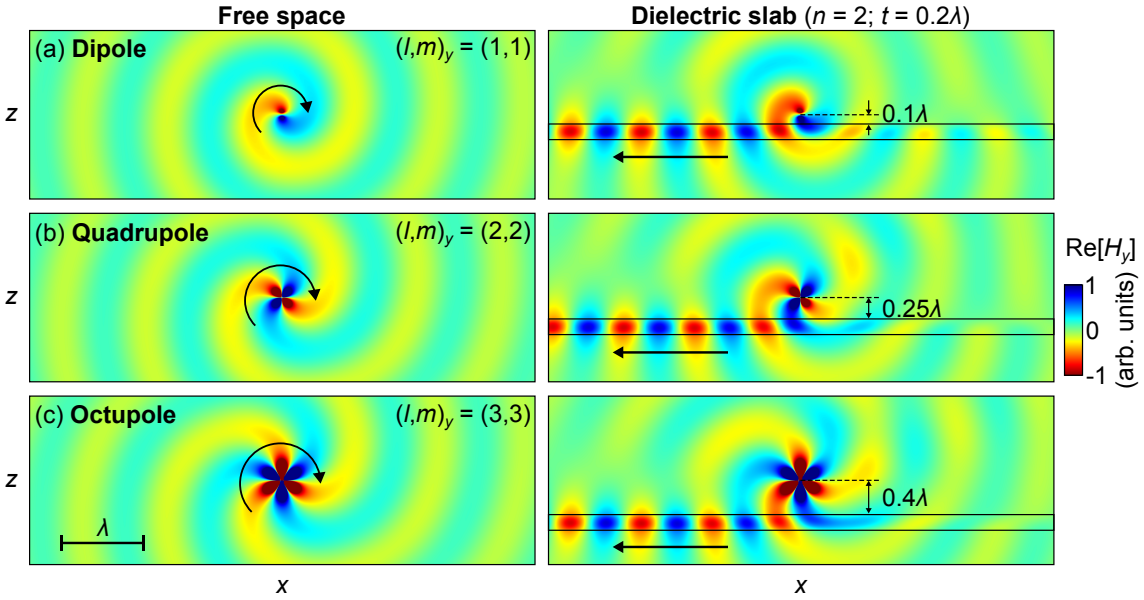

Figure B.2: The electromagnetic field calculation of electric multipolar sources in free space (left) and near a dielectric slab waveguide (right), showing the directional excitation of TM guided modes. The analytical angular spectra of multipolar sources is combined with a transfer matrix method to obtain the angular spectra at various z planes and the fields are calculated using a numerical inverse fast Fourier transform on each plane. (a) A circularly polarized electric dipole $\mathbf{p} = (1, 0, i)$ corresponding to electric multipole $(l, m)_y = (1, 1)$, where the subscript y denotes the angular-momentum axis oriented toward y. (b) A "circularly" polarized electric quadrupole with nonzero elements $\mathcal{Q}_{11} = -\mathcal{Q}_{33} = -1$ and $\mathcal{Q}_{13} = \mathcal{Q}_{31} = i$, corresponding to electric multipole $(l, m)_y = (2, 2)$. (c) A "circularly" polarized electric octupole corresponding to electric multipole $(l, m)_y = (3, 3)$. An animated version of the field evolution is available as a video in the Supplemental Material [50].

applications. Furthermore, the additional $\mathbf{k}^{\pm}$ dependence on the spectral amplitude of the electric quadrupole has advantageous implications that should be accounted for [4]. Specifically, as will be shown below, this leads up to a broader spatial range over which the evanescent modes have a significant contribution in comparison with the dipole case, hence increasing the range at which the quadrupole may couple to the guided mode [compare the coupling distances in Fig. B.2]. In addition, it also leads to a spatially broadband enhancement of the contrast ratio between guided modes coupled to opposite directions as we increase the order of the source [compare the amplitude ratios coupled to opposite directions in Fig. B.2].

B.IV Angular Spectrum of Higher-Order Electromagnetic Multipole Fields

In an experimentally realistic situation, optical sources are actually emitters (quantum dots or atoms) or scatterers (single or assemblies of nanoparticles). In both cases, the

multipole expansion of EM fields, expressed in terms of *vector spherical harmonics* [48], affords a suitable tool, because it provides a complete description of the fields emanating from or coupling to localized optical systems, regardless of the material composition, shape, or size [24]. This is crucial in nanophotonics, which typically deals with strongly confined optical fields that may lead to steep field gradients. Likewise, it should be highly valuable for near-field directional scattering when accounting for higher-order spectroscopic resonances [37,38].

In this case, instead of considering the standard vector potentials, in order to treat the electric and magnetic multipole fields on an equal footing we will use a formulation based on the Hertz potentials [53,54]. In this representation, the magnetic and electric fields are, respectively, related to the electriclike and magneticlike Hertz potentials [55], in the following manner:

$$\mathbf{H}^{(\mathrm{e})}_{l,m}(\mathbf{r}) = -i\omega[\nabla \times \mathbf{\Pi}^{(\mathrm{e})}_{l,m}], \qquad \mathbf{E}^{(\mathrm{m})}_{l,m}(\mathbf{r}) = i\mu_0\omega[\nabla \times \mathbf{\Pi}^{(\mathrm{m})}_{l,m}]. \tag{B.13}$$

After some manipulations taking into account the definitions of the EM multipole fields and fulfillment of the Helmholtz wave equation [48], one can find a closed expression for the Hertz vector potential of any electric and magnetic multipolar source of order (l, m) (see Sec. V in the Supplemental Material [50] for details). Finally, from the partial Fourier transform, it can be proven that the spectral amplitude of the Hertz potentials associated with the electriclike sources on the plane $z = 0$ reads as follows:

$$\tilde{\mathbf{\Pi}}^{(\mathrm{e})}_{l,m}(\kappa_x, \kappa_y; 0) = \frac{-k}{4\pi\omega}\frac{(-i)^m C_{l,m}}{\sqrt{l(l+1)}}\left[\tilde{\Pi}^{(\mathrm{e}),\mathrm{x}}_{l,m}, \tilde{\Pi}^{(\mathrm{e}),\mathrm{y}}_{l,m}, \tilde{\Pi}^{(\mathrm{e}),\mathrm{z}}_{l,m}\right], \tag{B.14}$$

where

$$\tilde{\Pi}^{(\mathrm{e}),\mathrm{x}}_{l,m} = i\left[(m-l)\tilde{\mathcal{K}}^{l,m}_{l,m+1}e^{i\phi} + (m+l)\tilde{\mathcal{K}}^{l,m}_{l,m-1}e^{-i\phi}\right]e^{im\phi}, \tag{B.15a}$$

$$\tilde{\Pi}^{(\mathrm{e}),\mathrm{y}}_{l,m} = \left[(m-l)\tilde{\mathcal{K}}^{l,m}_{l,m+1}e^{i\phi} - (m+l)\tilde{\mathcal{K}}^{l,m}_{l,m-1}e^{-i\phi}\right]e^{im\phi}, \tag{B.15b}$$

$$\tilde{\Pi}^{(\mathrm{e}),\mathrm{z}}_{l,m} = 2(l+m)\tilde{\mathcal{K}}^{l-1,m}_{l,m}e^{im\phi}. \tag{B.15c}$$

The same results also hold for magneticlike sources, just by noting that $\tilde{\mathbf{\Pi}}^{(\mathrm{m})}_{l,m}(\kappa_x, \kappa_y; 0) = -c\sqrt{\mu_r/\varepsilon_r}\tilde{\mathbf{\Pi}}^{(\mathrm{e})}_{l,m}(\kappa_x, \kappa_y; 0)$ [52]. These expressions depend on the function $\mathcal{K}^{l',m'}_{l,m}$ in the limit as $z \to 0$ [56]:

$$\tilde{\mathcal{K}}^{l',m'}_{l,m}(k, \kappa_R) \equiv \lim_{z\to 0} P^{m'}_{l'}(z)\mathcal{I}_{l,m}(k, \kappa_R; z), \tag{B.16}$$

where $P^{m'}_{l'}$ are the associated Legendre polynomials of degree l' and order m', and

$$\mathcal{I}_{l,m}(k, \kappa_R; 0) = \frac{\sqrt{\pi}\kappa_R^m}{k^2}\left[\frac{\Gamma\left[\frac{1+l+m}{2}\right]}{\Gamma\left[\frac{l-m}{2}\right]} + i(-1)^l\frac{\Gamma\left[\frac{2-l+m}{2}\right]}{\Gamma\left[\frac{1-l-m}{2}\right]}\right]\frac{{}_2F_1\left[\frac{1}{2}(2-l+m), \frac{1}{2}(1+l+m), 1+m; \kappa_R^2\right]}{\Gamma[1+m]}, \tag{B.17}$$

in which ${}_2F_1(a, b, c; z)$ is the Gaussian hypergeometric function [57]. Equation (B.17) is the second main result of this work; it can be regarded as a generalization of Weyl's identity, in the sense that it enables the calculation of the angular-spectrum representation

of any EM multipole field. It should be noted that a similar result has previously been obtained [58,59], but using a very different notation. Importantly, as shown in Sec. VI of the Supplemental Material [50], apart from the prefactors, these analytical and closed forms are in perfect agreement with the particular cases of the electric dipole ($l = 1$) [Eq. (B.6)] and quadrupole ($l = 2$) [Eq. (B.8)], thereby confirming their validity, at least up to the electric quadrupole case.

Practical applications usually require the angular spectra of the EM fields themselves instead of that of the vector potential. As pointed out above when addressing the simplest cases of dipolar and quadrupolar sources, this can be straightforwardly done by means of the substitution $\nabla \rightarrow i\mathbf{k}^{\pm}$. Then, the EM field angular spectra (expressed in the partial Fourier space) are directly obtained from Eq. (B.13) (given in real-space representation) in such a way that $\tilde{\mathbf{H}}^{(\mathrm{e})}_{l,m}(\kappa_x, \kappa_y; 0) = \omega[\mathbf{k}^{\pm} \times \tilde{\mathbf{\Pi}}^{(\mathrm{e})}_{l,m}]$ and $\tilde{\mathbf{E}}^{(\mathrm{m})}_{l,m}(\kappa_x, \kappa_y; 0) = \mu_0\omega[\tilde{\mathbf{\Pi}}^{(\mathrm{m})}_{l,m} \times \mathbf{k}^{\pm}]$, where $\kappa_x = \kappa_R \cos(\phi)$ and $\kappa_y = \kappa_R \sin(\phi)$, as long as we consider the corresponding spectral amplitude of the Hertz potentials explicitly given in Eqs. (B.14)–(B.17). Furthermore, our online tool performs all the necessary calculations and substitutions, providing the final EM field angular spectra as a function of κ_x and κ_y [33].

The circularly polarized dipole and quadrupole shown in Figs. B.2(a) and B.2(b) may be expressed in multipole form as $(l, m)_y = (1, 1)$ and $(2, 2)$, respectively. The y subindex denotes the angular-momentum axis of the source; therefore, they correspond to dipolar and quadrupolar sources with the highest angular momentum along y, i.e., parallel to the interface. This sets up a circular phase gradient that sweeps the surface of the waveguide along $-x$, causing unidirectional excitation. In Fig. B.2(c), we confirm the trend by considering the $(l, m)_y = (3, 3)$ octupole source. As previously anticipated, a main advantage of higher-order sources is their longer spatial range for near-field directional coupling as multipoles of increasing order are successively considered [see Fig. B.2]. This statement relies on the assumption that the same amplitude (or power fraction) is coupled to the guided mode at increasing distances for higher-order multipoles from the waveguiding structure. Note that to make this a fair comparison, we impose an identical far-field radiation amplitude for every multipolar source. This is more precisely depicted in Fig. B.3, where we show the electric field amplitude angular spectra of different multipolar sources of order $(l, m = l)$. In this regard, it is worth noting that the fraction of power generated by the source that is coupled to a specific mode is proportional to the angular spectrum of the source at the transverse wave vector of the mode. This is valid in all directions of the x-y plane, so for simplicity in the graphical depiction and without any loss of generality, we assume that $\kappa_y = 0$, thus representing the amplitude angular spectra along κ_x to show the directionality in the left or right direction [see Figs. B.2 and B.3]. So as to perform a proper comparison among all the multipolar orders, the spectral amplitudes have all been scaled in such a way that the far-field radiation power is exactly the same for all multipoles in all directions. This is clearly shown in Fig. B.3, where all of the multipoles have been normalized to have exactly the same spectral amplitude for all far-field propagating modes (i.e., within the range $|\kappa_x| < 1$). Taking the above considerations into account, it can

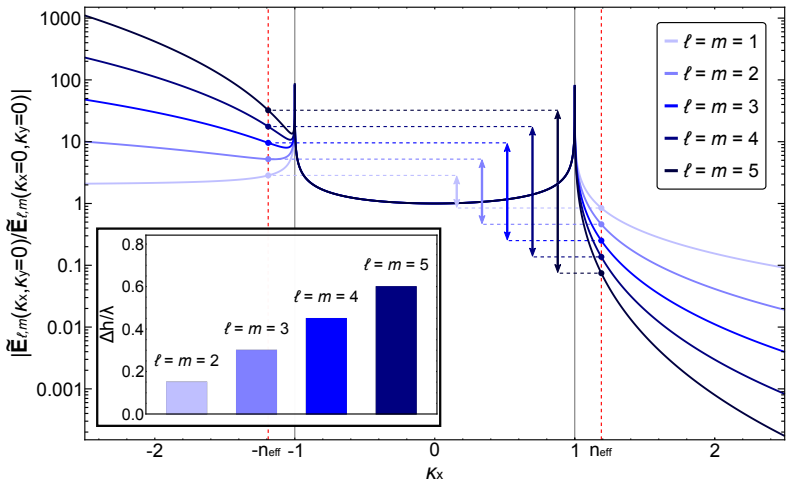

Figure B.3: The electric field amplitude angular spectra of electriclike multipolar sources of order $(l, m = l)_y$ as a function of the spatial frequency κ_x ($\kappa_y = 0$). Note that all the spectra are normalized to have identical far-field radiation. The contrast ratio between guided modes coupled to opposite directions, $\kappa_x = \mp n_{\text{eff}}$, is indicated for each of the multipolar orders, thus showing a spatially broadband enhancement as higher orders are considered. The inset displays the additional spatial range of higher-order multipoles, with respect to that of the electric dipole, to achieve the same coupling to the guided mode for $n_{\text{eff}} = 1.19$, corresponding to the effective index of the slab shown in Fig. B.2.

be demonstrated that the spatial range of higher-order multipoles with respect to that of the electric dipole, to obtain the same near-field coupling amplitude for the same far-field radiation, is given by the following:

$$\frac{\Delta h_{l,m}}{\lambda} = \frac{1}{2\pi\sqrt{\kappa_x^2 - 1}} \ln\left[\frac{|\tilde{\mathbf{E}}_{l,m=l}(\kappa_x, 0; 0)|}{|\tilde{\mathbf{E}}_{1,1}(\kappa_x, 0; 0)|}\right], \tag{B.18}$$

where $\Delta h_{l,m} = h_{l,m} - h_{1,1}$ and κ_x corresponds to the propagation constant of the guided mode. Hence, this analytical result informs us about the amount of additional distance at which an arbitrary multipole can be placed to achieve the same coupling to the guided mode as the dipolar source would achieve. Explicit values are represented in the inset of Fig. B.3, where, for the sake of simplicity in the representation, we have restricted it to sources of order $(l, m = l)$, but, of course, it can be applied to any other m. An alternative interpretation for the higher amplitude of the evanescent components is that, for a fixed distance, greater power is coupled to the guided mode from higher-order multipoles, while the radiated power stays the same. This implies an increased coupling efficiency. From Fig. B.3, it is also straightforward to determine the contrast ratio between light coupled in two opposite directions just by comparing the angular spectra at opposite κ_x. It is worth remarking on the stark enhancement as higher orders are considered. Importantly, unlike dipolar sources, which can be fine tuned to achieve a perfect contrast ratio for a specific mode [25,26,29], in this case the enhancement exhibits a spatially broadband behavior, thus increasing its efficiency and the effectiveness for potential applications.

From a theoretical approach, these features (i.e., the longer range and higher coupling efficiency for near-field directional coupling as well as the enhanced contrast ratio) are reflected in the analytical angular spectra as multiplicative "κ_R" terms, which enhance the amplitude of the higher frequencies, thus broadening the spectrum. As a final remark, note that our analytical Eqs. (B.14)–(B.17) assume $(l,m)_z$ sources, the angular momentum of which is around the z axis such that they do not show near-field directionality in the x-y plane. Yet, the same expression can be used to compute the angular spectra of the $(l,m)_y$ sources used in Figs. B.2 and B.3, by properly rotating the κ_x, κ_y, and κ_z axes; our online spectrum calculator allows this selection [33].

B.V Concluding Remarks

Taking advantage of the angular-spectrum representation, we present a general, systematic, and ready-to-use formulation for the near-field directionality beyond the dipole approximation. Additionally, for the readers' convenience, we include an online tool to retrieve the angular spectra of arbitrary multipoles [33]. Specifically, we derive an analytical and closed expression for the angular spectrum of EM multipole fields of arbitrary order. We see that successively higher-order multipole fields provide several advantages: a longer spatial range for near-field directional coupling, a higher coupling efficiency, an enhanced contrast ratio of the directionality over the whole angular spectrum (i.e., showing a spatially broadband behavior), and an increased number of degrees of freedom, giving us a greater design flexibility. This could be useful, for instance, to promote the spin-controlled (coherent) multidirectional excitation of guided waves on a large number of nearby waveguides, simultaneously, using a single multipolar source. Hence, besides underpinning and upgrading the already known framework on near-field directionality [5–14,60,61], the full consideration of higher-order multipole moments may unveil additional spin-dependent directional features in, for instance, the context of nonlinear nanophotonics [62].

Near-field directionality was, until recently, based on electric dipoles only. The addition of the magnetic dipole to the picture increases the richness and variety of the achievable physical effects, such as the Janus source, which combines electric and magnetic dipoles. Hence, by extending the study of near-field directionality even further, to consider higher-order multipoles of arbitrary order and their combinations, we expect novel interesting physics to arise in optical nanorouting, quantum optics, photonic logical circuits, optical forces, and many other fields of application.

Acknowledgments

This work was supported by ERC Starting Grant No. ERC-2016-STG-714151-PSINFONI. J.E.V.-L. is grateful for the kind hospitality of the Department of Physics, King's College London, where this research was partially

carried out. A.M. acknowledges the support of the Spanish Ministry of Science, Innovation and Universities under Grant No. PRX18/00126.

References

[1] K. Y. Bliokh, F. J. Rodríguez-Fortuño, F. Nori, and A. V. Zayats, *Spin-orbit interactions of light*, Nat. Photonics **9**, 796 (2015).

[2] F. Cardano and L. Marrucci, *Spin-orbit photonics*, Nat. Photonics **9**, 776 (2015).

[3] V. S. Liberman and B. Y. Zel'dovich, *Spin-orbit interaction of a photon in an inhomogeneous medium*, Phys. Rev. A **46**, 5199 (1992).

[4] J. E. Vázquez-Lozano and A. Martínez, *Classical emergence of intrinsic spin-orbit interaction of light at the nanoscale*, Phys. Rev. A **97**, 033804 (2018).

[5] F. J. Rodríguez-Fortuño, G. Marino, P. Ginzburg, D. O'Connor, A. Martínez, G. A. Wurtz, and A. V. Zayats, *Near-field interference for the unidirectional excitation of electromagnetic guided modes*, Science **340**, 328 (2013).

[6] F. J. Rodríguez-Fortuño, D. Puerto, A. Griol, L. Bellieres, J. Martí, and A. Martínez, *Universal method for the synthesis of arbitrary polarization states radiated by a nanoantenna*, Laser Photonics Rev. **8**, L27 (2014).

[7] F. J. Rodríguez-Fortuño, I. Barber-Sanz, D. Puerto, A. Griol, and A. Martínez, *Resolving light handedness with an on-chip silicon microdisk*, ACS Photonics **1**, 762 (2014).

[8] F. J. Rodríguez-Fortuño, D. Puerto, A. Griol, L. Bellieres, J. Martí, and A. Martínez, *Sorting linearly polarized photons with a single scatterer*, Opt. Lett. **39**, 1394 (2014).

[9] D. O'Connor, P. Ginzburg, F. J. Rodríguez-Fortuño, G. A. Wurtz, and A. V. Zayats, *Spin-orbit coupling in surface plasmon scattering by nanostructures*, Nat. Commun. **5**, 5327 (2014).

[10] P. V. Kapitanova, P. Ginzburg, F. J. Rodríguez-Fortuño, D. S. Filonov, P. M. Voroshilov, P. A. Belov, A. N. Poddubny, Y. S. Kivshar, G. A. Wurtz, and A. V. Zayats, *Photonic spin Hall effect in hyperbolic metamaterials for polarization-controlled routing of subwavelength modes*, Nat. Commun. **5**, 3226 (2014).

[11] B. le Feber, N. Rotenberg, and L. Kuipers, *Nanophotonic control of circular dipole emission*, Nat. Commun. **6**, 6695 (2015).

[12] I. Söllner, S. Mahmoodian, S. L. Hansen, L. Midolo, A. Javadi, G. Kiršanskė, T. Pregnolato, H. El-Ella, E. H. Lee, J. D. Song, S. Stobbe, and P. Lodahl, *Deterministic photon-emitter coupling in chiral photonic circuits*, Nat. Nanotechnol. **10**, 775 (2015).

[13] J. Carbonell, F. J. Rodríguez-Fortuño, A. Díaz-Rubio, A. Martínez, F. Cervera, and J. Sánchez-Dehesa, *Directive excitation of guided electromagnetic waves through polarization control*, Phys. Rev. B **89**, 155121 (2014).

[14] J. Petersen, J. Volz, and A. Rauschenbeutel, *Chiral nanophotonic waveguide interface based on spin-orbit interaction of light*, Science **346**, 67 (2014).

[15] M. F. Picardi, K. Y. Bliokh, F. J. Rodríguez-Fortuño, F. Alpeggiani, and F. Nori, *Angular momenta, helicity, and other properties of dielectric-fiber and metallic-wire modes*, Optica **5**, 1016 (2018).

[16] K. Y. Bliokh, D. Smirnova, and F. Nori, *Quantum spin Hall effect of light*, Science **348**, 1448 (2015).

[17] K. Y. Bliokh and F. Nori, *Transverse spin of a surface polariton*, Phys. Rev. A **85**, 061801 (2012).

[18] K. Y. Bliokh, A. Y. Bekshaev, and F. Nori, *Extraordinary momentum and spin in evanescent waves*, Nat. Commun. **5**, 3300 (2014).

[19] T. Van Mechelen and Z. Jacob, *Universal spin-momentum locking of evanescent waves*, Optica **3**, 118 (2016).

[20] M. Wang, H. Zhang, T. Kovalevich, R. Salut, M.-S. Kim, M. A. Suarez, M.-P. Bernal, H.-P. Herzig, H. Lu, and T. Grosjean, *Magnetic spin-orbit interaction of light*, Light Sci. Appl. **7**, 24 (2018).

[21] L. Marrucci, *Spin gives direction*, Nat. Phys. **11**, 9 (2015).

[22] A. Aiello, P. Banzer, M. Neugebauer, and G. Leuchs, *From transverse angular momentum to photonic wheels*, Nat. Photonics **9**, 789 (2015).

[23] A. Espinosa-Soria and A. Martínez, *Transverse spin and spin-orbit coupling in silicon waveguides*, IEEE Photonics Technol. Lett. **28**, 1561 (2016).

[24] L. Novotny and B. Hecht, *Principles of Nano-Optics* (Cambridge University Press, Cambridge, England, 2012).

[25] M. F. Picardi, A. Manjavacas, A. V. Zayats, and F. J. Rodríguez-Fortuño, *Unidirectional evanescent-wave coupling from circularly polarized electric and magnetic dipoles: An angular spectrum approach*, Phys. Rev. B **95**, 245416 (2017).

[26] M. F. Picardi, A. V. Zayats, and F. J. Rodríguez-Fortuño, *Janus and Huygens dipoles: Near-field directionality beyond spin-momentum locking*, Phys. Rev. Lett. **120**, 117402 (2018).

[27] M. Neugebauer, T. Bauer, P. Banzer, and G. Leuchs, *Polarization tailored light driven directional optical nanobeacon*, Nano Lett. **14**, 2546 (2014).

[28] M. Neugebauer, P. Woźniak, A. Bag, G. Leuchs, and P. Banzer, *Polarization-controlled directional scattering for nanoscopic position sensing*, Nat. Commun. **7**, 11286 (2016).

[29] M. F. Picardi, M. Neugebauer, J. S. Eismann, G. Leuchs, P. Banzer, F. J. Rodríguez-Fortuño, and A. V. Zayats, *Experimental demonstration of linear and spinning Janus dipoles for polarisation- and wavelength-selective near-field coupling*, Light Sci. Appl. **8**, 52 (2019).

[30] L. Wei, M. F. Picardi, J. J. Kingsley-Smith, A. V. Zayats, and F. J. Rodríguez-Fortuño, *Directional scattering from particles under evanescent wave illumination: the role of reactive power*, Opt. Lett. **43**, 3393 (2018).

[31] O. Keller, *Quantum Theory of Near-Field Electrodynamics* (Springer, Berlin, Heidelberg, 2012).

[32] I. Fernandez-Corbaton, X. Zambrana-Puyalto, N. Bonod, and C. Rockstuhl, *Transverse multipolar light-matter couplings in evanescent waves*, Phys. Rev. A **94**, 053822 (2016).

[33] The calculator for the angular spectra of arbitrary EM multipole sources is available online, at https://doi.org/10.5281/zenodo.2677908.

[34] A. G. Curto, T. H. Taminiau, G. Volpe, M. P. Kreuzer, R. Quidant, and N. F. van Hulst, *Multipolar radiation of quantum emitters with nanowire optical antennas*, Nat. Commun. **4**, 1750 (2013).

[35] A. B. Evlyukhin, C. Reinhardt, E. Evlyukhin, and B. N. Chichkov, *Multipole analysis of light scattering by arbitrary-shaped nanoparticles on a plane surface*, J. Opt. Soc. Am. B **30**, 2589 (2013).

[36] A. B. Evlyukhin, T. Fischer, C. Reinhardt, and B. N. Chichkov, *Optical theorem and multipole scattering of light by arbitrarily shaped nanoparticles*, Phys. Rev. B **94**, 205434 (2016).

[37] R. Alaee, C. Rockstuhl, and I. Fernandez-Corbaton, *An electromagnetic multipole expansion beyond the long-wavelength approximation*, Opt. Commun. **407**, 17 (2018).

[38] R. Alaee, C. Rockstuhl, and I. Fernandez-Corbaton, *Exact multipolar decompositions with applications in nanophotonics*, Adv. Opt. Mater. **7**, 1800783 (2019).

[39] A. J. Devaney and E. Wolf, *Multipole expansions and plane wave representations of the electromagnetic field*, J. Math. Phys. **15**, 234 (1974).

[40] L. Mandel and E. Wolf, *Optical Coherence and Quantum Optics* (Cambridge University Press, Cambridge, UK, 1995).

[41] G. C. Sherman, J. J. Stamnes, and E. Lalor, *Asymptotic approximations to angular-spectrum representations*, J. Math. Phys. **17**, 760 (1976).

[42] A. T. Friberg and E. Wolf, *Angular spectrum representation of scattered electromagnetic fields*, J. Opt. Soc. Am. **73**, 26 (1983).

[43] E. Wolf and M. Nieto-Vesperinas, *Analyticity of the angular spectrum amplitude of scattered fields and some of its consequences*, J. Opt. Soc. Am. A **2**, 886 (1985).

[44] T. Inoue and H. Hori, *Theoretical treatment of electric and magnetic multipole radiation near a planar dielectric surface based on angular spectrum representation of vector field*, Opt. Rev. **5**, 295 (1998).

[45] H. F. Arnoldus, *Angular spectrum representation of the electromagnetic multipole fields, and their reflection at a perfect conductor*, Surf. Sci. **590**, 101 (2005).

[46] J. W. Goodman, *Introduction to Fourier Optics* (McGraw-Hill, New York, USA, 1988).

[47] T. Setälä, M. Kaivola, and A. T. Friberg, *Decomposition of the point-dipole field into homogeneous and evanescent parts*, Phys. Rev. E **59**, 1200 (1999).

[48] J. D. Jackson, *Classical Electrodynamics* (Wiley, New York, USA, 1999).

[49] H. Weyl, *Ausbreitung elektromagnetischer Wellen über einem ebenen Leiter* [*Propagation of electromagnetic waves on an even conductor*], Ann. Phys. **365**, 481 (1919).

[50] See the Supplemental Material at http://link.aps.org/supplemental/10.1103/PhysRevApplied.12.024065 for further details on the angular-spectrum formalism, Weyl's identity, and the Hertz potentials (Sec. I). It also includes a detailed derivation of the angular spectrum of both the electric dipole (Sec. II) and quadrupole (Sec. III), and the EM fields (Sec. IV). Finally, we provide a step-by-step derivation of the angular spectrum of EM multipolar sources of arbitrary order (Sec. V) and set a relationship with the particular cases of the electric dipole and quadrupole (Sec. VI). See the accompanying video for an animated version of Fig. B.2.

[51] G. N. Watson, *A Treatise on the Theory of Bessel Functions* (Cambridge University Press, New York, USA, 1995).

[52] A. Ishimaru, *Electromagnetic Wave Propagation, Radiation, and Scattering* (Prentice-Hall, Englewood Cliffs, NJ, 1991).

[53] E. A. Essex, *Hertz vector potentials of electromagnetic theory*, Am. J. Phys. **45**, 1099 (1977).

[54] M. Ornigotti and A. Aiello, *The Hertz vector revisited: a simple physical picture*, J. Opt. **16**, 105705 (2014).

[55] Note that, in the context of guiding systems, the terminology "electric" and "magnetic," referring to the nature of the optical source, is often replaced by "transverse magnetic" and "transverse electric," respectively.

[56] It should be noted that the limit $z \to 0$ in Eq. (B.16) is actually a formal representation that gives a physically consistent meaning to the singular behavior at the origin [40]. In practice, though, this calculation is to be carried out by considering Eq. (B.17) and taking the corresponding limit on either of the indexes l and m.

[57] M. Abramowitz and I. A. Stegun, *Handbook of Mathematical Functions* (Dover, New York, USA, 1972).

[58] P. A. Bobbert and J. Vlieger, *Light scattering by a sphere on a substrate*, Physica A **137**, 209 (1986).

[59] R. Borghi, *On the angular-spectrum representation of multipole wave fields*, J. Opt. Soc. Am. A **21**, 1805 (2004).

[60] F. J. Rodríguez-Fortuño, N. Engheta, A. Martínez, and A. V. Zayats, *Lateral forces on circularly polarizable particles near a surface*, Nat. Commun. **6**, 8799 (2015).

[61] A. Espinosa-Soria, F. J. Rodríguez-Fortuño, A. Griol, and A. Martínez, *On-chip optimal Stokes nanopolarimetry based on spin-orbit interaction of light*, Nano Lett. **17**, 3139 (2017).

[62] D. Smirnova and Y. S. Kivshar, *Multipolar nonlinear nanophotonics*, Optica **3**, 1241 (2016).

Chapter 3

PAPER B: Supplemental Material

Near-Field Directionality Beyond the Dipole Approximation: Electric Quadrupole and Higher-Order Multipole Angular Spectra

---

Phys. Rev. Applied 12, 024065 (2019)

Supplemental Material: Near-Field Directionality Beyond the Dipole Approximation: Electric Quadrupole and Higher-Order Multipole Angular Spectra

J. Enrique Vázquez-Lozano,[1,2] Alejandro Martínez,[1] and Francisco J. Rodríguez-Fortuño[2]

[1]*Nanophotonics Technology Center, Universitat Politècnica de València, Camino de Vera s/n, 46022 Valencia, Spain*

[2]*Department of Physics, King's College London, Strand, London WC2R 2LS, United Kingdom*

In this supplemental material we provide a step-by-step derivation of the angular spectrum representation of any electromagnetic multipole field. For completeness, and for convenience throughout this work, we first briefly review the angular spectrum of the electric dipole, which relies on Weyl's identity. In a similar but slightly trickier way, we are also able to get the angular spectrum of the electric quadrupole. Due to the similarity between these two particular results, we look into the possibility of addressing a general approach valid to any multipolar order. In this way, we find an analytical and closed expression that generalizes Weyl's identity thus enabling the angular spectrum representation of any multipole field.

B.SM.I Angular Spectrum Representation, Weyl's Identity and Hertz Potentials

The angular spectrum representation is a classical technique that allows us to express any electromagnetic (EM) field in homogeneous media as a superposition of elementary plane waves which can be propagating (homogeneous) or evanescent (inhomogeneous) [S1,S2]. Within the dipole approximation [S3] this formalism essentially relies on *Weyl's identity* [S4]:

$$\frac{e^{ikr}}{r} = \frac{ik}{2\pi}\iint_{-\infty}^{+\infty} \frac{1}{\kappa_z} e^{ik(\kappa_x x + \kappa_y y \pm \kappa_z z)} d\kappa_x d\kappa_y, \tag{B.S1}$$

where the wave vector is defined as $\mathbf{k}^{\pm} = k\,(\kappa_x, \kappa_y, \pm\kappa_z)$, and the signs $+$ and $-$ stand for the wave propagation through the half-spaces $z > 0$ and $z < 0$, respectively. Moreover, assuming that $\mathbf{k}^{\pm} \cdot \mathbf{k}^{\pm} = k^2$, it follows that

$$\kappa_z = \begin{cases} \sqrt{1 - \kappa_x^2 - \kappa_y^2}, & \text{if} \quad \kappa_x^2 + \kappa_y^2 \leq 1; \\ i\sqrt{\kappa_x^2 + \kappa_y^2 - 1}, & \text{if} \quad \kappa_x^2 + \kappa_y^2 > 1. \end{cases} \tag{B.S2}$$

This fundamental result allows us to represent any diverging spherical wave as a superposition of plane waves in the partial Fourier (or momentum) space (κ_x, κ_y) [S5]. As it will be shown below, beyond this simple case concerning scalar waves, the importance of the Weyl's identity becomes much more evident when studying the propagation of properly defined EM vector waves.

Let us consider a time-harmonic optical field, $\mathbf{\Psi}(\mathbf{r}, t) = \mathbf{\Psi}_0(\mathbf{r})e^{-i\omega t}$, propagating in a linear, homogeneous, isotropic, and source-free medium. The time-independent complex amplitude $\mathbf{\Psi}_0$ must satisfy the Helmholtz wave equation:

$$\left(\nabla^2 + k^2\right) \mathbf{\Psi}_0(\mathbf{r}) = 0, \tag{B.S3}$$

where $\mathbf{\Psi}_0$ can be either the electric or the magnetic field, $k \equiv nk_0$ is the wave number of the medium, $k_0 \equiv \omega/c$ is the wave number in vacuum, and $n \equiv \sqrt{\varepsilon_r \mu_r}$ is the refractive index, being ε_r and μ_r the corresponding relative permittivity and permeability of the medium. If we assume that there exists a translational symmetry along two directions of a plane, we can define a direction $\mathbf{r}_\perp$ which is perpendicular to this plane of symmetry, and then $\mathbf{\Psi}_0$ can be represented by means of the inverse spatial Fourier transform on the partial space spanned by $\mathbf{r}_\parallel$ as

$$\mathbf{\Psi}_0(\mathbf{r}) = \iint_{-\infty}^{+\infty} \tilde{\mathbf{\Psi}}_0(\mathbf{k}_\parallel; \mathbf{r}_\perp) e^{i\mathbf{k}_\parallel \cdot \mathbf{r}_\parallel} d\mathbf{k}_\parallel, \tag{B.S4}$$

where we have expressed both position and wave vectors in terms of their projections parallel and perpendicular to the plane of translational symmetry. Substituting Eq. (B.S4) into (B.S3) it is straightforward to demonstrate that

$$\iint_{-\infty}^{+\infty} \left[\nabla_\perp^2 \tilde{\mathbf{\Psi}}_0(\mathbf{k}_\parallel; \mathbf{r}_\perp) + \left(k^2 - \mathbf{k}_\parallel \cdot \mathbf{k}_\parallel\right) \tilde{\mathbf{\Psi}}_0(\mathbf{k}_\parallel; \mathbf{r}_\perp)\right] e^{i\mathbf{k}_\parallel \cdot \mathbf{r}_\parallel} d\mathbf{k}_\parallel = 0. \tag{B.S5}$$

For simplicity, and without loss of generality, we particularize to the case in which $\mathbf{k}_\parallel = k\,(\kappa_x, \kappa_y, 0)$, and $\mathbf{k}_\perp^\pm = k\,(0, 0, \pm\kappa_z)$, and so, it is easy to realize that the expression in the square brackets of Eq. (B.S5) actually is a Helmholtz-like equation reduced to the one-dimensional case:

$$\frac{\partial^2 \tilde{\mathbf{\Psi}}_0(\kappa_x, \kappa_y; z)}{\partial z^2} + k^2 \kappa_z^2 \tilde{\mathbf{\Psi}}_0(\kappa_x, \kappa_y; z) = 0. \tag{B.S6}$$

Hence, the angular spectrum amplitude $\tilde{\mathbf{\Psi}}_0$ can be simply expressed as

$$\tilde{\mathbf{\Psi}}_0(\kappa_x, \kappa_y; z) = \tilde{\mathbf{\Psi}}_0(\kappa_x, \kappa_y; 0) e^{\pm ik\kappa_z z}. \tag{B.S7}$$

Finally, in order to get the *angular spectrum representation* we only have to insert this result in Eq. (B.S4):

$$\mathbf{\Psi}_0(\mathbf{r}) = \iint_{-\infty}^{+\infty} \tilde{\mathbf{\Psi}}_0(\kappa_x, \kappa_y; 0) e^{ik(\kappa_x x + \kappa_y y \pm \kappa_z z)} d\kappa_x d\kappa_y, \tag{B.S8}$$

where, once again, the signs + and − refer to a wave propagating in each of the half-spaces $z > 0$ and $z < 0$, respectively. Thus, provided that there exists a well defined translation symmetry, e.g., along the plane (x, y), one can always describe the whole EM field just from looking at the field over one of these planes, let us say the plane $z = 0$. As previously anticipated, this characterization is very useful because allows us to obtain a *mode representation* of the optical field in terms of propagating and evanescent plane waves [S1]. Specifically, these characteristic solutions can be easily distinguished in the transverse momentum space (κ_x, κ_y) taking into account their relative position with respect to the unit circumference $\kappa_x^2 + \kappa_y^2 = 1$ [S2]. In this manner, from Eqs. (B.S2) and (B.S7) we see that $\kappa_x^2 + \kappa_y^2 < 1$ leads to oscillating functions in z, thereby representing propagating plane waves. Otherwise, $\kappa_x^2 + \kappa_y^2 > 1$ gives rise to exponentially decaying solutions, which are in turn identified with evanescent waves.

Under the premises so far established, the above scheme is completely general, and can be applied to any scalar or vector field as long as it satisfies the Helmholtz wave equation. This enables a systematic analysis of the angular spectrum of any localized optical source (i.e., the electric dipole, quadrupole, and in general any higher-order multipole moment) by means of their corresponding vector potentials. More precisely, we can make use of the so-called electric and magnetic Hertz potentials [S6,S7], which might be introduced in terms of the standard scalar and vector potentials, $\Phi(\mathbf{r}, t)$ and $\boldsymbol{\mathcal{A}}(\mathbf{r}, t)$ respectively, as follows [S8]

$$\begin{aligned} \boldsymbol{\mathcal{A}}(\mathbf{r}, t) &= \mu \partial_t \boldsymbol{\Pi}^{(\mathrm{e})}(\mathbf{r}, t) + \mu_0 [\nabla \times \boldsymbol{\Pi}^{(\mathrm{m})}(\mathbf{r}, t)], \\ \Phi(\mathbf{r}, t) &= -\frac{1}{\varepsilon} \nabla \cdot \boldsymbol{\Pi}^{(\mathrm{e})}(\mathbf{r}, t), \end{aligned} \tag{B.S9}$$

where $\varepsilon \equiv \varepsilon_0 \varepsilon_r$ and $\mu \equiv \mu_0 \mu_r$, with ε_0 and μ_0 being the permittivity and permeability of free space, respectively. It is interesting to point out that the superscript refers to the nature of the source that originates the EM radiation, that may be either electric or magnetic [S9]. Furthermore, it should be noted that these definitions arise directly from the relationships between the time-dependent EM fields and the gauge standard potentials, $\boldsymbol{\mathcal{E}}(\mathbf{r}, t) \equiv -\nabla \Phi(\mathbf{r}, t) - \partial_t \boldsymbol{\mathcal{A}}(\mathbf{r}, t)$ and $\boldsymbol{\mathcal{B}}(\mathbf{r}, t) \equiv \nabla \times \boldsymbol{\mathcal{A}}(\mathbf{r}, t)$, together with the Lorenz condition, $\nabla \cdot \boldsymbol{\mathcal{A}}(\mathbf{r}, t) + \varepsilon_0 \mu_0 \partial_t \Phi(\mathbf{r}, t) = 0$ (a complete derivation can be found in Ref. [S8]). All in all, for our purposes the key point to bear in mind is that both the electric and magnetic Hertz potentials, $\boldsymbol{\Pi}^{(\mathrm{e})}(\mathbf{r}, t)$ and $\boldsymbol{\Pi}^{(\mathrm{m})}(\mathbf{r}, t)$, by construction, satisfy the vector Helmholtz wave equation, and are susceptible of an expansion into their angular spectrum.

The latter relations between the time-dependent EM fields and the potentials can be applied to both electric and magnetic-like multipole sources. For the sake of clarity and simplicity, and without any loss of generality, hereinafter it will be assumed fields with harmonic time dependence of the form $e^{-i\omega t}$. Then, from the definitions given in

Eq. (B.S9), the complex field amplitudes read as

$$\mathbf{E}(\mathbf{r}) = \mathbf{E}^{(\mathrm{e})}(\mathbf{r}) + \mathbf{E}^{(\mathrm{m})}(\mathbf{r}) = \frac{1}{\varepsilon}\left\{k^2\boldsymbol{\Pi}^{(\mathrm{e})}(\mathbf{r}) + \nabla[\nabla\cdot\boldsymbol{\Pi}^{(\mathrm{e})}(\mathbf{r})]\right\} + i\mu_0\omega[\nabla\times\boldsymbol{\Pi}^{(\mathrm{m})}(\mathbf{r})], \tag{B.S10}$$

$$\mathbf{H}(\mathbf{r}) = \mathbf{H}^{(\mathrm{e})}(\mathbf{r}) + \mathbf{H}^{(\mathrm{m})}(\mathbf{r}) = -i\omega[\nabla\times\boldsymbol{\Pi}^{(\mathrm{e})}(\mathbf{r})] + \frac{1}{\mu_r}\left\{k^2\boldsymbol{\Pi}^{(\mathrm{m})}(\mathbf{r}) + \nabla[\nabla\cdot\boldsymbol{\Pi}^{(\mathrm{m})}(\mathbf{r})]\right\}. \tag{B.S11}$$

It is worth remarking that there exist some other definitions for the Hertz potentials that may yield simpler expressions for the EM fields. In particular, in Ref. [S10] it can be found that the electric and magnetic Hertz potentials are presented separately, thus leading to EM fields associated to electric- and magnetic-like sources that are related to each other just through the *duality principle* and the symmetry of Maxwell's equations. Despite that, in order to build on a sound and self-consistent framework, we will mainly focus on the approach provided in Ref. [S8], and so we will regard the potentials as given in Eq. (B.S9). In this respect, it is important to recall that owing to the gauge freedom, we can always find out a gauge function $\chi(\mathbf{r},t)$ enabling the transformation of any scalar and vector potential so as to meet the Lorenz condition, and thereby giving rise to Hertz-like vector potentials. This fact will be profitably exploited later in dealing with the angular spectrum representation of the EM multipole fields.

Taking into account the appropriateness of the Hertz potentials for characterizing any multipole field, the main advantage of the angular spectrum formalism becomes evident when representing the EM fields, because the previous expressions involving spatial derivatives are greatly simplified in the partial Fourier space:

$$\tilde{\mathbf{E}}^{(\mathrm{e})}(\kappa_x,\kappa_y;z) = \frac{1}{\varepsilon}\left\{k^2\tilde{\boldsymbol{\Pi}}^{(\mathrm{e})}(\kappa_x,\kappa_y;z) - \mathbf{k}^{\pm}[\mathbf{k}^{\pm}\cdot\tilde{\boldsymbol{\Pi}}^{(\mathrm{e})}(\kappa_x,\kappa_y;z)]\right\}, \tag{B.S12}$$

$$\tilde{\mathbf{H}}^{(\mathrm{e})}(\kappa_x,\kappa_y;z) = \frac{ck}{n}\left[\mathbf{k}^{\pm}\times\tilde{\boldsymbol{\Pi}}^{(\mathrm{e})}(\kappa_x,\kappa_y;z)\right], \tag{B.S13}$$

$$\tilde{\mathbf{E}}^{(\mathrm{m})}(\kappa_x,\kappa_y;z) = -\frac{Z_0 k}{n}\left[\mathbf{k}^{\pm}\times\tilde{\boldsymbol{\Pi}}^{(\mathrm{m})}(\kappa_x,\kappa_y;z)\right], \tag{B.S14}$$

$$\tilde{\mathbf{H}}^{(\mathrm{m})}(\kappa_x,\kappa_y;z) = \frac{1}{\mu_r}\left\{k^2\tilde{\boldsymbol{\Pi}}^{(\mathrm{m})}(\kappa_x,\kappa_y;z) - \mathbf{k}^{\pm}[\mathbf{k}^{\pm}\cdot\tilde{\boldsymbol{\Pi}}^{(\mathrm{m})}(\kappa_x,\kappa_y;z)]\right\}, \tag{B.S15}$$

where $Z_0 \equiv \sqrt{\mu_0/\varepsilon_0}$ is the impedance of free space. These expressions are readily obtained by the substitution $\nabla \to i\mathbf{k}^{\pm}$. Hence, cumbersome analysis involving the computation of gradients, divergences, curls, and Laplacian, is reduced to simple algebraic operations relying upon the product between the wave vector $\mathbf{k}^{\pm}$ and the spectral amplitudes $\tilde{\boldsymbol{\Pi}}^{(\mathrm{e/m})}$.

B.SM.II Angular Spectrum Representation of the Electric Dipole

Below, for the sake of completeness and for convenience in the subsequent analysis, we will briefly sketch the derivation of the angular spectrum representation of an electric

dipole. To do so, let us start by considering the corresponding complex-like vector potential associated to an oscillating electric dipole as given in Ref. [S8]:

$$\mathbf{A}^{\mathrm{ED}}(\mathbf{r}) = \frac{\mu}{4\pi}\left[\int_{-\infty}^{+\infty}\mathbf{J}(\mathbf{r}')d\mathbf{r}'\right]\frac{e^{ikr}}{r}. \tag{B.S16}$$

After integration by parts and using the continuity equation for the electric charge, i.e., $\nabla\cdot\mathbf{J}+\partial_t\rho=0$, we can recast the latter expression in a more familiar form,

$$\mathbf{A}^{\mathrm{ED}}(\mathbf{r}) = -\frac{i\mu\omega}{4\pi}\mathbf{p}\frac{e^{ikr}}{r}, \tag{B.S17}$$

where $\mathbf{p}=\int_{-\infty}^{+\infty}\mathbf{r}'\rho(\mathbf{r}')d\mathbf{r}'$ is the *electric dipole moment*. This means that the electric current density can be actually expressed as $\mathbf{J}(\mathbf{r})=-i\omega\delta^3(\mathbf{r}-\mathbf{r}')\mathbf{p}$, and so the dipolar source is simply characterized by a constant vector $\mathbf{p}$. As pointed out above, to proceed with the angular spectrum representation, it is crucial to be certain that the vector potential given by Eq. (B.S17) really satisfies the Helmholtz equation:

$$\left(\nabla^2+k^2\right)\mathbf{A}^{\mathrm{ED}}(\mathbf{r})=0. \tag{B.S18}$$

In this regard, it should be noted that, besides a constant prefactor, the vector potential only consists of a diverging spherical wave (i.e., e^{ikr}/r) which is in fact the scalar Green's function of the Helmholtz operator [S1], thereby satisfying in its own the Helmholtz equation everywhere except at the origin. Despite that singularity, we might formally get the angular spectrum of e^{ikr}/r in each of the half-spaces $z>0$ and $z<0$ [S1]. Hence, appealing to Weyl's identity given in Eq. (B.S1), it is straightforward to show that

$$\mathbf{A}^{\mathrm{ED}}(\mathbf{r}) = -\frac{i\mu\omega}{4\pi}\mathbf{p}\left[\frac{ik}{2\pi}\iint_{-\infty}^{+\infty}\frac{1}{\kappa_z}e^{ik(\kappa_x x+\kappa_y y\pm\kappa_z z)}d\kappa_x d\kappa_y\right]. \tag{B.S19}$$

By comparing the above expression with the general results given in Eqs. (B.S7) and (B.S8), it is easy to see that the angular spectrum amplitude of the electric dipole is given by:

$$\tilde{\mathbf{A}}^{\mathrm{ED}}(\kappa_x,\kappa_y;z)=\tilde{\mathbf{A}}_0^{\mathrm{ED}}(\kappa_x,\kappa_y;0)e^{\pm ik\kappa_z z}, \tag{B.S20}$$

where

$$\tilde{\mathbf{A}}_0^{\mathrm{ED}}(\kappa_x,\kappa_y;0)=\frac{\mu c k^2}{8\pi^2 n}\frac{1}{\kappa_z}\mathbf{p}. \tag{B.S21}$$

A more detailed description of the above derivation, in particular the explicit calculations to obtain Weyl's identity analytically [Eq. (B.S1)], can be found in Ref. [S1].

B.SM.III Angular Spectrum Representation of the Electric Quadrupole

Building on the above scheme, in this section we will address the angular spectrum representation of the electric quadrupole. To this aim, we start once again from the corresponding vector potential as given in Ref. [S8]:

$$\mathbf{A}^{\mathrm{EQ}}(\mathbf{r}) = \frac{\mu\omega k}{8\pi}\left(\frac{1}{ikr}-1\right)\left[\int_{-\infty}^{+\infty}\mathbf{r}'\left(\mathbf{e}_r\cdot\mathbf{r}'\right)\rho(\mathbf{r}')d\mathbf{r}'\right]\frac{e^{ikr}}{r}, \tag{B.S22}$$

where $\mathbf{e}_r$ is the unit vector in the radial direction. Notice that this latter expression is given in terms of an integral involving the second moments of the charge density. Still, it can be readily simplified by using the following definitions:

$$\frac{\mathbf{Q}(\mathbf{e}_r)}{3} \equiv \int_{-\infty}^{+\infty} \mathbf{r}' \left(\mathbf{e}_r \cdot \mathbf{r}'\right) \rho(\mathbf{r}') d\mathbf{r}', \tag{B.S23}$$

where $Q_i = \sum_j \mathcal{Q}_{ij} (\mathbf{e}_r)_j$, and

$$\mathcal{Q}_{ij} = \int_{-\infty}^{+\infty} \left(3 r_i r_j - r^2 \delta_{ij}\right) \rho(\mathbf{r}) d\mathbf{r} \tag{B.S24}$$

is the *quadrupole moment tensor* characterizing the charge distribution. This is a rank-two tensor, usually represented by a 3×3 traceless, complex, and symmetric matrix, i.e., $\mathcal{Q}_{xx} + \mathcal{Q}_{yy} + \mathcal{Q}_{zz} = 0$, and $\mathcal{Q}_{ij} = \mathcal{Q}_{ji}$, thus reducing the number of unknowns to 5. Hence, the vector potential can be recast as

$$\mathbf{A}^{\mathrm{EQ}}(\mathbf{r}) = \frac{\mu\omega k}{24\pi} \left(\frac{1}{ikr} - 1\right) \mathbf{Q}(\mathbf{e}_r) \frac{e^{ikr}}{r}. \tag{B.S25}$$

Looking at this expression more closely, one realizes that there are important discrepancies in comparison with the previous case of the electric dipole. On the one side, it should be noticed that $\mathbf{Q}(\mathbf{e}_r)$ depends on the direction of observation. As a consequence, the scalar contribution of the electric quadrupole's vector potential is no longer a proper solution of the Helmholtz equation, and so we have to regard the whole vector expression of $\mathbf{A}^{\mathrm{EQ}}$ when addressing the angular spectrum representation.

After verifying that Eq. (B.S25) does indeed satisfy the Helmholtz equation (it can be readily checked by means of a symbolic calculation software), we can then proceed to the computation of the angular spectrum amplitude for the electric quadrupole from the partial Fourier transform:

$$\begin{aligned}\tilde{\mathbf{A}}^{\mathrm{EQ}}(\kappa_x, \kappa_y; z) &= \left(\frac{k}{2\pi}\right)^2 \iint_{-\infty}^{+\infty} \mathbf{A}^{\mathrm{EQ}}(x, y, z) e^{-ik(\kappa_x x + \kappa_y y)} dx dy \\ &= \frac{\mu\omega k^3}{96\pi^3} \iint_{-\infty}^{+\infty} \left(\frac{1}{ik\sqrt{x^2+y^2+z^2}} - 1\right) \mathbf{Q}(\mathbf{e}_r) \frac{e^{ik\sqrt{x^2+y^2+z^2}}}{\sqrt{x^2+y^2+z^2}} e^{-ik(\kappa_x x + \kappa_y y)} dx dy.\end{aligned} \tag{B.S26}$$

This integral can be easily solved making the following change of variables to cylindrical polar coordinates in both real and momentum space:

$$\begin{aligned} &x = R\cos\theta, && y = R\sin\theta, && z = z; \\ &\kappa_x = \kappa_R \cos\phi, && \kappa_y = \kappa_R \sin\phi, && \kappa_z = \kappa_z. \end{aligned} \tag{B.S27}$$

Therefore, Eq. (B.S26) reads as

$$\tilde{\mathbf{A}}^{\mathrm{EQ}}(\kappa_x, \kappa_y; z) = \frac{\mu\omega k^3}{96\pi^3} \int_0^{+\infty} \int_0^{2\pi} \left(\frac{1}{ik\sqrt{R^2+z^2}} - 1\right) \mathbf{Q}(\mathbf{e}_r) \frac{e^{ik\sqrt{R^2+z^2}}}{\sqrt{R^2+z^2}} e^{-ik\kappa_R R\cos(\theta-\phi)} R d\theta dR, \tag{B.S28}$$

where $R \equiv (x^2+y^2)^{1/2}$ and $\kappa_R \equiv (\kappa_x^2+\kappa_y^2)^{1/2}$ are both real and positive quantities. It is important to emphasize that $\mathbf{Q}(\mathbf{e}_r)$ depends in magnitude and direction on the integration variables R and θ, so it cannot be taken outside the integral (as in the previous case for the electric dipole). Furthermore, this is indeed the term that conveys the "quadrupolar character" to the vector potential and it can be expressed as follows:

$$\mathbf{Q} \equiv \vec{\vec{\mathcal{Q}}} \cdot \mathbf{e}_r = Q_x \mathbf{e}_x + Q_y \mathbf{e}_y + Q_z \mathbf{e}_z, \tag{B.S29}$$

where

$$Q_n = \frac{1}{\sqrt{R^2+z^2}} \left[R \left(\mathcal{Q}_{nx} \cos\theta + \mathcal{Q}_{ny} \sin\theta \right) + z \mathcal{Q}_{nz} \right], \tag{B.S30}$$

with $n = \{x, y, z\}$. Then, with the aid of the following identities

$$\int_0^{2\pi} e^{-i\alpha\cos(\theta-\beta)} d\theta = 2\pi J_0(\alpha), \tag{B.S31a}$$

$$\int_0^{2\pi} e^{-i\alpha\cos(\theta-\beta)} \begin{Bmatrix} \cos\theta \\ \sin\theta \end{Bmatrix} d\theta = -2\pi i J_1(\alpha) \begin{Bmatrix} \cos\beta \\ \sin\beta \end{Bmatrix}, \tag{B.S31b}$$

where $J_l(x)$ is the Bessel function of the first kind and order l, it follows at once that the integration with respect to the angle θ reduces to

$$\begin{aligned} \Omega_n &= \int_0^{2\pi} \left[\vec{\vec{\mathcal{Q}}} \cdot \mathbf{e}_r \right]_n e^{-ik\kappa_R R\cos(\theta-\phi)} d\theta \\ &= \frac{2\pi}{\sqrt{R^2+z^2}} \left[\mathcal{Q}_{nz} z J_0(k\kappa_R R) - iR J_1(k\kappa_R R) \left(\mathcal{Q}_{nx}\cos\phi + \mathcal{Q}_{ny}\sin\phi \right) \right]. \end{aligned} \tag{B.S32}$$

It is worth remarking in this case the presence of Bessel functions of order 1, in contrast with the case of the electric dipole where there are only Bessel functions of order 0. In addition, it should be noted that the whole vectorial expression would become much simpler provided that we use the properties of the quadrupole moment tensor (traceless, symmetries, ...). From the latter result it can be observed that we can actually work with all vector components simultaneously by using an index $n = \{x, y, z\}$. In doing so it follows that

$$\tilde{A}_n^{\mathrm{EQ}}(\kappa_x, \kappa_y; z) = \frac{\mu\omega k^3}{48\pi^2} \int_0^{+\infty} \left(\frac{1}{ik\sqrt{R^2+z^2}} - 1 \right) \frac{e^{ik\sqrt{R^2+z^2}}}{R^2+z^2} \left[\mathcal{Q}_{nz} z J_0 - iR J_1 (\mathcal{Q}_{nx}\cos\phi + \mathcal{Q}_{ny}\sin\phi) \right] R dR. \tag{B.S33}$$

Now we only have to perform the integration over the radial variable. In order to do that analytically, likewise as for the electric dipole, we ought to take the limit $z \to 0$. Nonetheless, in this case, it is important to realize that taking the limit to the plane $z = 0$ may lead to misleading outcomes wherein the z-dependent contribution of the quadrupole moment tensor would seem to be dismissed. Thus, to overcome this issue we should carry out the integration separately for the xy and z components of the quadrupole moment

(i.e., $\tilde{A}_n^{\mathrm{EQ}} = \tilde{A}_{n,xy}^{\mathrm{EQ}} + \tilde{A}_{n,z}^{\mathrm{EQ}}$), where:

$$\tilde{A}_{n,xy}^{\mathrm{EQ}}(\kappa_x,\kappa_y;z) = \frac{i\mu\omega k^3}{48\pi^2}\int_0^{+\infty}\left(1-\frac{1}{ik\sqrt{R^2+z^2}}\right)\frac{e^{ik\sqrt{R^2+z^2}}}{R^2+z^2}R^2J_1\left(\mathcal{Q}_{nx}\cos\phi+\mathcal{Q}_{ny}\sin\phi\right)dR$$

$$\xrightarrow[z\to 0]{} \frac{i\mu\omega k^3}{48\pi^2}\int_0^{+\infty}\left(1-\frac{1}{ikR}\right)e^{ikR}J_1(k\kappa_R R)\left(\mathcal{Q}_{nx}\cos\phi+\mathcal{Q}_{ny}\sin\phi\right)dR$$

$$= -\frac{i\mu\omega k^2}{48\pi^2}\frac{\kappa_R}{\kappa_z}\left(\mathcal{Q}_{nx}\cos\phi+\mathcal{Q}_{ny}\sin\phi\right) = \tilde{A}_{n,xy}^{\mathrm{EQ}}(\kappa_x,\kappa_y;0). \tag{B.S34}$$

As anticipated earlier, special care must be taken with the integral involving the z-dependent contribution of $\ddot{\mathcal{Q}}$. Then, we make use of integration by parts:

$$\tilde{A}_{n,z}^{\mathrm{EQ}}(\kappa_x,\kappa_y;z) = \frac{\mu\omega k^3}{48\pi^2}\int_0^{+\infty}\left(\frac{1}{ik\sqrt{R^2+z^2}}-1\right)\frac{e^{ik\sqrt{R^2+z^2}}}{R^2+z^2}RzJ_0\mathcal{Q}_{nz}dR$$

$$= \begin{Bmatrix} u = J_0 & \Rightarrow & du = -k\kappa_R J_1 dR \\ dv = \left(\dfrac{1}{ik\sqrt{R^2+z^2}}-1\right)\dfrac{Rz}{R^2+z^2}e^{ik\sqrt{R^2+z^2}}dR & \Rightarrow & v = \dfrac{ize^{ik\sqrt{R^2+z^2}}}{k\sqrt{R^2+z^2}} \end{Bmatrix}$$

$$= \frac{\mu\omega k^3}{48\pi^2}\mathcal{Q}_{nz}\left[\frac{iz}{k\sqrt{R^2+z^2}}J_0e^{ik\sqrt{R^2+z^2}}\Big|_{R=0}^{R\to\infty} + \int_0^{+\infty}\frac{iz\kappa_R}{\sqrt{R^2+z^2}}J_1e^{ik\sqrt{R^2+z^2}}dR\right]$$

$$= \frac{\mu\omega k^3}{48\pi^2}\mathcal{Q}_{nz}\left[-\frac{i}{k}\frac{z}{|z|}e^{ik|z|} + \int_0^{+\infty}\frac{iz\kappa_R}{\sqrt{R^2+z^2}}J_1(k\kappa_R R)e^{ik\sqrt{R^2+z^2}}dR\right]$$

$$\xrightarrow[z\to 0]{} \mp\frac{i\mu\omega k^2}{48\pi^2}\mathcal{Q}_{nz} = \tilde{A}_{n,z}^{\mathrm{EQ}}(\kappa_x,\kappa_y;0). \tag{B.S35}$$

Hence, gathering together the above calculations, the spectral amplitude of the electric quadrupole reads

$$\tilde{A}_{0,n}^{\mathrm{EQ}}(\kappa_x,\kappa_y;0) = -\frac{i\mu\omega k^2}{48\pi^2}\frac{1}{\kappa_z}\left[\kappa_R\left(\mathcal{Q}_{nx}\cos\phi+\mathcal{Q}_{ny}\sin\phi\right)\pm k_z\mathcal{Q}_{nz}\right]$$

$$= -\frac{i\mu\omega k^2}{48\pi^2}\frac{1}{\kappa_z}\left[\kappa_x\mathcal{Q}_{nx}+\kappa_y\mathcal{Q}_{ny}\pm\kappa_z\mathcal{Q}_{nz}\right]. \tag{B.S36}$$

Since $\mathbf{k}^{\pm} = k(\kappa_x,\kappa_y,\pm\kappa_z)$ (where signs $+$ and $-$ correspond to $z>0$ and $z<0$, respectively), the above result can be expressed in a closed form:

$$\tilde{\mathbf{A}}_0^{\mathrm{EQ}}(\kappa_x,\kappa_y;0) = \frac{\mu c k^2}{8\pi^2 n}\frac{1}{\kappa_z}\frac{(-i)\left[\ddot{\mathcal{Q}}\cdot\mathbf{k}^{\pm}\right]}{6}. \tag{B.S37}$$

Notice that we have deliberately written down the latter expression in such a way that is straightforward to compare it with the angular spectrum amplitude of the electric dipole [Eq. (B.S21)]. In this respect, it is worth pointing out that we can attain the spectral amplitude of the electric quadrupole from that of the electric dipole by simply performing the substitution $\mathbf{p} \to (-i)\left[\ddot{\mathcal{Q}}\cdot\mathbf{k}^{\pm}\right]/6$. This additional $\mathbf{k}$ dependence on the spectral amplitude has important consequences regarding the spatial range where the evanescent modes have a significant contribution.

B.SM.IV Spectral Amplitudes for the Electric and Magnetic Fields of the Electric Dipole and Quadrupole

Until now, we have been mainly focused on the angular spectra of the vector potentials. However, we are typically more interested in knowing the angular spectrum representation of the EM fields themselves. As has been already pointed out above, we can write the complex fields $\mathbf{E}(\mathbf{r})$ and $\mathbf{H}(\mathbf{r})$ from the standard vector potential $\mathbf{A}(\mathbf{r})$ by means of the following relations:

$$\mathbf{B}(\mathbf{r}) = \nabla \times \mathbf{A}(\mathbf{r}) \qquad \Longrightarrow \qquad \mathbf{H}(\mathbf{r}) = \frac{1}{\mu}[\nabla \times \mathbf{A}(\mathbf{r})]; \tag{B.S38}$$

$$\nabla \times \mathbf{H}(\mathbf{r}) = -i\omega\varepsilon\mathbf{E}(\mathbf{r}) \qquad \Longrightarrow \qquad \mathbf{E}(\mathbf{r}) = \frac{ic}{kn}\left[\nabla\left(\nabla \cdot \mathbf{A}(\mathbf{r})\right) - \nabla^2\mathbf{A}(\mathbf{r})\right]. \tag{B.S39}$$

It should be noted that, for the moment, we skip the usage of Hertz potentials (they will turn out to be relevant below when dealing with EM multipole fields). Taking advantage of the angular spectrum formalism, one can easily represent the complex field amplitudes of both the electric dipole and quadrupole in a compact notation as

$$\begin{aligned}
\tilde{\mathbf{E}}^{\mathrm{ED}}(\kappa_x, \kappa_y; 0) &= \frac{ic}{kn}[k^2\tilde{\mathbf{A}}_0^{\mathrm{ED}} - \mathbf{k}^{\pm}(\mathbf{k}^{\pm} \cdot \tilde{\mathbf{A}}_0^{\mathrm{ED}})] \\
&= \frac{ik}{8\pi^2\varepsilon}\frac{1}{\kappa_z}\left\{k^2\mathbf{p} - \mathbf{k}^{\pm}(\mathbf{k}^{\pm} \cdot \mathbf{p})\right\}, \qquad \text{(B.S40)} \\
\tilde{\mathbf{H}}^{\mathrm{ED}}(\kappa_x, \kappa_y; 0) &= \frac{i}{\mu}[\mathbf{k}^{\pm} \times \tilde{\mathbf{A}}_0^{\mathrm{ED}}] \\
&= \frac{i\omega k}{8\pi^2}\frac{1}{\kappa_z}\left[\mathbf{k}^{\pm} \times \mathbf{p}\right]; \qquad \text{(B.S41)} \\
\tilde{\mathbf{E}}^{\mathrm{EQ}}(\kappa_x, \kappa_y; 0) &= \frac{ic}{kn}[k^2\tilde{\mathbf{A}}_0^{\mathrm{EQ}} - \mathbf{k}^{\pm}(\mathbf{k}^{\pm} \cdot \tilde{\mathbf{A}}_0^{\mathrm{EQ}})] \\
&= \frac{k}{48\pi^2\varepsilon}\frac{1}{\kappa_z}\left\{k^2(\vec{\mathcal{Q}} \cdot \mathbf{k}^{\pm}) - \mathbf{k}^{\pm}[\mathbf{k}^{\pm} \cdot (\vec{\mathcal{Q}} \cdot \mathbf{k}^{\pm})]\right\}, \qquad \text{(B.S42)} \\
\tilde{\mathbf{H}}^{\mathrm{EQ}}(\kappa_x, \kappa_y; 0) &= \frac{i}{\mu}[\mathbf{k}^{\pm} \times \tilde{\mathbf{A}}_0^{\mathrm{EQ}}] \\
&= \frac{\omega k}{48\pi^2}\frac{1}{\kappa_z}[\mathbf{k}^{\pm} \times (\vec{\mathcal{Q}} \cdot \mathbf{k}^{\pm})], \qquad \text{(B.S43)}
\end{aligned}$$

where, so as to avoid cumbersome notation, $\tilde{\mathbf{A}}_0^{\mathrm{ED/EQ}} \equiv \tilde{\mathbf{A}}^{\mathrm{ED/EQ}}(\kappa_x, \kappa_y; z = 0)$. Further simplifications can be made by introducing the polarization vector basis [S11]:

$$\mathbf{e}_s \equiv \frac{\mathbf{e}_z \times \mathbf{k}^{\pm}}{\sqrt{(\mathbf{e}_z \times \mathbf{k}^{\pm}) \cdot (\mathbf{e}_z \times \mathbf{k}^{\pm})}} = \frac{(-\kappa_y, \kappa_x, 0)}{\kappa_R}, \tag{B.S44}$$

$$\mathbf{e}_p^{\pm} \equiv \mathbf{e}_s \times \mathbf{k}^{\pm}/k = \frac{(\pm\kappa_x\kappa_z, \pm\kappa_y\kappa_z, -(\kappa_x^2 + \kappa_y^2))}{\kappa_R}, \tag{B.S45}$$

where the subscripts indicate the s and p polarizations [S9], and $\mathbf{e}_z$ is the unit vector perpendicular to the plane in which we perform the angular spectrum representation. Notice that in the propagating lossless case (i.e., when $\mathbf{k}^{\pm}$ is real), these two polarization

vectors correspond to the usual unit vectors in spherical coordinates $\mathbf{e}_\varphi$ and $\mathbf{e}_\theta$, respectively, and form, together with $\mathbf{k}^\pm/k$ an orthonormal basis. However, even when we consider a complex $\mathbf{k}^\pm$, the triad $\left\{\mathbf{e}_s, \mathbf{e}_p^\pm, \mathbf{k}^\pm/k\right\}$ remains orthonormal as long as we define the inner product as the dot product with no complex conjugation: $\mathbf{e}_s\cdot\mathbf{e}_s = \mathbf{e}_p^\pm\cdot\mathbf{e}_p^\pm = (\mathbf{k}^\pm\cdot\mathbf{k}^\pm)/k^2 = 1$, and $\mathbf{e}_s\cdot\mathbf{e}_p^\pm = \mathbf{k}^\pm\cdot\mathbf{e}_s = \mathbf{k}^\pm\cdot\mathbf{e}_p^\pm = 0$. Moreover, it can be shown that

$$\mathbf{k}^\pm\times\mathbf{e}_s = -k\mathbf{e}_p^\pm, \qquad \mathbf{k}^\pm\times\mathbf{e}_p^\pm = k\mathbf{e}_s. \tag{B.S46}$$

Therefore, taking into account the above relations together with the scalar triple product identity, $\mathbf{A}\cdot(\mathbf{B}\times\mathbf{C}) = \mathbf{B}\cdot(\mathbf{C}\times\mathbf{A}) = \mathbf{C}\cdot(\mathbf{A}\times\mathbf{B})$, we can recast the EM fields as the projections along the polarization vectors:

$$\tilde{\mathbf{E}}^{\mathrm{ED}}(\kappa_x,\kappa_y;0) = \frac{ik^3}{8\pi^2\varepsilon}\frac{1}{\kappa_z}\left\{[\mathbf{e}_s\cdot\mathbf{p}]\mathbf{e}_s + [\mathbf{e}_p^\pm\cdot\mathbf{p}]\mathbf{e}_p^\pm\right\}, \tag{B.S47}$$

$$\tilde{\mathbf{H}}^{\mathrm{ED}}(\kappa_x,\kappa_y;0) = \frac{ik^3}{8\pi^2\varepsilon}\sqrt{\frac{\varepsilon}{\mu}}\frac{1}{\kappa_z}\left\{[\mathbf{e}_p^\pm\cdot\mathbf{p}]\mathbf{e}_s - [\mathbf{e}_s\cdot\mathbf{p}]\mathbf{e}_p^\pm\right\}; \tag{B.S48}$$

$$\tilde{\mathbf{E}}^{\mathrm{EQ}}(\kappa_x,\kappa_y;0) = \frac{k^3}{48\pi^2\varepsilon}\frac{1}{\kappa_z}\left\{[\mathbf{e}_s\cdot(\vec{\mathcal{Q}}\cdot\mathbf{k}^\pm)]\mathbf{e}_s + [\mathbf{e}_p^\pm\cdot(\vec{\mathcal{Q}}\cdot\mathbf{k}^\pm)]\mathbf{e}_p^\pm\right\}, \tag{B.S49}$$

$$\tilde{\mathbf{H}}^{\mathrm{EQ}}(\kappa_x,\kappa_y;0) = \frac{k^3}{48\pi^2\varepsilon}\sqrt{\frac{\varepsilon}{\mu}}\frac{1}{\kappa_z}\left\{[\mathbf{e}_p^\pm\cdot(\vec{\mathcal{Q}}\cdot\mathbf{k}^\pm)]\mathbf{e}_s - [\mathbf{e}_s\cdot(\vec{\mathcal{Q}}\cdot\mathbf{k}^\pm)]\mathbf{e}_p^\pm\right\}. \tag{B.S50}$$

Summarizing all the above, so far we have presented the Weyl's identity, the expression for the angular spectrum representation and the Hertz potentials. We have also sketched the angular spectrum for the particular case of the electric dipole and afterwards, we have performed the corresponding full derivation for the electric quadrupole (notice that we have omitted the magnetic dipole as yet; see appendix for details). This has enabled us to get the spectral representation of the EM fields in a very simple manner in terms of the s and p transverse unit vectors. Even so, this approach essentially relies on the ability to determine firstly the vector potential from the following expansion [S8]:

$$\mathbf{A}(\mathbf{r}) = \frac{\mu}{4\pi}\int_{-\infty}^{+\infty}\mathbf{J}(\mathbf{r}')\frac{e^{ik|\mathbf{r}-\mathbf{r}'|}}{|\mathbf{r}-\mathbf{r}'|}d\mathbf{r}'. \tag{B.S51}$$

Moreover we must be able to identify either the electric or the magnetic nature of the corresponding optical source. Thus, to find a formulation as general as possible, including the angular spectrum representation of any multipole field, we would have to go through higher-order terms in the previous expansion of the standard vector potential one by one. However, as pointed out by Jackson in Ref. [S8], this is only feasible for the lowest orders, i.e., just for the electric and magnetic dipole, or even for the electric quadrupole at best:

> *"[...] The labor involved in manipulating higher terms in expansion of the vector potential becomes increasingly prohibitive as the expansion is extended beyond the electric quadrupole terms. Another disadvantage of the present approach is that physically distinct fields such as those of the magnetic dipole and the electric quadrupole must be disentangled from the separate terms [...]"*

Owing to these considerations, in the next section we shall draw on the concepts previously introduced to provide a more suitable and systematic formulation for multipolar sources of arbitrary order.

B.SM.V Angular Spectrum Representation of the Electromagnetic Multipole Fields

In this section we aim to find the angular spectrum representation of the general electric and magnetic multipole fields. Leaving aside the detailed procedure to obtain their explicit expressions, which can be found elsewhere (see, e.g., Refs. [S2,S8]), the electric (e) and magnetic (m) multipole fields of arbitrary order can be written as follows:

$$\mathbf{H}^{(\mathrm{e})}_{l,m}(\mathbf{r}) = \frac{f_l(kr)}{\sqrt{l(l+1)}}\mathbf{L}Y_{l,m}(\Omega), \tag{B.S52}$$

$$\mathbf{E}^{(\mathrm{e})}_{l,m}(\mathbf{r}) = \frac{i}{\varepsilon\omega}[\nabla\times\mathbf{H}^{(\mathrm{e})}_{l,m}(\mathbf{r})], \tag{B.S53}$$

$$\mathbf{E}^{(\mathrm{m})}_{l,m}(\mathbf{r}) = \frac{\mu c}{n}\frac{f_l(kr)}{\sqrt{l(l+1)}}\mathbf{L}Y_{l,m}(\Omega), \tag{B.S54}$$

$$\mathbf{H}^{(\mathrm{m})}_{l,m}(\mathbf{r}) = -\frac{i}{\mu\omega}[\nabla\times\mathbf{E}^{(\mathrm{m})}_{l,m}(\mathbf{r})], \tag{B.S55}$$

where $Y_{l,m}(\Omega)$ are the spherical harmonics of order (l,m), $\Omega \equiv (\theta,\varphi)$ stands for the standard angular coordinates (i.e., polar and azimuthal angles, respectively), $f_l(kr) \equiv \{j_l(kr), y_l(kr)\}$ are the l-dependent spherical Bessel functions of first and second kind, and $\mathbf{L} \equiv -i\,(\mathbf{r}\times\nabla)$ is the orbital angular momentum operator. Since there are two independent radial dependent solutions [$j_l(kr)$ and $y_l(kr)$], any linear combination will also be a solution, and specifically the spherical Hankel functions $h_l^{(\pm)}(kr) = j_l(kr) \pm iy_l(kr)$ are used to represent propagating spherical waves.

Rather than dealing with the EM fields themselves, it is convenient to resort to the vector potentials. In this case, however, instead of considering the standard vector potentials, we will use a formulation based on the Hertz potentials to treat the electric and magnetic multipole fields on an equal footing. Under this representation, the first step will consist in determining an explicit expression for both the electric and magnetic Hertz potentials associated to the multipole fields of arbitrary order. This can be easily done just by looking at the Eqs. (B.S10) and (B.S11), which allow us to relate the magnetic and the electric fields to the electric and magnetic Hertz potentials, respectively:

$$\mathbf{H}^{(\mathrm{e})}_{l,m}(\mathbf{r}) = -i\omega[\nabla\times\mathbf{\Pi}^{(\mathrm{e})}_{l,m}(\mathbf{r})], \tag{B.S56}$$

$$\mathbf{E}^{(\mathrm{m})}_{l,m}(\mathbf{r}) = i\mu_0\omega[\nabla\times\mathbf{\Pi}^{(\mathrm{m})}_{l,m}(\mathbf{r})]. \tag{B.S57}$$

Taking also into account the definitions given in Eqs. (B.S52) and (B.S54) it follows that

$$\begin{aligned}\mathbf{H}^{(\mathrm{e})}_{l,m}(\mathbf{r}) &= -i\omega[\nabla\times\mathbf{\Pi}^{(\mathrm{e})}_{l,m}(\mathbf{r})]\\ &= \frac{h_l(kr)}{\sqrt{l(l+1)}}\mathbf{L}Y_{l,m}(\Omega) = \frac{h_l(kr)}{i\sqrt{l(l+1)}}\left[\mathbf{r}\times\nabla Y_{l,m}(\Omega)\right],\end{aligned} \tag{B.S58}$$

$$\begin{aligned}\mathbf{E}^{(\mathrm{m})}_{l,m}(\mathbf{r}) &= i\mu_0\omega[\nabla\times\mathbf{\Pi}^{(\mathrm{m})}_{l,m}(\mathbf{r})]\\ &= \frac{\mu c}{n}\frac{h_l(kr)}{\sqrt{l(l+1)}}\mathbf{L}Y_{l,m}(\Omega) = \frac{\mu c}{n}\frac{h_l(kr)}{i\sqrt{l(l+1)}}\left[\mathbf{r}\times\nabla Y_{l,m}(\Omega)\right],\end{aligned} \tag{B.S59}$$

where we have particularized the spherical Hankel functions as the radial functions. With the help of the identity $\mathbf{v}\times\nabla f = f\nabla\times\mathbf{v} - \nabla\times(f\mathbf{v})$, the latter expressions can be recast as

$$\begin{aligned}\mathbf{H}^{(\mathrm{e})}_{l,m}(\mathbf{r}) &= \frac{h_l(kr)}{i\sqrt{l(l+1)}}\left[Y_{l,m}(\Omega)\nabla\times\mathbf{r} - \nabla\times(Y_{l,m}(\Omega)\mathbf{r})\right] \\ &= i\frac{h_l(kr)}{\sqrt{l(l+1)}}\left[\nabla\times(Y_{l,m}(\Omega)\mathbf{r})\right], \qquad \text{(B.S60)}\\ \mathbf{E}^{(\mathrm{m})}_{l,m}(\mathbf{r}) &= \frac{\mu c}{n}\frac{h_l(kr)}{i\sqrt{l(l+1)}}[Y_{l,m}(\Omega)\nabla\times\mathbf{r} - \nabla\times(Y_{l,m}(\Omega)\mathbf{r})] \\ &= \frac{i\mu c}{n}\frac{h_l(kr)}{\sqrt{l(l+1)}}[\nabla\times(Y_{l,m}(\Omega)\mathbf{r})], \qquad \text{(B.S61)}\end{aligned}$$

where we used the fact that $\nabla\times\mathbf{r} = 0$. It is important to realize that, since the only vector component is the radial one, we can judiciously insert the r-dependent prefactor inside the curl operator:

$$\mathbf{H}^{(\mathrm{e})}_{l,m}(\mathbf{r}) = \nabla\times\left(\frac{i}{\sqrt{l(l+1)}}rh_l(kr)Y_{l,m}(\Omega)\mathbf{e}_r\right), \qquad \text{(B.S62)}$$

$$\mathbf{E}^{(\mathrm{m})}_{l,m}(\mathbf{r}) = \nabla\times\left(\frac{i\mu c}{n\sqrt{l(l+1)}}rh_l(kr)Y_{l,m}(\Omega)\mathbf{e}_r\right). \qquad \text{(B.S63)}$$

By comparing these results with the definitions of the EM multipole fields in terms of the Hertz potentials [see Eqs. (B.S56) and (B.S57)], it is straightforward to show that a first attempt at finding potentials for arbitrary electric and magnetic multipole fields leads to

$$\mathbf{\Pi}^{\mathrm{rad(e)}}_{l,m}(\mathbf{r}) = -\frac{1}{\omega\sqrt{l(l+1)}}rh_l(kr)Y_{l,m}(\Omega)\mathbf{e}_r, \qquad \text{(B.S64)}$$

$$\mathbf{\Pi}^{\mathrm{rad(m)}}_{l,m}(\mathbf{r}) = \sqrt{\frac{\mu_r}{\varepsilon_r}}\frac{c}{\omega\sqrt{l(l+1)}}rh_l(kr)Y_{l,m}(\Omega)\mathbf{e}_r. \qquad \text{(B.S65)}$$

However, despite their simplicity, it can be demonstrated that the above expressions fail when we attempt to address the angular spectrum representation. This is because they do not satisfy the Helmholtz wave equation: $\left(\nabla^2 + k^2\right)\mathbf{\Pi}^{\mathrm{rad(e/m)}}_{l,m} \neq 0$. Therefore, referring to $\mathbf{\Pi}^{\mathrm{rad(e/m)}}_{l,m}$ as the Hertz potentials is somehow an abuse of terminology. Nonetheless, we can overcome this issue just by adding the corresponding gradient of the electric- and magnetic-like gauge functions:

$$\chi^{(\mathrm{e})}_{l,m}(\mathbf{r}) = -\frac{1}{\omega\sqrt{l(l+1)}}\frac{r}{k}h_{l-1}(kr)Y_{l,m}(\Omega), \qquad \text{(B.S66)}$$

$$\chi^{(\mathrm{m})}_{l,m}(\mathbf{r}) = \sqrt{\frac{\mu_r}{\varepsilon_r}}\frac{c}{\omega\sqrt{l(l+1)}}\frac{r}{k}h_{l-1}(kr)Y_{l,m}(\Omega). \qquad \text{(B.S67)}$$

Hence, the vector potentials now read as

$$\begin{aligned}\mathbf{\Pi}_{l,m}^{(\mathrm{e})} &= \mathbf{\Pi}_{l,m}^{\mathrm{rad(e)}} + \nabla\chi_{l,m}^{(\mathrm{e})} \\ &= -\frac{1}{\omega k\sqrt{l(l+1)}}\left\{krh_l(kr)Y_{l,m}(\Omega)\mathbf{e}_r + \nabla\left[rh_{l-1}(kr)Y_{l,m}(\Omega)\right]\right\}, \qquad \text{(B.S68)}\\ \mathbf{\Pi}_{l,m}^{(\mathrm{m})} &= \mathbf{\Pi}_{l,m}^{\mathrm{rad(m)}} + \nabla\chi_{l,m}^{(\mathrm{m})} \\ &= \sqrt{\frac{\mu_r}{\varepsilon_r}}\frac{c}{\omega k\sqrt{l(l+1)}}\left\{krh_l(kr)Y_{l,m}(\Omega)\mathbf{e}_r + \nabla\left[rh_{l-1}(kr)Y_{l,m}(\Omega)\right]\right\}. \qquad \text{(B.S69)}\end{aligned}$$

These results can be further simplified by expanding the gradient of the gauge function:

$$\begin{aligned}\nabla\left[rh_{l-1}(kr)Y_{l,m}(\Omega)\right] &= \left[h_{l-1}(kr) + r\partial_r h_{l-1}(kr)\right]Y_{l,m}(\Omega)\mathbf{e}_r + rh_{l-1}(kr)\nabla Y_{l,m}(\Omega) \\ &= \left[krh_{l-2} - (l-1)h_{l-1}(kr)\right]Y_{l,m}(\Omega)\mathbf{e}_r + rh_{l-1}(kr)\nabla Y_{l,m}(\Omega). \qquad \text{(B.S70)}\end{aligned}$$

By means of the recurrence relation $krh_{l-2} - (l-1)h_{l-1} + krh_l = lh_{l-1}$ we then arrive at

$$\mathbf{\Pi}_{l,m}^{(\mathrm{e})}(\mathbf{r}) = -\frac{1}{\omega k\sqrt{l(l+1)}}h_{l-1}(kr)\left[lY_{l,m}(\Omega)\mathbf{e}_r + r\nabla Y_{l,m}(\Omega)\right], \qquad \text{(B.S71)}$$

$$\mathbf{\Pi}_{l,m}^{(\mathrm{m})}(\mathbf{r}) = \sqrt{\frac{\mu_r}{\varepsilon_r}}\frac{c}{\omega k\sqrt{l(l+1)}}h_{l-1}(kr)\left[lY_{l,m}(\Omega)\mathbf{e}_r + r\nabla Y_{l,m}(\Omega)\right]. \qquad \text{(B.S72)}$$

Furthermore, aiming to get a closed expression, we make use of the explicit definition of the spherical harmonics [S8]:

$$Y_{l,m}(\Omega) \equiv \sqrt{\frac{2l+1}{4\pi}\frac{(l-m)!}{(l+m)!}}P_l^m(\cos\theta)e^{im\varphi} = C_{l,m}P_l^m(\cos\theta)e^{im\varphi}, \qquad \text{(B.S73)}$$

where $P_l^m(\cos\theta)$ are the associated Legendre polynomials of degree l and order m, and $C_{l,m}$ is used as a shorthand notation for the prefactor. In addition, it should be noted that $Y_{l,-m} = (-1)^m Y_{l,m}^*$, with the asterisk denoting complex conjugation. Then, it can be shown that

$$lY_{l,m}(\Omega)\mathbf{e}_r + r\nabla Y_{l,m}(\Omega) = C_{l,m}\left[lP_l^m(\cos\theta)\mathbf{e}_r + \partial_\theta P_l^m(\cos\theta)\mathbf{e}_\theta + \frac{im}{\sin\theta}P_l^m(\cos\theta)\mathbf{e}_\varphi\right]e^{im\varphi}, \qquad \text{(B.S74)}$$

where $\mathbf{e}_r \equiv (\sin\theta\cos\varphi, \sin\theta\sin\varphi, \cos\theta)$, $\mathbf{e}_\theta \equiv (\cos\theta\cos\varphi, \cos\theta\sin\varphi, -\sin\theta)$, and $\mathbf{e}_\varphi \equiv (-\sin\varphi, \cos\varphi, 0)$, are the spherical unit vectors in Cartesian basis. Finally, after some straightforward but lengthy manipulations we arrive at a closed expression for a valid Hertz potential of any electric and magnetic multipolar source of arbitrary order:

$$\mathbf{\Pi}_{l,m}^{(\mathrm{e})}(\mathbf{r}) = -\frac{C_{l,m}h_{l-1}(kr)}{\omega k\sqrt{l(l+1)}}\left[\alpha_{l,m}\cos\varphi - m\beta_{l,m}e^{i\varphi}, \alpha_{l,m}\sin\varphi + im\beta_{l,m}e^{i\varphi}, \gamma_{l,m}\right]e^{im\varphi}, \qquad \text{(B.S75)}$$

and

$$\mathbf{\Pi}_{l,m}^{(\mathrm{m})}(\mathbf{r}) = -c\sqrt{\frac{\mu_r}{\varepsilon_r}}\mathbf{\Pi}_{l,m}^{(\mathrm{e})}(\mathbf{r}), \qquad \text{(B.S76)}$$

with

$$\alpha_{l,m}(\theta) = \frac{1}{\sin\theta}\left[(l+m)\left(P_l^m(\cos\theta) - \cos\theta P_{l-1}^m(\cos\theta)\right)\right], \tag{B.S77a}$$

$$\beta_{l,m}(\theta) = \frac{1}{\sin\theta}P_l^m(\cos\theta), \tag{B.S77b}$$

$$\gamma_{l,m}(\theta) = (l+m)P_{l-1}^m(\cos\theta). \tag{B.S77c}$$

As we can see, using spherical coordinates, the radial, polar and azimuthal dependences appear to be separated, thereby simplifying the subsequent calculations of the partial Fourier transform. In addition, it should also be noted that these expressions can be greatly simplified when we restrict ourselves to the plane $z = 0$, i.e., for $\theta = \pi/2$. In fact, in this particular case the θ-dependent functions become,

$$\alpha_{l,m}(\pi/2) = (l+m)\,P_l^m(0) = \left(\frac{l+m}{l+m+1}\right)\gamma_{l+1,m}(\pi/2), \tag{B.S78a}$$

$$\beta_{l,m}(\pi/2) = P_l^m(0) = \left(\frac{1}{l+m+1}\right)\gamma_{l+1,m}(\pi/2), \tag{B.S78b}$$

$$\gamma_{l,m}(\pi/2) = (l+m)\,P_{l-1}^m(0), \tag{B.S78c}$$

where

$$P_l^m(0) = \begin{cases} (-1)^{l+\frac{l-m}{2}}\dfrac{(l-m+2m)!}{2^l\left(\frac{l-m}{2}\right)!\left(\frac{l+m}{2}\right)!}, & \text{for} \quad l+m \quad \text{even;} \\ 0 & \text{for} \quad l+m \quad \text{odd.} \end{cases} \tag{B.S79}$$

Having an explicit expression for both the electric and magnetic Hertz vector potential [Eqs. (B.S75) and (B.S76)], we now proceed with finding their angular spectrum at the plane $z = 0$. Indeed, since $\mathbf{\Pi}_{l,m}^{(\mathrm{e})}$ (and consequently $\mathbf{\Pi}_{l,m}^{(\mathrm{m})}$) satisfies the Helmholtz equation, the spectral amplitudes of the electric multipole fields are given by the partial Fourier transform of Eq. (B.S75):

$$\begin{aligned}\tilde{\mathbf{\Pi}}_{l,m}^{(\mathrm{e})}(\kappa_x,\kappa_y;z) &= \left(\frac{k}{2\pi}\right)^2\iint_{-\infty}^{+\infty}\mathbf{\Pi}_{l,m}^{(\mathrm{e})}(x,y,z)e^{-ik(\kappa_x x+\kappa_y y)}dxdy \\ &= \frac{-k}{4\pi^2\omega}\frac{C_{l,m}}{\sqrt{l(l+1)}}\int_0^{+\infty}\int_0^{2\pi}h_{l-1}(kr)\left\{\mathcal{X}_{l,m}^{(\mathrm{e})},\mathcal{Y}_{l,m}^{(\mathrm{e})},\mathcal{Z}_{l,m}^{(\mathrm{e})}\right\}e^{-ik\kappa_R r\sin\theta\cos(\varphi-\phi)}r\sin\theta d\varphi dr,\end{aligned} \tag{B.S80}$$

where

$$\mathcal{X}_{l,m}^{(\mathrm{e})}(\Omega) = \left[\alpha_{l,m}(\theta)\cos\varphi - m\beta_{l,m}(\theta)e^{i\varphi}\right]e^{im\varphi}, \tag{B.S81}$$

$$\mathcal{Y}_{l,m}^{(\mathrm{e})}(\Omega) = \left[\alpha_{l,m}(\theta)\sin\varphi + im\beta_{l,m}(\theta)e^{i\varphi}\right]e^{im\varphi}, \tag{B.S82}$$

$$\mathcal{Z}_{l,m}^{(\mathrm{e})}(\Omega) = \gamma_{l,m}(\theta)e^{im\varphi}. \tag{B.S83}$$

To perform the integration along the angle φ we will consider each of the vector components separately:

$$\begin{aligned}\int_0^{2\pi} \mathcal{X}_{l,m}^{(\mathrm{e})} e^{-ik\kappa_R r\sin\theta\cos(\varphi-\phi)}d\varphi &= \int_0^{2\pi} \alpha_{l,m}\cos\varphi e^{i(m\varphi-k\kappa_R r\sin\theta\cos(\varphi-\phi))}d\varphi \\ &\quad - \int_0^{2\pi} m\beta_{l,m} e^{i[(m+1)\varphi-k\kappa_R r\sin\theta\cos(\varphi-\phi)]}d\varphi \\ &= \pi(-i)^{m+1}\left[(\alpha_{l,m}-2m\beta_{l,m})\,J_{m+1}(k\kappa_R r\sin\theta)e^{i\phi} - \alpha_{l,m}J_{m-1}(k\kappa_R r\sin\theta)e^{-i\phi}\right]e^{im\phi},\end{aligned}$$

$$\begin{aligned}\int_0^{2\pi} \mathcal{Y}_{l,m}^{(\mathrm{e})} e^{-ik\kappa_R r\sin\theta\cos(\varphi-\phi)}d\varphi &= \int_0^{2\pi} \alpha_{l,m}\sin\varphi e^{i(m\varphi-k\kappa_R r\sin\theta\cos(\varphi-\phi))}d\varphi \\ &\quad + \int_0^{2\pi} im\beta_{l,m} e^{i[(m+1)\varphi-k\kappa_R r\sin\theta\cos(\varphi-\phi)]}d\varphi \\ &= \pi(-i)^{m}\left[(2m\beta_{l,m}-\alpha_{l,m})\,J_{m+1}(k\kappa_R r\sin\theta)e^{i\phi} - \alpha_{l,m}J_{m-1}(k\kappa_R r\sin\theta)e^{-i\phi}\right]e^{im\phi},\end{aligned}$$

$$\begin{aligned}\int_0^{2\pi} \mathcal{Z}_{l,m}^{(\mathrm{e})} e^{-ik\kappa_R r\sin\theta\cos(\varphi-\phi)}d\varphi &= \int_0^{2\pi} \gamma_{l,m} e^{i(m\varphi-k\kappa_R r\sin\theta\cos(\varphi-\phi))}d\varphi \\ &= 2\pi\,(-i)^m\,\gamma_{l,m}J_m(k\kappa_R r\sin\theta)e^{im\phi}.\end{aligned}$$

Even though these results appear to be somewhat complicated, we still have to carry out the integration along the radius and particularize to the case of the plane $z=0$. Thereupon, it turns out to be more convenient to express the latter integrals in cylindrical coordinates:

$$\tilde{\mathbf{\Pi}}_{l,m}^{(\mathrm{e})}(\kappa_x,\kappa_y;z) = \frac{-k}{4\pi\omega}\frac{(-i)^m C_{l,m}}{\sqrt{l(l+1)}}\int_0^{+\infty}\left\{\tilde{\mathcal{X}}_{l,m}^{(\mathrm{e})}(R,z),\tilde{\mathcal{Y}}_{l,m}^{(\mathrm{e})}(R,z),\tilde{\mathcal{Z}}_{l,m}^{(\mathrm{e})}(R,z)\right\}dR, \quad \text{(B.S84)}$$

where $R\equiv r\sin\theta$, $z\equiv r\cos\theta$, and

$$\tilde{\mathcal{X}}_{l,m}^{(\mathrm{e})}(R,z) = h_{l-1}(k\sqrt{R^2+z^2})R\left[(2im\beta_{l,m}-i\alpha_{l,m})\,J_{m+1}(k\kappa_R R)e^{i\phi}+i\alpha_{l,m}J_{m-1}(k\kappa_R R)e^{-i\phi}\right]e^{im\phi}, \quad \text{(B.S85)}$$

$$\tilde{\mathcal{Y}}_{l,m}^{(\mathrm{e})}(R,z) = h_{l-1}(k\sqrt{R^2+z^2})R\left[(2m\beta_{l,m}-\alpha_{l,m})\,J_{m+1}(k\kappa_R R)e^{i\phi}-\alpha_{l,m}J_{m-1}(k\kappa_R R)e^{-i\phi}\right]e^{im\phi}, \quad \text{(B.S86)}$$

$$\tilde{\mathcal{Z}}_{l,m}^{(\mathrm{e})}(R,z) = h_{l-1}(k\sqrt{R^2+z^2})R[2\gamma_{l,m}J_m(k\kappa_R R)]e^{im\phi}. \quad \text{(B.S87)}$$

The explicit integrand functions given above are presented up to the fourth order in Table B.SI. From these results we can make an important observation: for each l-order, the different mathematical structures appearing in the x and y components (i.e., in the functions $\tilde{\mathcal{X}}_{l,m}^{(\mathrm{e})}$ and $\tilde{\mathcal{Y}}_{l,m}^{(\mathrm{e})}$), are actually linear combinations of the ones that appear in the z component. Moreover, it can be seen that $\tilde{\mathcal{Z}}_{l,m}^{(\mathrm{e})}(R,z)=0$ for all $l=m$. Therefore the problem is strongly reduced to the analysis of l integrals associated to the z component

$\{l,m\}$	$\tilde{\mathcal{X}}^{(\mathrm{e})}_{l,m}(R,z)$	$\tilde{\mathcal{Y}}^{(\mathrm{e})}_{l,m}(R,z)$	$\tilde{\mathcal{Z}}^{(\mathrm{e})}_{l,m}(R,z)$
$\{1,0\}$	0	0	$2Rh_0J_0$
$\{1,1\}$	$-2iRh_0J_0$	$2Rh_0J_0$	0
$\{2,0\}$	$\left[\frac{2iR^2h_1J_1}{(R^2+z^2)^{1/2}}\right]\cos\phi$	$\left[\frac{2iR^2h_1J_1}{(R^2+z^2)^{1/2}}\right]\sin\phi$	$\frac{4Rzh_1J_0}{(R^2+z^2)^{1/2}}$
$\{2,1\}$	$\frac{-6iRzh_1J_0}{(R^2+z^2)^{1/2}}$	$\frac{6Rzh_1J_0}{(R^2+z^2)^{1/2}}$	$\left[\frac{-6R^2h_1J_1}{(R^2+z^2)^{1/2}}\right]e^{i\phi}$
$\{2,2\}$	$\left[\frac{12iR^2h_1J_1}{(R^2+z^2)^{1/2}}\right]e^{i\phi}$	$\left[\frac{-12R^2h_1J_1}{(R^2+z^2)^{1/2}}\right]e^{i\phi}$	0
$\{3,0\}$	$\left[\frac{6iR^2zh_2J_1}{R^2+z^2}\right]\cos\phi$	$\left[\frac{6iR^2zh_2J_1}{R^2+z^2}\right]\sin\phi$	$\frac{-3R(R^2-2z^2)h_2J_0}{R^2+z^2}$
$\{3,1\}$	$\frac{3iRh_2\left[2(R^2-2z^2)J_0-R^2J_2e^{2i\phi}\right]}{R^2+z^2}$	$\frac{-3Rh_2\left[2(R^2-2z^2)J_0+R^2J_2e^{2i\phi}\right]}{R^2+z^2}$	$\left[\frac{-24R^2zh_2J_1}{R^2+z^2}\right]e^{i\phi}$
$\{3,2\}$	$\left[\frac{60iR^2zh_2J_1}{R^2+z^2}\right]e^{i\phi}$	$\left[\frac{-60R^2zh_2J_1}{R^2+z^2}\right]e^{i\phi}$	$\left[\frac{30R^3h_2J_2}{R^2+z^2}\right]e^{2i\phi}$
$\{3,3\}$	$\left[\frac{-90iR^3h_2J_2}{R^2+z^2}\right]e^{2i\phi}$	$\left[\frac{90R^3h_2J_2}{R^2+z^2}\right]e^{2i\phi}$	0
$\{4,0\}$	$\left[\frac{-3iR^2(R^2-4z^2)h_3J_1}{(R^2+z^2)^{3/2}}\right]\cos\phi$	$\left[\frac{-3iR^2(R^2-4z^2)h_3J_1}{(R^2+z^2)^{3/2}}\right]\sin\phi$	$\frac{-4Rz(3R^2-2z^2)h_3J_0}{(R^2+z^2)^{3/2}}$
$\{4,1\}$	$\frac{5iRzh_3\left[2(3R^2-2z^2)J_0-3R^2J_2e^{2i\phi}\right]}{(R^2+z^2)^{3/2}}$	$\frac{-5Rzh_3\left[2(3R^2-2z^2)J_0+3R^2J_2e^{2i\phi}\right]}{(R^2+z^2)^{3/2}}$	$\left[\frac{15R^2(R^2-4z^2)h_3J_1}{(R^2+z^2)^{3/2}}\right]e^{i\phi}$
$\{4,2\}$	$\left[\frac{-15iR^2h_3\left[3(R^2-4z^2)J_1-R^2J_3e^{2i\phi}\right]}{(R^2+z^2)^{3/2}}\right]e^{i\phi}$	$\left[\frac{15R^2h_3\left[3(R^2-4z^2)J_1+R^2J_3e^{2i\phi}\right]}{(R^2+z^2)^{3/2}}\right]e^{i\phi}$	$\left[\frac{180R^3zh_3J_2}{(R^2+z^2)^{3/2}}\right]e^{2i\phi}$
$\{4,3\}$	$\left[\frac{-630iR^3zh_3J_2}{(R^2+z^2)^{3/2}}\right]e^{2i\phi}$	$\left[\frac{630R^3zh_3J_2}{(R^2+z^2)^{3/2}}\right]e^{2i\phi}$	$\left[\frac{-210R^4h_3J_3}{(R^2+z^2)^{3/2}}\right]e^{3i\phi}$
$\{4,4\}$	$\left[\frac{840iR^4h_3J_3}{(R^2+z^2)^{3/2}}\right]e^{3i\phi}$	$\left[\frac{-840R^4h_3J_3}{(R^2+z^2)^{3/2}}\right]e^{3i\phi}$	0

Table B.SI: Spectral amplitudes of the Hertz potential associated to the first four electric-like multipole moments.

for each order l. Taking into account these considerations, in order to find a closed and analytical result, we shall first look into the possibility of integrating $\tilde{\mathcal{Z}}^{(\mathrm{e})}_{l,m}(R,z)$ for these particular cases. This involves a judicious choice of integration by parts in those cases in

which setting $z = 0$ seems to cancel out the whole integral, greatly reminiscent of what happened in the previous case of the electric quadrupole. Thus, for the case $l = 1$:

$$\int_0^{+\infty} Rh_0(k\sqrt{R^2+z^2})P_0^0\left[\frac{z}{\sqrt{R^2+z^2}}\right]J_0 dR = \frac{-i}{k}\int_0^{+\infty}\frac{Re^{ik\sqrt{R^2+z^2}}}{\sqrt{R^2+z^2}}J_0 dR$$
$$\xrightarrow[z\to 0]{} \frac{-i}{k}\int_0^{+\infty} e^{ikR}J_0 dR = \frac{1}{k^2\kappa_z}. \tag{B.S88}$$

For $l = 2$:

$$\int_0^{+\infty} Rh_1(k\sqrt{R^2+z^2})P_1^1\left[\frac{z}{\sqrt{R^2+z^2}}\right]J_1 dR = \frac{1}{k}\int_0^{+\infty}\left(1-\frac{1}{ik\sqrt{R^2+z^2}}\right)\frac{R^2e^{ik\sqrt{R^2+z^2}}}{R^2+z^2}J_1 dR$$
$$\xrightarrow[z\to 0]{} \frac{1}{k}\int_0^{+\infty}\left(1-\frac{1}{ikR}\right)e^{ikR}J_1 dR = -\frac{\kappa_R}{k^2\kappa_z}; \tag{B.S89}$$

$$\int_0^{+\infty} Rh_1(k\sqrt{R^2+z^2})P_1^0\left[\frac{z}{\sqrt{R^2+z^2}}\right]J_0 dR = \int_0^{+\infty}\left(\frac{1}{ik\sqrt{R^2+z^2}}-1\right)\frac{Rze^{ik\sqrt{R^2+z^2}}}{k(R^2+z^2)}J_0 dR$$
$$= \begin{Bmatrix} u = J_0 & \Longrightarrow & du = -k\kappa_R J_1 dR \\ dv = Rh_1P_1^1 dR & \Longrightarrow & v = -\dfrac{\sqrt{R^2+z^2}}{k}h_0P_1^0 \end{Bmatrix}$$
$$= -\frac{i}{k^2}\frac{z}{|z|}e^{ik|z|} - \kappa_R\int_0^{+\infty}\sqrt{R^2+z^2}h_0P_1^0J_1 dR$$
$$\xrightarrow[z\to 0]{} \mp\frac{i}{k^2}. \tag{B.S90}$$

For the case $l = 3$ we have that:

$$\int_0^{+\infty} Rh_2(k\sqrt{R^2+z^2})P_2^2\left[\frac{z}{\sqrt{R^2+z^2}}\right]J_2 dR = \frac{i}{k}\int_0^{+\infty}\left(3+\frac{9i}{k\sqrt{R^2+z^2}}-\frac{9}{k^2(R^2+z^2)}\right)\frac{R^3e^{ik\sqrt{R^2+z^2}}}{(R^2+z^2)^{3/2}}J_2 dR$$
$$\xrightarrow[z\to 0]{} \frac{i}{k}\int_0^{+\infty}\left(3+\frac{9i}{kR}-\frac{9}{k^2R^2}\right)e^{ikR}J_2 dR = \frac{3\kappa_R^2}{k^2\kappa_z}; \tag{B.S91}$$

$$\int_0^{+\infty} Rh_2(k\sqrt{R^2+z^2})P_2^1\left[\frac{z}{\sqrt{R^2+z^2}}\right]J_1 dR = \frac{i}{k}\int_0^{+\infty}\left(\frac{9}{k^2(R^2+z^2)}-\frac{9i}{k\sqrt{R^2+z^2}}-3\right)\frac{R^2ze^{ik\sqrt{R^2+z^2}}}{(R^2+z^2)^{3/2}}J_1 dR$$
$$= \begin{Bmatrix} u = RJ_1 & \Longrightarrow & du = k\kappa_R RJ_0 dR \\ dv = h_2P_2^1 dR & \Longrightarrow & v = \dfrac{3}{k}h_1P_1^0 \end{Bmatrix}$$
$$= \frac{3R}{k}h_1P_1^0J_1\Big|_{R=0}^{R\to\infty} - 3\kappa_R\int_0^{+\infty}Rh_1P_1^0J_0 dR$$
$$\xrightarrow[z\to 0]{} \pm\frac{3i\kappa_R}{k^2}; \tag{B.S92}$$

$$\int_0^{+\infty} Rh_2(k\sqrt{R^2+z^2})P_2^0\left[\frac{z}{\sqrt{R^2+z^2}}\right]J_0dR = \frac{i}{k}\int_0^{+\infty}\left(\frac{3}{k^2\sqrt{R^2+z^2}} - \frac{3i}{k\sqrt{R^2+z^2}} - 1\right)\frac{R(R^2-2z^2)e^{ik\sqrt{R^2+z^2}}}{2(R^2+z^2)^{3/2}}J_0dR$$

$$= \left\{\begin{array}{lll} u = J_0 & \Longrightarrow & du = -k\kappa_R J_1 dR \\ dv = Rh_2P_2^0dR & \Longrightarrow & v = \left[2kz^2\sqrt{R^2+z^2} - R^2(3i+k\sqrt{R^2+z^2})\right]\dfrac{e^{ik\sqrt{R^2+z^2}}}{2k^3(R^2+z^2)^{3/2}} \end{array}\right\}$$

$$= -\frac{e^{ik|z|}}{k^2} + \kappa_R\int_0^{+\infty}\left[\frac{2kz^2\sqrt{R^2+z^2} - R^2(3i+k\sqrt{R^2+z^2})}{2k^2(R^2+z^2)^{3/2}}\right]e^{ik\sqrt{R^2+z^2}}J_1dR$$

$$\xrightarrow[z\to 0]{} -\frac{1}{k^2} - \kappa_R\int_0^{+\infty}\frac{(3i+kR)e^{ikR}}{2k^2R}J_1dR = \frac{3\kappa_R^2-2}{2k^2\kappa_z}. \tag{B.S93}$$

And finally, for the case $l = 4$:

$$\int_0^{+\infty} Rh_3(k\sqrt{R^2+z^2})P_3^3\left[\frac{z}{\sqrt{R^2+z^2}}\right]J_3(k\kappa_R R)dR \xrightarrow[z\to 0]{} \frac{-15\kappa_R^3}{k^2\kappa_z}; \tag{B.S94}$$

$$\int_0^{+\infty} Rh_3(k\sqrt{R^2+z^2})P_3^2\left[\frac{z}{\sqrt{R^2+z^2}}\right]J_2(k\kappa_R R)dR \xrightarrow[z\to 0]{} \mp\frac{15i\kappa_R^2}{k^2}; \tag{B.S95}$$

$$\int_0^{+\infty} Rh_3(k\sqrt{R^2+z^2})P_3^1\left[\frac{z}{\sqrt{R^2+z^2}}\right]J_1(k\kappa_R R)dR \xrightarrow[z\to 0]{} \frac{3\kappa_R(4-5\kappa_R^2)}{2k^2\kappa_z}; \tag{B.S96}$$

$$\int_0^{+\infty} Rh_3(k\sqrt{R^2+z^2})P_3^0\left[\frac{z}{\sqrt{R^2+z^2}}\right]J_0(k\kappa_R R)dR \xrightarrow[z\to 0]{} \mp\frac{i(5\kappa_R^2-2)}{2k^2}. \tag{B.S97}$$

After verifying that all the integrands showed in Table B.SI are actually integrable functions, we are in the position to derive a general formula enabling this integration for all the possible cases of l and m. To this aim, we first observe that the above integrals involving the radial variable all have the same form:

$$\mathcal{K}_{l,m}^{l',m'}(k,\kappa_R;z) = \int_0^{+\infty} Rh_{l-1}\left(k\sqrt{R^2+z^2}\right)P_{l'}^{m'}\left[\frac{z}{\sqrt{R^2+z^2}}\right]J_m(k\kappa_R R)dR. \tag{B.S98}$$

It is important to stress that the latter integral involves the product of both spherical and cylindrical Bessel-like functions. This fact hinders the direct utilization of usual integral properties involving Bessel functions. We may yet write the spherical Bessel functions of first and second kinds in terms of the (cylindrical) Bessel functions of first kind and half-integer order [S12]:

$$j_l(kr) = \sqrt{\frac{\pi}{2kr}}J_{l+\frac{1}{2}}(kr), \tag{B.S99a}$$

$$y_l(kr) = \sqrt{\frac{\pi}{2kr}}Y_{l+\frac{1}{2}}(kr) = (-1)^{l+1}\sqrt{\frac{\pi}{2kr}}J_{-l-\frac{1}{2}}(kr). \tag{B.S99b}$$

So, the spherical Hankel functions can be expressed as

$$h_l(kr) = j_l(kr) + iy_l(kr) = \sqrt{\frac{\pi}{2kr}}\left[J_{l+\frac{1}{2}}(kr) + i(-1)^{l+1}J_{-l-\frac{1}{2}}(kr)\right], \tag{B.S100}$$

and the integral given in Eq. (B.S98) is then recast as

$$\mathcal{K}_{l,m}^{l',m'}(k,\kappa_R;z)=\sqrt{\frac{\pi}{2k}}\int_0^{+\infty}\frac{R}{(R^2+z^2)^{1/4}}\left[J_{l-\frac{1}{2}}+i(-1)^l J_{-l+\frac{1}{2}}\right]P_{l'}^{m'}J_m dR, \tag{B.S101}$$

where we have omitted the argument in both the Bessel and associated Legendre functions. Furthermore, since we are ultimately considering the plane $z=0$, according to the results given in Eq. (B.S79) we can take the Legendre functions outside the integral, and then, it turns out to be convenient to define $\mathcal{K}_{l,m}^{l',m'}(k,\kappa_R;z)\equiv P_{l'}^{m'}(z)\mathcal{I}_{l,m}(k,\kappa_R;z)$. Under this condition, it can be explicitly demonstrated (by means of a symbolic calculation software, e.g., Wolfram *Mathematica*) that Eq. (B.S101) yields a closed result:

$$\begin{aligned}\mathcal{I}_{l,m}^{(\mathrm{odd})}(k,\kappa_R;0)&=\sqrt{\frac{\pi}{2k}}\int_0^{+\infty}\sqrt{R}J_{l-\frac{1}{2}}J_m dR\\&=\frac{\sqrt{\pi}\kappa_R^m}{k^2}\frac{\Gamma\left[\frac{1+l+m}{2}\right]}{\Gamma\left[\frac{l-m}{2}\right]}\frac{{}_2F_1\left[\frac{1}{2}(2-l+m),\frac{1}{2}(1+l+m),1+m;\kappa_R^2\right]}{\Gamma\left[1+m\right]},\end{aligned} \tag{B.S102}$$

$$\begin{aligned}\mathcal{I}_{l,m}^{(\mathrm{even})}(k,\kappa_R;0)&=\sqrt{\frac{\pi}{2k}}\int_0^{+\infty}\sqrt{R}J_{\frac{1}{2}-l}J_m dR\\&=\frac{\sqrt{\pi}\kappa_R^m}{k^2}\frac{\Gamma\left[\frac{2-l+m}{2}\right]}{\Gamma\left[\frac{1-l-m}{2}\right]}\frac{{}_2F_1\left[\frac{1}{2}(2-l+m),\frac{1}{2}(1+l+m),1+m;\kappa_R^2\right]}{\Gamma\left[1+m\right]},\end{aligned} \tag{B.S103}$$

where ${}_2F_1(a,b,c;z)$ is the Gaussian hypergeometric function defined as [S13]

$${}_2F_1(a,b,c;z)\equiv\frac{\Gamma[c]}{\Gamma[a]\Gamma[b]}\sum_{t=0}^{\infty}\frac{\Gamma[a+t]\Gamma[b+t]}{\Gamma[c+t]}\frac{z^t}{t!}. \tag{B.S104}$$

Hence, by summing up Eqs. (B.S102) and (B.S103), it follows that

$$\mathcal{I}_{l,m}(k,\kappa_R;0)=\frac{\sqrt{\pi}\kappa_R^m}{k^2}\frac{{}_2F_1\left[\frac{1}{2}(2-l+m),\frac{1}{2}(1+l+m),1+m;\kappa_R^2\right]}{\Gamma\left[1+m\right]}\left[\frac{\Gamma\left[\frac{1+l+m}{2}\right]}{\Gamma\left[\frac{l-m}{2}\right]}+i(-1)^l\frac{\Gamma\left[\frac{2-l+m}{2}\right]}{\Gamma\left[\frac{1-l-m}{2}\right]}\right]. \tag{B.S105}$$

Looking at this result carefully one realizes that there are two situations that should be distinguished when $z\to 0$. On the one hand, if $l+m$ is odd, $\mathcal{I}_{l,m}^{(\mathrm{odd})}$ is a well behaved function of k and κ_R (indeed this happens regardless of the parity of $l+m$) and $\mathcal{I}_{l,m}^{(\mathrm{even})}=0$. However, if $l+m$ is even the function $\mathcal{I}_{l,m}^{(\mathrm{even})}$ strikingly blows up. As pointed out by Mandel regarding the simplest case of the spherical wave e^{ikr}/r (when addressing the classical Weyl's identity) [S1], such divergent behavior is a direct consequence of the presence of a singularity at the origin. Still, as shown above, we can perform the integration by hand, thereby indicating that these singularities are actually removable. In fact, our calculations up to order four show that in the limit $z\to 0$, the infinities of $\mathcal{I}_{l,m}$ are compensated by the zeros of $P_{l'}^{m'}$ [S14] in such a way that the function $\mathcal{K}_{l,m}^{l',m'}(k,\kappa_R;z)$ can always be evaluated for whatever order (l,m), thus leading to a well defined function of k and κ_R. Hence, the integral given in Eq. (B.S98) ought to be redefined as a limit [S15]:

$$\tilde{\mathcal{K}}_{l,m}^{l',m'}(k,\kappa_R)\equiv\lim_{z\to 0}\mathcal{K}_{l,m}^{l',m'}(k,\kappa_R;z)=\lim_{z\to 0}P_{l'}^{m'}(z)\mathcal{I}_{l,m}(k,\kappa_R;z). \tag{B.S106}$$

Putting it all together, the spectral amplitude of the Hertz vector potential associated to electric-like sources of order (l,m) on the plane $z=0$ finally reads as

$$\tilde{\mathbf{\Pi}}^{(\mathrm{e})}_{l,m}(\kappa_x,\kappa_y;z\to 0)=\frac{-k}{4\pi\omega}\frac{(-i)^m C_{l,m}}{\sqrt{l(l+1)}}\left[\tilde{\Pi}^{(\mathrm{e}),\mathrm{x}}_{l,m}(\kappa_x,\kappa_y;z\to 0),\tilde{\Pi}^{(\mathrm{e}),\mathrm{y}}_{l,m}(\kappa_x,\kappa_y;z\to 0),\tilde{\Pi}^{(\mathrm{e}),\mathrm{z}}_{l,m}(\kappa_x,\kappa_y;z\to 0)\right], \tag{B.S107}$$

where

$$\begin{aligned}
\tilde{\Pi}^{(\mathrm{e}),\mathrm{x}}_{l,m}(\kappa_x,\kappa_y;z\to 0) &= i\left[(m-l)\tilde{\mathcal{K}}^{l,m}_{l,m+1}(k,\kappa_R)e^{i\phi}+(m+l)\tilde{\mathcal{K}}^{l,m}_{l,m-1}(k,\kappa_R)e^{-i\phi}\right]e^{im\phi},\\
\tilde{\Pi}^{(\mathrm{e}),\mathrm{y}}_{l,m}(\kappa_x,\kappa_y;z\to 0) &= \left[(m-l)\tilde{\mathcal{K}}^{l,m}_{l,m+1}(k,\kappa_R)e^{i\phi}-(m+l)\tilde{\mathcal{K}}^{l,m}_{l,m-1}(k,\kappa_R)e^{-i\phi}\right]e^{im\phi},\\
\tilde{\Pi}^{(\mathrm{e}),\mathrm{z}}_{l,m}(\kappa_x,\kappa_y;z\to 0) &= 2(l+m)\tilde{\mathcal{K}}^{l-1,m}_{l,m}(k,\kappa_R)e^{im\phi}.
\end{aligned}$$

And those of magnetic sources can be readily obtained from these, as detailed in Eq. (B.S76). Then, using this general expression, we can analytically obtain the angular spectra for the Hertz potential of arbitrary multipoles. For the first four orders in l, these are given by:

$$\begin{aligned}
\tilde{\mathbf{\Pi}}^{(\mathrm{e})}_{1,0}(\kappa_x,\kappa_y;z\to 0) &= \frac{-C_{1,0}}{4\sqrt{2}\pi}\frac{2}{k\omega}\frac{1}{\kappa_z}\{0,0,1\},\\
\tilde{\mathbf{\Pi}}^{(\mathrm{e})}_{1,1}(\kappa_x,\kappa_y;z\to 0) &= \frac{iC_{1,1}}{4\sqrt{2}\pi}\frac{4}{k\omega}\frac{1}{\kappa_z}\frac{1}{2}\{-i,1,0\};
\end{aligned}$$

$$\begin{aligned}
\tilde{\mathbf{\Pi}}^{(\mathrm{e})}_{2,0}(\kappa_x,\kappa_y;z\to 0) &= \frac{-C_{2,0}}{4\sqrt{6}\pi}\frac{4}{k\omega}\frac{1}{\kappa_z}\frac{1}{2}\{i\kappa_x,i\kappa_y,\mp 2i\kappa_z\},\\
\tilde{\mathbf{\Pi}}^{(\mathrm{e})}_{2,1}(\kappa_x,\kappa_y;z\to 0) &= \frac{iC_{2,1}}{4\sqrt{6}\pi}\frac{6}{k\omega}\frac{1}{\kappa_z}\{\mp\kappa_z,\mp i\kappa_z,-(\kappa_x+i\kappa_y)\},\\
\tilde{\mathbf{\Pi}}^{(\mathrm{e})}_{2,2}(\kappa_x,\kappa_y;z\to 0) &= \frac{C_{2,2}}{4\sqrt{6}\pi}\frac{8}{k\omega}\frac{1}{\kappa_z}\frac{3}{2}\{i(\kappa_x+i\kappa_y),-(\kappa_x+i\kappa_y),0\};
\end{aligned}$$

$$\begin{aligned}
\tilde{\mathbf{\Pi}}^{(\mathrm{e})}_{3,0}(\kappa_x,\kappa_y;z\to 0) &= \frac{-C_{3,0}}{4\sqrt{12}\pi}\frac{6}{k\omega}\frac{1}{\kappa_z}\frac{1}{2}\left\{\pm 2\kappa_x\kappa_z,\pm 2\kappa_y\kappa_z,3(\kappa_x^2+\kappa_y^2)-2\right\},\\
\tilde{\mathbf{\Pi}}^{(\mathrm{e})}_{3,1}(\kappa_x,\kappa_y;z\to 0) &= \frac{iC_{3,1}}{4\sqrt{12}\pi}\frac{8}{k\omega}\frac{1}{\kappa_z}\frac{3}{8}\left\{-i(7\kappa_x^2+5\kappa_y^2+2i\kappa_x\kappa_y-4),5\kappa_x^2+7\kappa_y^2-2i\kappa_x\kappa_y-4,\pm 8i\kappa_z(\kappa_x+i\kappa_y)\right\},\\
\tilde{\mathbf{\Pi}}^{(\mathrm{e})}_{3,2}(\kappa_x,\kappa_y;z\to 0) &= \frac{C_{3,2}}{4\sqrt{12}\pi}\frac{10}{k\omega}\frac{1}{\kappa_z}3\left\{\pm 2(\kappa_x+i\kappa_y)\kappa_z,\pm 2i(\kappa_x+i\kappa_y)\kappa_z,(\kappa_x+i\kappa_y)^2\right\},\\
\tilde{\mathbf{\Pi}}^{(\mathrm{e})}_{3,3}(\kappa_x,\kappa_y;z\to 0) &= \frac{-iC_{3,3}}{4\sqrt{12}\pi}\frac{12}{k\omega}\frac{1}{\kappa_z}\frac{15}{2}\left\{-i(\kappa_x+i\kappa_y)^2,(\kappa_x+i\kappa_y)^2,0\right\};
\end{aligned}$$

$$\begin{aligned}
\tilde{\mathbf{\Pi}}^{(\mathrm{e})}_{4,0}(\kappa_x,\kappa_y;z\to 0) &= \frac{-C_{4,0}}{4\sqrt{20}\pi}\frac{8}{k\omega}\frac{1}{\kappa_z}\frac{1}{8}\left\{3i(5\kappa_R^2-4)\kappa_R\cos\phi,3i(5\kappa_R^2-4)\kappa_R\sin\phi,\pm 4i\kappa_z(2-5\kappa_R^2)\right\},\\
\tilde{\mathbf{\Pi}}^{(\mathrm{e})}_{4,1}(\kappa_x,\kappa_y;z\to 0) &= \frac{iC_{4,1}}{4\sqrt{20}\pi}\frac{10}{k\omega}\frac{1}{\kappa_z}\frac{1}{2}\left\{\pm\kappa_z\left[(10+3e^{2i\phi})\kappa_R^2-4\right],\pm i\kappa_z\left[(10-3e^{2i\phi})\kappa_R^2-4\right],3(4-5\kappa_R^2)\kappa_R e^{i\phi}\right\},\\
\tilde{\mathbf{\Pi}}^{(\mathrm{e})}_{4,2}(\kappa_x,\kappa_y;z\to 0) &= \frac{C_{4,2}}{4\sqrt{20}\pi}\frac{12}{k\omega}\frac{1}{\kappa_z}\frac{5}{4}\left\{i\left[(15+e^{2i\phi})\kappa_R^2-12\right]\kappa_R e^{i\phi},\left[(e^{2i\phi}-15)\kappa_R^2+12\right]\kappa_R e^{i\phi},\mp 12i\kappa_z\kappa_R^2 e^{2i\phi}\right\},\\
\tilde{\mathbf{\Pi}}^{(\mathrm{e})}_{4,3}(\kappa_x,\kappa_y;z\to 0) &= \frac{-iC_{4,3}}{4\sqrt{20}\pi}\frac{14}{k\omega}\frac{1}{\kappa_z}15\left\{\mp 3\kappa_z\kappa_R^2 e^{2i\phi},\mp 3i\kappa_z\kappa_R^2 e^{2i\phi},-\kappa_R^3 e^{3i\phi}\right\},\\
\tilde{\mathbf{\Pi}}^{(\mathrm{e})}_{4,4}(\kappa_x,\kappa_y;z\to 0) &= \frac{-C_{4,4}}{4\sqrt{20}\pi}\frac{16}{k\omega}\frac{1}{\kappa_z}\frac{105}{2}\left\{i\kappa_R^3 e^{3i\phi},-\kappa_R^3 e^{3i\phi},0\right\}.
\end{aligned}$$

As a final remark, it should be noted that a similar derivation of the angular spectra of EM multipole fields of arbitrary order has already been addressed with other

approaches [S16–S18]. Yet, even though the final results are explicitly expressed by means of an analytical and closed form (see, e.g., those shown in Ref. [S18]), both the formalism and the notation used makes them hard to interpret and handle, thus being not very practical.

B.SM.VI Verification and Relationship between the Results Obtained via the Hertz's and Standard Vector Potentials for both the Electric Dipole and Quadrupole

Below, in order to verify our results, we will compare the above general expression of the spectral amplitude [Eq. (B.S107)] for the particular cases of the electric dipole ($l = 1$) and quadrupole ($l = 2$), with those explicitly obtained in Sec. II and Sec. III [Eqs. (B.S21) and (B.S37)], respectively.

In the first place, focusing on the electric dipole, we have to consider $l = 1$ and $m = 0, \pm 1$, which correspond to the different characteristic polarizations of the electric dipole moment $\mathbf{p}$. To determine their explicit relationship we should look into the EM fields. Specifically, just by looking at the magnetic field stemmed from the standard vector potential of the electric dipole given in Eq. (B.S17), we have that

$$\mathbf{H}^{\mathrm{ED}} = \frac{\omega k^2}{4\pi} h_1(kr) \left\{ \left[p_y \cos\varphi - p_x \sin\varphi \right] \mathbf{e}_\theta + \left[p_z \sin\theta - \cos\theta \left(p_x \cos\varphi + p_y \sin\varphi \right) \right] \mathbf{e}_\varphi \right\},$$

where, for comparison purposes, we have expressed the dipole moment in the spherical basis. This magnetic field should be related to the one derived from the multipole expansion for $l = 1$:

$$\mathbf{H}^{(\mathrm{e})}_{1,m} = \frac{-ir h_1(kr)}{\sqrt{2}} \left[\mathbf{e}_r \times \nabla Y_{1,m} \right] \Rightarrow \begin{cases} m = 0 \quad \rightarrow \mathbf{H}^{(\mathrm{e})}_{1,0} = \dfrac{i h_1(kr)}{\sqrt{2}} \sqrt{\dfrac{3}{4\pi}} \sin\theta \mathbf{e}_\varphi, \\ m = \pm 1 \rightarrow \mathbf{H}^{(\mathrm{e})}_{1,\pm 1} = \dfrac{i h_1(kr)}{\sqrt{2}} \sqrt{\dfrac{3}{8\pi}} \left(-i\mathbf{e}_\theta \pm \cos\theta \mathbf{e}_\varphi \right) e^{\pm i\varphi}. \end{cases}$$

Then, leaving aside the prefactors, it is easy to see that, for $m = 0$, the functional form of $\mathbf{H}^{\mathrm{ED}}$ coincides with that of $\mathbf{H}^{(\mathrm{e})}_{1,m}$ as long as $p_x = p_y = 0$. Likewise, for $m = \pm 1$, the matching is satisfied for $p_x = \mp i p_y$ and $p_z = 0$. Taking into account these relations, one can directly observe that:

$$\mathbf{H}^{\mathrm{ED}} = \frac{\omega k^2}{4\pi} \frac{(-1)^m \sqrt{2}}{i C_{1,m}} \mathbf{H}^{(\mathrm{e})}_{1,m} \Rightarrow \begin{cases} \mathbf{H}^{\mathrm{ED}} = -\dfrac{\omega k^2}{4\pi} h_1(kr) \left[\mathbf{e}_r \times \mathbf{p}_0 \right] = \dfrac{\omega k^2}{4\pi} \dfrac{\sqrt{2}}{i C_{1,0}} \mathbf{H}^{(\mathrm{e})}_{1,0}, \\ \mathbf{H}^{\mathrm{ED}} = -\dfrac{\omega k^2}{4\pi} h_1(kr) \left[\mathbf{e}_r \times \mathbf{p}_\pm \right] = \dfrac{\omega k^2}{4\pi} \dfrac{(-1)\sqrt{2}}{i C_{1,\pm 1}} \mathbf{H}^{(\mathrm{e})}_{1,\pm 1}, \end{cases}$$

where $C_{1,0}=\sqrt{3/4\pi}$, $C_{1,+1}=\sqrt{3/8\pi}$, and $C_{1,-1}=(-1)C_{1,+1}$. Therefore it can be shown that for $l=1$, the following relationship holds:

$$\{l,m\}=\{1,0\} \qquad \Longleftrightarrow \qquad \mathbf{p}_0=\{0,0,1\}\,,$$

$$\{l,m\}=\{1,\pm1\} \qquad \Longleftrightarrow \qquad \mathbf{p}_\pm=\{1,\pm i,0\}\,.$$

With this in mind, we can directly compare the result shown in Eq. (B.S21) with that given in Eq. (B.S107) for $l=1$:

$$\tilde{\mathbf{A}}_0^{\mathrm{ED}(0)}=\frac{\mu c k^2}{8\pi^2 n}\frac{1}{\kappa_z}\mathbf{p}_0 \;\Leftrightarrow\; \tilde{\mathbf{\Pi}}_{1,0}^{(\mathrm{e})}=\frac{-C_{1,0}}{2\sqrt{2}\pi}\frac{1}{k\omega}\frac{1}{\kappa_z}\mathbf{p}_0 \;\Rightarrow\; \tilde{\mathbf{A}}_0^{\mathrm{ED}(0)}=\frac{-\sqrt{2}}{4\pi C_{1,0}}\frac{\mu c k^3\omega}{n}\tilde{\mathbf{\Pi}}_{1,0}^{(\mathrm{e})},$$

$$\tilde{\mathbf{A}}_0^{\mathrm{ED}(\pm1)}=\frac{\mu c k^2}{8\pi^2 n}\frac{1}{\kappa_z}\mathbf{p}_\pm \Leftrightarrow \tilde{\mathbf{\Pi}}_{1,\pm1}^{(\mathrm{e})}=\frac{C_{1,\pm1}}{2\sqrt{2}\pi}\frac{1}{k\omega}\frac{1}{\kappa_z}\mathbf{p}_\pm \;\Rightarrow\; \tilde{\mathbf{A}}_0^{\mathrm{ED}(\pm1)}=\frac{\sqrt{2}}{4\pi C_{1,\pm1}}\frac{\mu c k^3\omega}{n}\tilde{\mathbf{\Pi}}_{1,\pm1}^{(\mathrm{e})},$$

where it should be noted that $\tilde{\mathbf{A}}_0^{\mathrm{ED}(-1)}=[\tilde{\mathbf{A}}_0^{\mathrm{ED}(+1)}]^*$ and $\tilde{\mathbf{\Pi}}_{1,-1}^{(e)}=[-\tilde{\mathbf{\Pi}}_{1,+1}^{(e)}]^*$. Hence, for this particular case, apart from the prefactors that account for the dimensional constants, both approaches are in perfect agreement, as expected.

Following a similar procedure for the electric quadrupole, we need first to identify the explicit relationship between the components of the quadrupole moment tensor, $\vec{\vec{\mathcal{Q}}}$, and the different pairs $\{l,m\}$, with $l=2$ and $m=0,\pm1,\pm2$. For this, we will write the magnetic field associated to the electric quadrupole from the corresponding standard vector potential given in Eq. (B.S25):

$$\begin{aligned}\mathbf{H}^{\mathrm{EQ}}=&\frac{\omega k^3}{48\pi}h_2(kr)\,[2\cos\theta(\mathcal{Q}_{yz}\cos\varphi-\mathcal{Q}_{xz}\sin\varphi)\\&\qquad+\sin\theta(2\mathcal{Q}_{xy}\cos(2\varphi)+(\mathcal{Q}_{yy}-\mathcal{Q}_{xx})\sin(2\varphi))]\,\mathbf{e}_\theta\\&-\frac{\omega k^3}{96\pi}h_2(kr)\,\{4\cos(2\theta)(\mathcal{Q}_{xz}\cos\varphi+\mathcal{Q}_{yz}\sin\varphi)\\&\qquad+\sin(2\theta)\,[3(\mathcal{Q}_{xx}+\mathcal{Q}_{yy})+(\mathcal{Q}_{xx}-\mathcal{Q}_{yy})\cos(2\varphi)+2\mathcal{Q}_{xy}\sin(2\varphi)]\}\,\mathbf{e}_\varphi.\end{aligned}$$

Analogously to the dipole case, this expression of the magnetic field has to be related to that obtained from the multipole expansion for $l=2$:

$$\mathbf{H}_{2,m}^{(\mathrm{e})}=\frac{-irh_2(kr)}{\sqrt{6}}\,[\mathbf{e}_r\times\nabla Y_{2,m}]\Rightarrow\begin{cases}\mathbf{H}_{2,0}^{(\mathrm{e})}=\dfrac{ih_2(kr)}{\sqrt{6}}\dfrac{3}{4}\sqrt{\dfrac{5}{\pi}}\sin(2\theta)\mathbf{e}_\varphi,\\[2ex]\mathbf{H}_{2,\pm1}^{(\mathrm{e})}=\dfrac{ih_2(kr)}{\sqrt{6}}\sqrt{\dfrac{15}{8\pi}}\,[-i\cos\theta\mathbf{e}_\theta\pm\cos(2\theta)\mathbf{e}_\varphi]\,e^{\pm i\varphi},\\[2ex]\mathbf{H}_{2,\pm2}^{(\mathrm{e})}=\dfrac{ih_2(kr)}{\sqrt{6}}\sqrt{\dfrac{15}{32\pi}}\,[\pm2i\sin\theta\mathbf{e}_\theta-\sin(2\theta)\mathbf{e}_\varphi]\,e^{\pm2i\varphi}.\end{cases}$$

Thus, by comparing the functional form of $\mathbf{H}^{\mathrm{EQ}}$ with that of $\mathbf{H}_{2,m}^{(\mathrm{e})}$, it is easy to see that, for $m=0$ we have to require that $\mathcal{Q}_{xx}=\mathcal{Q}_{yy}$, and $\mathcal{Q}_{yz}=\mathcal{Q}_{xz}=\mathcal{Q}_{xy}=0$. Likewise, for

$m=\pm1$, $\mathcal{Q}_{xx}=\mathcal{Q}_{yy}=\mathcal{Q}_{xy}=0$, and $\mathcal{Q}_{yz}=\pm i\mathcal{Q}_{xz}$. And finally, for $m=\pm2$ we have that $\mathcal{Q}_{xy}=\pm i\mathcal{Q}_{xx}=\mp i\mathcal{Q}_{yy}$, and $\mathcal{Q}_{xz}=\mathcal{Q}_{yz}=0$. With these conditions, it follows that

$$\mathbf{H}^{\mathrm{EQ}}=\frac{\omega k^2}{24\pi}\frac{(-1)^m\sqrt{6}}{iC_{2,m}}\mathbf{H}^{(\mathrm{e})}_{2,m}\Rightarrow\begin{cases}\mathbf{H}^{\mathrm{EQ}}=\dfrac{-\omega k^3}{24\pi}h_2(kr)[\mathbf{e}_r\times(\vec{\vec{\mathcal{Q}}}_0\cdot\mathbf{e}_r)]=\dfrac{\omega k^2}{24\pi}\dfrac{\sqrt{6}}{iC_{2,0}}\mathbf{H}^{(\mathrm{e})}_{2,0},\\[2ex]\mathbf{H}^{\mathrm{EQ}}=\dfrac{-\omega k^3}{24\pi}h_2(kr)[\mathbf{e}_r\times(\vec{\vec{\mathcal{Q}}}_{\pm1}\cdot\mathbf{e}_r)]=\dfrac{\omega k^2}{24\pi}\dfrac{(-1)\sqrt{6}}{iC_{2,\pm1}}\mathbf{H}^{(\mathrm{e})}_{2,\pm1},\\[2ex]\mathbf{H}^{\mathrm{EQ}}=\dfrac{-\omega k^3}{24\pi}h_2(kr)[\mathbf{e}_r\times(\vec{\vec{\mathcal{Q}}}_{\pm2}\cdot\mathbf{e}_r)]=\dfrac{\omega k^2}{24\pi}\dfrac{\sqrt{6}}{iC_{2,\pm2}}\mathbf{H}^{(\mathrm{e})}_{2,\pm2},\end{cases}$$

where $C_{2,0}=\sqrt{5/4\pi}$, $C_{2,1}=\sqrt{5/24\pi}$, $C_{2,2}=\sqrt{5/96\pi}$, and $C_{2,-m}=(-1)^mC_{2,m}$. Therefore, for $l=2$, we get the following correspondence between the m multipolar order and the matrices associated to the quadrupole moment tensor (expressed in Cartesian basis):

$$\{l,m\}=\{2,0\}\qquad\Longleftrightarrow\qquad\vec{\vec{\mathcal{Q}}}_0=\frac{1}{k}\begin{pmatrix}-1&0&0\\0&-1&0\\0&0&2\end{pmatrix},$$

$$\{l,m\}=\{2,\pm1\}\qquad\Longleftrightarrow\qquad\vec{\vec{\mathcal{Q}}}_{\pm1}=\frac{3}{k}\begin{pmatrix}0&0&1\\0&0&\pm i\\1&\pm i&0\end{pmatrix},$$

$$\{l,m\}=\{2,\pm2\}\qquad\Longleftrightarrow\qquad\vec{\vec{\mathcal{Q}}}_{\pm2}=\frac{6}{k}\begin{pmatrix}\pm1&i&0\\i&\mp1&0\\0&0&0\end{pmatrix}.$$

Taking into account these latter relations we can now compare the particular result of Eq. (B.S37) with the general one given in Eq. (B.S107) for $l=2$:

$$\tilde{\mathbf{A}}_0^{\mathrm{EQ}(0)}=\frac{\mu ck^2}{8\pi^2n}\frac{(-i)}{6\kappa_z}\left[\vec{\vec{\mathcal{Q}}}_0\cdot\mathbf{k}^{\pm}\right]\quad\Longleftrightarrow\quad\tilde{\mathbf{\Pi}}^{(\mathrm{e})}_{2,0}=\frac{iC_{2,0}}{2\sqrt{6}\pi}\frac{1}{k\omega}\frac{1}{\kappa_z}\left[\vec{\vec{\mathcal{Q}}}_0\cdot\mathbf{k}^{\pm}\right]$$
$$\Longrightarrow\tilde{\mathbf{A}}_0^{\mathrm{EQ}(0)}=\frac{-\sqrt{6}}{24\pi C_{2,0}}\frac{\mu ck^3\omega}{n}\tilde{\mathbf{\Pi}}^{(\mathrm{e})}_{2,0},$$

$$\tilde{\mathbf{A}}_0^{\mathrm{EQ}(\pm1)}=\frac{\mu ck^2}{8\pi^2n}\frac{(-i)}{6\kappa_z}\left[\vec{\vec{\mathcal{Q}}}_{\pm1}\cdot\mathbf{k}^{\pm}\right]\quad\Longleftrightarrow\quad\tilde{\mathbf{\Pi}}^{(\mathrm{e})}_{2,\pm1}=\frac{\mp iC_{2,\pm1}}{2\sqrt{6}\pi}\frac{1}{k\omega}\frac{1}{\kappa_z}\left[\vec{\vec{\mathcal{Q}}}_{\pm1}\cdot\mathbf{k}^{\pm}\right]$$
$$\Longrightarrow\tilde{\mathbf{A}}_0^{\mathrm{EQ}(\pm1)}=\frac{\pm\sqrt{6}}{24\pi C_{2,\pm1}}\frac{\mu ck^3\omega}{n}\tilde{\mathbf{\Pi}}^{(\mathrm{e})}_{2,\pm1},$$

$$\tilde{\mathbf{A}}_0^{\mathrm{EQ}(\pm2)}=\frac{\mu ck^2}{8\pi^2n}\frac{(-i)}{6\kappa_z}\left[\vec{\vec{\mathcal{Q}}}_{\pm2}\cdot\mathbf{k}^{\pm}\right]\quad\Longleftrightarrow\quad\tilde{\mathbf{\Pi}}^{(\mathrm{e})}_{2,\pm2}=\frac{iC_{2,\pm2}}{2\sqrt{6}\pi}\frac{1}{k\omega}\frac{1}{\kappa_z}\left[\vec{\vec{\mathcal{Q}}}_{\pm2}\cdot\mathbf{k}^{\pm}\right]$$
$$\Longrightarrow\tilde{\mathbf{A}}_0^{\mathrm{EQ}(\pm2)}=\frac{-\sqrt{6}}{24\pi C_{2,\pm2}}\frac{\mu ck^3\omega}{n}\tilde{\mathbf{\Pi}}^{(\mathrm{e})}_{2,\pm2},$$

with $\tilde{\mathbf{A}}_0^{\mathrm{EQ}(-1)} = [-\tilde{\mathbf{A}}_0^{\mathrm{EQ}(+1)}]^*$, $\tilde{\mathbf{A}}_0^{\mathrm{EQ}(-2)} = [\tilde{\mathbf{A}}_0^{\mathrm{EQ}(+2)}]^*$, $\tilde{\mathbf{\Pi}}_{2,-1}^{(e)} = [-\tilde{\mathbf{\Pi}}_{2,+1}^{(e)}]^*$, and $\tilde{\mathbf{\Pi}}_{2,-2}^{(e)} = [-\tilde{\mathbf{\Pi}}_{2,+2}^{(e)}]^*$. Hence, once again, apart from the prefactors, both approaches are straightforwardly related to each other, thus confirming the validity of the general expression given in Eq. (B.S107) up to the electric quadrupole case.

Appendix: Angular Spectrum Representation of the Magnetic Dipole and its Relation with the Electric Dipole

From a similar procedure as in the previous sections for the electric dipole and quadrupole, in order to obtain the angular spectrum of an oscillating magnetic dipole, we start by considering its associated vector potential [S8]:

$$\mathbf{A}^{\mathrm{MD}}(\mathbf{r}) = \frac{i\mu k}{4\pi}\left(1-\frac{1}{ikr}\right)(\mathbf{e}_r\times\mathbf{m})\,\frac{e^{ikr}}{r}, \tag{B.S108}$$

where $\mathbf{m}$ is the *magnetic dipole moment*. The corresponding spectral amplitude is obtained from its partial Fourier transform:

$$\begin{aligned}\tilde{\mathbf{A}}^{\mathrm{MD}}(\kappa_x,\kappa_y;z) &= \left(\frac{k}{2\pi}\right)^2\iint_{-\infty}^{+\infty}\mathbf{A}^{\mathrm{MD}}(x,y,z)e^{-ik(\kappa_x x+\kappa_y y)}dxdy\\ &= \frac{i\mu k^3}{16\pi^3}\iint_{-\infty}^{+\infty}\left(1-\frac{1}{ik\sqrt{x^2+y^2+z^2}}\right)(\mathbf{e}_r\times\mathbf{m})\,\frac{e^{ik\sqrt{x^2+y^2+z^2}}}{\sqrt{x^2+y^2+z^2}}e^{-ik(\kappa_x x+\kappa_y y)}dxdy.\end{aligned} \tag{B.S109}$$

Making the change of variables to cylindrical coordinates, as given in Eq. (B.S27), it follows that

$$\begin{aligned}\tilde{\mathbf{A}}^{\mathrm{MD}}(\kappa_x,\kappa_y;z) &= \frac{i\mu k^3}{16\pi^3}\int_0^{+\infty}\int_0^{2\pi}\left(1-\frac{1}{ik\sqrt{R^2+z^2}}\right)(\mathbf{e}_r\times\mathbf{m})\,\frac{e^{ik\sqrt{R^2+z^2}}}{\sqrt{R^2+z^2}}e^{-ik\kappa_R R\cos(\theta-\phi)}Rd\theta dR\\ &= \frac{\mu k^3}{8\pi^2}\int_0^{+\infty}\left(1-\frac{1}{ik\sqrt{R^2+z^2}}\right)\boldsymbol{\Omega}\frac{e^{ik\sqrt{R^2+z^2}}}{R^2+z^2}RdR,\end{aligned} \tag{B.S110}$$

where

$$\begin{aligned}\boldsymbol{\Omega} &\equiv \boldsymbol{\Omega}_R+\boldsymbol{\Omega}_z\\ &= RJ_1\left[m_z\left(\sin\phi\mathbf{e}_x-\cos\phi\mathbf{e}_y\right)+\left(m_y\cos\phi-m_x\sin\phi\right)\mathbf{e}_z\right]-izJ_0\left(m_y\mathbf{e}_x-m_x\mathbf{e}_y\right).\end{aligned}$$

Similarly to the electric quadrupole case, special care must be taken with the integral involving the z-dependent contribution. We thus perform the integration separately for

the R- and the z-dependent contributions as follows:

$$\tilde{\mathbf{A}}_R^{\mathrm{MD}}(\kappa_x,\kappa_y;z)=\frac{\mu k^3}{8\pi^2}\int_0^{+\infty}\left(1-\frac{1}{ik\sqrt{R^2+z^2}}\right)\boldsymbol{\Omega}_R\frac{e^{ik\sqrt{R^2+z^2}}}{R^2+z^2}RdR$$

$$\xrightarrow[z\to 0]{}\frac{\mu k^3}{8\pi^2}\int_0^{+\infty}\left(1-\frac{1}{ikR}\right)\left[m_z\left(\sin\phi\mathbf{e}_x-\cos\phi\mathbf{e}_y\right)+\left(m_y\cos\phi-m_x\sin\phi\right)\mathbf{e}_z\right]J_1e^{ikR}dR$$

$$=-\frac{\mu k^2}{8\pi^2}\frac{\kappa_R}{\kappa_z}\left[m_z\left(\sin\phi\mathbf{e}_x-\cos\phi\mathbf{e}_y\right)+\left(m_y\cos\phi-m_x\sin\phi\right)\mathbf{e}_z\right];\tag{B.S111}$$

$$\tilde{\mathbf{A}}_z^{\mathrm{MD}}(\kappa_x,\kappa_y;z)=\frac{\mu k^3}{8\pi^2}\int_0^{+\infty}\left(1-\frac{1}{ik\sqrt{R^2+z^2}}\right)\boldsymbol{\Omega}_z\frac{e^{ik\sqrt{R^2+z^2}}}{R^2+z^2}RdR$$

$$=\frac{i\mu k^3}{8\pi^2}\left(m_y\mathbf{e}_x-m_x\mathbf{e}_y\right)\int_0^{+\infty}\left(\frac{1}{ik\sqrt{R^2+z^2}}-1\right)\frac{e^{ik\sqrt{R^2+z^2}}}{R^2+z^2}RzJ_0(k\kappa_RR)dR$$

$$=\left\{\begin{array}{lll}u=J_0(k\kappa_RR) & \Longrightarrow & du=-k\kappa_RJ_1(k\kappa_RR)dR\\ dv=\left(\dfrac{1}{ik\sqrt{R^2+z^2}}-1\right)\dfrac{Rz}{R^2+z^2}e^{ik\sqrt{R^2+z^2}}dR & \Longrightarrow & v=\dfrac{ize^{ik\sqrt{R^2+z^2}}}{k\sqrt{R^2+z^2}}\end{array}\right\}$$

$$=\frac{i\mu k^3}{8\pi^2}\left(m_y\mathbf{e}_x-m_x\mathbf{e}_y\right)\left[\frac{izJ_0e^{ik\sqrt{R^2+z^2}}}{k\sqrt{R^2+z^2}}\bigg|_{R=0}^{R\to\infty}+\int_0^{+\infty}\frac{iz\kappa_R}{\sqrt{R^2+z^2}}J_1e^{ik\sqrt{R^2+z^2}}dR\right]$$

$$\xrightarrow[z\to 0]{}\pm\frac{\mu k^2}{8\pi^2}\left(m_y\mathbf{e}_x-m_x\mathbf{e}_y\right).\tag{B.S112}$$

Hence, summing up the above results we obtain that

$$\begin{aligned}\tilde{\mathbf{A}}_0^{\mathrm{MD}}(\kappa_x,\kappa_y;0)&=\frac{\mu k^2}{8\pi^2}\frac{\kappa_R}{\kappa_z}\left[m_z\left(-\sin\phi\mathbf{e}_x+\cos\phi\mathbf{e}_y\right)-\left(m_y\cos\phi-m_x\sin\phi\right)\mathbf{e}_z\right]\\&\qquad\pm\frac{\mu k^2}{8\pi^2}\left(m_y\mathbf{e}_x-m_x\mathbf{e}_y\right)\\&=\frac{\mu k^2}{8\pi^2}\frac{1}{\kappa_z}\left[\left(\pm m_y\kappa_z-m_z\kappa_y\right)\mathbf{e}_x+\left(m_z\kappa_x\mp m_x\kappa_z\right)\mathbf{e}_y+\left(m_x\kappa_y-m_y\kappa_x\right)\mathbf{e}_z\right]\\&=\frac{\mu ck^2}{8\pi^2n}\frac{1}{\kappa_z}\frac{\left[\mathbf{m}\times\mathbf{k}^{\pm}\right]}{\omega}.\end{aligned}\tag{B.S113}$$

Then, the spectral amplitudes of the EM fields for the magnetic dipole reads

$$\tilde{\mathbf{E}}^{\mathrm{MD}}(\kappa_x,\kappa_y;0)=\frac{ic}{kn}[k^2\tilde{\mathbf{A}}_0^{\mathrm{MD}}-\mathbf{k}^{\pm}(\mathbf{k}^{\pm}\cdot\tilde{\mathbf{A}}_0^{\mathrm{MD}})]=\frac{i\omega k}{8\pi^2}\frac{\mu}{\kappa_z}\left[\mathbf{m}\times\mathbf{k}^{\pm}\right],\tag{B.S114}$$

$$\tilde{\mathbf{H}}^{\mathrm{MD}}(\kappa_x,\kappa_y;0)=\frac{i}{\mu}[\mathbf{k}^{\pm}\times\tilde{\mathbf{A}}_0^{\mathrm{MD}}]=\frac{ik}{8\pi^2}\frac{1}{\kappa_z}\left\{k^2\mathbf{m}-\mathbf{k}^{\pm}\left(\mathbf{k}^{\pm}\cdot\mathbf{m}\right)\right\},\tag{B.S115}$$

where $\tilde{\mathbf{A}}_0^{\mathrm{MD}}\equiv\tilde{\mathbf{A}}^{\mathrm{MD}}(\kappa_x,\kappa_y;z=0)$. Comparing the above expressions for the magnetic dipole with that given in Eqs. (B.S40) and (B.S41) for the electric dipole we find that there exists a relationship between them. Indeed, taking into account the duality principle

and the symmetry of Maxwell's equations [S10], we can get the EM fields of the magnetic dipole from that of the electric dipole by simply performing the following transformations:

$$\tilde{\mathbf{E}}^{\mathrm{ED}} \longrightarrow \sqrt{\frac{\mu}{\varepsilon}}\tilde{\mathbf{H}}^{\mathrm{MD}}, \qquad \tilde{\mathbf{H}}^{\mathrm{ED}} \longrightarrow -\sqrt{\frac{\varepsilon}{\mu}}\tilde{\mathbf{E}}^{\mathrm{MD}}, \qquad \mathbf{p} \longrightarrow \frac{n}{c}\mathbf{m}. \tag{B.S116}$$

Notice that, unlike the substitutions pointed out in Ref. [S11], the above transformation rule does not require the interchange of ε and μ, thereby becoming more useful for dealing with EM fields in the same medium [S10].

References

[S1] L. Mandel and E. Wolf, *Optical Coherence and Quantum Optics* (Cambridge University Press, Cambridge, UK, 1995).

[S2] L. Novotny and B. Hecht, *Principles of Nano-Optics* (Cambridge University Press, Cambridge, England, 2012).

[S3] T. Setälä, M. Kaivola, and A. T. Friberg, *Decomposition of the point-dipole field into homogeneous and evanescent parts*, Phys. Rev. E **59**, 1200 (1999).

[S4] H. Weyl, *Ausbreitung elektromagnetischer Wellen über einem ebenen Leiter* [*Propagation of electromagnetic waves on an even conductor*], Ann. Phys. **365**, 481 (1919).

[S5] J. W. Goodman, *Introduction to Fourier Optics* (McGraw-Hill, New York, USA, 1988).

[S6] E. A. Essex, *Hertz vector potentials of electromagnetic theory*, Am. J. Phys. **45**, 1099 (1977).

[S7] M. Ornigotti and A. Aiello, *The Hertz vector revisited: a simple physical picture*, J. Opt. **16**, 105705 (2014).

[S8] J. D. Jackson, *Classical Electrodynamics* (Wiley, New York, USA, 1999).

[S9] In the context of guiding systems, the terminology electric and magnetic, referring to the nature of the optical source, is often replaced by transverse magnetic (TM) (or *p*-polarized) and transverse electric (TE) (or *s*-polarized) modes, respectively.

[S10] A. Ishimaru, *Electromagnetic Wave Propagation, Radiation, and Scattering* (Prentice-Hall, Englewood Cliffs, NJ, 1991).

[S11] M. F. Picardi, A. Manjavacas, A. V. Zayats, and F. J. Rodríguez-Fortuño, *Unidirectional evanescent-wave coupling from circularly polarized electric and magnetic dipoles: An angular spectrum approach*, Phys. Rev. B **95**, 245416 (2017).

[S12] G. N. Watson, *A Treatise on the Theory of Bessel Functions* (Cambridge University Press, New York, USA, 1995).

[S13] M. Abramowitz and I. A. Stegun, *Handbook of Mathematical Functions* (Dover, New York, USA, 1972).

[S14] Notice that the matching between $\mathcal{I}_{l,m}$ and $P_{l'}^{m'}$ works since $\mathcal{I}_{l,m}$ appears multiplied by P_{l-1}^{m}, and $\mathcal{I}_{l,m\pm1}$ by P_{l}^{m}.

[S15] It should be noted that the limit $z \to 0$ in Eq. (B.S106) is actually a formal representation that yields a physically consistent meaning to the singular behavior at the origin. However, in practice, this calculation is to be carried out by considering Eq. (B.S105), and taking the corresponding limit either on the index l or m. Notice that, by doing this, one has to assume deliberately that l and/or m are continuous variables.

[S16] A. J. Devaney and E. Wolf, *Multipole expansions and plane wave representations of the electromagnetic field*, J. Math. Phys. **15**, 234 (1974).

[S17] P. A. Bobbert and J. Vlieger, *Light scattering by a sphere on a substrate*, Physica A **137**, 209 (1986).

[S18] R. Borghi, *On the angular-spectrum representation of multipole wave fields*, J. Opt. Soc. Am. A **21**, 1805 (2004).

Part II

Original Contributions on Optical Chirality

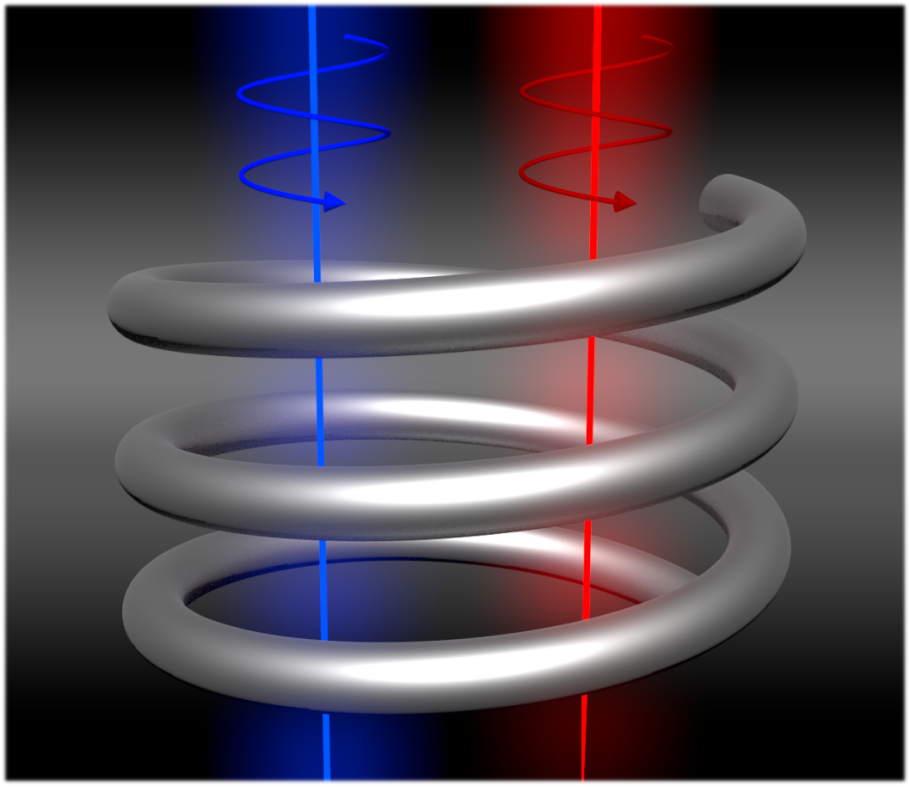

Chapter 4

PAPER C

Optical Chirality in Dispersive and Lossy Media

Phys. Rev. Lett. 121, 043901 (2018)

Optical Chirality in Dispersive and Lossy Media

J. Enrique Vázquez-Lozano and Alejandro Martínez

Nanophotonics Technology Center, Universitat Politècnica de València, Camino de Vera s/n, 46022 Valencia, Spain

Several dynamical properties of electromagnetic waves such as energy, momentum, angular momentum, and optical helicity have been recently reexamined in dispersive and lossless media. Here, we address an alternative derivation for the optical chirality, extending it so as to include dissipative effects as well. To this end, we first elaborate on the most complete form of the conservation law for the optical chirality, without any restrictions on the nature of the medium. As a result we find a general expression for the optical chirality density both in lossless and lossy dispersive media. Our definition is perfectly consistent with that originally introduced for electromagnetic fields in free space, and is applicable to any material system, including dielectrics, plasmonic nanostructures, and left-handed metamaterials.

C.I Introduction

Local dynamical properties such as energy, linear momentum, and angular momentum, are conserved quantities for electric and magnetic fields in vacuum [1,2]. In fact, leaving aside the physical meaning, there exists an infinite class of conserved quantities for free-space electromagnetic (EM) fields [3,4]. In particular, in 1964 Lipkin demonstrated the existence of a set containing ten new independent conservation laws for EM radiation in vacuum [5]. Originally, these tensorial quantities were merely conceived as mathematical entities theretofore unknown, and having no ready physical significance. That is why they were collectively referred to as the *ij-zilches* (which literally means "nothingness"), where i and j stand for the labels indicating the tensor indices. Since then, there have been many efforts in searching for a physically meaningful picture for these quantities [6–8].

Recent advances in near-field optics attempting to achieve full spatiotemporal control of light-matter interactions [9] has led to a renewed interest in Lipkin's zilches as a measure of the handedness, or knottedness, of the streamlines describing highly contorted optical fields [10]. In this regard, and motivated by the possibility for enhancing the chiroptical effects (such as circular dichroism (CD) [11]), which leads to enantioselective signals far larger than that due to circularly polarized light (CPL), Tang and Cohen introduced the 00-zilch as a measure of the local density of optical chirality [12]:

$$\mathcal{C}_{\text{vacuum}} \equiv \left[\varepsilon_0 \boldsymbol{\mathcal{E}} \cdot (\nabla \times \boldsymbol{\mathcal{E}}) + \mu_0 \boldsymbol{\mathcal{H}} \cdot (\nabla \times \boldsymbol{\mathcal{H}})\right]/2, \tag{C.1}$$

where ε_0 and μ_0 are the permittivity and permeability of vacuum, respectively, and $\boldsymbol{\mathcal{E}}(\mathbf{r},t)$ and $\boldsymbol{\mathcal{H}}(\mathbf{r},t)$ are the local, time-dependent electric and magnetic fields. Shortly after, this definition for the optical chirality was successfully used in enhanced CD spectroscopic measurements for the experimental detection and characterization of chiral biomolecules [13], thus confirming its physical significance, and highlighting the feasibility for practical applications. The extremely high sensitivity in the chiroptical responses (enhancement factors up to 6 orders of magnitude were reported) was attributed to *superchiral fields* [14]. However, on account of the energy conservation, there should be an upper bound lowering those enhancements [15,16]. It was argued that this fundamental restriction ought to limit the enhancement factor up to 2 orders of magnitude [15]; the other 4 orders should come from the highly twisted evanescent near-field modes [16,17]. It then follows that, essentially, the main requirement for the occurrence of strengthened chiroptical influence in light-matter interaction relies on the complexity in the structure of the EM field distribution [10,17,18]. For this reason, metallic nanostructures represent ideal candidates for investigating chirality-based applications and functionalities in nanophotonics [19–26]. It is certainly surprising, however, that, most of the previous studies on this issue build on the earliest definition for the optical chirality density [5], which is only valid for monochromatic optical fields in free space [12,14,16,27]. Still, there are few works attempting to extend such definition to linear [15], gyrotropic [28], or lossless dispersive media [29].

Inspired by the latest theoretical results concerning the dispersive features of the EM energy momentum, the optical orbital and spin angular momentum [30–32], and the EM helicity [33], in this Letter we report on the optical chirality in lossless and lossy dispersive media. Special emphasis is placed on the role of the mathematical structure of the corresponding conservation law. Indeed, building on previous approaches addressing the EM energy density considering dispersion as well as dissipation [34], we put forward a complete description for the optical chirality conservation law valid for arbitrarily structured optical fields. The only restriction we need to impose relies on the EM characterization of the medium, which must be fitted by Lorentzian line shapes. Hence, our results are completely general [64], and are applicable to any material system, including dielectrics, semiconductors, metals, as well as metamaterials. Further, our findings are perfectly consistent with the ones so far established for optical fields in free space [12,16].

C.II Conservation Law for the Optical Chirality

Conservation laws and symmetry properties of a physical system are, arguably, among the most important cornerstones of modern physics [65]. Indeed, appealing to the principle of least action, Noether's theorem states that, in the absence of sources, conserved quantities and symmetries can be regarded as equivalent features [66]. These theoretical concepts are mathematically described via continuous or discrete symmetry groups, which are in turn related to the corresponding physical transformations [67]. Typical examples of continuous symmetries lead to the conservation of energy, linear momentum and, angular

momentum, which are associated with the invariance under the universal space-time transformations [68]. An insightful picture of the conserved quantities, reminiscent of the quantum formalism [69], allows one to deal with the conserved quantities as differential operators representing the generators of the corresponding infinitesimal symmetry transformations. For the above dynamical properties, the generators simply involve first derivatives with respect to the space-time coordinates acting on the EM fields, and are given explicitly by $\{i\partial_t, i\nabla\}$, for the space-time translations [30], and $i\,(\mathbf{r}\times\nabla)$, for the spatial rotations [31]. Furthermore, it was recently demonstrated that the conservation of the optical chirality is underpinned by $i\,(\partial_t\nabla\times)$ [29], which must be applied on the vector potentials. Importantly, these generators can be used to find the eigenstates of the aforementioned conserved quantities. In this regard, just as the plane waves are the eigenstates of the energy-momentum differential operator, the corresponding eigenstates associated to the optical chirality are the circularly polarized plane waves [29].

The above scheme for identifying continuous conserved quantities only holds in the absence of sources. In the presence of charges and/or currents, conservation laws are to be expressed through the continuity equations [70,71]. Within the EM field theory, the most well-known example is perhaps Poynting's theorem [72], accounting for the energy conservation [1,2]:

$$\nabla\cdot\boldsymbol{\mathcal{S}} = -\left[\boldsymbol{\mathcal{E}}\cdot\partial_t\boldsymbol{\mathcal{D}} + \boldsymbol{\mathcal{H}}\cdot\partial_t\boldsymbol{\mathcal{B}} + \boldsymbol{\mathcal{J}}\cdot\boldsymbol{\mathcal{E}}\right], \tag{C.2}$$

where $\boldsymbol{\mathcal{S}} \equiv \boldsymbol{\mathcal{E}}\times\boldsymbol{\mathcal{H}}$ is the Poynting vector, which represents the energy flux density, and $\boldsymbol{\mathcal{D}}$, $\boldsymbol{\mathcal{B}}$, and $\boldsymbol{\mathcal{J}}$ are the time-dependent electric displacement, magnetic induction, and electric current density, respectively. This expression is generally valid, and can be readily obtained by taking the divergence of the energy flux density. Likewise, we can derive the time-dependent conservation law for the optical chirality from the corresponding chirality flux density [5,12,16]:

$$\boldsymbol{\mathcal{F}} \equiv \left[\boldsymbol{\mathcal{E}}\times(\nabla\times\boldsymbol{\mathcal{H}}) - \boldsymbol{\mathcal{H}}\times(\nabla\times\boldsymbol{\mathcal{E}})\right]/2. \tag{C.3}$$

With the aid of the structural Maxwell's equations and the vector identity, $\nabla\cdot(\boldsymbol{\mathcal{A}}\times\boldsymbol{\mathcal{B}}) = \boldsymbol{\mathcal{B}}\cdot(\nabla\times\boldsymbol{\mathcal{A}}) - \boldsymbol{\mathcal{A}}\cdot(\nabla\times\boldsymbol{\mathcal{B}})$, it follows that

$$\nabla\cdot\boldsymbol{\mathcal{F}} = -\left[\boldsymbol{\mathcal{E}}\cdot\partial_t\left(\nabla\times\boldsymbol{\mathcal{D}}\right) + \boldsymbol{\mathcal{H}}\cdot\partial_t\left(\nabla\times\boldsymbol{\mathcal{B}}\right) + \mathcal{S}_{\mathcal{J}}\right]/2, \tag{C.4}$$

where $\mathcal{S}_{\mathcal{J}} = \boldsymbol{\mathcal{E}}\cdot(\nabla\times\boldsymbol{\mathcal{J}})$ is the current-related sourcelike contribution. Taking into account the general structure of the continuity equation [34], Eq. (C.4) can be recast as

$$\nabla\cdot\boldsymbol{\mathcal{F}} + \partial_t\mathcal{C} = \mathcal{S}, \tag{C.5}$$

where

$$\mathcal{C} \equiv \left[\boldsymbol{\mathcal{E}}\cdot(\nabla\times\boldsymbol{\mathcal{D}}) + \boldsymbol{\mathcal{H}}\cdot(\nabla\times\boldsymbol{\mathcal{B}})\right]/2, \tag{C.6}$$

$$\mathcal{S} \equiv \left[\partial_t\boldsymbol{\mathcal{E}}\cdot(\nabla\times\boldsymbol{\mathcal{D}}) + \partial_t\boldsymbol{\mathcal{H}}\cdot(\nabla\times\boldsymbol{\mathcal{B}}) - \mathcal{S}_{\mathcal{J}}\right]/2, \tag{C.7}$$

are the optical chirality density and the sourcelike terms, respectively. The above expressions represent the most general result for the conservation law of optical chirality, without any restrictions on the nature of the medium. However, they differ significantly from the previously established continuity equation [5,12,16,26],

$$\nabla \cdot \boldsymbol{\mathcal{F}} + \partial_t \mathcal{C}_{\text{vacuum}} = \mathcal{S}_{\text{vacuum}}, \tag{C.8}$$

where $\mathcal{C}_{\text{vacumm}}$ is the optical chirality density as defined in Eq. (C.1), and $\mathcal{S}_{\text{vacuum}} \equiv -\left[\boldsymbol{\mathcal{J}} \cdot (\nabla \times \boldsymbol{\mathcal{E}}) + \boldsymbol{\mathcal{E}} \cdot (\nabla \times \boldsymbol{\mathcal{J}})\right]/2$ is the sourcelike term in free space. The essential discrepancy arises on account of the dispersion-related terms [34]. In particular, it is easy to prove that $\mathcal{C} = \mathcal{C}_{\text{vacuum}} + \mathcal{C}_{\text{medium}}$, where $\mathcal{C}_{\text{medium}} \equiv \left[\boldsymbol{\mathcal{E}} \cdot (\nabla \times \boldsymbol{\mathcal{P}}) + \mu_0 \boldsymbol{\mathcal{H}} \cdot (\nabla \times \boldsymbol{\mathcal{M}})\right]/2$, and $\boldsymbol{\mathcal{P}}$ and $\boldsymbol{\mathcal{M}}$ are the macroscopic polarization and magnetization fields. Strikingly, up to our knowledge, these considerations have never been properly analyzed in previous approaches [12,15,16,29,73]. In fact, even though both the dispersion-related and the dissipation terms are explicitly disregarded in Eq. (C.8), it has been widely used for investigating chiroptical effects in media where the permittivity is highly dispersive, including plasmonic nanostructures as well as metamaterials [19–26]. Thus, as shown below, the dispersion of the material systems brings about important corrections into the original expressions for the optical chirality density [compare Eqs. (C.1) and (C.6)] and the sourcelike terms of the continuity equation [compare Eqs. (C.5) and (C.8)], and hence, it must be generally considered.

C.III Optical Chirality in Lossless Dispersive Media: Brillouin's Approach

For monochromatic electric and magnetic fields in free space, $\boldsymbol{\mathcal{E}}(\mathbf{r},t) = \text{Re}\left[\mathbf{E}(\mathbf{r})e^{-i\omega t}\right]$ and $\boldsymbol{\mathcal{H}}(\mathbf{r},t) = \text{Re}\left[\mathbf{H}(\mathbf{r})e^{-i\omega t}\right]$, the time-averaged optical chirality density is given by [12,16]

$$C_{\text{vacuum}} = \frac{\omega}{2c^2}\text{Im}[\mathbf{E} \cdot \mathbf{H}^*], \tag{C.9}$$

where bold letters stand for complex field amplitudes and the asterisk denotes complex conjugation. A straightforward calculation allows us to show that, for freely propagating EM plane waves, the maximum value of C is achieved for CPL:

$$C_{\text{vacuum}}^{(\pm)\text{CPL}} = \pm\frac{\omega}{2c^2}\frac{1}{Z_0}\left|\mathbf{E}\right|^2, \tag{C.10}$$

where $Z_0 \equiv \sqrt{\mu_0/\varepsilon_0}$ is the vacuum impedance, and the signs $+$ and $-$ correspond to left- and right-handed CPL.

In general, CPL is considered as the paradigmatic example of field displaying optical chirality, and has been widely used for chiroptical measurements [13,14]. Unfortunately, mainly due to the mismatch between the scales of the wavelength and the typical size of chiral objects [10], chiral responses are inherently very weak [11,74]. To overcome this drawback, several efforts have been undertaken for improving the

detection schemes [14,18,75,76], with special emphasis on metallic nanostructures, which are regarded as well suited platforms for strengthening chiroptical light-matter interactions [19–26].

Metals are inherently absorptive and highly dispersive. Something similar happens with semiconductors at energies around the band gap. These features are characterized in terms of the electric permittivity ε (and eventually with the magnetic permeability μ) depending on the frequency ω. According to the Kramers-Kronig relations [1,77], dispersion is necessarily tied to dissipation. Thus, in order to avoid misleading outcomes, the analysis of the local dynamical properties have to be carefully carried out from a material standpoint as well. This is well known for the EM field energy in metals, for which a general treatment has been developed [1,2]. Indeed, in a lossless dispersive medium the energy density is described by the Brillouin's formula [78,79]. Following a similar procedure we may obtain a closed expression for the optical chirality density. For simplicity, we will assume a linear, homogeneous, and isotropic medium such that $\mathbf{D} = \varepsilon_0\varepsilon(\omega)\mathbf{E}$ and $\mathbf{B} = \mu_0\mu(\omega)\mathbf{H}$. From the continuity equation as given in Eq. (C.4), and using the Fourier transforms, the instantaneous distribution of the optical chirality density can be obtained by integrating $\boldsymbol{\mathcal{E}} \cdot \partial_t (\nabla \times \boldsymbol{\mathcal{D}})$ and $\boldsymbol{\mathcal{H}} \cdot \partial_t (\nabla \times \boldsymbol{\mathcal{B}})$ over time. Notice that the integral convergence is constrained by the *slowly varying amplitude approximation* [2]. Within this assumption, the electric contribution reads as

$$\mathcal{C}^{\text{elec}} = \frac{i}{2c^2} \iint \left[\frac{\omega^2 \varepsilon_\omega \mu_\omega}{\omega' + \omega} \right] \mathbf{E}_{\omega'} \cdot \mathbf{H}_\omega e^{-i(\omega'+\omega)t} d\omega' d\omega. \tag{C.11}$$

By proceeding in the same way for the magnetic contribution, summing up both expressions, and integrating them properly over the frequencies ω and ω' [34], we can get the time-averaged optical chirality density in a lossless dispersive media:

$$C_{\text{lossless}} = \text{Re}[n(\omega)\tilde{n}(\omega)] C_{\text{vacuum}} = \frac{\omega}{2} \frac{\text{Im}[\mathbf{E} \cdot \mathbf{H}^*]}{v_p(\omega) v_g(\omega)}, \tag{C.12}$$

where $v_p(\omega) \equiv c/\text{Re}[n(\omega)]$ and $v_g(\omega) \equiv c/\text{Re}[\tilde{n}(\omega)]$, are the phase and group velocities [80,81], respectively, which are in turn expressed in terms of the phase refractive index $n(\omega) \equiv \sqrt{\varepsilon(\omega)\mu(\omega)}$ and the corresponding dispersion-modified group index $\tilde{n}(\omega) \equiv n(\omega) + \omega\,[\partial n(\omega)/\partial\omega]$. A detailed description of the above derivation as well as the current-related contribution can be found in Sec. III B of the Supplemental Material [34].

It should be noted that the same expression for the optical chirality density was previously obtained, but using a more complicated approach (see Eq. (33) in Ref. [29]). Importantly, this definition [Eq. (C.12)] reduces to the standard result [Eq. (C.9)] for freely propagating optical fields, i.e., when $n = 1$. Furthermore, it is important to emphasize the dependence of Eq. (C.12) on the dispersion-related phase and group velocities. From this simple relation, it is easy to realize that we may enhance the optical chirality in artificially engineered materials directly by lowering both velocities [80,81]. This is specifically accomplished in the vicinity of the resonance frequency, i.e., in the anomalous dispersion region [see upper panel of Fig. C.1]. However, in a dispersive and

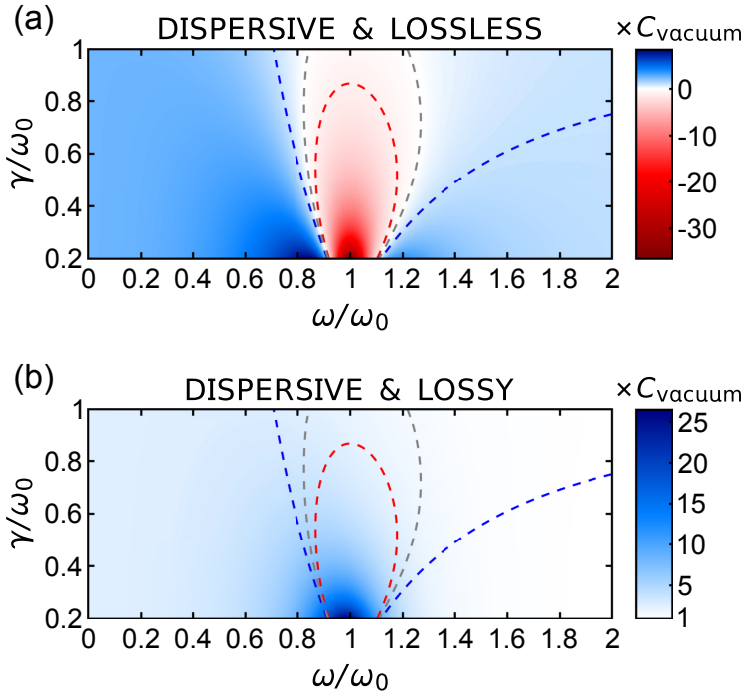

Figure C.1: Optical chirality density in (a) lossless and (b) lossy dispersive media. Material parameters correspond to a nonmagnetic medium ($\mu = 1$), with ε being described by a single Lorentz pole with $\omega_p = \omega_0$. Red, gray, and blue dashed lines indicate the curves where the optical chirality in the lossless case is $-C_{\text{vacuum}}$, 0, and C_{vacuum}, respectively.

lossy media, there are certain frequency ranges where the precise physical meaning of the group velocity turns out to be somewhat unclear [78,79], and Eq. (C.12) may not be valid.

C.IV Optical Chirality in Lossy Dispersive Media: Loudon's Approach

A more physically realistic description of dispersive media requires careful considerations of dissipative effects. In this regard, as previously reported (see, e.g., Refs. [82,83]), the expression of the energy density in dispersive and lossy media crucially depends on the specific model characterizing the medium. In classical theory, ε can be modeled as a collection of Lorentz oscillators [2,84]:

$$\varepsilon_{\text{Drude-Lorentz}}(\omega) = 1 - \sum_n \frac{f_n \omega_p^2}{\omega^2 - \omega_n^2 + i\omega\gamma_n}, \tag{C.13}$$

where f_n, ω_p, ω_n, ω, and γ_n are, respectively, the relative strength of the oscillators, the plasma frequency, the nth resonance frequency, the excitation frequency, and the nth damping constant. This multiresonant model has been proved to fit very well with experiments [64,85,86], and thus, it can generally characterize the electric response of any material system for any frequency and bandwidth. A similar expression can also

be introduced for the magnetic permeability μ, e.g., when describing negative-index metamaterials [87–89]. It should be noted that the latter expression for ε follows from the dynamic equation of the polarization field:

$$\frac{\partial^2 \boldsymbol{\mathcal{P}}_n}{\partial t^2} + \gamma_n \frac{\partial \boldsymbol{\mathcal{P}}_n}{\partial t} + \omega_n^2 \boldsymbol{\mathcal{P}}_n = \varepsilon_0 f_n \omega_p^2 \boldsymbol{\mathcal{E}}_{\mathrm{loc}}, \tag{C.14}$$

with $\boldsymbol{\mathcal{E}}_{\mathrm{loc}}$ being the time-varying external electric field. This relation between the electric and the polarization field is actually the key point to get the general form of the energy density [82,83]. Likewise, taking into account the underlying mathematical structure of the continuity equation [34], we can use Eq. (C.14) (and the corresponding one for the magnetization field) to identify the electric (and the magnetic) contribution of the optical chirality density in dispersive and lossy media. To this aim, we start again from the continuity equation as given in Eq. (C.4). Attempting to find the total time derivative for the electric contribution, we have to express $\boldsymbol{\mathcal{E}} \cdot \partial_t (\nabla \times \boldsymbol{\mathcal{D}})$ in terms of the electric and the polarization fields (and similarly for the magnetic contribution [34]):

$$\boldsymbol{\mathcal{E}} \cdot \partial_t (\nabla \times \boldsymbol{\mathcal{D}}) = \left[\varepsilon_0 \boldsymbol{\mathcal{E}} \cdot \partial_t (\nabla \times \boldsymbol{\mathcal{E}}) + \boldsymbol{\mathcal{E}} \cdot \partial_t (\nabla \times \boldsymbol{\mathcal{P}})\right]. \tag{C.15}$$

In this way, we can also account for the influence of the medium on the chirality density. In the latter expression, the first term of the right-hand side can be rewritten as

$$\boldsymbol{\mathcal{E}} \cdot \partial_t (\nabla \times \boldsymbol{\mathcal{E}}) = \partial_t \left[\boldsymbol{\mathcal{E}} \cdot (\nabla \times \boldsymbol{\mathcal{E}})\right] - \partial_t \boldsymbol{\mathcal{E}} \cdot (\nabla \times \boldsymbol{\mathcal{E}}), \tag{C.16}$$

thereby leading to a total time derivative plus a residual term. This residual term exactly cancels with the one appearing for the magnetic contribution in vacuum [34], thus allowing us to recover the usual expression for the optical chirality in free space [Eq. (C.1)]. On the other hand, the second term in the right-hand side of Eq. (C.15) can be addressed by using the dynamic equation for the polarization field given in Eq. (C.14) (see Sec. III A in the Supplemental Material [34] for further details). Following the same procedure for the magnetic contribution and summing up both expressions, we finally find that the time-averaged optical chirality density in a lossy dispersive medium is

$$C_{\mathrm{lossy}} = \frac{\omega}{4c^2} \mathrm{Im}[(\varepsilon(\omega)\mu_{\mathrm{eff}}(\omega) + \varepsilon_{\mathrm{eff}}(\omega)\mu^*(\omega))\, \mathbf{E} \cdot \mathbf{H}^*], \tag{C.17}$$

where $\varepsilon_{\mathrm{eff}}$ and μ_{eff} are the real-valued effective material parameters, which are defined as

$$\varepsilon_{\mathrm{eff}}(\omega) \equiv 1 + \sum_n \left(\chi_n' + 2\omega\chi_n''/\gamma_n\right), \tag{C.18a}$$

$$\mu_{\mathrm{eff}}(\omega) \equiv 1 + \sum_n \left(\xi_n' + 2\omega\xi_n''/\tilde{\gamma}_n\right), \tag{C.18b}$$

with $\chi = \chi' + i\chi'' \equiv \varepsilon - 1$ and $\xi = \xi' + i\xi'' \equiv \mu - 1$ being the electric and magnetic susceptibilities. Furthermore, as pointed out in the Supplemental Material [34], there is also a current-related contribution which should be included.

As shown in Fig. C.1, both of the above approaches yield different results. Indeed, whereas C_{lossless} [Eq. (C.12)] can display both positive and negative values, the total

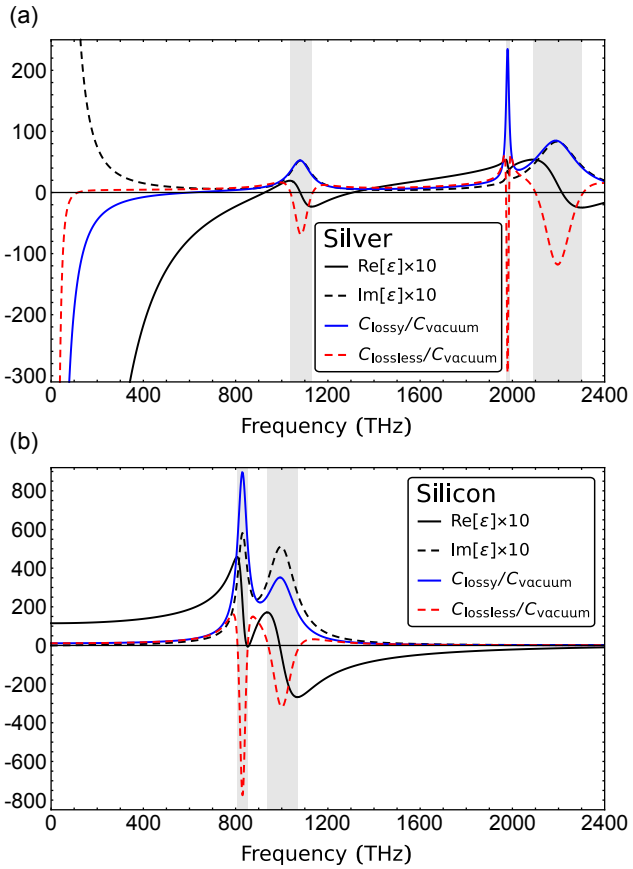

Figure C.2: Optical chirality density for (a) silver and (b) silicon. Material parameters describing ε are taken from Refs. [85,86], respectively. For comparison, we represent the results for lossless (red dashed lines) [Eq. (C.12)] and lossy (blue solid lines) [Eq. (C.17)] dispersive media in terms of C_{vacuum}. The gray shaded areas indicate the spectral ranges with anomalous dispersion.

contribution of C_{lossy} [Eq. (C.17)] remains always positive, with a minimum value of C_{vacuum} that is reached in the high-frequency limit. The largest discrepancies occur close to the resonance frequency. Still, the peaks for both approaches are almost equal in absolute value. These signatures can also be appreciated in Fig. C.2, where we plot the optical chirality density of silver and silicon. Both materials have been modeled using Eq. (C.13) with parameters taken from Refs. [85,86]. From the results in Fig. C.2 we note that C_{lossless} overlaps almost exactly with C_{lossy} for all frequencies, except in the vicinity of the region of anomalous dispersion, i.e., where $d\varepsilon'/d\omega < 0$. There, the curves drastically separate from each other, thereby highlighting the importance of considering dissipative effects.

Equation (C.17) is the main result of this work. To the best of our knowledge, it provides the most general definition for the optical chirality density in dispersive and lossy media, being applicable to any material system, including plasmonic nanostructures [26] and left-handed metamaterials [89]. Yet, our definition differs significantly from the

standard formula for optical fields in free space [12,16], and even from previous suggestions attempting to tackle optical chirality in dispersive media [29,73]. The distinction between our result and those found in previous approaches essentially arises from considering properly the dynamic response of the time-dependent EM fields within a dispersive medium [34]. In this regard, it should be noted that the time derivative of the fields $\boldsymbol{\mathcal{D}}$ and $\boldsymbol{\mathcal{B}}$, must be expressed as convolution integrals in the time domain. Furthermore, in this particular case, regarding lossy dispersive media, the mathematical structure of the continuity equation plays a central role in the identification of the optical chirality density as a conserved dynamical property.

C.V Summary

We have carried out a theoretical analysis of the conservation law for the optical chirality. Taking advantage of previous approaches addressing the EM energy density, we have undertaken a parallel derivation for the optical chirality both in lossless and lossy dispersive media. Remarkably, our description is completely general, i.e., is valid for arbitrarily varying radiation fields, and can be applied to any medium, including dielectrics, semiconductors, as well as highly lossy material systems such as metals and metamaterials. In view of the growing interest in chirality and chiral light-matter interaction, we expect that these results will aid the development of plasmonic and metamaterial nanostructures for advanced chiroptical applications [17,89], especially in the context of enhanced enantioselectivity, and detection and characterization of chiral biomolecules via tailored chiral and nonchiral structures [90,91].

Acknowledgments

The authors are grateful to C. García-Meca for valuable comments and discussions. This work was supported by funding from Ministerio de Economía y Competitividad (MINECO) of Spain under Contract No. TEC2014-51902-C2-1-R.

References

[1] J. D. Jackson, *Classical Electrodynamics* (Wiley, New York, USA, 1999).

[2] L. Novotny and B. Hecht, *Principles of Nano-Optics* (Cambridge University Press, Cambridge, England, 2012).

[3] T. W. B. Kibble, *Conservation laws for free fields*, J. Math. Phys. **6**, 1022 (1965).

[4] W. I. Fushchich and A. G. Nikitin, *The complete sets of conservation laws for the electromagnetic field*, J. Phys. A **25**, L231 (1992).

[5] D. M. Lipkin, *Existence of a new conservation law in electromagnetic theory*, J. Math. Phys. **5**, 696 (1964).

[6] T. A. Morgan, *Two classes of new conservation laws for the electromagnetic field and for other massless fields*, J. Math. Phys. **5**, 1659 (1964).

[7] M. G. Calkin, *An invariance property of the free electromagnetic field*, Am. J. Phys. **33**, 958 (1965).

[8] D. J. Candlin, *Analysis of the new conservation law in electromagnetic theory*, Nuovo Cimento **37**, 1390 (1965).

[9] T. Brixner, F. J. García de Abajo, J. Schneider, and W. Pfeiffer, *Nanoscopic ultrafast space-time-resolved spectroscopy*, Phys. Rev. Lett. **95**, 093901 (2005).

[10] N. Yang, Y. Tang, and A. E. Cohen, *Spectroscopy in sculpted fields*, Nano Today **4**, 269 (2009).

[11] L. D. Barron, *Molecular Light Scattering and Optical Activity* (Cambridge University Press, Cambridge, England, 2004).

[12] Y. Tang and A. E. Cohen, *Optical chirality and its interaction with matter*, Phys. Rev. Lett. **104**, 163901 (2010).

[13] E. Hendry, T. Carpy, J. Johnston, M. Popland, R. V. Mikhaylovskiy, A. J. Lapthorn, S. M. Kelly, L. D. Barron, N. Gadegaard, and M. Kadodwala, *Ultrasensitive detection and characterization of biomolecules using superchiral fields*, Nat. Nanotechnol. **5**, 783 (2010).

[14] Y. Tang and A. E. Cohen, *Enhanced enantioselectivity in excitation of chiral molecules by superchiral light*, Science **332**, 333 (2011).

[15] J. S. Choi and M. Cho, *Limitations of a superchiral field*, Phys. Rev. A **86**, 063834 (2012).

[16] K. Y. Bliokh and F. Nori, *Characterizing optical chirality*, Phys. Rev. A **83**, 021803 (2011).

[17] L. E. Barr, S. A. R. Horsley, I. R. Hooper, J. K. Eager, C. P. Gallagher, S. M. Hornett, A. P. Hibbins, and E. Hendry, *Investigating the nature of chiral near-field interactions*, Phys. Rev. B **97**, 155418 (2018).

[18] C. Kramer, M. Schäferling, T. Weiss, H. Giessen, and T. Brixner, *Analytic optimization of near-field optical chirality enhancement*, ACS Photonics **4**, 396 (2017).

[19] M. Schäferling, D. Dregely, M. Hentschel, and H. Giessen, *Tailoring enhanced optical chirality: Design principles for chiral plasmonic nanostructures*, Phys. Rev. X **2**, 031010 (2012).

[20] N. Meinzer, E. Hendry, and W. L. Barnes, *Probing the chiral nature of electromagnetic fields surrounding plasmonic nanostructures*, Phys. Rev. B **88**, 041407 (2013).

[21] V. K. Valev, J. J. Baumberg, C. Sibilia, and T. Verbiest, *Chirality and chiroptical effects in plasmonic nanostructures: Fundamentals, recent progress, and outlook*, Adv. Mater. **25**, 2517 (2013).

[22] M. L. Nesterov, X. Yin, M. Schäferling, H. Giessen, and T. Weiss, *The role of plasmon-generated near fields for enhanced circular dichroism spectroscopy*, ACS Photonics **3**, 578 (2016).

[23] J. T. Collins, C. Kuppe, D. C. Hooper, C. Sibilia, M. Centini, and V. K. Valev, *Chirality and chiroptical effects in metal nanostructures: Fundamentals and current trends*, Adv. Opt. Mater. **5**, 1700182 (2017).

[24] Y. Luo, C. Chi, M. Jiang, R. Li, S. Zu, Y. Li, and Z. Fang, *Plasmonic chiral nanostructures: Chiroptical effects and applications*, Adv. Opt. Mater. **5**, 1700040 (2017).

[25] M. Hentschel, M. Schäferling, X. Duan, H. Giessen, and N. Liu, *Chiral plasmonics*, Sci. Adv. **3**, e1602735 (2017).

[26] M. Schäferling, *Chiral Nanophotonics: Chiral Optical Properties of Plasmonic Systems* (Springer, Berlin, 2017).

[27] M. M. Coles and D. L. Andrews, *Chirality and angular momentum in optical radiation*, Phys. Rev. A **85**, 063810 (2012).

[28] I. Proskurin, A. S. Ovchinnikov, P. Nosov, and J. Kishine, *Optical chirality in gyrotropic media: symmetry approach*, New J. Phys. **19**, 063021 (2017).

[29] T. G. Philbin, *Lipkin's conservation law, Noether's theorem, and the relation to optical helicity*, Phys. Rev. A **87**, 043843 (2013).

[30] T. G. Philbin, *Electromagnetic energy momentum in dispersive media*, Phys. Rev. A **83**, 013823 (2011); Erratum, Phys. Rev. A **85**, 059902 (2012).

[31] T. G. Philbin and O. Allanson, *Optical angular momentum in dispersive media*, Phys. Rev. A **86**, 055802 (2012).

[32] K. Y. Bliokh, A. Y. Bekshaev, and F. Nori, *Optical momentum, spin, and angular momentum in dispersive media*, Phys. Rev. Lett. **119**, 073901 (2017).

[33] F. Alpeggiani, K. Y. Bliokh, F. Nori, and L. Kuipers, *Electromagnetic helicity in complex media*, Phys. Rev. Lett. **120**, 243605 (2018).

[34] See Supplemental Material at http://link.aps.org/supplemental/10.1103/PhysRevLett.121.043901 for further details on the derivation of the continuity equation (or conservation law) for both the energy (Sec. I), which includes Refs. [35–63], and the optical chirality (Sec. II) in dispersive and lossy media. The Supplemental Material also contains a detailed derivation of the optical chirality density and the corresponding rate of losses, considering dispersion as well as dissipation (Sec. III).

[35] V. G. Veselago, *The electrodynamics of substances with simultaneously negative values of ϵ and μ*, Sov. Phys. Usp. **10**, 509 (1968).

[36] J. B. Pendry, *Negative refraction makes a perfect lens*, Phys. Rev. Lett. **85**, 3966 (2000).

[37] H. J. Lezec, J. A. Dionne, and H. A. Atwater, *Negative refraction at visible frequencies*, Science **316**, 430 (2007).

[38] N. Engheta, *Circuits with light at nanoscales: Optical nanocircuits inspired by metamaterials*, Science **317**, 1698 (2007).

[39] J. Valentine, S. Zhang, T. Zentgraf, E. Ulin-Avila, D. A. Genov, G. Bartal, and X. Zhang, *Three-dimensional optical metamaterial with a negative refractive index*, Nature (London) **455**, 376 (2008).

[40] T. J. Cui and J. A. Kong, *Time-domain electromagnetic energy in a frequency-dispersive left-handed medium*, Phys. Rev. B **70**, 205106 (2004).

[41] S. A. Tretyakov, *Electromagnetic field energy density in artificial microwave materials with strong dispersion and loss*, Phys. Lett. A **343**, 231 (2005).

[42] A. D. Boardman and K. Marinov, *Electromagnetic energy in a dispersive metamaterial*, Phys. Rev. B **73**, 165110 (2006).

[43] P.-G. Luan, *Power loss and electromagnetic energy density in a dispersive metamaterial medium*, Phys. Rev. E **80**, 046601 (2009).

[44] A. Raman and S. Fan, *Photonic band structure of dispersive metamaterials formulated as a Hermitian eigenvalue problem*, Phys. Rev. Lett. **104**, 087401 (2010).

[45] W. Shin, A. Raman, and S. Fan, *Instantaneous electric energy and electric power dissipation in dispersive media*, J. Opt. Soc. Am. B **29**, 1048 (2012).

[46] F. S. S. Rosa, D. A. R. Dalvit, and P. W. Milonni, *Electromagnetic energy, absorption, and Casimir forces: Uniform dielectric media in thermal equilibrium*, Phys. Rev. A **81**, 033812 (2010).

[47] K. J. Webb and Shivanand, *Electromagnetic field energy in dispersive materials*, J. Opt. Soc. Am. B **27**, 1215 (2010).

[48] F. D. Nunes, T. C. Vasconcelos, M. Bezerra, and J. Weiner, *Electromagnetic energy density in dispersive and dissipative media*, J. Opt. Soc. Am. B **28**, 1544 (2011).

[49] J. Askne and B. Lind, *Energy of electromagnetic waves in the presence of absorption and dispersion*, Phys. Rev. A **2**, 2335 (1970).

[50] C.-G. Huang and Y.-Z. Zhang, *Poynting vector, energy density, and energy velocity in an anomalous dispersion medium*, Phys. Rev. A **65**, 015802 (2001).

[51] R. W. Ziolkowski, *Superluminal transmission of information through an electromagnetic metamaterial*, Phys. Rev. E **63**, 046604 (2001).

[52] R. A. Shelby, D. R. Smith, and S. Schultz, *Experimental verification of a negative index of refraction*, Science **292**, 77 (2001).

[53] L. J. Wang, A. Kuzmich, and A. Dogariu, *Gain-assisted superluminal light propagation*, Nature (London) **406**, 277 (2000).

[54] S. Glasgow, M. Ware, and J. Peatross, *Poynting's theorem and luminal total energy transport in passive dielectric media*, Phys. Rev. E **64**, 046610 (2001).

[55] G. Dolling, C. Enkrich, M. Wegener, C. M. Soukoulis, and S. Linden, *Simultaneous negative phase and group velocity of light in a metamaterial*, Science **312**, 892 (2006).

[56] E. Feigenbaum, N. Kaminski, and M. Orenstein, *Negative dispersion: a backward wave or fast light? Nanoplasmonic examples*, Opt. Express **17**, 18934 (2009).

[57] D. F. Nelson, *Momentum, pseudomomentum, and wave momentum: Toward resolving the Minkowski-Abraham controversy*, Phys. Rev. A **44**, 3985 (1991).

[58] S. M. Barnett and R. Loudon, *The enigma of optical momentum in a medium*, Phil. Trans. R. Soc. A **368**, 927 (2010).

[59] S. M. Barnett, *Resolution of the Abraham-Minkowski dilemma*, Phys. Rev. Lett. **104**, 070401 (2010).

[60] K. Y. Bliokh, A. Y. Bekshaev, and F. Nori, *Optical momentum and angular momentum in complex media: from the Abraham-Minkowski debate to unusual properties of surface plasmon-polaritons*, New J. Phys. **19**, 123014 (2017).

[61] M. G. Silveirinha, *Reexamination of the Abraham-Minkowski dilemma*, Phys. Rev. A **96**, 033831 (2017).

[62] K. E. Oughstun and S. Shen, *Velocity of energy transport for a time-harmonic field in a multiple-resonance Lorentz medium*, J. Opt. Soc. Am. B **5**, 2395 (1988).

[63] F. D. Nunes, B.-H. V. Borges, and J. Weiner, *Analysis of dispersive and dissipative media with optical resonances*, Opt. Express **20**, 15679 (2012).

[64] H. S. Sehmi, W. Langbein, and E. A. Muljarov, *Optimizing the Drude-Lorentz model for material permittivity: Method, program, and examples for gold, silver, and copper*, Phys. Rev. B **95**, 115444 (2017).

[65] W. I. Fushchich and A. G. Nikitin, *Symmetries of Maxwell's Equations. Mathematics and its Applications* (Springer, Amsterdam, 1987).

[66] E. Noether, *Invariant variation problems*, Gott. Nachr. **1918**, 235 (1918) [Transp. Theory Stat. Phys. **1**, 186 (1971)].

[67] W.-K Tung, *Group Theory in Physics* (World Scientific, Singapore, 1985).

[68] R. P. Cameron, J. B. Götte, S. M. Barnett, and A. M. Yao, *Chirality and the angular momentum of light*, Phil. Trans. R. Soc. A **375**, 20150433 (2017).

[69] S. Weinberg, *The Quantum Theory of Fields* (Cambridge University Press, Cambridge, UK, 1995).

[70] G. Nienhuis, *Conservation laws and symmetry transformations of the electromagnetic field with sources*, Phys. Rev. A **93**, 023840 (2016).

[71] I. Fernandez-Corbaton and C. Rockstuhl, *Unified theory to describe and engineer conservation laws in light-matter interactions*, Phys. Rev. A **95**, 053829 (2017).

[72] J. H. Poynting, *On the transfer of energy in the electromagnetic field*, Phil. Trans. R. Soc. London **175**, 343 (1884).

[73] L. V. Poulikakos, P. Gutsche, K. M. McPeak, S. Burger, J. Niegemann, C. Hafner, and D. J. Norris, *Optical chirality flux as a useful far-field probe of chiral near fields*, ACS Photonics **3**, 1619 (2016).

[74] H. Rhee, J. S. Choi, D. J. Starling, J. C. Howell, and M. Cho, *Amplifications in chiroptical spectroscopy, optical enantioselectivity, and weak value measurement*, Chem. Sci. **4**, 4107 (2013).

[75] C. Rosales-Guzmán, K. Volke-Sepulveda, and J. P. Torres, *Light with enhanced optical chirality*, Opt. Lett. **37**, 3486 (2012).

[76] I. Fernandez-Corbaton, M. Fruhnert, and C. Rockstuhl, *Objects of maximum electromagnetic chirality*, Phys. Rev. X **6**, 031013 (2016).

[77] M. V. Gorkunov, V. E. Dmitrienko, A. A. Ezhov, V. V. Artemov, and O. Y. Rogov, *Implications of the causality principle for ultra chiral metamaterials*, Sci. Rep. **5**, 9273 (2015).

[78] L. Brillouin, *Wave Propagation and Group Velocity* (Academic, New York, USA, 1960).

[79] L. D. Landau, E. M. Lifshitz, and L. P. Pitaevskii, *Electrodynamics of Continuous Media* (Pergamon, New York, USA, 1984).

[80] R. W. Boyd and D. J. Gauthier, *Controlling the velocity of light pulses*, Science **326**, 1074 (2009).

[81] V. Gerasik and M. Stastna, *Complex group velocity and energy transport in absorbing media*, Phys. Rev. E **81**, 056602 (2010).

[82] R. Loudon, *The propagation of electromagnetic energy through an absorbing dielectric*, J. Phys. A: Gen. Phys. **3**, 233 (1970).

[83] R. Ruppin, *Electromagnetic energy density in a dispersive and absorptive material*, Phys. Lett. A **299**, 309 (2002).

[84] S. A. Maier, *Plasmonics: Fundamentals and Applications* (Springer, New York, USA, 2007).

[85] A. D. Rakić, A. B. Djurišić, J. M. Elazar, and M. L. Majewski, *Optical properties of metallic films for vertical-cavity optoelectronic devices*, Appl. Opt. **37**, 5271 (1998).

[86] E. D. Palik, *Handbook of Optical Constants of Solids* (Academic Press, New York, USA, 1985).

[87] D. R. Smith, W. J. Padilla, D. C. Vier, S. C. Nemat-Nasser, and S. Schultz, *Composite medium with simultaneously negative permeability and permittivity*, Phys. Rev. Lett. **84**, 4184 (2000).

[88] C. García-Meca, J. Hurtado, J. Martí, A. Martínez, W. Dickson, and A. V. Zayats, *Low-loss multilayered metamaterial exhibiting a negative index of refraction at visible wavelengths*, Phys. Rev. Lett. **106**, 067402 (2011).

[89] S. J. Yoo, M. Cho, and Q.-Han Park, *Globally enhanced chiral field generation by negative-index metamaterials*, Phys. Rev. B **89**, 161405 (2014); S. J. Yoo and Q.-Han Park, *Chiral light-matter interaction in optical resonators*, Phys. Rev. Lett. **114**, 203003 (2015).

[90] A. García-Etxarri and J. A. Dionne, *Surface-enhanced circular dichroism spectroscopy mediated by nonchiral nanoantennas*, Phys. Rev. B **87**, 235409 (2013).

[91] G. Pellegrini, M. Finazzi, M. Celebrano, L. Duò, and P. Biagioni, *Chiral surface waves for enhanced circular dichroism*, Phys. Rev. B **95**, 241402 (2017).

Chapter 5

PAPER C: Supplemental Material

Optical Chirality in Dispersive and Lossy Media

Phys. Rev. Lett. 121, 043901 (2018)

Supplemental Material: Optical Chirality in Dispersive and Lossy Media

J. Enrique Vázquez-Lozano and Alejandro Martínez

Nanophotonics Technology Center, Universitat Politècnica de València, Camino de Vera s/n, 46022 Valencia, Spain

Building on the earlier approaches addressing the electromagnetic energy density in dispersive and lossy media, in this supplemental material we provide a parallel derivation for the optical chirality density considering dispersion as well as dissipation. To this aim, we first elaborate on the most general form of the continuity equation for the optical chirality. As a result we find a complete description, valid for arbitrary structured optical fields regardless of the time dependence. The only restriction we need to impose relies on the characterization of the material parameters, which must be fitted by Lorentzian line shapes. In the particular case of time-harmonic fields in a linear medium, we show that our findings are perfectly consistent with the ones so far established for electromagnetic fields in free space.

C.SM.I Energy Conservation in Dispersive and Lossy Media: Energy Density and Flow

The energy conservation law, also referred to as the Poynting's theorem, is a fundamental statement of electrodynamics [S1]. Even though at a first glance it seems to be a somewhat trivial concern, the situation may become more complicated when considering an optical field traveling through a dispersive medium, i.e., a material system whose electromagnetic response depends on the frequency of the applied field. In the time domain field representation this means that the material response is not instantaneous, but it relies on the electromagnetic fields at all previous time instants. Indeed, according to the basic properties of Fourier transform, this is described in terms of a convolution in the time domain of material equations [S2]. This behavior is actually characterized by means of the electric permittivity ε, and the magnetic permeability, μ, both depending on the frequency ω, and described by the corresponding constitutive relations, which account for the influence of the electromagnetic radiation on matter. Importantly, it should be noted that, strictly speaking, dispersion is necessarily tied to dissipation. This connection is well established by the so-called Kramers-Kronig relations [S3], according to which the real and imaginary parts of the material parameters ($\varepsilon(\omega) = \varepsilon' + i\varepsilon''$ and $\mu(\omega) = \mu' + i\mu''$) appear to be coupled together. In addition, it has been demonstrated that Kramers-Kronig relations underpin the fundamental principle of causality, and hence,

initial assumptions regarding dispersion and dissipation have to be carefully considered, otherwise they may lead to misleading outcomes. Still, we can find many cases where is assumed a dispersive medium neglecting the losses.

The relatively recent advent of left-handed materials [S4–S7], and the development of metamaterial photonics in general [S8–S10], have led to reexamine both the treatment and the formulation [S11–S21] of the field energy in dispersive media [S1,S2,S22,S23]. In this respect, one of the main difficulties arises on account of a *bona fide* interpretation about each of the contributions appearing in the continuity equation, e.g., the sense of negative values for the energy density (in regards to the thermodynamic significance of the stability conditions [S23]) in the anomalous dispersion region (near the resonance frequencies) [S24–S27], or the attainable superluminal (or even backward) light propagation [S28–S31]. Furthermore, owing to the close relation between the Poynting vector and the electromagnetic momentum [S32], the long-standing controversy known as the Abraham-Minkowski dilemma [S33], that still remains as a subject of current interest around the proper definition of the linear momentum for optical field in media, may also be an additional source of puzzling discussions and conclusions [S34–S36].

Below, we briefly sketch the derivation outlined by Loudon [S11] (and extended by Ruppin [S12]) in order to settle out an appropriate framework for the subsequent analysis dealing with the optical chirality conservation law. Moreover, aiming to find a closed expression, we also look into the adiabatic-like classical approaches put forward by Brillouin [S22], and Landau [S23]. For the sake of clarity, throughout this work we will use a distinct notation either for the real-valued electromagnetic radiation in the time domain, or for the complex fields in the frequency domain. It is well known that both representations are related to each other via (inverse) Fourier transform [S37]:

$$\boldsymbol{\mathcal{F}}(\mathbf{r},t)=\int_{-\infty}^{+\infty}\mathbf{F}(\mathbf{r},\omega)e^{-i\omega t}d\omega \qquad \Longleftrightarrow \qquad \mathbf{F}(\mathbf{r},\omega)=\frac{1}{2\pi}\int_{-\infty}^{+\infty}\boldsymbol{\mathcal{F}}(\mathbf{r},t)e^{i\omega t}dt, \quad \text{(C.S1)}$$

where the vector field $\boldsymbol{\mathcal{F}}(\mathbf{r},t)$ (or $\mathbf{F}(\mathbf{r},\omega)$) stands for the electric field $\boldsymbol{\mathcal{E}}$, the electric displacement $\boldsymbol{\mathcal{D}}$, the magnetic field $\boldsymbol{\mathcal{H}}$, or the magnetic induction $\boldsymbol{\mathcal{B}}$ (or their corresponding complex-like counterparts). Moreover, so as to avoid cumbersome notations, we shall omit the argument in the field expressions.

Taking into account the above convention, the general expression for the time-dependent energy conservation law can be straightforwardly stemmed from the vector identity $\nabla\cdot(\boldsymbol{\mathcal{A}}\times\boldsymbol{\mathcal{B}})=\boldsymbol{\mathcal{B}}\cdot(\nabla\times\boldsymbol{\mathcal{A}})-\boldsymbol{\mathcal{A}}\cdot(\nabla\times\boldsymbol{\mathcal{B}})$, with the aid of the structural (or curl-like) Maxwell's equations $\nabla\times\boldsymbol{\mathcal{E}}=-\partial_t\boldsymbol{\mathcal{B}}$ and $\nabla\times\boldsymbol{\mathcal{H}}=\partial_t\boldsymbol{\mathcal{D}}+\boldsymbol{\mathcal{J}}$:

$$\nabla\cdot\boldsymbol{\mathcal{S}}=-\boldsymbol{\mathcal{E}}\cdot\partial_t\boldsymbol{\mathcal{D}}-\boldsymbol{\mathcal{H}}\cdot\partial_t\boldsymbol{\mathcal{B}}-\boldsymbol{\mathcal{J}}\cdot\boldsymbol{\mathcal{E}}, \quad \text{(C.S2)}$$

where $\boldsymbol{\mathcal{S}}\equiv\boldsymbol{\mathcal{E}}\times\boldsymbol{\mathcal{H}}$ is the Poynting vector, which represent the energy flux density [S1], and $\boldsymbol{\mathcal{J}}$ is the electric current density. The previous equation is known as the differential form of Poynting's theorem and is an absolutely general result, i.e., holds for both lossy

and lossless media [S1,S2,S23,S37]. Besides to express the energy balance over the whole system, due to its mathematical structure,

$$\nabla \cdot [\text{FLUX}] + \partial_t [\text{CONSERVED PROPERTY}] = [\text{SOURCE or SINK}], \tag{C.S3}$$

the continuity equation, in conjunction with Noether's theorem, constitutes a powerful tool for identifying and analyzing dynamical properties that are often, but not always, conserved, such as the energy, the linear momentum, or the optical chirality, among many others. Therefore, in the simplest case of linear and nondispersive media, i.e, if $\boldsymbol{\mathcal{D}} = \varepsilon_0 \varepsilon \boldsymbol{\mathcal{E}}$ and $\boldsymbol{\mathcal{B}} = \mu_0 \mu \boldsymbol{\mathcal{H}}$, with $\varepsilon, \mu \in \mathbb{R}$, Eq. (C.S2) can be recast as

$$\nabla \cdot \boldsymbol{\mathcal{S}} + \partial_t \mathcal{W} = -\boldsymbol{\mathcal{J}} \cdot \boldsymbol{\mathcal{E}}, \tag{C.S4}$$

where $\mathcal{W} = [\boldsymbol{\mathcal{E}} \cdot \boldsymbol{\mathcal{D}} + \boldsymbol{\mathcal{H}} \cdot \boldsymbol{\mathcal{B}}]/2$ is the instantaneous energy density stored (or conserved) in the electromagnetic field, and $\boldsymbol{\mathcal{J}} \cdot \boldsymbol{\mathcal{E}}$ represent the power loss dissipated to the medium on account of external current sources [S2,S23,S37]. However, a more physically realistic description requires careful considerations of dispersion and, consequently, dissipation [S38]. In such a case, as pointed out above, the dynamic response of a time-dependent electric field passing through a dispersive medium is expressed as [S2]

$$\boldsymbol{\mathcal{D}}(\mathbf{r}, t) = \int_{-\infty}^{t} \varepsilon(t - t') \boldsymbol{\mathcal{E}}(\mathbf{r}, t') dt' = \int_{-\infty}^{+\infty} \varepsilon(t - t') \boldsymbol{\mathcal{E}}(\mathbf{r}, t') dt'. \tag{C.S5}$$

Notice that a similar expression can be posed for the magnetic contribution in terms of μ. Here it is worth observing that Eq. (C.S2) involves the time derivative of the fields $\boldsymbol{\mathcal{D}}$ and $\boldsymbol{\mathcal{B}}$, which are in turn written as the convolution integral given in Eq. (C.S5). This is in fact the main difficulty for obtaining, in this case, a general and closed expression for the instantaneous electromagnetic energy density. Nevertheless, there are several routes to overcome the evaluation of the time derivative [S11–S23], each of them subject to well distinct prescriptions relying upon assumptions concerning both the characteristics of the medium, and the time dependence of the electromagnetic fields. In the present work we pursue an approach as general as possible, so that it can be applied to an arbitrarily varying radiation field which propagates within a truly dispersive media, namely, including the absorption losses as well. However it should be emphasized that the expressions accounting for both the energy density stored and the dissipation, will crucially depend upon the specific features of the model characterizing the medium [S14–S16]. Hence, for practical purposes, we will focus on the pragmatic treatment provided by Loudon [S11], which consider an absorbing classical dielectric with a single resonance frequency, i.e., a Lorentz-like medium. This approach has been further extended by many other authors to account for dispersive magnetic permeabilities [S12–S16], as well as the possibility of multiple resonance frequencies describing the influence of interband transition effects [S17,S18,S39,S40]. For completeness, and for convenience in subsequent analysis, we shall take into account these generalizations throughout this work.

Optical properties of metals (often regarded as the paradigmatic example of dispersive media) may be classically modeled by distinguishing between the response owing to the free

electrons moving within the conduction band (usually referred to as the intraband effects), and that of the bound carriers, giving rise to the interband transitions [S37,S41]. This can be generally described as a collection of N oscillators in the following form [S42,S43]:

$$\varepsilon_{\mathrm{D-L}}(\omega) = 1 - \frac{f_0\omega_p^2}{\omega^2 + i\omega\gamma_0} - \sum_{n=1}^{N-1} \frac{f_n\omega_p^2}{\omega^2 - \omega_n^2 + i\omega\gamma_n} = 1 - \sum_{n=0}^{N-1} \frac{f_n\omega_p^2}{\omega^2 - \omega_n^2 + i\omega\gamma_n}, \tag{C.S6}$$

where f_n, ω_p, ω_n, ω and γ_n are, respectively, the relative strength of the oscillators, the plasma frequency, the nth resonance (or restoring) frequency, the excitation frequency, and the nth damping constant (or characteristic collision frequency). Note that, since the Drude model only holds for intraband effects, there is no resonant behavior for the first term in Eq. (C.S6), and thus $\omega_0 \equiv 0$. In any case, each of the Lorentz-like oscillators is described as a pole in the dielectric function [Eq. (C.S6)], and can be readily achieved from the equation of motion for a bound electron with undamped resonance frequency ω_n, experiencing a damping force characterized by γ_n, and subjected to a time-varying external electric field $\boldsymbol{\mathcal{E}}_{\mathrm{loc}}$ [S44]:

$$\frac{\partial^2\mathbf{r}_n}{\partial t^2} + \gamma_n\frac{\partial\mathbf{r}_n}{\partial t} + \omega_n^2\mathbf{r}_n = -\frac{q_\mathrm{e}}{m_\mathrm{e}}\boldsymbol{\mathcal{E}}_{\mathrm{loc}}, \tag{C.S7}$$

where m_e, q_e and $\mathbf{r}_n$ stand for the effective mass, charge, and the displacement of the electrons, respectively. If we further interpret each mode as an electron gas of uniform density ρ_n, the collective effect emerging from all individual displacement leads to a polarization field $\boldsymbol{\mathcal{P}}_n = \rho_n\mathbf{p}_n = (-q_\mathrm{e}\rho_n)\,\mathbf{r}_n$, where $\mathbf{p}_n$ is the electric dipole moment associated to the nth mode. Hence, Eq. (C.S7) can be rewritten as

$$\frac{\partial^2\boldsymbol{\mathcal{P}}_n}{\partial t^2} + \gamma_n\frac{\partial\boldsymbol{\mathcal{P}}_n}{\partial t} + \omega_n^2\boldsymbol{\mathcal{P}}_n = \varepsilon_0 f_n\omega_p^2\boldsymbol{\mathcal{E}}_{\mathrm{loc}}, \tag{C.S8}$$

where ε_0 is the electric permittivity of vacuum, $\omega_p \equiv \sqrt{q_\mathrm{e}^2\rho_\mathrm{e}/(m_\mathrm{e}\varepsilon_0)}$, and $f_n \equiv \rho_n/\rho_\mathrm{e}$, with ρ_e being the total density of Drude and Lorentz oscillators. By solving Eq. (C.S8) for fields with harmonic time dependence of the form $e^{-i\omega t}$, one can obtain the individual contribution of the oscillators:

$$\mathbf{P}_n = \rho_n\alpha_n^{(\mathrm{e})}(\omega)\mathbf{E}_{\mathrm{loc}} = \varepsilon_0\left[\frac{f_n\omega_p^2}{\omega_n^2 - \omega^2 - i\omega\gamma_n}\right]\mathbf{E}_{\mathrm{loc}}, \tag{C.S9}$$

where $\alpha_n^{(\mathrm{e})}(\omega)$ is the electric dipole polarizability. Therefore, each of the Lorentz poles contribute to the electric permittivity given in Eq. (C.S6) in such a way that

$$\mathbf{D} = \varepsilon_0\left[1 - \sum_{n=0}^{N-1}\frac{f_n\omega_p^2}{\omega^2 - \omega_n^2 + i\omega\gamma_n}\right]\mathbf{E}, \tag{C.S10}$$

where the total polarization field is defined as $\mathbf{P} \equiv \sum_n \langle\mathbf{P}_n\rangle$, and the macroscopic electric field is $\mathbf{E} \equiv \langle\mathbf{E}_{\mathrm{loc}}\rangle$, with the angular brackets indicating an average over space [S44]. This procedure is specific for getting the electric permittivity in a linear medium modeled as a combination of Drude and Lorentz oscillators [S39–S43]. Still, provided the magnetic

permeability can be properly tailored by Lorentzian line shapes, it may also be extended to magnetically dispersive media [S12–S16] by means of the corresponding dynamic equation associated to the magnetization field $\boldsymbol{\mathcal{M}}_n$:

$$\frac{\partial^2 \boldsymbol{\mathcal{M}}_n}{\partial t^2} + \tilde{\gamma}_n \frac{\partial \boldsymbol{\mathcal{M}}_n}{\partial t} + \tilde{\omega}_n^2 \boldsymbol{\mathcal{M}}_n = \tilde{f}_n \tilde{\omega}_n^2 \boldsymbol{\mathcal{H}}_{\mathrm{loc}}, \tag{C.S11}$$

where, analogously to the previous case, $\tilde{\omega}_n$, $\tilde{\gamma}_n$, and $\tilde{f}_n$ are, respectively, the nth resonance frequency of the magnetic dipole oscillators, the nth magnetic damping constant and the magnetic-like oscillator strength. It should be noted that in earlier works addressing magnetic dispersion (e.g., when characterizing split-ring resonator-based structures) only a single Lorentzian resonance takes place [S12–S16]. Nonetheless, for completeness, we shall express the magnetic permeability by considering the possible appearance of N magnetic dipole oscillators of the form

$$\mathbf{M}_n = \left[\frac{\tilde{f}_n \tilde{\omega}_n^2}{\tilde{\omega}_n^2 - \omega^2 - i\omega\tilde{\gamma}_n} \right] \mathbf{H}_{\mathrm{loc}}. \tag{C.S12}$$

Hence, if we define the total magnetization field as $\mathbf{M} \equiv \sum_n \langle \mathbf{M}_n \rangle$, and the macroscopic magnetic field $\mathbf{H} \equiv \langle \mathbf{H}_{\mathrm{loc}} \rangle$ [S44], the magnetic permeability is given by

$$\mu_{\mathrm{D-L}}(\omega) = 1 - \sum_{n=0}^{N-1} \frac{\tilde{f}_n \tilde{\omega}_n^2}{\omega^2 - \tilde{\omega}_n^2 + i\omega\tilde{\gamma}_n}. \tag{C.S13}$$

After this brief outline, we are now in the position to show the expression for the energy conservation law in dispersive and lossy media, fully accounting for both the energy density and the power density lost due to light-matter interactions. Whatever the specific electromagnetic properties of the medium, it can always be represented in terms of the polarization and the magnetization vector fields as follows:

$$\boldsymbol{\mathcal{D}} = \varepsilon_0 \boldsymbol{\mathcal{E}} + \boldsymbol{\mathcal{P}}, \tag{C.S14}$$

$$\boldsymbol{\mathcal{B}} = \mu_0 \boldsymbol{\mathcal{H}} + \mu_0 \boldsymbol{\mathcal{M}}. \tag{C.S15}$$

Then, the first two terms in the right-hand side of Eq. (C.S2) can be straightforwardly evaluated by using the dynamic equations for the polarization and magnetization fields [Eqs. (C.S8) and (C.S11)], with the aid of Eqs. (C.S14) and (C.S15):

$$\boldsymbol{\mathcal{E}} \cdot \frac{\partial \boldsymbol{\mathcal{D}}}{\partial t} = \partial_t \left\{ \frac{\varepsilon_0}{2} \boldsymbol{\mathcal{E}}^2 + \sum_{n=0}^{N-1} \frac{1}{2\varepsilon_0 f_n \omega_p^2} \left[\left(\partial_t \langle \boldsymbol{\mathcal{P}}_n \rangle \right)^2 + \omega_n^2 \langle \boldsymbol{\mathcal{P}}_n \rangle^2 \right] \right\} + \sum_{n=0}^{N-1} \frac{\gamma_n}{\varepsilon_0 f_n \omega_p^2} \left(\partial_t \langle \boldsymbol{\mathcal{P}}_n \rangle \right)^2, \tag{C.S16}$$

$$\boldsymbol{\mathcal{H}} \cdot \frac{\partial \boldsymbol{\mathcal{B}}}{\partial t} = \partial_t \left\{ \frac{\mu_0}{2} \boldsymbol{\mathcal{H}}^2 + \sum_{n=0}^{N-1} \frac{\mu_0}{2\tilde{f}_n \tilde{\omega}_n^2} \left[\left(\partial_t \langle \boldsymbol{\mathcal{M}}_n \rangle \right)^2 + \tilde{\omega}_n^2 \left(\langle \boldsymbol{\mathcal{M}}_n \rangle \right)^2 \right] \right\} + \sum_{n=0}^{N-1} \frac{\mu_0 \tilde{\gamma}_n}{\tilde{f}_n \tilde{\omega}_n^2} \left(\partial_t \langle \boldsymbol{\mathcal{M}}_n \rangle \right)^2. \tag{C.S17}$$

The above results are completely general, and they are applicable independently of the time dependence considered for the electromagnetic fields. The only restriction we need

to impose is that the material parameters of the medium must be fitted by Lorentzian line shapes. In such a case, they allow us to identify accurately both the electric and the magnetic contributions to the energy density stored either by the fields themselves or by the material system, as well as the terms accounting for the power loss densities:

$$\boldsymbol{\mathcal{E}} \cdot \partial_t \boldsymbol{\mathcal{D}} = \partial_t \left[\mathcal{W}^{\text{(e)lectric}}_{\text{vacuum}} + \mathcal{W}^{\text{(e)lectric}}_{\text{medium}} \right] + \mathcal{L}^{\text{(e)lectric}}_{\text{energy}}, \tag{C.S18}$$

$$\boldsymbol{\mathcal{H}} \cdot \partial_t \boldsymbol{\mathcal{B}} = \partial_t \left[\mathcal{W}^{\text{(m)agnetic}}_{\text{vacuum}} + \mathcal{W}^{\text{(m)agnetic}}_{\text{medium}} \right] + \mathcal{L}^{\text{(m)agnetic}}_{\text{energy}}. \tag{C.S19}$$

Taking into account the above expressions, it is worth mentioning that both the energy and losses can be directly identified by comparing them with the general structure of the continuity equation given in Eq. (C.S3):

$$\nabla \cdot \boldsymbol{\mathcal{S}} + \partial_t \left[\mathcal{W}^{(\text{e})}_{\text{vac}} + \mathcal{W}^{(\text{e})}_{\text{med}} + \mathcal{W}^{(\text{m})}_{\text{vac}} + \mathcal{W}^{(\text{m})}_{\text{med}} \right] = - \left[\mathcal{L}^{(\text{e})}_{\text{energy}} + \mathcal{L}^{(\text{m})}_{\text{energy}} + \mathcal{L}^{\text{current}}_{\text{energy}} \right], \tag{C.S20}$$

where $\mathcal{L}^{\text{current}}_{\text{energy}} = \boldsymbol{\mathcal{J}} \cdot \boldsymbol{\mathcal{E}}$. Notice that in the case of only one Lorentz oscillator, i.e., $N = 1$, the results reduce to those of Ref. [S12]. A deeper understanding of the role played by these terms deserves further efforts beyond the scope of this work (c.f. Refs. [S11–S18,S39,S40]). Despite that, turns out to be convenient to compare the results provided by this procedure, wherein the dispersion and dissipation are truly considered, with those stemmed from the classical approaches put forward by Brillouin and Landau [S22,S23]. To this aim we calculate the time average of the energy density by considering time harmonic fields. Thus, from Eqs. (C.S16) and (C.S17), we can obtain

$$\langle \mathcal{W}^{(\text{e})} \rangle_{\text{T}} = \frac{\varepsilon_0}{4} |\mathbf{E}|^2 \left[1 + \sum_{n=0}^{N-1} \frac{f_n \left(\omega^2 + \omega_n^2 \right) \omega_p^2}{\left(\omega_n^2 - \omega^2 \right)^2 + \omega^2 \gamma_n^2} \right] = \frac{\varepsilon_0 \varepsilon_{\text{eff}}(\omega)}{4} |\mathbf{E}|^2, \tag{C.S21}$$

$$\langle \mathcal{W}^{(\text{m})} \rangle_{\text{T}} = \frac{\mu_0}{4} |\mathbf{H}|^2 \left[1 + \sum_{n=0}^{N-1} \frac{\tilde{f}_n \left(\omega^2 + \tilde{\omega}_n^2 \right) \tilde{\omega}_n^2}{\left(\tilde{\omega}_n^2 - \omega^2 \right)^2 + \omega^2 \tilde{\gamma}_n^2} \right] = \frac{\mu_0 \mu_{\text{eff}}(\omega)}{4} |\mathbf{H}|^2, \tag{C.S22}$$

where the angle brackets indicate time averaging over one period of oscillation, and ε_{eff} and μ_{eff} are the real-valued effective material parameters (i.e., the electric permittivity and magnetic permeability), which are defined as

$$\varepsilon_{\text{eff}}(\omega) \equiv 1 + \sum_{n=0}^{N-1} \left(\chi_n' + \frac{2\omega \chi_n''}{\gamma_n} \right), \qquad \mu_{\text{eff}}(\omega) \equiv 1 + \sum_{n=0}^{N-1} \left(\xi_n' + \frac{2\omega \xi_n''}{\tilde{\gamma}_n} \right), \tag{C.S23}$$

with $\chi = \sum_n \chi_n = \chi' + i\chi'' \equiv \varepsilon - 1$ and $\xi = \sum_n \xi_n = \xi' + i\xi'' \equiv \mu - 1$ being the electric and magnetic susceptibilities:

$$\chi_n = \frac{f_n \omega_p^2 \left(\omega_n^2 - \omega^2 \right)}{\left(\omega_n^2 - \omega^2 \right)^2 + \omega^2 \gamma_n^2} + i \left(\frac{f_n \omega_p^2 \omega \gamma_n}{\left(\omega_n^2 - \omega^2 \right)^2 + \omega^2 \gamma_n^2} \right), \tag{C.S24}$$

$$\xi_n = \frac{\tilde{f}_n \tilde{\omega}_n^2 \left(\tilde{\omega}_n^2 - \omega^2 \right)}{\left(\tilde{\omega}_n^2 - \omega^2 \right)^2 + \omega^2 \tilde{\gamma}_n^2} + i \left(\frac{\tilde{f}_n \tilde{\omega}_n^2 \omega \tilde{\gamma}_n}{\left(\tilde{\omega}_n^2 - \omega^2 \right)^2 + \omega^2 \tilde{\gamma}_n^2} \right). \tag{C.S25}$$

On the other hand, according to the approach of Brillouin, it is known that the time average of the energy density is

$$\langle \mathcal{W}^{(\text{e})}_{\text{Brillouin}} \rangle = \frac{\varepsilon_0 \tilde{\varepsilon}(\omega)}{4} |\mathbf{E}|^2, \qquad \langle \mathcal{W}^{(\text{m})}_{\text{Brillouin}} \rangle = \frac{\mu_0 \tilde{\mu}(\omega)}{4} |\mathbf{H}|^2. \tag{C.S26}$$

where $\tilde{\varepsilon}(\omega) \equiv \varepsilon' + \omega[\partial\varepsilon'/\partial\omega]$ and $\tilde{\mu}(\omega) \equiv \mu' + \omega[\partial\mu'/\partial\omega]$ are the dispersion-modified material parameters. After some calculations it is tedious but straightforward to show that $\tilde{\varepsilon}(\omega) = \varepsilon_{\text{eff}}(\omega)$ and $\tilde{\mu}(\omega) = \mu_{\text{eff}}(\omega)$ if and only if

$$\left(\omega^2 + \omega_n^2\right)\gamma_n^2 = 0, \qquad \text{and} \qquad \left(\omega^2 + \tilde{\omega}_n^2\right)\tilde{\gamma}_n^2 = 0, \tag{C.S27}$$

namely, if $\gamma_n = 0$ and/or $\omega = \pm i\omega_n$, and $\tilde{\gamma}_n = 0$ and/or $\omega = \pm i\tilde{\omega}_n$, for all n. Hence, both approaches exactly coincide only in the case of lossless media, and/or otherwise under the a priori physically meaningless condition of imaginary operating frequencies [S21].

C.SM.II Continuity Equation for Optical Chirality in Dispersive and Lossy Media

Building on the above scheme, below we will provide a step-by-step derivation of the correct form of the continuity equation (or conservation law) for the optical chirality in dispersive and lossy media. As was previously pointed out, in a proper sense, dispersion and dissipation are needly related to each other, and therefore we are forced to consider them together. Furthermore, regarding the corresponding dynamical property, the source-like contributions, containing loss or gain terms, afford valuable insights into fundamental aspects of light-matter interaction [S45,S46].

The literature concerning with optical chirality and its interaction with matter mostly deals with electromagnetic fields in free space [S47–S51]. That is why we often find several expressions for the chirality flux density where the fields $\boldsymbol{\mathcal{B}}$ and $\boldsymbol{\mathcal{H}}$ are used interchangeably yielding the same result, as of course it must. However, this does not occur in dispersive media, and special care should be taken in dealing with electromagnetic fields either in free-space ($\boldsymbol{\mathcal{E}}$ and $\boldsymbol{\mathcal{H}}$), or within a material system ($\boldsymbol{\mathcal{D}}$ and $\boldsymbol{\mathcal{B}}$). For symmetry reasons, we may heuristically assume that the chirality flux density reads as

$$\boldsymbol{\mathcal{F}} \equiv \frac{1}{2}\left[\boldsymbol{\mathcal{E}} \times (\nabla \times \boldsymbol{\mathcal{H}}) - \boldsymbol{\mathcal{H}} \times (\nabla \times \boldsymbol{\mathcal{E}})\right]. \tag{C.S28}$$

This axiomatic definition is in fact that used in Ref. [S52], and coincides with that originally introduced by Tang and Cohen [S48] for electromagnetic fields in free space. Following a similar procedure as before for the energy conservation law, from Eq. (C.S28) we can readily calculate the divergence of the chirality flux density as:

$$\begin{aligned}\nabla \cdot \boldsymbol{\mathcal{F}} &= \frac{1}{2}\left[\boldsymbol{\mathcal{H}} \cdot \nabla \times (\nabla \times \boldsymbol{\mathcal{E}}) - \boldsymbol{\mathcal{E}} \cdot \nabla \times (\nabla \times \boldsymbol{\mathcal{H}})\right] \\ &= -\frac{1}{2}\left[\boldsymbol{\mathcal{H}} \cdot \partial_t (\nabla \times \boldsymbol{\mathcal{B}}) + \boldsymbol{\mathcal{E}} \cdot \partial_t (\nabla \times \boldsymbol{\mathcal{D}}) + \boldsymbol{\mathcal{E}} \cdot (\nabla \times \boldsymbol{\mathcal{J}})\right]. \end{aligned} \tag{C.S29}$$

For obtaining an expression with the structure of the continuity equation as given in Eq. (C.S3), we need to find a total time derivative term. Thus, from the latter expression it is straightforward to show that

$$\partial_t\left[\boldsymbol{\mathcal{H}} \cdot (\nabla \times \boldsymbol{\mathcal{B}})\right] = \boldsymbol{\mathcal{H}} \cdot \partial_t (\nabla \times \boldsymbol{\mathcal{B}}) + \partial_t \boldsymbol{\mathcal{H}} \cdot (\nabla \times \boldsymbol{\mathcal{B}}), \tag{C.S30}$$

$$\partial_t\left[\boldsymbol{\mathcal{E}} \cdot (\nabla \times \boldsymbol{\mathcal{D}})\right] = \boldsymbol{\mathcal{E}} \cdot \partial_t (\nabla \times \boldsymbol{\mathcal{D}}) + \partial_t \boldsymbol{\mathcal{E}} \cdot (\nabla \times \boldsymbol{\mathcal{D}}). \tag{C.S31}$$

By means of the above expressions we can recast Eq. (C.S29) as

$$\nabla \cdot \boldsymbol{\mathcal{F}} + \partial_t \mathcal{C} = \mathcal{S}, \tag{C.S32}$$

where the optical chirality density and the source-like terms have been defined as

$$\mathcal{C} \equiv \frac{1}{2}\left[\boldsymbol{\mathcal{E}} \cdot (\nabla \times \boldsymbol{\mathcal{D}}) + \boldsymbol{\mathcal{H}} \cdot (\nabla \times \boldsymbol{\mathcal{B}})\right], \tag{C.S33}$$

$$\mathcal{S} \equiv \frac{1}{2}\left[\partial_t \boldsymbol{\mathcal{E}} \cdot (\nabla \times \boldsymbol{\mathcal{D}}) + \partial_t \boldsymbol{\mathcal{H}} \cdot (\nabla \times \boldsymbol{\mathcal{B}}) - \boldsymbol{\mathcal{E}} \cdot (\nabla \times \boldsymbol{\mathcal{J}})\right]. \tag{C.S34}$$

It is worth pointing out that the above expressions represent the most general result for the conservation law of optical chirality without restrictions on the nature of the medium, namely, Eqs. (C.S32), (C.S33) and (C.S34) are valid regardless of the linearity, homogeneity, isotropy, or dispersion. Nonetheless, they differ considerably from the previously established continuity equation [S47–S54]:

$$\nabla \cdot \boldsymbol{\mathcal{F}}_{\text{vacuum}} + \partial_t \mathcal{C}_{\text{vacuum}} = \mathcal{S}_{\text{vacuum}}, \tag{C.S35}$$

where $\boldsymbol{\mathcal{F}}_{\text{vacuum}} \equiv \boldsymbol{\mathcal{F}}$, $\mathcal{C}_{\text{vacuum}} \equiv \left[\varepsilon_0 \boldsymbol{\mathcal{E}} \cdot (\nabla \times \boldsymbol{\mathcal{E}}) + \mu_0 \boldsymbol{\mathcal{H}} \cdot (\nabla \times \boldsymbol{\mathcal{H}})\right]/2$, and $\mathcal{S}_{\text{vacuum}} \equiv -\left[\boldsymbol{\mathcal{J}} \cdot (\nabla \times \boldsymbol{\mathcal{E}}) + \boldsymbol{\mathcal{E}} \cdot (\nabla \times \boldsymbol{\mathcal{J}})\right]/2$ are, respectively, the chirality flux density, the optical chirality density and the source-like terms in free space. Curiously, albeit Eq. (C.S35) was initially posed for optical fields in vacuum, has been widely used for investigating chiroptical effects occurring in material systems, including metals as well. However, it can be demonstrated that the general result given in Eq. (C.S32) reduces to Eq. (C.S35) only for linear and nonabsorbing media, i.e., as long as $\boldsymbol{\mathcal{D}} = \varepsilon_0 \varepsilon \boldsymbol{\mathcal{E}}$ and $\boldsymbol{\mathcal{B}} = \mu_0 \mu \boldsymbol{\mathcal{H}}$, with $\varepsilon = \mu = 1$:

$$\begin{aligned} \mathcal{C} &= \frac{1}{2}\left[\boldsymbol{\mathcal{E}} \cdot (\nabla \times \boldsymbol{\mathcal{D}}) + \boldsymbol{\mathcal{H}} \cdot (\nabla \times \boldsymbol{\mathcal{B}})\right] \\ &= \frac{1}{2}\left[\varepsilon_0 \boldsymbol{\mathcal{E}} \cdot (\nabla \times \boldsymbol{\mathcal{E}}) + \mu_0 \boldsymbol{\mathcal{H}} \cdot (\nabla \times \boldsymbol{\mathcal{H}})\right] = \mathcal{C}_{\text{vacuum}}, \end{aligned} \tag{C.S36}$$

and

$$\begin{aligned} \mathcal{S} &= \frac{1}{2}\left[\partial_t \boldsymbol{\mathcal{E}} \cdot (\nabla \times \boldsymbol{\mathcal{D}}) + \partial_t \boldsymbol{\mathcal{H}} \cdot (\nabla \times \boldsymbol{\mathcal{B}}) - \boldsymbol{\mathcal{E}} \cdot (\nabla \times \boldsymbol{\mathcal{J}})\right] \\ &= \frac{1}{2}\left[\varepsilon_0 \partial_t \boldsymbol{\mathcal{E}} \cdot (-\mu_0 \partial_t \boldsymbol{\mathcal{H}}) + \mu_0 \partial_t \boldsymbol{\mathcal{H}} \cdot (\varepsilon_0 \partial_t \boldsymbol{\mathcal{E}} + \boldsymbol{\mathcal{J}}) - \boldsymbol{\mathcal{E}} \cdot (\nabla \times \boldsymbol{\mathcal{J}})\right] \\ &= \frac{1}{2}\left[\mu_0 \partial_t \boldsymbol{\mathcal{H}} \cdot \boldsymbol{\mathcal{J}} - \boldsymbol{\mathcal{E}} \cdot (\nabla \times \boldsymbol{\mathcal{J}})\right] \\ &= -\frac{1}{2}\left[\boldsymbol{\mathcal{J}} \cdot (\nabla \times \boldsymbol{\mathcal{E}}) + \boldsymbol{\mathcal{E}} \cdot (\nabla \times \boldsymbol{\mathcal{J}})\right] = \mathcal{S}_{\text{vacuum}}, \end{aligned} \tag{C.S37}$$

where $\mu_0 \partial_t \boldsymbol{\mathcal{H}} = -(\nabla \times \boldsymbol{\mathcal{E}})$. Hence, we stress here the relevance for considering dispersive-like terms. This becomes much more evident by rewriting the above expressions in terms of those for vacuum. Indeed, since

$$\boldsymbol{\mathcal{E}} \cdot (\nabla \times \boldsymbol{\mathcal{D}}) = \boldsymbol{\mathcal{D}} \cdot (\nabla \times \boldsymbol{\mathcal{E}}) + \nabla \cdot (\boldsymbol{\mathcal{P}} \times \boldsymbol{\mathcal{E}}), \tag{C.S38}$$

$$\boldsymbol{\mathcal{H}} \cdot (\nabla \times \boldsymbol{\mathcal{B}}) = \boldsymbol{\mathcal{B}} \cdot (\nabla \times \boldsymbol{\mathcal{H}}) + \mu_0 \nabla \cdot (\boldsymbol{\mathcal{M}} \times \boldsymbol{\mathcal{H}}), \tag{C.S39}$$

the optical chirality density given in Eq. (C.S33) can be generally expressed as

$$\begin{aligned}\mathcal{C} &= \mathcal{C}_{\text{vacuum}} + \mathcal{C}_{\text{medium}} \\ &= \frac{1}{2}\left\{\boldsymbol{\mathcal{D}}\cdot(\nabla\times\boldsymbol{\mathcal{E}}) + \boldsymbol{\mathcal{B}}\cdot(\nabla\times\boldsymbol{\mathcal{H}}) + \nabla\cdot\left[\boldsymbol{\mathcal{P}}\times\boldsymbol{\mathcal{E}} + \mu_0\left(\boldsymbol{\mathcal{M}}\times\boldsymbol{\mathcal{H}}\right)\right]\right\},\end{aligned} \tag{C.S40}$$

where $\mathcal{C}_{\text{medium}} \equiv \left[\boldsymbol{\mathcal{E}}\cdot(\nabla\times\boldsymbol{\mathcal{P}}) + \mu_0\boldsymbol{\mathcal{H}}\cdot(\nabla\times\boldsymbol{\mathcal{M}})\right]/2$. On the other hand, the source-like term can also be recast as

$$\mathcal{S} = \mathcal{S}_{\text{vacuum}} + \mathcal{S}_{\text{medium}}, \tag{C.S41}$$

where $\mathcal{S}_{\text{medium}} \equiv \{\partial_t\boldsymbol{\mathcal{E}}\cdot(\nabla\times\boldsymbol{\mathcal{P}}) - \partial_t\boldsymbol{\mathcal{P}}\cdot(\nabla\times\boldsymbol{\mathcal{E}}) + \mu_0\left[\partial_t\boldsymbol{\mathcal{H}}\cdot(\nabla\times\boldsymbol{\mathcal{M}}) - \partial_t\boldsymbol{\mathcal{M}}\cdot(\nabla\times\boldsymbol{\mathcal{H}})\right]\}/2$. Therefore, by assuming a monochromatic optical field represented by $\mathbf{E}(\omega) = \left[\mathbf{E}\delta(\omega-\omega_0) + \mathbf{E}^*\delta(\omega+\omega_0)\right]/2$, it can be demonstrated that in a linear medium

$$\langle\boldsymbol{\mathcal{E}}\cdot(\nabla\times\boldsymbol{\mathcal{P}})\rangle_{\text{T}} = \frac{\varepsilon_0\mu_0}{2}\text{Im}[\omega\left(1-\varepsilon\right)\mu\mathbf{E}^*\cdot\mathbf{H}] + \frac{i\varepsilon_0\left(\mathbf{E}\times\mathbf{E}^*\right)}{2}\text{Im}[\nabla\varepsilon], \tag{C.S42}$$

$$\langle\boldsymbol{\mathcal{H}}\cdot(\nabla\times\boldsymbol{\mathcal{M}})\rangle_{\text{T}} = \frac{\varepsilon_0}{2}\text{Im}[\omega\left(1-2\varepsilon^*\right)\left(\mu^*-1\right)\mathbf{E}^*\cdot\mathbf{H}] + \frac{i\left(\mathbf{H}\times\mathbf{H}^*\right)}{2}\text{Im}[\nabla\mu], \tag{C.S43}$$

thus showing that

$$\begin{aligned}\langle\mathcal{C}_{\text{medium}}\rangle_{\text{T}} = \frac{1}{4c^2}\text{Im}\left\{\left[\frac{i\sigma^*\xi^*}{\varepsilon_0} - \omega\chi\mu - \omega\varepsilon^*\xi^*\right]\mathbf{E}^*\cdot\mathbf{H}\right\} \\ + \frac{i\varepsilon_0\left(\mathbf{E}\times\mathbf{E}^*\right)}{4}\text{Im}[\nabla\varepsilon] + \frac{i\mu_0\left(\mathbf{H}\times\mathbf{H}^*\right)}{4}\text{Im}[\nabla\mu],\end{aligned} \tag{C.S44}$$

where $\sigma(\omega) = i\varepsilon_0\omega\left[1-\varepsilon(\omega)\right]$ is the complex-valued conductivity. Likewise, the time average over the terms comprising the source-like contributions yields

$$\langle\partial_t\boldsymbol{\mathcal{E}}\cdot(\nabla\times\boldsymbol{\mathcal{P}})\rangle_{\text{T}} = -\frac{\varepsilon_0\mu_0}{2}\text{Re}\left[\omega^2\chi\mu\mathbf{E}^*\cdot\mathbf{H}\right] + \frac{i\omega\varepsilon_0\left(\mathbf{E}\times\mathbf{E}^*\right)}{2}\text{Re}[\nabla\varepsilon], \tag{C.S45}$$

$$\langle\partial_t\boldsymbol{\mathcal{P}}\cdot(\nabla\times\boldsymbol{\mathcal{E}})\rangle_{\text{T}} = -\frac{\varepsilon_0\mu_0}{2}\text{Re}\left[\omega^2\chi^*\mu\mathbf{E}^*\cdot\mathbf{H}\right], \tag{C.S46}$$

$$\langle\partial_t\boldsymbol{\mathcal{H}}\cdot(\nabla\times\boldsymbol{\mathcal{M}})\rangle_{\text{T}} = \frac{\varepsilon_0}{2}\text{Re}\left[\omega^2\left(2\varepsilon^*-1\right)\xi^*\mathbf{E}^*\cdot\mathbf{H}\right] + \frac{i\omega\left(\mathbf{H}\times\mathbf{H}^*\right)}{2}\text{Re}[\nabla\mu], \tag{C.S47}$$

$$\langle\partial_t\boldsymbol{\mathcal{M}}\cdot(\nabla\times\boldsymbol{\mathcal{H}})\rangle_{\text{T}} = \frac{\varepsilon_0}{2}\text{Re}\left[\omega^2\left(2\varepsilon^*-1\right)\xi\mathbf{E}^*\cdot\mathbf{H}\right], \tag{C.S48}$$

and then

$$\langle\partial_t\boldsymbol{\mathcal{E}}\cdot(\nabla\times\boldsymbol{\mathcal{P}}) - \partial_t\boldsymbol{\mathcal{P}}\cdot(\nabla\times\boldsymbol{\mathcal{E}})\rangle_{\text{T}} = \varepsilon_0\mu_0\omega^2\text{Im}[\varepsilon]\text{Im}[\mu\mathbf{E}^*\cdot\mathbf{H}] + \frac{i\omega\varepsilon_0\left(\mathbf{E}\times\mathbf{E}^*\right)}{2}\text{Re}[\nabla\varepsilon], \tag{C.S49}$$

$$\langle\partial_t\boldsymbol{\mathcal{H}}\cdot(\nabla\times\boldsymbol{\mathcal{M}}) - \partial_t\boldsymbol{\mathcal{M}}\cdot(\nabla\times\boldsymbol{\mathcal{H}})\rangle_{\text{T}} = \varepsilon_0\omega^2\text{Im}[\mu]\text{Im}[\left(2\varepsilon^*-1\right)\mathbf{E}^*\cdot\mathbf{H}] + \frac{i\omega\left(\mathbf{H}\times\mathbf{H}^*\right)}{2}\text{Re}[\nabla\mu]. \tag{C.S50}$$

For the sake of simplicity, let us focus our attention here in the case of homogeneous media, i.e., $\varepsilon \neq \varepsilon(\mathbf{r})$, and $\mu \neq \mu(\mathbf{r})$, in such a way that $\nabla\varepsilon = \nabla\mu = 0$. In this simple case it can be found that

$$\langle\mathcal{C}_{\text{medium}}\rangle_{\text{T}} = \frac{1}{4c^2}\text{Im}\left\{\left[\frac{i\sigma^*\xi^*}{\varepsilon_0} - \omega\chi\mu - \omega\varepsilon^*\xi^*\right]\mathbf{E}^*\cdot\mathbf{H}\right\}, \tag{C.S51}$$

and

$$\langle \mathcal{S}_{\text{medium}} \rangle_{\text{T}} = \frac{\omega^2}{2c^2} \left\{ \text{Im}[\varepsilon]\text{Im}[\mu \mathbf{E}^* \cdot \mathbf{H}] + \text{Im}[\mu]\text{Im}[(2\varepsilon^* - 1)\, \mathbf{E}^* \cdot \mathbf{H}] \right\}. \tag{C.S52}$$

By analyzing the latter results it can be shown that, irrespectively of the input polarization, $\langle \mathcal{C}_{\text{medium}} \rangle_{\text{T}} = 0$ if $\varepsilon = \mu = 1$, i.e., in vacuum. On the other hand, as long as the medium is nondispersive, i.e., provided that $\text{Im}[\varepsilon] = \text{Im}[\mu] = 0$, $\langle \mathcal{S}_{\text{medium}} \rangle_{\text{T}} = 0$.

Summarizing, in this section we have shown that the conservation law for the optical chirality established up to now (see, e.g., Refs. [S47–S54]) is only valid for electromagnetic waves in free space or, at most, in dispersive and lossless media. Starting from the definition of the chirality flux density as given in Eq. (C.S28), we have provided a detailed derivation showing that there are terms which have been neglected in previous works. Significantly, the dispersion of the material system leads to important corrections into the expressions for the optical chirality density as well as for the source-like terms of the continuity equation, which must be generally considered.

C.SM.III Optical Chirality Density in Linear Dispersive and Lossy Media

Following a similar approach as in previous studies [S11–S21], we will properly derive the optical chirality density in dispersive and lossy media. As mentioned above for the case of energy, our results will be valid provided the material parameters can be modeled by Lorentzian line shapes. Within this approach, the expression for the chirality density does not rely on the time dependence of the electromagnetic fields. For comparison, we will also determine the optical chirality density via the classical procedure leading to the Brillouin formula for the energy density [S22,S23]. Just as previously found, there are certain conditions where both approaches exactly coincide. We will show that these conditions for the chirality density are analogous to that obtained for the energy density.

A. Optical chirality density in dispersive and lossy media: Loudon's approach

Starting from the continuity equation as given in Eq. (C.S29) and attempting to express the electric contribution in terms of the electric and polarization fields, $\boldsymbol{\mathcal{E}}$ and $\boldsymbol{\mathcal{P}}$ respectively, it follows that

$$\frac{1}{2}\boldsymbol{\mathcal{E}} \cdot \partial_t \left(\nabla \times \boldsymbol{\mathcal{D}} \right) = \frac{1}{2} \left[\varepsilon_0 \boldsymbol{\mathcal{E}} \cdot \partial_t \left(\nabla \times \boldsymbol{\mathcal{E}} \right) + \boldsymbol{\mathcal{E}} \cdot \partial_t \left(\nabla \times \boldsymbol{\mathcal{P}} \right) \right]. \tag{C.S53}$$

In this expression the first term of the right-hand side can be rewritten as

$$\frac{\varepsilon_0}{2}\boldsymbol{\mathcal{E}} \cdot \partial_t \left(\nabla \times \boldsymbol{\mathcal{E}} \right) = \frac{\varepsilon_0}{2} \left\{ \partial_t \left[\boldsymbol{\mathcal{E}} \cdot \left(\nabla \times \boldsymbol{\mathcal{E}} \right) \right] - \partial_t \boldsymbol{\mathcal{E}} \cdot \left(\nabla \times \boldsymbol{\mathcal{E}} \right) \right\}, \tag{C.S54}$$

thereby leading to a total time derivative term plus a residual one. As will be shown below, this residual term exactly cancel with the one appearing for the magnetic contribution in

vacuum, thus allowing us to recover the usual expression for the optical chirality in free space. Likewise, the second term in the right-hand side of Eq. (C.S53) can be addressed by using the dynamic equation for the polarization field given in Eq. (C.S8):

$$\begin{aligned}\frac{1}{2}\boldsymbol{\mathcal{E}}\cdot\partial_t\left(\nabla\times\boldsymbol{\mathcal{P}}\right)=\partial_t\left\{\sum_{n=0}^{N-1}\frac{1}{2\varepsilon_0 f_n\omega_p^2}\left[\partial_t\left\langle\boldsymbol{\mathcal{P}}_n\right\rangle\cdot\left(\nabla\times\partial_t\left\langle\boldsymbol{\mathcal{P}}_n\right\rangle\right)+\omega_n^2\left\langle\boldsymbol{\mathcal{P}}_n\right\rangle\cdot\left(\nabla\times\left\langle\boldsymbol{\mathcal{P}}_n\right\rangle\right)\right]\right\}\\ -\sum_{n=0}^{N-1}\frac{1}{2\varepsilon_0 f_n\omega_p^2}\left\{\omega_n^2\partial_t\left\langle\boldsymbol{\mathcal{P}}_n\right\rangle\cdot\left(\nabla\times\left\langle\boldsymbol{\mathcal{P}}_n\right\rangle\right)+\partial_t\left\langle\boldsymbol{\mathcal{P}}_n\right\rangle\cdot\left(\nabla\times\partial_t^2\left\langle\boldsymbol{\mathcal{P}}_n\right\rangle\right)\right\}\\ +\sum_{n=0}^{N-1}\frac{1}{2\varepsilon_0 f_n\omega_p^2}\left\{\gamma_n\partial_t\left\langle\boldsymbol{\mathcal{P}}_n\right\rangle\cdot\left(\nabla\times\partial_t\left\langle\boldsymbol{\mathcal{P}}_n\right\rangle\right)\right\}.\end{aligned}\tag{C.S55}$$

Analogously, we can write the magnetic contribution in terms of $\boldsymbol{\mathcal{H}}$ and $\boldsymbol{\mathcal{M}}$:

$$\frac{1}{2}\boldsymbol{\mathcal{H}}\cdot\partial_t\left(\nabla\times\boldsymbol{\mathcal{B}}\right)=\frac{\mu_0}{2}\left[\boldsymbol{\mathcal{H}}\cdot\partial_t\left(\nabla\times\boldsymbol{\mathcal{H}}\right)+\boldsymbol{\mathcal{H}}\cdot\partial_t\left(\nabla\times\boldsymbol{\mathcal{M}}\right)\right],\tag{C.S56}$$

where

$$\frac{\mu_0}{2}\boldsymbol{\mathcal{H}}\cdot\partial_t\left(\nabla\times\boldsymbol{\mathcal{H}}\right)=\frac{\mu_0}{2}\left\{\partial_t\left[\boldsymbol{\mathcal{H}}\cdot\left(\nabla\times\boldsymbol{\mathcal{H}}\right)\right]-\partial_t\boldsymbol{\mathcal{H}}\cdot\left(\nabla\times\boldsymbol{\mathcal{H}}\right)\right\},\tag{C.S57}$$

$$\begin{aligned}\frac{\mu_0}{2}\boldsymbol{\mathcal{H}}\cdot\partial_t\left(\nabla\times\boldsymbol{\mathcal{M}}\right)=\partial_t\left\{\sum_{n=0}^{N-1}\frac{\mu_0}{2\tilde{f}_n\tilde{\omega}_n^2}\left[\partial_t\left\langle\boldsymbol{\mathcal{M}}_n\right\rangle\cdot\left(\nabla\times\partial_t\left\langle\boldsymbol{\mathcal{M}}_n\right\rangle\right)+\tilde{\omega}_n^2\left\langle\boldsymbol{\mathcal{M}}_n\right\rangle\cdot\left(\nabla\times\left\langle\boldsymbol{\mathcal{M}}_n\right\rangle\right)\right]\right\}\\ -\sum_{n=0}^{N-1}\frac{\mu_0}{2\tilde{f}_n\tilde{\omega}_n^2}\left\{\tilde{\omega}_n^2\partial_t\left\langle\boldsymbol{\mathcal{M}}_n\right\rangle\cdot\left(\nabla\times\left\langle\boldsymbol{\mathcal{M}}_n\right\rangle\right)+\partial_t\left\langle\boldsymbol{\mathcal{M}}_n\right\rangle\cdot\left(\nabla\times\partial_t^2\left\langle\boldsymbol{\mathcal{M}}_n\right\rangle\right)\right\}\\ +\sum_{n=0}^{N-1}\frac{\mu_0}{2\tilde{f}_n\tilde{\omega}_n^2}\left\{2\tilde{\gamma}_n\partial_t\left\langle\boldsymbol{\mathcal{M}}_n\right\rangle\cdot\left(\nabla\times\partial_t\left\langle\boldsymbol{\mathcal{M}}_n\right\rangle\right)\right\}.\end{aligned}\tag{C.S58}$$

Then, taking into account the structure of the continuity equation as given in Eq. (C.S3) we can easily identify the electric and magnetic contributions of the optical chirality density stored either by the fields or by the medium, as well as the terms accounting for the loss rate of the chirality density [S45,S46]:

$$\frac{1}{2}\boldsymbol{\mathcal{E}}\cdot\partial_t\left(\nabla\times\boldsymbol{\mathcal{D}}\right)=\partial_t\left[\mathcal{C}^{(\mathrm{e})\mathrm{lectric}}_{\mathrm{vacuum}}+\mathcal{C}^{(\mathrm{e})\mathrm{lectric}}_{\mathrm{medium}}\right]+\mathcal{L}^{(\mathrm{e})\mathrm{lectric}}_{\mathrm{chirality}},\tag{C.S59}$$

$$\frac{1}{2}\boldsymbol{\mathcal{H}}\cdot\partial_t\left(\nabla\times\boldsymbol{\mathcal{B}}\right)=\partial_t\left[\mathcal{C}^{(\mathrm{m})\mathrm{agnetic}}_{\mathrm{vacuum}}+\mathcal{C}^{(\mathrm{m})\mathrm{agnetic}}_{\mathrm{medium}}\right]+\mathcal{L}^{(\mathrm{m})\mathrm{agnetic}}_{\mathrm{chirality}}.\tag{C.S60}$$

From the above equations one can directly observe that $\boldsymbol{\mathcal{E}}\cdot\partial_t\left(\nabla\times\boldsymbol{\mathcal{D}}\right)$ and $\boldsymbol{\mathcal{H}}\cdot\partial_t\left(\nabla\times\boldsymbol{\mathcal{B}}\right)$ enclose generally the joint action of stored together with the dissipative (or gained) contributions. Aiming to compare these results with those obtained via the Fourier transform, we should calculate the time average of the optical chirality density by considering time harmonic fields in a linear medium. Therefore, from Eqs. (C.S54), (C.S55), (C.S57) and (C.S58), and with the help of Eqs. (C.S9) and (C.S12), it can be demonstrated that

$$\langle\mathcal{C}^{(\mathrm{e})}_{\mathrm{vacuum+medium}}\rangle_{\mathrm{T}}=\frac{\omega}{4c^2}\mathrm{Im}[\mu^*(\omega)\mathbf{E}\cdot\mathbf{H}^*]\varepsilon_{\mathrm{eff}}(\omega),\tag{C.S61}$$

and

$$\langle \mathcal{C}^{(\mathrm{m})}_{\mathrm{vacuum+medium}} \rangle_{\mathrm{T}} = \frac{\omega}{4c^2} \mathrm{Im}[\varepsilon(\omega) \mathbf{E} \cdot \mathbf{H}^*] \mu_{\mathrm{eff}}(\omega), \tag{C.S62}$$

where $\varepsilon_{\mathrm{eff}}$ and μ_{eff} are the real-valued effective material parameters defined in Eq. (C.S23). Hence, the sum of the above quantities allow us to write the total optical chirality density for dispersive and lossy media:

$$\langle \mathcal{C} \rangle_{\mathrm{T}} \equiv \langle \mathcal{C}^{(\mathrm{e})+(\mathrm{m})}_{\mathrm{vac+med}} \rangle_{\mathrm{T}} = \frac{\omega}{4c^2} \mathrm{Im}[(\varepsilon(\omega) \mu_{\mathrm{eff}}(\omega) + \varepsilon_{\mathrm{eff}}(\omega) \mu^*(\omega)) \, \mathbf{E} \cdot \mathbf{H}^*]. \tag{C.S63}$$

It should also be noticed that in the magnetic contribution there appears an additional term associated with the current density $\mathbf{J}$:

$$\langle \mathcal{C}^{(\mathrm{c})\mathrm{urrent}}_{\mathrm{medium}} \rangle_{\mathrm{T}} = \frac{\omega}{4c^2} \mathrm{Im}[(\varepsilon(\omega) - 1) \mathbf{E} \cdot \mathbf{H}^*] \mu_{\mathrm{eff}}(\omega). \tag{C.S64}$$

Then, the complete expression for the optical chirality conservation law actually reads as follows:

$$\nabla \cdot \boldsymbol{\mathcal{F}} + \partial_t \left[\mathcal{C}^{(\mathrm{e})}_{\mathrm{vac+med}} + \mathcal{C}^{(\mathrm{m})}_{\mathrm{vac+med}} + \mathcal{C}^{(\mathrm{c})}_{\mathrm{med}} \right] = - \left[\mathcal{L}^{(\mathrm{e})}_{\mathrm{chirality}} + \mathcal{L}^{(\mathrm{m})}_{\mathrm{chirality}} + \mathcal{L}^{(\mathrm{c})}_{\mathrm{chirality}} \right], \tag{C.S65}$$

where $\mathcal{L}^{(\mathrm{c})}_{\mathrm{chirality}} = \boldsymbol{\mathcal{E}} \cdot (\nabla \times \boldsymbol{\mathcal{J}}) / 2$. However it is interesting to realize that $\mathcal{L}^{(\mathrm{c})}_{\mathrm{chirality}}$ actually leads to conserved-like contributions. This can be easily shown by turning to the Drude model [S41], where the current density satisfies

$$\frac{\partial \boldsymbol{\mathcal{J}}}{\partial t} + \gamma_0 \boldsymbol{\mathcal{J}} = \varepsilon_0 \omega_p^2 \boldsymbol{\mathcal{E}}. \tag{C.S66}$$

Indeed, by using the latter dynamic equation, it follows that

$$\frac{1}{2} \boldsymbol{\mathcal{E}} \cdot (\nabla \times \boldsymbol{\mathcal{J}}) = \frac{1}{2\varepsilon_0 \omega_p^2} \left\{ \partial_t \left[\boldsymbol{\mathcal{J}} \cdot (\nabla \times \boldsymbol{\mathcal{J}}) \right] - \boldsymbol{\mathcal{J}} \cdot (\nabla \times \partial_t \boldsymbol{\mathcal{J}}) + \gamma_0 \boldsymbol{\mathcal{J}} \cdot (\nabla \times \boldsymbol{\mathcal{J}}) \right\}. \tag{C.S67}$$

The source-like contribution given in Eq. (C.S67) may also be written as the field contributions [Eqs. (C.S59) and (C.S60)]:

$$\frac{1}{2} \boldsymbol{\mathcal{E}} \cdot (\nabla \times \boldsymbol{\mathcal{J}}) = \partial_t \left[\mathcal{C}^{(\mathrm{c})}_{\mathrm{sources}} \right] + \mathcal{L}^{(\mathrm{c})}_{\mathrm{chirality}}. \tag{C.S68}$$

Taking into account the latter results, in a linear, homogeneous and isotropic medium it follows that

$$\langle \mathcal{C}^{(\mathrm{c})}_{\mathrm{sources}} \rangle_{\mathrm{T}} = \frac{\omega \mu_0 |\sigma_{\mathrm{Drude}}|^2}{4\varepsilon_0 \omega_p^2} \mathrm{Im}[\mu^*(\omega) \mathbf{E} \cdot \mathbf{H}^*] = \frac{\omega}{4c^2} \left[\frac{\omega_p^2}{\omega^2 + \gamma_0^2} \right] \mathrm{Im}[\mu^*(\omega) \mathbf{E} \cdot \mathbf{H}^*], \tag{C.S69}$$

where it has been used that

$$\mathbf{J} = \left[\frac{i\omega\varepsilon_0 \omega_p^2}{\omega^2 + i\omega\gamma_0} \right] \mathbf{E} = i\omega\varepsilon_0 \left(1 - \varepsilon_{\mathrm{Drude}}(\omega) \right) \mathbf{E} \equiv \sigma_{\mathrm{Drude}} \mathbf{E}. \tag{C.S70}$$

For simplicity we focus here on the simpler case of nonmagnetic medium, $\mu = \mu_{\mathrm{eff}} = 1$, thus obtaining that

$$\langle \mathcal{C}^{(\mathrm{c})}_{\mathrm{medium}} \rangle_{\mathrm{T}} + \langle \mathcal{C}^{(\mathrm{c})}_{\mathrm{sources}} \rangle_{\mathrm{T}} = \frac{1}{4c^2} \left[\frac{\gamma_0 \omega_p^2}{\omega^2 + \gamma_0^2} \right] \mathrm{Re}[\mathbf{E} \cdot \mathbf{H}^*], \tag{C.S71}$$

and

$$\langle \mathcal{C}^{(\mathrm{e})}_{\mathrm{vac+med}} \rangle_{\mathrm{T}} + \langle \mathcal{C}^{(\mathrm{m})}_{\mathrm{vac+med}} \rangle_{\mathrm{T}} = \frac{\omega}{2c^2} \mathrm{Im}[\mathbf{E} \cdot \mathbf{H}^*] + \frac{1}{4c^2} \left[\frac{\gamma_0 \omega_p^2}{\omega^2 + \gamma_0^2} \right] \mathrm{Re}[\mathbf{E} \cdot \mathbf{H}^*]. \tag{C.S72}$$

Notice that, since we are considering the Drude model, we should use Eqs. (C.S23), (C.S24) and (C.S25) in the simplest case of $N = 1$, $f_0 = 1$, and $\omega_n = \tilde{\omega}_n = 0$ for all n. Summing up the above expressions we get the chirality density:

$$\langle \mathcal{C}^{(\mathrm{e})}_{\mathrm{vac+med}} \rangle_{\mathrm{T}} + \langle \mathcal{C}^{(\mathrm{m})}_{\mathrm{vac+med}} \rangle_{\mathrm{T}} + \langle \mathcal{C}^{(\mathrm{c})}_{\mathrm{sou+med}} \rangle_{\mathrm{T}} = \frac{\omega}{2c^2} \mathrm{Im}[\mathbf{E} \cdot \mathbf{H}^*] + \frac{1}{2c^2} \left[\frac{\gamma_0 \omega_p^2}{\omega^2 + \gamma_0^2} \right] \mathrm{Re}[\mathbf{E} \cdot \mathbf{H}^*]. \tag{C.S73}$$

In the last result one can observe that contributions involving the damping parameter γ_0, i.e., accounting for the material absorption effects, are $\pi/2$ out of phase with respect to that of free space. We can also see that this result reduces to the well known and widely studied expression for the optical chirality density in vacuum provided that $\gamma_0 = 0$, as it should be expected. Furthermore, at least in this simple example, it is interesting to note that the terms involving the current density arrange in such a way that only yield outcomes depending on $\mathrm{Re}[\mathbf{E} \cdot \mathbf{H}^*]$. In this regard, it is straightforward to show that in general,

$$\mathbf{E} \cdot \mathbf{H}^* \equiv \frac{i}{\omega \mu_0 \mu^*} [\mathbf{E} \cdot (\nabla \times \mathbf{E}^*)] = \frac{i}{\omega \mu_0 \mu^*} \left[\mathrm{Re}[\mathbf{E} \cdot (\nabla \times \mathbf{E}^*)] + \frac{1}{2} \nabla \cdot (\mathbf{E}^* \times \mathbf{E}) \right]. \tag{C.S74}$$

Because we are assuming a nonmagnetic medium, the first term in the right-hand side of the latter equation always vanishes when taking the real part. On the other hand, the second term only contributes for nonlinear polarizations. Still, even for circularly polarized light, due to the spatial derivatives, such a contribution is in general zero, except in very special cases involving the spatial dependence of the complex field amplitude, e.g., when considering an oscillating electric dipole.

It is worth remarking that the whole development for obtaining the correct expression of the optical chirality density in dispersive and lossy media relies on the underlying structure of the continuity equation [Eq. (C.S3)]. Indeed, according to this approach, we have specially focused on representing the right-hand side of Eq. (C.S29) in terms of total time derivatives. To look into this possibility we attempted to reproduce the treatment employed for the derivation of the energy density [S11,S12]. However, the occurrence of curl terms hinders this realization and special care must be taken with the residual terms so as to avoid meaningless results. Still, it is important to realize that, when combining the electric and magnetic contributions [Eqs. (C.S53) and (C.S56), respectively] in free space, these terms completely cancel each other:

$$\frac{1}{2} [\boldsymbol{\mathcal{E}} \cdot \partial_t (\nabla \times \boldsymbol{\mathcal{D}}) + \boldsymbol{\mathcal{H}} \cdot \partial_t (\nabla \times \boldsymbol{\mathcal{B}})] = \frac{1}{2} \{\varepsilon_0 \partial_t [\boldsymbol{\mathcal{E}} \cdot (\nabla \times \boldsymbol{\mathcal{E}})] + \mu_0 \partial_t [\boldsymbol{\mathcal{H}} \cdot (\nabla \times \boldsymbol{\mathcal{H}})]\} = \partial_t \mathcal{C}_{\mathrm{vac}}. \tag{C.S75}$$

However, taking into account Eqs. (C.S59) and (C.S60), the residual terms, $\partial_t \boldsymbol{\mathcal{E}} \cdot (\nabla \times \boldsymbol{\mathcal{E}})$ and $\partial_t \boldsymbol{\mathcal{H}} \cdot (\nabla \times \boldsymbol{\mathcal{H}})$, and the corresponding terms accounting for the light-matter interaction (given by the second and third summation in Eqs. (C.S55) and (C.S58)), must be generally interpreted as the loss rate of the field chirality density.

B. Optical chirality density in dispersive and lossless media: Brillouin's approach

We will now determine a closed expression for the optical chirality density by direct evaluation of the Fourier integrals. This procedure resembles that gives rise to the Brillouin formula for the energy density [S22,S23], and then is constrained by the same prescriptions. For simplicity, hereinafter it will be assumed a linear, homogeneous and isotropic medium.

To start with, let us expand the left-hand side of Eq. (C.S53) by using the Fourier integrals as given in Eq. (C.S1):

$$\begin{aligned}\frac{1}{2}\boldsymbol{\mathcal{E}}\cdot\partial_t\left(\nabla\times\boldsymbol{\mathcal{D}}\right)&=\frac{1}{2}\int_{-\infty}^{+\infty}\mathbf{E}(\omega')e^{-i\omega' t}d\omega'\cdot\partial_t\left\{\nabla\times\left[\int_{-\infty}^{+\infty}\mathbf{D}(\omega)e^{-i\omega t}d\omega\right]\right\}\\&=\frac{-i}{2}\int_{-\infty}^{+\infty}\int_{-\infty}^{+\infty}\omega\mathbf{E}(\omega')\cdot\left[\nabla\times\mathbf{D}(\omega)\right]e^{-i(\omega'+\omega)t}d\omega' d\omega.\end{aligned}\tag{C.S76}$$

According to Eq. (C.S59), this is actually the time rate of change of optical chirality. The instantaneous distribution of the optical chirality density can then be obtained by integrating the latter expression over time:

$$\begin{aligned}\mathcal{C}^{(\mathrm{e})}(t')&=\frac{-i}{2}\int_{-\infty}^{t'}\int_{-\infty}^{+\infty}\int_{-\infty}^{+\infty}\omega\mathbf{E}(\omega')\cdot\left[\nabla\times\mathbf{D}(\omega)\right]e^{-i(\omega'+\omega)t}d\omega' d\omega dt\\&=\frac{1}{2}\int_{-\infty}^{+\infty}\int_{-\infty}^{+\infty}\left[\frac{\omega}{\omega'+\omega}\right]\mathbf{E}(\omega')\cdot\left[\nabla\times\mathbf{D}(\omega)\right]e^{-i(\omega'+\omega)t'}d\omega' d\omega,\end{aligned}\tag{C.S77}$$

where it has been implicitly assumed fields tending sufficiently rapidly to zero as $t\to-\infty$. This is indeed a crucial assumption that necessarily restricts the applicability of this procedure to electromagnetic fields under the *slowly varying amplitude approximation* [S37]. In linear, homogeneous and isotropic media, $\nabla\times\mathbf{D}(\omega)=i\omega\varepsilon_0\mu_0\varepsilon(\omega)\mu(\omega)\mathbf{H}(\omega)$, and then we have

$$\mathcal{C}^{(\mathrm{e})}(t)=\frac{i}{2c^2}\int_{-\infty}^{+\infty}\int_{-\infty}^{+\infty}\left[\frac{\omega^2\varepsilon(\omega)\mu(\omega)}{\omega'+\omega}\right]\mathbf{E}(\omega')\cdot\mathbf{H}(\omega)e^{-i(\omega'+\omega)t}d\omega' d\omega.\tag{C.S78}$$

Likewise, performing the same calculation for the magnetic contribution it follows that

$$\begin{aligned}\mathcal{C}^{(\mathrm{m})}(t)=&\frac{-i}{2c^2}\int_{-\infty}^{+\infty}\int_{-\infty}^{+\infty}\left[\frac{\omega^2\varepsilon(\omega)\mu(\omega)}{\omega'+\omega}\right]\mathbf{E}(\omega)\cdot\mathbf{H}(\omega')e^{-i(\omega'+\omega)t}d\omega' d\omega\\&+\frac{\mu_0}{2}\int_{-\infty}^{+\infty}\int_{-\infty}^{+\infty}\left[\frac{\omega\sigma(\omega)\mu(\omega)}{\omega'+\omega}\right]\mathbf{E}(\omega)\cdot\mathbf{H}(\omega')e^{-i(\omega'+\omega)t}d\omega' d\omega.\end{aligned}\tag{C.S79}$$

Therefore, summing up the latter results we obtain that

$$\mathcal{C}(t)=\frac{i}{4c^2}\iint\left[\frac{\omega^2\varepsilon(\omega)\mu(\omega)\Xi(\omega',\omega)e^{-i(\omega'+\omega)t}+\omega'^2\varepsilon^*(\omega')\mu^*(\omega')\Xi^*(\omega',\omega)e^{i(\omega'+\omega)t}}{\omega'+\omega}\right]d\omega' d\omega,\tag{C.S80}$$

where $\Xi(\omega',\omega) = \mathbf{E}(\omega')\cdot\mathbf{H}(\omega) - \mathbf{E}(\omega)\cdot\mathbf{H}(\omega')$. Note that in the above expression it has only been accounted the first term of the right-hand side of Eq. (C.S79). By regarding monochromatic optical fields, it can be shown that

$$\Xi_{\rm av}(\omega',\omega) = \frac{i}{2}\mathrm{Im}[\mathbf{E}^*\cdot\mathbf{H}]\left[\delta(\omega-\omega_0)\delta(\omega'+\omega_0) - \delta(\omega+\omega_0)\delta(\omega'-\omega_0)\right] = -\Xi^*_{\rm av}(\omega',\omega), \quad \text{(C.S81)}$$

where there are only the terms contributing to the time average. Hence, substituting this into Eq. (C.S80) we find that the time-averaged optical chirality density is given by

$$\langle\mathcal{C}\rangle_{\rm T} \equiv \langle\mathcal{C}^{(\rm e)} + \mathcal{C}^{(\rm m)}\rangle_{\rm T} = \frac{1}{4c^2}\mathrm{Im}[\mathbf{E}\cdot\mathbf{H}^*]\mathrm{Re}\left[\frac{\omega_0'^2\varepsilon(\omega_0')\mu(\omega_0') - \omega_0^2\varepsilon(\omega_0)\mu(\omega_0)}{\omega_0'-\omega_0}\right]. \quad \text{(C.S82)}$$

The latter result has a singular behavior when $\omega_0' = \omega_0$. To overcome this issue we should take the limit $\omega_0' \to \omega_0$, thus transforming the above expression into a derivative with respect to ω:

$$\langle\mathcal{C}\rangle_{\rm T} = \frac{1}{4c^2}\mathrm{Re}\left[\frac{d\left[\omega^2\varepsilon(\omega)\mu(\omega)\right]}{d\omega}\right]\mathrm{Im}[\mathbf{E}\cdot\mathbf{H}^*] = \frac{\omega}{2c^2}\mathrm{Re}[n(\omega)\tilde{n}(\omega)]\mathrm{Im}[\mathbf{E}\cdot\mathbf{H}^*], \quad \text{(C.S83)}$$

where $n(\omega) = \sqrt{\varepsilon\mu}$ is the phase refractive index and $\tilde{n}(\omega) \equiv n + \omega[\partial n/\partial\omega]$ is the dispersion-modified group refractive index [S35]. A more elegant form for expressing the above result may be made regarding the phase and group velocities, $v_p(\omega) \equiv c/n$ and $v_g(\omega) \equiv c/\tilde{n}$, respectively:

$$\langle\mathcal{C}\rangle_{\rm T} = \mathrm{Re}\left[\frac{\omega}{2v_p(\omega)v_g(\omega)}\right]\mathrm{Im}[\mathbf{E}\cdot\mathbf{H}^*], \quad \text{(C.S84)}$$

thus showing that the stored optical chirality increases as the group and/or phase velocities tend to get smaller [S55].

In order to compare with the results derived following the Loudon's approach [Eq. (C.S64)], we should also consider the second integral of Eq. (C.S79). This is carried out in the same way as the former calculations, and leads to

$$\langle\mathcal{C}^{(\rm c)}\rangle_{\rm T} = \frac{1}{8c^2}\mathrm{Im}\left[\frac{d\left[\omega^2\left(\varepsilon(\omega)-1\right)\mu(\omega)\right]}{d\omega}\mathbf{E}\cdot\mathbf{H}^*\right]. \quad \text{(C.S85)}$$

C. Brillouin's approach vs Loudon's approach: some additional remarks

To complete the analysis, we now show that there exists certain condition under which the expression for the optical chirality density associated to the fields, exactly coincide for both the above approaches. Indeed, it is easy to see that the optical chirality density given in Eq. (C.S63) is equal to that expressed in Eq. (C.S83) (or Eq. (C.S84)) when

$$2\mathrm{Re}\left[\varepsilon(\omega)\mu(\omega) + \frac{\omega\mu(\omega)}{2}\frac{\partial\varepsilon(\omega)}{\partial\omega} + \frac{\omega\varepsilon(\omega)}{2}\frac{\partial\mu(\omega)}{\partial\omega}\right] = \varepsilon_{\rm eff}\mu^*(\omega) + \varepsilon(\omega)\mu_{\rm eff}. \quad \text{(C.S86)}$$

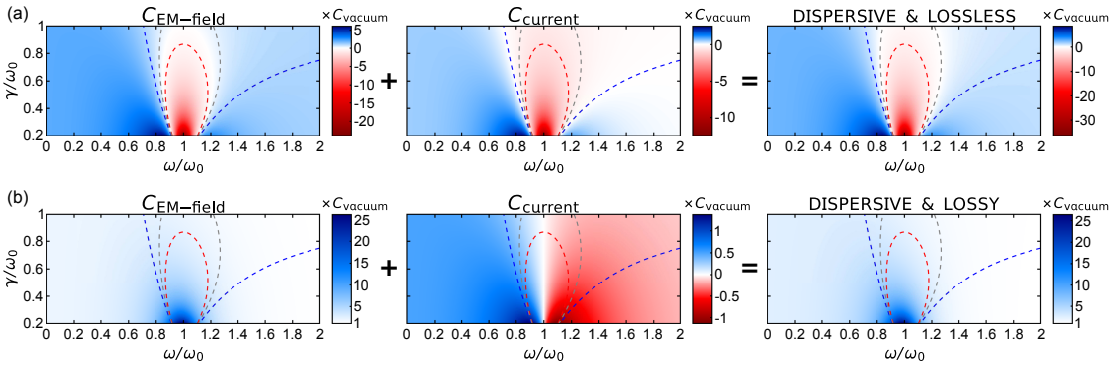

Figure C.S1: Optical chirality density in (a) lossless and (b) lossy dispersive media. Material parameters correspond to a nonmagnetic medium ($\mu = 1$) whose permittivity is described by a single Lorentz pole with $\omega_p = \omega_0$. In all the cases, red, gray and blue dashed lines indicate the curves where the total contribution of the optical chirality in the lossless case is $-C_{\text{vacuum}}$, 0 and C_{vacuum}, respectively.

From the latter equation it is straightforward to observe that the imaginary part of the right-hand side must be zero. This translates into the following condition:

$$\chi_n'' \left(1 + \xi_n'\right) - \xi_n'' \left(1 + \chi_n'\right) + 2\omega \chi_n'' \xi_n'' \left(\frac{1}{\tilde{\gamma}_n} - \frac{1}{\gamma_n}\right) = 0, \tag{C.S87}$$

which is fulfilled when $\gamma_n = \tilde{\gamma}_n = 0$ for all n. At the same time, we can verify that this solution is indeed the correct one, just by substituting it into the real part of Eq. (C.S86).

Finally, we would like to highlight once again that the key point throughout this derivation relies on the underlying mathematical structure of the conservation laws [Eq. (C.S3)]. The classical approaches provided by Brillouin and Landau enable us to obtain a closed expression, but it is only valid under the slowly varying amplitude approximation, i.e., in a relatively narrow frequency range where the effects of material absorption are negligible [see upper panel of Fig. C.S1]. Therefore, Eqs. (C.S26) and (C.S83) are suitable for describing energy and chirality solely in lossless dispersive media. In order to further include the dissipation, we have to consider explicitly the material features as well. This is carried out by means of the corresponding dynamic equations characterizing the polarization and the magnetization fields of the medium, thereby introducing additional terms that must be explicitly included in the time derivative of Eq. (C.S3). By doing so, we are able to find a more general definition for the energy and the optical chirality densities, thus capturing analytically the dispersion as well as the absorption processes [see lower panel of Fig. C.S1]. These results, given in Eqs. (C.S21), (C.S22) and (C.S63), are schematically summarized in Fig. C.S2. Importantly, departing from the top of the scheme, i.e., from the most general expressions, it is possible to arrive at the standard definitions, displayed in the intermediate and the lower panels of the scheme, by means of the corresponding approximations, thus progressively particularizing our general result. Hence, we can conclude that our approach leads to a consistent and meaningful definition for describing the optical chirality in dispersive and lossy media.

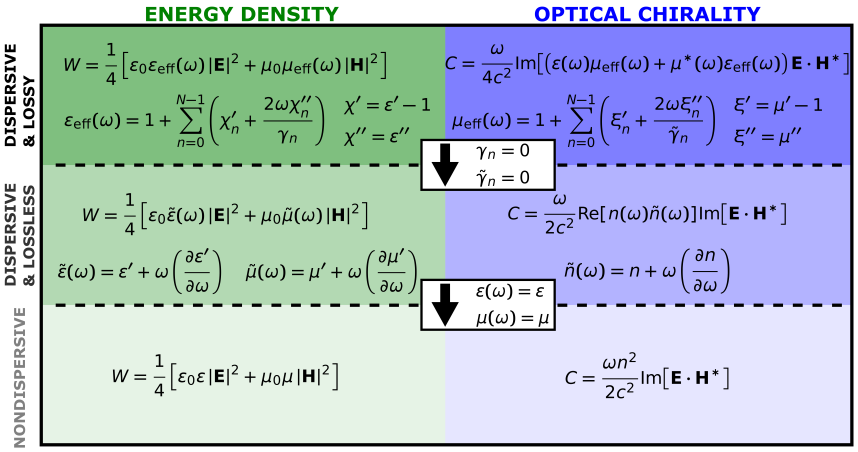

Figure C.S2: Schematic representation summarizing the main results showed in this supplementary material. For comparison, we also draw a parallel between the electromagnetic energy and the optical chirality densities derived by using different approaches.

D. Loss rate of the optical chirality in dispersive and lossy media

For the sake of completeness, we will show the expressions for describing the loss (or gain) rate of the field chirality density in dispersive media. The source-like contribution associated with the energy conservation, $\boldsymbol{\mathcal{J}} \cdot \boldsymbol{\mathcal{E}}$, can be directly related to the power lost (or the work exerted) by the electromagnetic fields to the sources. However, the physical significance of the source-like terms associated with the optical chirality, $\boldsymbol{\mathcal{E}} \cdot (\nabla \times \boldsymbol{\mathcal{J}})/2$, is not so obvious. This limits to some extent the concept of source (or sink) of optical chirality, and thus, hinders a proper interpretation of the loss rate associated with its conservation law [S45,S46]. Despite that, as pointed out above, these contributions are important because would enable us to get deeper insights into fundamental aspects regarding the interaction between chiral light with matter [S56].

Leaving aside the difficulty surrounding the physical interpretation, from a mathematical point of view, the loss rate of the optical chirality can be derived taking into account the structure of the continuity equation [Eq. (C.S3)]. Then, according to the complete expression of the conservation law for the optical chirality given in Eq. (C.S65), we will focus on the source-like terms $\mathcal{L}^{(\text{e})}_{\text{chirality}}$, $\mathcal{L}^{(\text{m})}_{\text{chirality}}$, and $\mathcal{L}^{(\text{c})}_{\text{chirality}}$. For simplicity, we will consider a nonmagnetic medium, so that $\mathcal{L}^{(\text{m})}_{\text{chirality}} = 0$. The electric contribution, $\mathcal{L}^{(\text{e})}_{\text{chirality}}$, is given by the second term of the right-hand side of Eq. (C.S54) together with the second and the third summation in Eq. (C.S55). Once again, in order to compare these results with those obtained via the Fourier transform we have to calculate the time average by considering time harmonic fields. In this manner it can be demonstrated that the residual term of Eq. (C.S54) leads to

$$-\frac{\varepsilon_0}{2}\left\langle \partial_t \boldsymbol{\mathcal{E}} \cdot (\nabla \times \boldsymbol{\mathcal{E}})\right\rangle_{\text{T}} = \frac{\omega^2}{4c^2}\text{Re}[\mu^* \mathbf{E}\cdot\mathbf{H}^*]. \tag{C.S88}$$

By summing this latter result and the time-average of the second and third summation in Eq. (C.S55) we obtain that

$$\langle \mathcal{L}^{(\mathrm{e})}_{\mathrm{chirality}} \rangle_{\mathrm{T}} = \frac{\omega^2}{4c^2} \left\{ \mathrm{Re}[\varepsilon] \mathrm{Re}[\mu^* \mathbf{E} \cdot \mathbf{H}^*] + \mathrm{Im}[\varepsilon] \mathrm{Im}[\mu^* \mathbf{E} \cdot \mathbf{H}^*] \right\}. \tag{C.S89}$$

On the other hand, assuming a linear, homogeneous and isotropic medium the current-like term is

$$\begin{aligned} \langle \mathcal{L}^{(\mathrm{c})}_{\mathrm{chirality}} \rangle_{\mathrm{T}} &= \frac{1}{2} \langle \boldsymbol{\mathcal{E}} \cdot (\nabla \times \boldsymbol{\mathcal{J}}) \rangle_{\mathrm{T}} \\ &= \frac{\omega^2}{4c^2} \left\{ \mathrm{Re}[(\varepsilon - 1)] \mathrm{Re}[\mu^* \mathbf{E} \cdot \mathbf{H}^*] + \mathrm{Im}[\varepsilon] \mathrm{Im}[\mu^* \mathbf{E} \cdot \mathbf{H}^*] \right\}. \end{aligned} \tag{C.S90}$$

Hence, the loss rate of the optical chirality in a nonmagnetic, dispersive and lossy medium is given by

$$\begin{aligned} \langle \mathcal{L}_{\mathrm{chirality}} \rangle_{\mathrm{T}} &= \langle \mathcal{L}^{(\mathrm{e})}_{\mathrm{chirality}} \rangle_{\mathrm{T}} + \langle \mathcal{L}^{(\mathrm{c})}_{\mathrm{chirality}} \rangle_{\mathrm{T}} \\ &= \frac{\omega^2}{2c^2} \left\{ \mathrm{Re}\left[\varepsilon - \frac{1}{2} \right] \mathrm{Re}[\mathbf{E} \cdot \mathbf{H}^*] + \mathrm{Im}[\varepsilon] \mathrm{Im}[\mathbf{E} \cdot \mathbf{H}^*] \right\}. \end{aligned} \tag{C.S91}$$

E. Loss rate of the optical chirality in dispersive and lossless media

Since we are assuming a lossless medium, the only term accounting for chirality dissipation is the current-like term $\boldsymbol{\mathcal{E}} \cdot (\nabla \times \boldsymbol{\mathcal{J}})/2$. Taking the Fourier transform we arrive at

$$\begin{aligned} \frac{1}{2} \boldsymbol{\mathcal{E}} \cdot (\nabla \times \boldsymbol{\mathcal{J}}) &= \frac{1}{2} \int_{-\infty}^{+\infty} \mathbf{E}(\omega') e^{-i\omega' t} d\omega' \cdot \left(\nabla \times \left[\int_{-\infty}^{+\infty} \mathbf{J}(\omega) e^{-i\omega t} d\omega \right] \right) \\ &= \frac{1}{2} \int_{-\infty}^{+\infty} \int_{-\infty}^{+\infty} \sigma(\omega) \mathbf{E}(\omega') \cdot [\nabla \times \mathbf{E}(\omega)] \, e^{-i(\omega' + \omega)t} d\omega' d\omega \\ &= \frac{i\mu_0}{2} \int_{-\infty}^{+\infty} \int_{-\infty}^{+\infty} \omega \mu(\omega) \sigma(\omega) \mathbf{E}(\omega') \cdot \mathbf{H}(\omega) e^{-i(\omega' + \omega)t} d\omega' d\omega. \end{aligned} \tag{C.S92}$$

By considering monochromatic optical fields, and integrating over frequencies we finally obtain

$$\frac{1}{2} \langle \boldsymbol{\mathcal{E}} \cdot (\nabla \times \boldsymbol{\mathcal{J}}) \rangle_{\mathrm{T}} = \frac{\omega^2}{4c^2} \left\{ \mathrm{Re}[(\varepsilon - 1)] \mathrm{Re}[\mu^* \mathbf{E} \cdot \mathbf{H}^*] + \mathrm{Im}[\varepsilon] \mathrm{Im}[\mu^* \mathbf{E} \cdot \mathbf{H}^*] \right\}. \tag{C.S93}$$

As we can see, this result exactly coincides with that given in Eq. (C.S90). However, in lossy media there are additional contributions that leads to the complete expression [Eq. (C.S91)] accounting for the sources or sinks of optical chirality.

Appendix: Values of the Drude-Lorentz model parameters characterizing silver and silicon

Figure C.2 in the main text shows the optical chirality density for silver and silicon. Material parameters describing the corresponding permittivities are taken from Refs. [S42]

and [S43], respectively (see values listed in Tables C.SI and C.SII). It should be noted that the material parameter for silver can be directly taken from Ref. [S42]. On the other hand, for the silicon, we have used fitting parameter from the experimental data given in Ref. [S43]. As a consequence, the expression for the permittivity is slightly different than Eq. (C.S6), and is given by

$$\varepsilon^{(\mathrm{Si})}_{\mathrm{D-L}}(\omega) = 1 - \frac{f_0\omega_0^2}{\omega^2 - \omega_0^2 + i\omega\gamma_0} - \frac{f_1\omega_1^2}{\omega^2 - \omega_1^2 + i\omega\gamma_1}. \tag{C.S94}$$

Table C.SI: Material parameters for the multi-resonant model as given in Eq. (C.S6), characterizing the permittivity of silver [S42]. The plasma frequency (ω_p), nth resonance frequencies (ω_n) and the nth damping constants (γ_n) are expressed in THz.

Ag [A. D. Rakić *et al.*, Appl. Opt. **37**, 5271 (1998)]								
ω_p	f_0	γ_0	f_1	γ_1	ω_1	f_2	γ_2	ω_2
2178.61	0.845	11.61	0.065	939.63	197.31	0.124	109.29	1083.50

f_3	γ_3	ω_3	f_4	γ_4	ω_4	f_5	γ_5	ω_5
0.011	15.72	1979.12	0.840	221.49	2196.26	5.646	584.91	4906.10

Table C.SII: Fitting parameters for the multi-resonant model as given in Eq. (C.S94), characterizing the permittivity of silicon [S43]. The nth resonance frequencies (ω_n) and the nth damping constants (γ_n) are expressed in THz.

Si [E. D. Palik, *Handbook of Optical Constants of Solids* (Academic Press, New York, 1985)]					
f_0	γ_0	ω_0	f_1	γ_1	ω_1
7.5	150	1000	3	50	830

References

[S1] J. H. Poynting, *On the transfer of energy in the electromagnetic field*, Phil. Trans. R. Soc. London **175**, 343 (1884).

[S2] J. D. Jackson, *Classical Electrodynamics* (Wiley, New York, USA, 1999).

[S3] M. V. Gorkunov, V. E. Dmitrienko, A. A. Ezhov, V. V. Artemov, and O. Y. Rogov, *Implications of the causality principle for ultra chiral metamaterials*, Sci. Rep. **5**, 9273 (2015).

[S4] V. G. Veselago, *The electrodynamics of substances with simultaneously negative values of ϵ and μ*, Sov. Phys. Usp. **10**, 509 (1968).

[S5] J. B. Pendry, *Negative refraction makes a perfect lens*, Phys. Rev. Lett. **85**, 3966 (2000).

[S6] D. R. Smith, W. J. Padilla, D. C. Vier, S. C. Nemat-Nasser, and S. Schultz, *Composite medium with simultaneously negative permeability and permittivity*, Phys. Rev. Lett. **84**, 4184 (2000).

[S7] H. J. Lezec, J. A. Dionne, and H. A. Atwater, *Negative refraction at visible frequencies*, Science **316**, 430 (2007).

[S8] N. Engheta, *Circuits with light at nanoscales: Optical nanocircuits inspired by metamaterials*, Science **317**, 1698 (2007).

[S9] J. Valentine, S. Zhang, T. Zentgraf, E. Ulin-Avila, D. A. Genov, G. Bartal, and X. Zhang, *Three-dimensional optical metamaterial with a negative refractive index*, Nature (London) **455**, 376 (2008).

[S10] C. García-Meca, J. Hurtado, J. Martí, A. Martínez, W. Dickson, and A. V. Zayats, *Low-loss multilayered metamaterial exhibiting a negative index of refraction at visible wavelengths*, Phys. Rev. Lett. **106**, 067402 (2011).

[S11] R. Loudon, *The propagation of electromagnetic energy through an absorbing dielectric*, J. Phys. A: Gen. Phys. **3**, 233 (1970).

[S12] R. Ruppin, *Electromagnetic energy density in a dispersive and absorptive material*, Phys. Lett. A **299**, 309 (2002).

[S13] T. J. Cui and J. A. Kong, *Time-domain electromagnetic energy in a frequency-dispersive left-handed medium*, Phys. Rev. B **70**, 205106 (2004).

[S14] S. A. Tretyakov, *Electromagnetic field energy density in artificial microwave materials with strong dispersion and loss*, Phys. Lett. A **343**, 231 (2005).

[S15] A. D. Boardman and K. Marinov, *Electromagnetic energy in a dispersive metamaterial*, Phys. Rev. B **73**, 165110 (2006).

[S16] P.-G. Luan, *Power loss and electromagnetic energy density in a dispersive metamaterial medium*, Phys. Rev. E **80**, 046601 (2009).

[S17] A. Raman and S. Fan, *Photonic band structure of dispersive metamaterials formulated as a Hermitian eigenvalue problem*, Phys. Rev. Lett. **104**, 087401 (2010).

[S18] W. Shin, A. Raman, and S. Fan, *Instantaneous electric energy and electric power dissipation in dispersive media*, J. Opt. Soc. Am. B **29**, 1048 (2012).

[S19] F. S. S. Rosa, D. A. R. Dalvit, and P. W. Milonni, *Electromagnetic energy, absorption, and Casimir forces: Uniform dielectric media in thermal equilibrium*, Phys. Rev. A **81**, 033812 (2010).

[S20] K. J. Webb and Shivanand, *Electromagnetic field energy in dispersive materials*, J. Opt. Soc. Am. B **27**, 1215 (2010).

[S21] F. D. Nunes, T. C. Vasconcelos, M. Bezerra, and J. Weiner, *Electromagnetic energy density in dispersive and dissipative media*, J. Opt. Soc. Am. B **28**, 1544 (2011).

[S22] L. Brillouin, *Wave Propagation and Group Velocity* (Academic, New York, USA, 1960).

[S23] L. D. Landau, E. M. Lifshitz, and L. P. Pitaevskii, *Electrodynamics of Continuous Media* (Pergamon, New York, USA, 1984).

[S24] J. Askne and B. Lind, *Energy of electromagnetic waves in the presence of absorption and dispersion*, Phys. Rev. A **2**, 2335 (1970).

[S25] C.-G. Huang and Y.-Z. Zhang, *Poynting vector, energy density, and energy velocity in an anomalous dispersion medium*, Phys. Rev. A **65**, 015802 (2001).

[S26] R. W. Ziolkowski, *Superluminal transmission of information through an electromagnetic metamaterial*, Phys. Rev. E **63**, 046604 (2001).

[S27] R. A. Shelby, D. R. Smith, and S. Schultz, *Experimental verification of a negative index of refraction*, Science **292**, 77 (2001).

[S28] L. J. Wang, A. Kuzmich, and A. Dogariu, *Gain-assisted superluminal light propagation*, Nature (London) **406**, 277 (2000).

[S29] S. Glasgow, M. Ware, and J. Peatross, *Poynting's theorem and luminal total energy transport in passive dielectric media*, Phys. Rev. E **64**, 046610 (2001).

[S30] G. Dolling, C. Enkrich, M. Wegener, C. M. Soukoulis, and S. Linden, *Simultaneous negative phase and group velocity of light in a metamaterial*, Science **312**, 892 (2006).

[S31] E. Feigenbaum, N. Kaminski, and M. Orenstein, *Negative dispersion: a backward wave or fast light? Nanoplasmonic examples*, Opt. Express **17**, 18934 (2009).

[S32] D. F. Nelson, *Momentum, pseudomomentum, and wave momentum: Toward resolving the Minkowski-Abraham controversy*, Phys. Rev. A **44**, 3985 (1991).

[S33] S. M. Barnett and R. Loudon, *The enigma of optical momentum in a medium*, Phil. Trans. R. Soc. A **368**, 927 (2010).

[S34] S. M. Barnett, *Resolution of the Abraham-Minkowski dilemma*, Phys. Rev. Lett. **104**, 070401 (2010).

[S35] K. Y. Bliokh, A. Y. Bekshaev, and F. Nori, *Optical momentum and angular momentum in complex media: from the Abraham-Minkowski debate to unusual properties of surface plasmon-polaritons*, New J. Phys. **19**, 123014 (2017).

[S36] M. G. Silveirinha, *Reexamination of the Abraham-Minkowski dilemma*, Phys. Rev. A **96**, 033831 (2017).

[S37] L. Novotny and B. Hecht, *Principles of Nano-Optics* (Cambridge University Press, Cambridge, England, 2012).

[S38] Notice that, strictly speaking, vacuum is the only nondispersive medium [S2,S37]. Still, dielectrics are often regarded in a simpler fashion as transparent (or nonabsorbing) and nondispersive material systems, or even as lossless dispersive media over some frequency bands for which absorption losses are negligibly small [S22,S23].

[S39] K. E. Oughstun and S. Shen, *Velocity of energy transport for a time-harmonic field in a multiple-resonance Lorentz medium*, J. Opt. Soc. Am. B **5**, 2395 (1988).

[S40] F. D. Nunes, B.-H. V. Borges, and J. Weiner, *Analysis of dispersive and dissipative media with optical resonances*, Opt. Express **20**, 15679 (2012).

[S41] S. A. Maier, *Plasmonics: Fundamentals and Applications* (Springer, New York, USA, 2007).

[S42] A. D. Rakić, A. B. Djurišić, J. M. Elazar, and M. L. Majewski, *Optical properties of metallic films for vertical-cavity optoelectronic devices*, Appl. Opt. **37**, 5271 (1998).

[S43] E. D. Palik, *Handbook of Optical Constants of Solids* (Academic Press, New York, USA, 1985).

[S44] Notice that the external electromagnetic fields, $\boldsymbol{\mathcal{E}}_{\rm loc}$ and $\boldsymbol{\mathcal{H}}_{\rm loc}$, are actually local microscopic fields acting as a driving force [S39]. The corresponding macroscopic counterpart comes when averaging over sufficiently large spatial distances [S2,S37,S41].

[S45] G. Nienhuis, *Conservation laws and symmetry transformations of the electromagnetic field with sources*, Phys. Rev. A **93**, 023840 (2016).

[S46] I. Fernandez-Corbaton and C. Rockstuhl, *Unified theory to describe and engineer conservation laws in light-matter interactions*, Phys. Rev. A **95**, 053829 (2017).

[S47] D. M. Lipkin, *Existence of a new conservation law in electromagnetic theory*, J. Math. Phys. **5**, 696 (1964).

[S48] Y. Tang and A. E. Cohen, *Optical chirality and its interaction with matter*, Phys. Rev. Lett. **104**, 163901 (2010).

[S49] Y. Tang and A. E. Cohen, *Enhanced enantioselectivity in excitation of chiral molecules by superchiral light*, Science **332**, 333 (2011).

[S50] K. Y. Bliokh and F. Nori, *Characterizing optical chirality*, Phys. Rev. A **83**, 021803 (2011).

[S51] M. M. Coles and D. L. Andrews, *Chirality and angular momentum in optical radiation*, Phys. Rev. A **85**, 063810 (2012).

[S52] L. V. Poulikakos, P. Gutsche, K. M. McPeak, S. Burger, J. Niegemann, C. Hafner, and D. J. Norris, *Optical chirality flux as a useful far-field probe of chiral near fields*, ACS Photonics **3**, 1619 (2016).

[S53] T. G. Philbin, *Lipkin's conservation law, Noether's theorem, and the relation to optical helicity*, Phys. Rev. A **87**, 043843 (2013).

[S54] R. P. Cameron, J. B. Götte, S. M. Barnett, and A. M. Yao, *Chirality and the angular momentum of light*, Phil. Trans. R. Soc. A **375**, 20150433 (2017).

[S55] R. W. Boyd and D. J. Gauthier, *Controlling the velocity of light pulses*, Science **326**, 1074 (2009).

[S56] M. Schäferling, *Chiral Nanophotonics: Chiral Optical Properties of Plasmonic Systems* (Springer, Berlin, 2017).

Chapter 6

PAPER D

Toward Chiral Sensing and Spectroscopy Enabled by All-Dielectric Integrated Photonic Waveguides

---

Laser Photonics Rev. 14, 1900422 (2020)

Toward Chiral Sensing and Spectroscopy Enabled by All-Dielectric Integrated Photonic Waveguides

J. Enrique Vázquez-Lozano and Alejandro Martínez

Nanophotonics Technology Center, Universitat Politècnica de València, Camino de Vera s/n, 46022 Valencia, Spain

Chiral spectroscopy is a powerful technique enabling to identify optically the chirality of matter. So far, most experiments to check the chirality of matter or nanostructures have been performed through arrangements wherein both the optical excitation and detection are realized via circularly polarized light propagating in free space. However, for the sake of miniaturization, it would be desirable to perform chiral spectroscopy in photonic integrated platforms, with the additional benefit of massive parallel detection, low-cost production, repeatability, and portability. Here it is shown that all-dielectric photonic waveguides can support chiral modes under proper combination of fundamental eigenmodes. Two mainstream configurations are investigated: a dielectric wire with square cross section and a slotted waveguide. Three different scenarios in which such waveguides could be used for chiral detection are numerically analyzed: waveguides as near-field probes, evanescent-induced chiral fields, and chiroptical interaction in void slots. In all the cases, a metallic nanohelix is considered as a chiral probe, though all the approaches can be extended to other kinds of chiral nanostructures as well as matter. These results establish that chiral applications such as sensing and spectroscopy could be realized in standard integrated optics, in particular, with silicon-based technology.

D.I Introduction

Chirality is the geometrical property by which an object cannot be superimposed on its mirror image. Even though this feature is ubiquitous in nature at the full range of scales, it is likely at the molecular level where it plays a key role from a practical point of view. Indeed, enantiomers, that is, pairs of stereoisomers having opposite handedness or chirality, may have well different pharmacological effects [1–3]. Besides in the molecular structure [4], chirality also applies to some elementary particles such as photons [5], electrons [6], or phonons [7]. In the case of photons, and using classical notation, we shall refer to it as optical chirality, which, just like the electromagnetic helicity [8,9], has been recognized as a fundamental property of light characterizing the local handedness, or

twistiness, of the electromagnetic field lines [10,11]. Thus, circularly polarized light (CPL) is typically considered as the paradigmatic example of chiral light [12].

Information about the chirality of matter at the micro or even molecular scale can then be directly retrieved by making it interact with chiral light. There are a number of techniques to discriminate enantiomers, but the most commonly performed is the so-called circular dichroism spectroscopy [13], which consists in determining the differential absorption rate of left (L) and right (R) CPL when propagating through a chiral medium [14]. Likewise, the efficiency of this asymmetric chiroptical response is generally quantified in terms of the dissymmetry factor:

$$g = 2\left[\frac{A^+ - A^-}{A^+ + A^-}\right], \tag{D.1}$$

where $A^{\pm}$ is the absorption rate of L-CPL (+) and R-CPL (−). This establishes a standard metric to quantify the enantioselectivity and its possible enhancement with respect to CPL [15,16]. Importantly, for free-space illumination under the dipole approximation, it has been proved that the dissymmetry factor is, in turn, proportional to the optical chirality density [10,12], thereby promoting an insightful pathway to control the chiroptical response via an all-optical approach, namely, regardless of the structural properties of the chiral analyte [17]. Notwithstanding that, this proportionality is not universal at all, and it would only be valid in the presence of non-structured environments; otherwise (i.e., in structured environments), local enhancement peaks of chirality and those of g, would appear to be slightly wavelength-shifted from each other, thus breaking such a proportionality [18]. In this regard, it should be noticed that, although known for years, only recently it has been put forward general and closed expressions for both the optical chirality [19], as well for the electromagnetic helicity [9], of fields propagating through dispersive and even lossy media.

Interaction between chiral light and chiral molecules is in general extremely weak [14], owing to the large scale difference between the operational wavelength of the input light and the typical size of the molecules [17]. Nevertheless, since the original suggestion [10] and preliminary demonstrations [12,16] of the existence of superchiral fields (i.e., optical fields carrying chirality larger than that of CPL) to enhance the chiroptical interactions, the interest in this field has grown considerably. In particular, metallic nanostructures supporting plasmonic resonances at subwavelength dimensions have been proven to be well-suited platforms for strengthening chiroptical effects [20–23], leading to local chiral enhancements by orders of magnitude [24,25]. Further developments have led to improve and simplify the chiroptical schemes to achieve ultrasensitive enantiomeric detection, recognition, and separation [26], for example, by stacking twisted planar metasurfaces [27], or in arrays of both chiral [28] and even achiral plasmonic nanostructures, such as spheres [29], nanoslits [30], or nanorods [31,32]. Much more recently, high-index dielectric nanoparticles in several geometries such as nanospheres [18,33], solid [34–37], or slotted [38] nanodisks, or bowtie-like nanostructures [39], have also been suggested

as suitable structures to boost near-field chirality [29,40,41]. Besides displaying lower absorption losses than its plasmonic counterparts, dielectric resonators are proving to be a promising platform with a number of important practical advantages for chiral sensing, spectroscopy, and enantioselectivity [42]: large areas of high and uniform-sign chirality (enantiopure enhancement) [34,35], spectral accessibility and tunability of chiral interactions [18,36], switchability upon reversing the input polarization [37], as well as large and spatially accessible chiral hot spots [38,39].

In recent years, there have been many efforts to implement sensing, spectrometry, and spectroscopy in photonic integrated platforms [43,44]. In all these cases, light is guided on a chip through lossless dielectric nanowires (i.e., waveguides with confinement dimensions of the order of $\lambda/2$, and propagation distances beyond the cm-scale), wherein some integrated elements are included to carry out the required optical processing. A similar conception may also be applicable to perform integrated chiral sensing and spectroscopy, since, up to now, prevailing approaches are considering arrangements in which the input light propagates through free space. While keeping the same working principle, the integrated approach should bring about numerous practical benefits, mainly if realized onto silicon-based platforms compatible with standard CMOS technology: low-cost and mass-volume production, repeatability, multiplexed detection, or integration with electronics, among others. Yet, in the context of integrated photonics, chiroptical effects have only been borne out as a consequence of the spin–orbit interaction of light for controlling near-field unidirectional excitation of guided modes [45–47], leaving aside other interesting capabilities such as enantiomeric discrimination, chiral spectroscopy, or sensing. In this regard, it should be noted that, apart from the case of plane-wave propagating in free space, studies on optical chirality (and/or helicity [8]) in integrated platforms are scarce, with the notable exception of cylindrical dielectric waveguides, for which there are analytical solutions [48–50].

In this work, we investigate the existence of (enhanced) optical chirality in lithographically defined integrated dielectric waveguides, as well as its potential in chiral applications such as sensing or spectroscopy. In particular we focus on two of the most common guiding structures used in nanophotonics: strip and slot waveguides [51]. Even though the fundamental eigenmodes of these structures, typically referred to as transverse electric (TE) and transverse magnetic (TM), yield no chirality, we show that a net optical chirality of opposite signs can arise from the adequate superposition of two orthogonally polarized guided modes, analogously to the conventional case of L- and R-CPL. Building on this analysis, we show that such waveguides can be used as near-field tips and probes for excitation and read-out of chiral nanostructures, in arrangements equivalent to that routinely performed in circular dichroism measurements. More strikingly, we find a strong interaction between the evanescent field of the chiral guided modes and the chiral metallic sample, which is different depending on whether or not the optical chirality of the field matches the handedness of the structure. These effects also allow us to disclose the active role of the absorption losses, recently introduced in the theoretical

framework of optical chirality [19], as well as the relationship between the chirality and the transverse spin [52,53]. Hence, besides suggesting the possibility of using photonic integrated platforms for chiral applications, these findings may lay the groundwork for a greater variety of chiroptical effects [54,55].

D.II Optical Chirality Density in All-Dielectric Integrated Photonic Waveguides

We start by considering a guiding system consisting of a silicon nitride (Si_3N_4) waveguide with square cross section that, for simplicity, is surrounded by vacuum. Silicon nitride is chosen as it is compatible with standard CMOS technology and enables guidance in an extremely broad wavelength regime [44], thus covering the relevant visible and near-infrared (NIR) spectral regions [56]. The waveguide can be suspended in air just by removing the substrate, as it is usually done in waveguide and cavity optomechanics. Moreover, by choosing a square cross section, we ensure that the two first guided modes (i.e., the TE and TM modes) appear to be degenerate. Unlike wires with circular cross section [48–50], there is no analytical solution for the propagating modes of square (or, in general, rectangular) dielectric waveguides, so we ought to calculate the corresponding guided modes by means of numerical simulations. This has been performed with the aid of the commercial 3D full-wave solver CST Microwave Studio (Section D.VI). After that, as done earlier when calculating the transverse spin of such guided modes [57], once determined the electric and magnetic components of each mode, we can straightforwardly obtain the optical chirality density from its general definition [19]:

$$C = \frac{\omega}{4c^2}\mathrm{Im}[(\varepsilon(\omega)\mu_{\mathrm{eff}}(\omega) + \varepsilon_{\mathrm{eff}}(\omega)\mu^*(\omega))\,\mathbf{E}\cdot\mathbf{H}^*], \tag{D.2}$$

wherein c is the speed of light in free space, $\mathbf{E}$ and $\mathbf{H}$ are, respectively, the electric and magnetic complex field amplitudes, with the asterisk denoting complex conjugation, and ε and μ are the standard permittivity and permeability of the medium. Additionally, to fully account for the dispersion of the guiding structure, we should use the real-valued effective material parameters $\varepsilon_{\mathrm{eff}}$ and μ_{eff}, depending on the angular frequency ω [19].

Figure D.1a shows the optical chirality density for right- and left-handed circularly polarized guided modes (CPGMs) in a silicon nitride strip waveguide, with equal width and thickness, $w = t = 450$ nm, at NIR frequencies (specifically, it is set at $f \approx 230$ THz). Notice that, in principle, lower wavelengths (or higher frequencies), that is, those ranging from visible to the near-UV spectral region, would be more suitable for chiral spectroscopy. Nonetheless, the transverse profile of the modes will be similar at any wavelength below the cut-off, so these results would qualitatively apply to the whole wavelength range supporting the TE and TM guided modes. Just like CPL propagating in free space, CPGMs may be built by superposing both degenerate TE and TM eigenmodes with a phase shift of $\pi/2$ between them. In this way, they result in a locally nonzero optical chirality within the waveguide core, being positive or negative depending on whether the

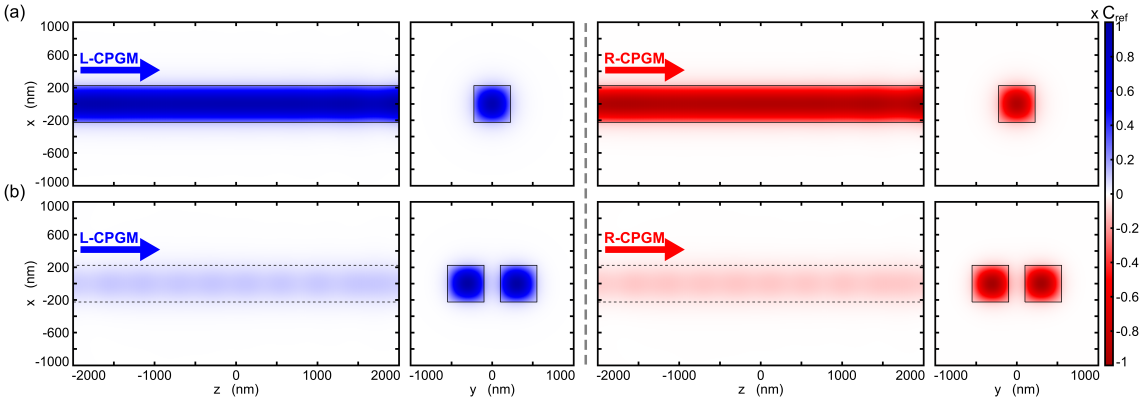

Figure D.1: Cross-sectional maps of the normalized chirality density for L- and R-CPGM in silicon nitride a) strip and b) slot waveguides with square cross section ($w = t = 450$ nm) and $d_{\text{slot}} = 200$ nm, at NIR frequencies (specifically, they are $f \approx 230$ THz and $f \approx 250$ THz, for the strip and the slotted case, respectively). The normalization is carried out with respect to the maximum chirality, dubbed as C_{ref}, for each configuration, and it will serve as a reference to quantify the corresponding chiral enhancement in the following results.

CPGM is left- or right-handed, respectively (Figure D.1). This is a feature that could be expected by considering that the waveguide core squeezes propagating light in a thin cross section of the order of $(\lambda/2n_{\text{eff}})^2$, being n_{eff} the effective refractive index of the corresponding guided mode. Noticeably, the evanescent tail of the propagating CPGM through the vacuum region surrounding the waveguide still yields chirality as well. This allows us to suggest the possibility of performing chiral spectroscopy or sensing just by placing chiral objects in such a near-field region [22,29,42,58]. As evident, the local chirality of the evanescent field is much lower than in the core, but still, its interaction with chiral structures can be even stronger than that of normal incidence, as will be shown in the next section. Moreover, since all-dielectric waveguides are inherently lossless (e.g., in silicon nitride technology, actual fabrication processes enable propagation losses as low as 5.5 dB m^{-1} at telecom wavelengths [59]), the optical chirality conveyed by the CPGMs can be transported over very long distances, thereby enlarging the active region where realizing chiral light–matter interaction.

Alternatively, dielectric slot waveguides are practical structures that enable guiding and strong field confinement in a thin low-index region separating two strip waveguides [60]. This makes them useful for biosensing [61], and thus amenable for the experimental realization of chiroptical applications. However, in contrast to the previous case, here the slot breaks the symmetry of the system so it is not possible to get an exact degeneracy between the TE and TM modes. It is, though, feasible to design the slot waveguide in such a way that the TE and TM modes have the same effective index for (or up to) a certain wavelength, namely, ensuring a sufficient degree of coherence for the CPGMs so that they can propagate along the required operational distance. As shown in Figure D.2, for a square cross-sectional silicon nitride waveguide with $w = t = 450$ nm, and $d_{\text{slot}} = 200$ nm,

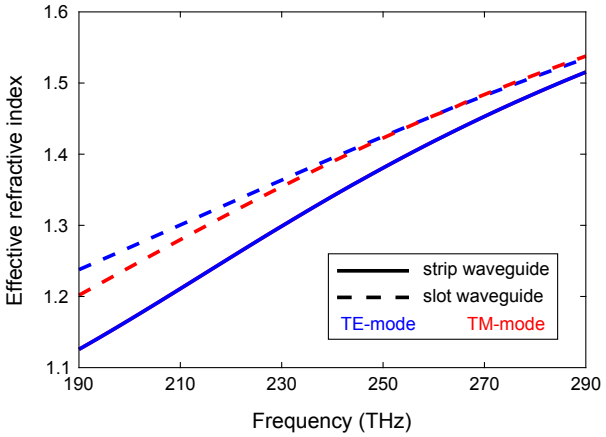

Figure D.2: Effective refractive index of the fundamental TE and TM eigenmodes of a silicon nitride strip (solid line) and slot (dashed line) waveguide with square cross section ($w = t = 450$ nm) and $d_{\text{slot}} = 200$ nm. In both cases the surrounding medium is assumed to be vacuum.

this overall degree of coherence between TE and TM modes is attained when $f \approx 250$ THz ($\lambda \approx 1200$ nm). With this restriction in mind, we performed similar calculations as in the former case, whose results are depicted in Figure D.1b. It can be seen that both L- and R-CPGM yield a roughly uniform distribution of optical chirality in the slot region, which should be extremely useful for multiple chiroptical applications (e.g., for enantioselective photochemical processes, such as photolysis or photoionization of racemic mixtures of chiral molecules [18,34,36]).

The optical chirality maps shown in Figure D.1 will be used as the reference for setting the corresponding enhancement when the chiral sample is included. In this regard, it is worth pointing out that, unlike in the case of plane-wave propagation in free space, wherein superchirality is well defined with respect to the chirality of CPL [10,12,16,62], in the case of waveguiding systems the situation can be slightly problematic as it would depend on the specific structure. So, in lieu of superchirality, we shall refer to it simply as the enhanced chirality [63], whose enhancement factor is relative to the reference chirality C_{ref}, that is, the maximum chirality for each specific configuration.

Now that we have shown that planar dielectric waveguides may support chiral light propagation, we will look into three different scenarios enabling integrated chiral applications: dielectric waveguides as near-field probes for excitation and read-out of chiral light–matter interaction (in-gap configuration); near-field optical chirality induced by evanescent fields neighboring waveguiding structures (on-top configuration); and chiroptical interaction in slot waveguides (slotted configuration). For simplicity, and without any loss of generality, throughout this work, we are going to consider a metallic nanohelix as a sample structure since it is often regarded as the prototypical example of chiral object [64–72]. It will lead to a differential absorption (or, equivalently, transmission, through the output waveguide) of L- and R-CPGM, depending on the handedness of the

metallic nanohelix. For comparison purposes, we will analyze the resonant behavior of this structure modeled either as a perfect electric conductor (PEC) or silver, whose material parameters are taken from ref. [73]. At any rate, we stress out that any other kind of chiral structure or material could be used as well [74–76].

D.III Probing the Chiroptical Response in Dielectric Strip Waveguides: Normal Incidence (in-gap configuration) and Evanescent-Induced Chiral Interaction (on-top configuration)

First we investigate a chiral metallic scatterer embedded in a narrow gap separating two silicon nitride waveguides with square cross section ($w = t = 450$ nm). The chiral nanostructure consists of a 4-turns single helix placed in between the waveguides, being centered and orientated along the propagation axis in the z-direction (Figure D.3a). As aforementioned, in this first approach, the metal is simply modeled as a PEC. This would give us some hints to understand the chiral behavior of the helix on account of its geometry itself, thereby dismissing any potential influence of dispersion or absorption effects. Regardless of the number of turns, a full geometrical description of this complex object is determined by the following set of structural parameters: helix radius (R_{helix}), pitch (p), and helix wire radius (r_{helix}), apart from the handedness, given by a relative phase shift between the x- and y-coordinates. By properly engineering each of these parameters one can gain control over the main spectral features, tuning the resonance position and depth, as well as the optical activity of the metallic chiral structure (see refs. [65,66,71,72] for further details). In this case, we shall consider a right-handed helix with geometrical parameters fixed to $p = 50$ nm, $r_{\text{helix}} = 20$ nm, and R_{helix} set as the control parameter, varying from 100 to 114 nm. Notice that this choice of the variable parameter is done so that we can keep constant the gap width, in this case to 240 nm.

As mentioned above, one can excite either L- and R-CPGM in the input waveguide by controlling the relative phase shift between the TE and TM modes (Section D.VI). Then, using an end-fire coupling setup, the light exiting the input waveguide will excite the chiral structure in the near-field, here acting as a probe. The output waveguide will collect the light both scattered by the structure and transmitted from waveguide to waveguide [77,78], thus enabling the read-out of the chiroptical interaction. To account for the chiral spectral response, we first represent the transmission and mode conversion spectra for L- and R-CPGM (Figure D.3b). From this, it can be seen that, while L-CPGM is nearly transparent to the presence of the helix, R-CPGM exhibits a narrow transmission dip depending on R_{helix}, thereby providing clear evidence of the underlying optical activity brought about when the handedness of the CPGM coincides with that of the chiral structure. These signals directly translate into an asymmetric response on the transmission spectra, whose strength can be quantified by means of the chiral dissymmetry factor g (Figure D.3c) [62,63,79]. In this regard, it should be noted that,

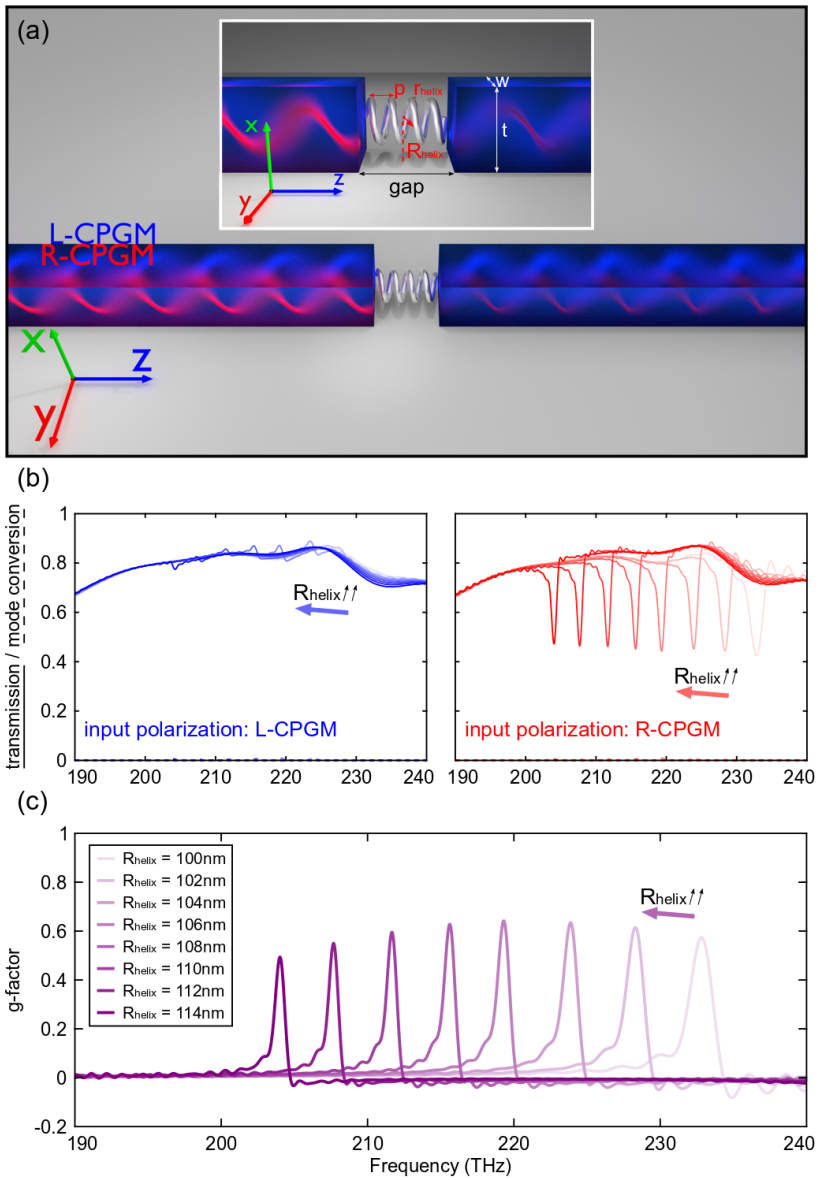

Figure D.3: a) Scheme of the arrangement for chiral sensing and spectroscopy enabled by a dielectric strip waveguide as a local probe for excitation and read-out under normal incidence with a gap width set to 240 nm (in-gap configuration). The chiral metallic structure is modeled as a right-handed 4-turns single helix made of PEC, with geometrical parameters fixed to $p = 50$ nm, $r_{\mathrm{helix}} = 20$ nm, and R_{helix} is varied from 100 to 114 nm. b) Numerical simulation of transmission and mode conversion spectra for different values of R_{helix}. c) Dissymmetry factor.

along with the definition given in Equation (D.1), involving the differential absorption rate, for simplicity, in this situation the dissymmetry factor may also be equivalently characterized in terms of the differential transmission of L- and R-CPGMs, along the ouput waveguides [21,68,70,72]. Thus, concerning our proposed scheme, such a definition will allow us from now on for a more direct and intuitive description of the chiroptical

interaction. It can be seen that the peak values of g (≥ 0.5) are attained at the helix resonance, which does depend on the radius R_{helix}. This then confirms the chiral response of the system in a region with a foot-print $< 1\ \mu\text{m}^2$. Remarkably, as shown in Figure D.3b, the strong chiral interaction at resonance also results in a negligible, but nonzero, mode conversion between L- and R-CPGM, and vice versa, that is, there is optical power from the input mode that is transferred to the orthogonal mode at the output of the system. For our purposes, this is a totally unwanted side effect since, ideally, the chiral sample should behave so that the transmitted incident circular polarization is maintained [65]. Still, this effect might be further mitigated by intertwining multiple helices [66].

A similar analysis holds for the near-field chirality induced by the evanescent field neighboring the silicon nitride waveguide over which a metallic chiral nanostructure is placed. The scheme of this approach is depicted in Figure D.4a. Again, maintaining the same geometrical parameters for the nanohelix and modeling it as a PEC, we obtain, via numerical simulations, the spectral behavior of the transmission of L- and R-CPGM for different radii of the helix, now ranging from 50 to 55 nm (Figure D.4b). From these results, and taking into account the above considerations, we can directly calculate the dissymmetry factor g (Figure D.4c). It can be seen that the peaks of g (or, analogously, the dips in transmission) become narrower and higher in comparison with the previous case. This is quite striking since the fields in the evanescent region are much weaker than in the gap spacing two waveguides, wherein they are essentially similar to those in the waveguide core [77,78]. Yet, this configuration still retain common features with respect to the previous case, in particular, the peak position (or resonance frequency) dependent on the helix radius, and the intermodal conversion between L- and R-CPGM, and vice versa, as a result of the interaction between the CPGMs and the chiral structure (Figure D.4b).

For a more intuitive description, we plot the cross-sectional maps of optical chirality density from the corresponding electromagnetic field distributions (Figure D.5), which, in turn, are obtained via numerical simulations (Section D.VI). For practical reasons, we have to decide a specific set of parameters to perform the graphical representation, including the working frequency. By looking at the results shown in Figures D.3c and D.4c, the best trade-off for a fair comparison is such that $R_{\text{helix}} = 108$ nm for the in-gap configuration, and $R_{\text{helix}} = 52$ nm for the on-top configuration, since in both cases there exists a well-localized resonance at approximately 216 THz. It should be noticed that this map brings about complementary information to be accounted for. In particular, it provides a clear visualization of the resonant behavior of the nanohelix. Indeed, as shown in Figure D.5, most of the optical chirality density is tightly localized and strongly enhanced in the surroundings of the chiral structure, reaching a value of up to 30 times C_{ref}, that is, the maximum chirality attainable when the chiral particle is ignored (Figure D.1). Remarkably, both the enhancement and the localization are even larger when the input mode possesses the same handedness as the chiral nanohelix, namely, for R-CPGM. This translates into a higher scattering and/or absorption by the sample we are probing (or a lower transmission at the output port), thus exhibiting a true chiroptical effect. It should

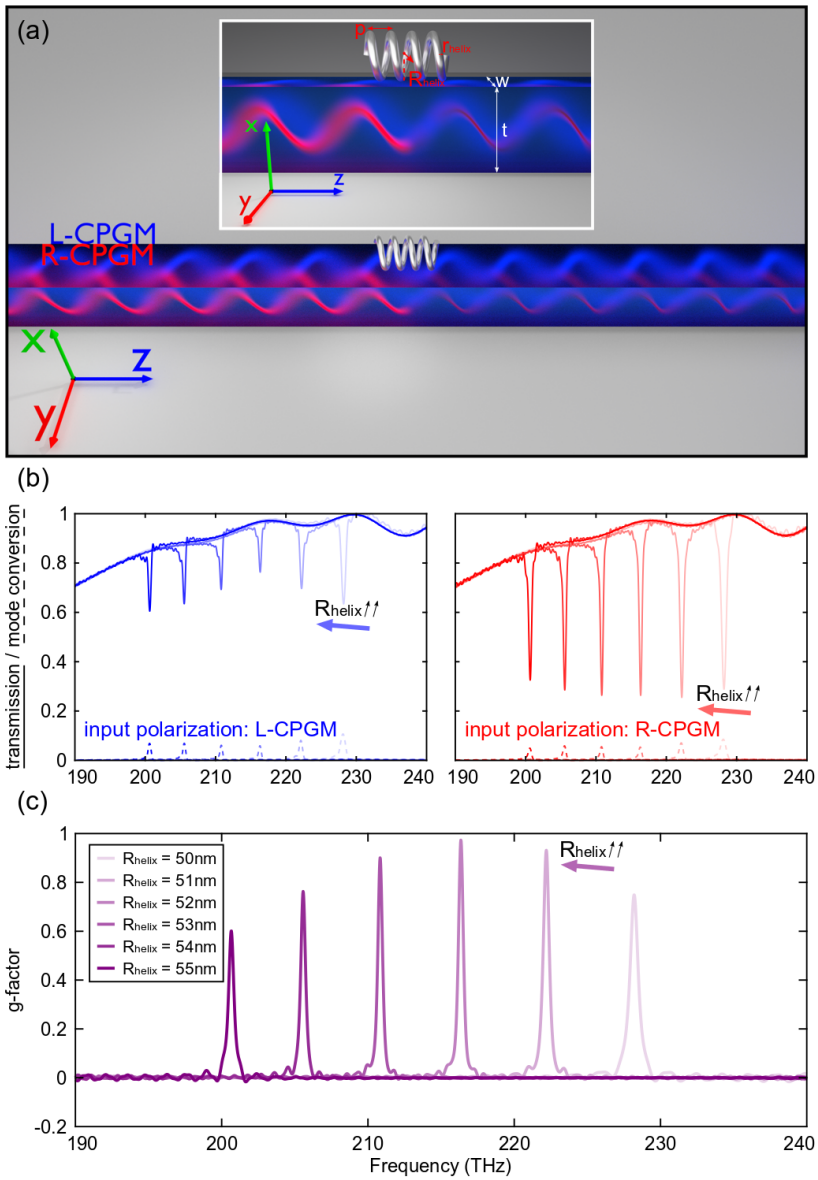

Figure D.4: a) Scheme of the arrangement for the evanescent-induced chiral response in a dielectric strip waveguide (on-top configuration). The characterization of the chiral metallic nanohelix is the same as in Figure D.3, but with R_{helix} ranging from 50 to 55 nm. b) Numerical simulation of transmission and modal conversion spectra for different values of R_{helix}. c) Calculated dissymmetry factor.

be noted that, since we are considering PEC made helices, the dominant response should be due to chirality-dependent scattering [71,72]. Furthermore, regardless of the input mode, the sign of chirality remains uniform in both the outer and the inner region of nanohelix. In this regard, it is worth observing that, inside the helix, the chiral sign is always opposed to that of its handedness. This fact becomes even more evident for the on-top configuration, in which the local optical chirality gets strikingly higher than in the in-gap configuration.

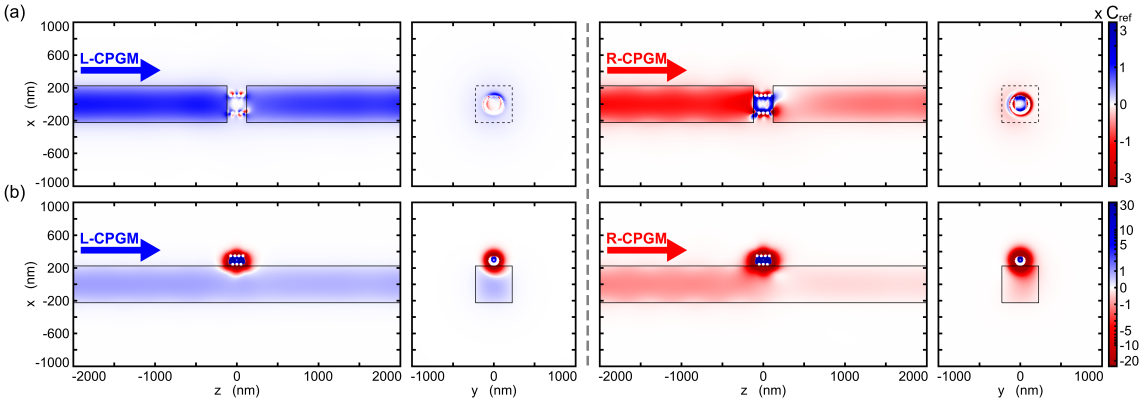

Figure D.5: Cross-sectional maps of the optical chirality density for L- and R-CPGM in silicon nitride strip waveguides for a) the in-gap configuration (Figure D.3a) and b) the on-top configuration (Figure D.4a). The chiral metallic structure is modeled as a PEC, and the geometrical parameters are the same as in Figures D.3 and D.4, setting a) $R_{\text{helix}} = 108$ nm, and b) $R_{\text{helix}} = 52$ nm. In both cases, we consider the working frequency $f = f_{\text{res}} \approx 216$ THz. The values are normalized with respect to C_{ref}, that is, the maximum chirality attainable for each configuration when ignoring the presence of the chiral structure.

D.IV Further Considerations for a Realistic Approach of Chiroptical Applications in Integrated Platforms

A. Beyond the ideal PEC model: Drude–Lorentz materials

For the sake of simplicity, thus far we have assumed the chiral probe particle as made of a PEC. However, this will not be the case in a real system, where at optical frequencies metals display a Drude–Lorentz-like response in which dispersion and absorption losses should be included. To account for this, we have further repeated our simulations considering a silver helix with material parameters taken from ref. [73]. Numerical results are summarized in Figure D.6. In order to compare with the case above, for the in-gap configuration, we have considered again a right-handed 4-turns single helix. Nonetheless, for a better representation of the results, small modifications in the geometrical parameters have been carried out, setting the gap width to 300 nm, $p = 70$ nm, $r_{\text{helix}} = 10$ nm, with R_{helix} varying from 90 to 120 nm. On the other side, for the on-top configuration we have used a helix with 16 turns, so that we can leverage further the chiroptical interaction induced by the evanescent tail of the CPGMs. Regardless of structural specifications of the chiral scatterer, in both cases, the system still retains the same general features mentioned above, that is, chiral-like resonances whose frequency depends on the helix radius, and the nonzero mode conversion between L- and R-CPGM, and vice versa. However, likely due to the absorption losses, the transmission dips, and consequently, the peaks in the dissymmetry factor spectra become wider. Moreover, g also exhibits opposite chiral behavior at frequencies just before the resonant peak. Despite that, it is worth emphasizing that the chiroptical responses characterized by the dissymmetry factor

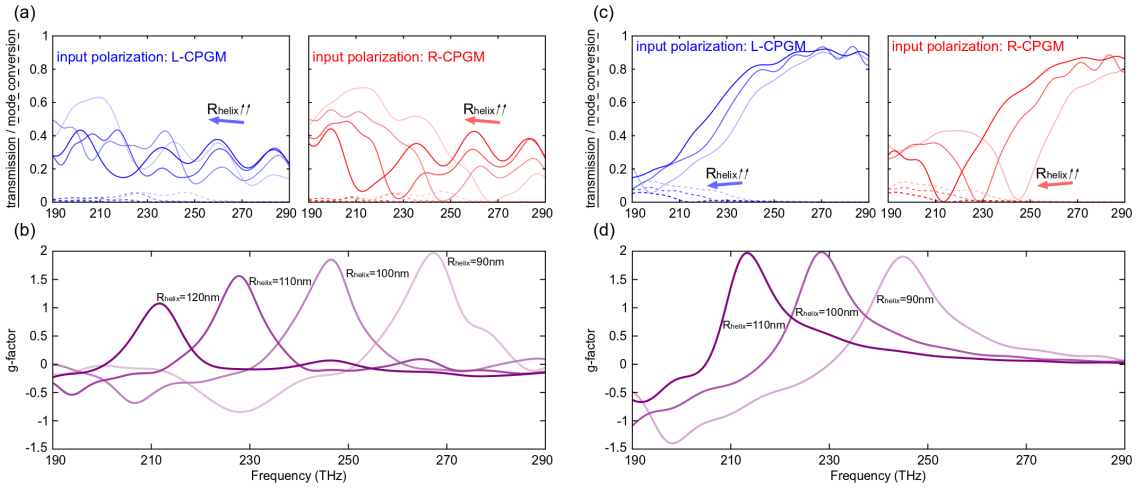

Figure D.6: a) Numerical results of transmission and mode conversion spectra and b) calculated dissymmetry factor for different values of R_{helix} for the in-gap configuration. Panels (c) and (d) plot the same for the on-top configuration. Note that in all panels we are considering a right-handed silver nanohelix with $p = 70$ nm and $r_{\text{helix}} = 10$ nm. For the in-gap configuration the gap width is fixed to 300 nm and the helix has 4 turns, whereas for the on-top case it has 16 turns.

are greatly increased in comparison with the previous results for PEC made helices. Once again, we illustrate this fact by means of the optical chirality density cross-sectional map shown in Figure D.7. Even though the enhancement is obviously lower than for the case of PEC helices, the contrast ratio between L- and R-CPGM at the output waveguide is now significantly higher. Namely, while the optical chirality density is roughly uniformly preserved along the entire waveguide for L-CPGM, the excitation of the chiral structure by the R-CPGM is so strong that the chirality is completely absorbed at the output port, a fact that can be likely attributed to the active role played by the absorption losses, as well as the dispersion features of the chiral scatterer [19].

B. Enhancing the evanescent effect: Slotted configuration

Slot waveguides, consisting of a thin air channel placed between two dielectric waveguides [60], present important advantages in a multitude of integrated photonics applications, in particular, in optical biosensing and spectroscopy [43,61]. Motivated by this, we also analyze chiroptical light–matter interactions in these kind of configurations. Indeed, the slotted approach can be regarded as an improved version of the on-top configuration in which we place a second waveguide close to the first one in order to produce more intense fields in the void region close to the waveguide interface. Therefore, as in the case of the on-top configuration, the main benefit of the slotted configuration relies on the long active region in which the chiroptical interaction takes place.

Based on this, we consider two square cross-sectional silicon nitride waveguides separated by a slot of width $d_{\text{slot}} = 200$ nm, where the optical field is strongly confined.

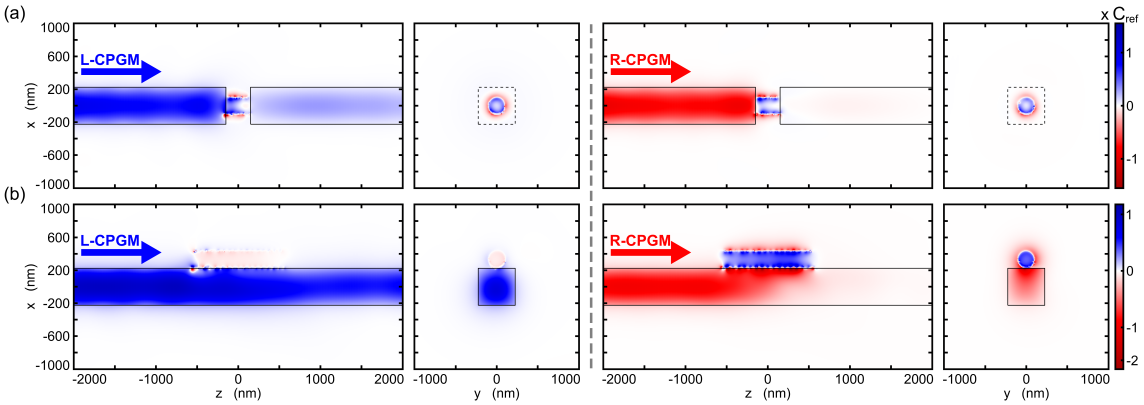

Figure D.7: Cross-sectional maps of the optical chirality density for L- and R-CPGM in silicon nitride strip waveguides for a) the in-gap configuration (Figure D.3a) and b) the on-top configuration (Figure D.4a). The chiral metallic structure is modeled as a right-handed silver nanohelix with geometrical parameters as indicated in Figure D.6. In both cases, the working frequencies are fixed to be that of resonance for $R_{\text{helix}} = 100$ nm, that is, a) $f = f_{\text{res}} \approx 247$ THz, and b) $f = f_{\text{res}} \approx 228$ THz. The values are normalized with respect to C_{ref}.

Here, we place the chiral analyte, in this case a 16-turns silver nanohelix (Figure D.8a). The rest of geometrical parameters are the same that previously used in Figure D.6. From the numerical results shown in Figure D.8 we observe that, like in the cases above, the transmission spectra display a sharp dip at the resonance frequency for the CPGM that matches the chirality of the helix. This translates into a peak in the corresponding dissymmetry factor spectrum, which, owing to the absorption losses of the material, has a broad spectral width.

A key issue arising with the slotted configuration is that the system does not display a C_4 rotational symmetry around the waveguide axis, which prevents TE and TM modes to be degenerate. This means that the chirality of the CPGMs will change when propagating through the slotted waveguide. Still, in the simplest case in which the waveguide is surrounded by a homogeneous low-index medium, for example, vacuum, the slot waveguide can be designed to be fully degenerate for (or up to) a given wavelength (Figure D.2) so that purely L- or R-CPGM can be generated and propagated for realizing chiral interaction. The C_4 symmetry also breaks when a substrate is introduced, and, as discussed below, this poses some limits in practice.

C. Breaking the C_4 rotational symmetry: Polarization beat length and its effect on chiroptical applications

All-dielectric waveguides with square cross section completely surrounded by vacuum support TE and TM modes fully degenerate, meaning that the chirality conveyed by the CPGMs will be maintained no matter how long the waveguide is. Notice that this kind of suspended dielectric nanowires can be technologically realized by releasing

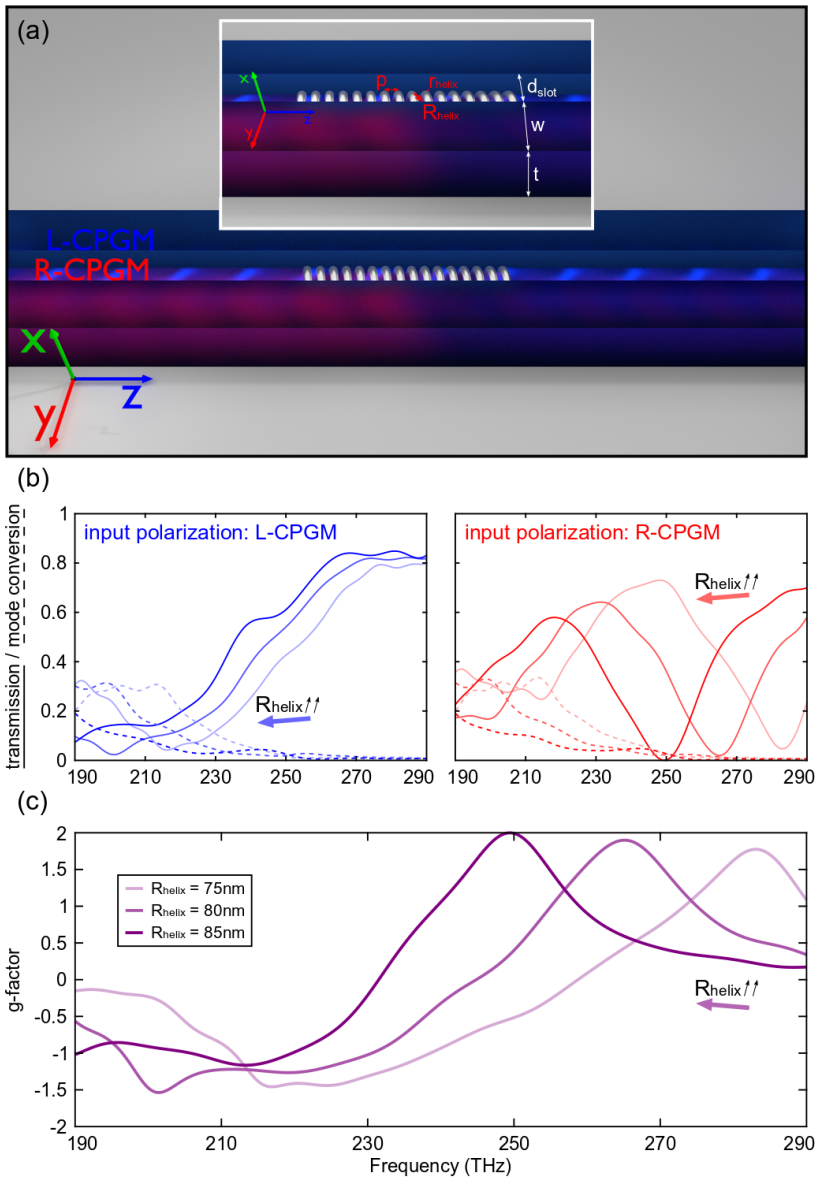

Figure D.8: a) Scheme of the arrangement for chiral sensing and spectroscopy enabled by a dielectric slotted waveguide with a slot width of $d_{\mathrm{slot}} = 200$ nm (slotted configuration). The chiral metallic structure is modeled as a right-handed 16-turns single nanohelix made of silver, with geometrical parameters fixed to $p = 70$ nm, $r_{\mathrm{helix}} = 10$ nm, and R_{helix} ranging from 75 to 85 nm. b) Numerical simulation of transmission and mode conversion spectra for different values of R_{helix}. c) Dissymmetry factor.

the waveguide core using standard processes, for instance, in the case of silicon-based materials, by employing an HF bath that removes the silica substrate as usually done in cavity and waveguide optomechanics. However, this limits the maximum distance for which the chirality is maintained, as very long waveguides may eventually break down and collapse. This can be solved by using a substrate, so that there is no limit on the

maximum guiding length, as long as we ensure low propagation losses [59], and providing a support for the addition of chiral scatterers (as the helix used in this work) or even chiral chemical compounds.

When the substrate is added, the C_4 rotational symmetry of the system is broken, and the TE and TM modes are no longer fully degenerate. In such a case, it is worth assessing how long the sign of the chirality can be kept in our system, thereby determining the maximum active length to carry out the required chiral processing. To characterize the degree of degeneracy between the TE and TM eigenmodes, and its influence on the coherent propagation through the waveguide structure to generate the required chiral CPGMs, we use the so-called polarization beat length:

$$\mathrm{PBL} = \frac{\lambda}{n_{\mathrm{TE}} - n_{\mathrm{TM}}}. \tag{D.3}$$

This is a parameter typically used to check the birefringence of optical waveguides [80], accounting for the fabrication deviations from the nominal values of the waveguide as well. Specifically, it fixes the distance traveled by the corresponding guided mode after which the original polarization state is recovered. Namely, this means that the chirality sign can be kept uniform over a distance of PBL/2. Therefore, in the cases of a suspended slotted waveguide or a dielectric wire with substrate, one can work out a design so that the TE and TM modes are fully degenerate at a certain frequency (for which PBL $\to \infty$), and look into the bandwidth around that frequency so that it achieves a PBL length over a given threshold. In Figure D.9, we plot the PBL for both strip (solid line) and slot (dashed line) waveguides. To do that, we first calculated the effective refractive index for the TE and TM modes in each case by means of a 3D full-wave solver (Section D.VI). In the strip case we consider a realistic system: a conventional silicon nitride wire with rectangular cross section, being $t = 300$ nm (available in commercial wafers) and $w = 350$ nm, on top of a silica substrate. On the other side, for the slotted case we choose square waveguides with the same dimensions as that indicated in Figure D.2, and, for comparison, we account for the cases with and without substrate. In the former scheme, we find that the TE and TM modes have the same index at a wavelength of 900 nm, with PBL ≈ 1.5 mm over a bandwidth of nearly 50 nm. Of course, this result is far from being satisfactory for a real application and it should be further optimized, by changing the dimensions as well as the characteristics of the cladding. Nevertheless, it serves to show the feasibility of such an approach taking into account the substrate. In fact, from a simple comparison with the slot waveguide, including the silica substrate, we observe a much better performance, increasing the PBL peak magnitude to 3.5 mm, located in this case at 1400 nm, and slightly widening the bandwidth. Finally, in the ideal case removing the substrate we can further enhance both the magnitude and the bandwidth of the PBL peak, centered at 1150 nm. Interestingly, all the PBL peaks appear located in a spectral range that, as reported in the recent literature, is highly appropriate for realizing chiroptical spectroscopy, especially when plasmonic nanostructures are involved (see, e.g., examples shown in ref. [20]). Therefore, we have shown that, even with a substrate, realistic dielectric waveguides may support chiral modes in a significant wavelength range and over

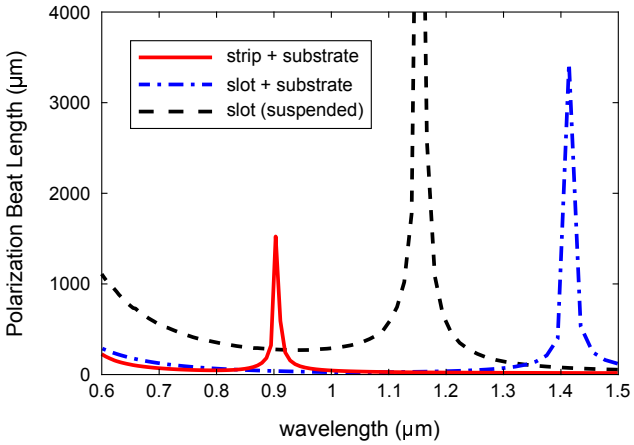

Figure D.9: Polarization beat length (PBL) of a silicon nitride strip (solid line) and slotted (dashed lines) waveguide as a function of the wavelength. For the strip case, the rectangular cross-sectional waveguide ($w = 350$ nm and $t = 300$ nm) is placed on a silica substrate. In the slotted case, for comparison, the PBL is plotted with and without substrate.

large propagation lengths, enabling chiral applications in active regions able to reach up to the mm-scale.

D.V Conclusion and Outlook

In summary, we have examined three possible configurations to get chiroptical responses enabled by all-dielectric strip and slotted waveguides in integrated photonic systems. To this aim, we have taken under consideration a metallic nanohelix acting as a chiral sample (a sort of metamolecule). For simplicity, the metal has been first modeled as a PEC, so that the chiral interaction is only due to the geometrical aspects, dismissing additional dispersive or absorption effects. Numerical results show that, in each of the configurations, there exists a very well localized single chiral-like resonance in the transmission spectra depending on the helix radius, which is chosen as the control parameter for sweeping. Consequently, the dissymmetry factor exhibits a narrow peak at such frequencies. Furthermore, intermodal conversion is also present everywhere. These features are illustrated by means of the chirality cross-sectional map, where it can be observed the strong enhancement in the chiral excitation of the nanohelix when its chirality coincides with that of the input CPGM.

For the in-gap configuration the system becomes ultra-compact, with an active area wherein realizing the chiroptical interaction smaller than 1 μm^2. In contrast, for both the on-top and the slotted configurations, the interaction lengths can be made much larger, which may be highly useful to sort the chirality of chemical and biological compounds in the context of lab-on-a-chip technologies. In these cases, breaking the rotational symmetry of the system, either by adding a substrate or in the slotted waveguides themselves, would result in TE and TM modes no longer fully degenerate, limiting the length over which a

certain sign of chirality can be kept uniform. Still, we have argued that, under a proper design of the waveguide and the cladding characteristics, the sign of the chirality could be conserved up to mm-scale distances over a wide bandwidth.

Hence, our results suggest that chiral applications such as sensing and spectroscopy, would be feasible using integrated photonic waveguides. Specifically, using silicon-compatible materials and technology would enable low-cost and large-volume production of chips for massive parallel detection, recognition, and separation of chiral molecules, thus completing current approaches for biosensing or spectroscopy in integrated platforms [43]. Notice that, far from providing fully optimized geometries [63], we only sought to show the viability of this working principle enabled by integrated photonic waveguides. Nonetheless, by comparing our results, in particular those of silver made helices, with those found in the existing literature (see, e.g., the overview table shown in the supplementary material of ref. [72]), it can be seen that the dissymmetry factors obtained here are comparable and even better than those already reported for freely propagating optical fields.

Although throughout this work we only focused on the chiroptical behavior of a metallic nanohelix, in real applications this would be extensible to other geometries and materials more relevant [74–76], specifically to chiral molecules [15]. Likewise, taking into account earlier schemes, plasmonic nanostructures [22], or high-index dielectric nanoparticles [29], might be added in order to enhance the chiroptical response when a certain substance is applied [81], thus leading to hybrid chiral plasmonic–photonic systems. Somehow connected with this, it is worth noticing that the chiral structure considered here has only been used as a chiral sample to probe the chiroptical interactions. However, in view of the chirality maps shown above, it can also be envisaged as a near-field chiral enhancer, retaining the most important features for practical purposes [42], namely, a large area of high and uniform-sign chirality, spectral accessibility, tunability, and switchability. In fact, we observe a clear analogy between the near-field chirality induced by the evanescent field and the scheme proposed in ref. [67], in which the optical chirality is longitudinally confined within the helical structure.

Following the current trends, the next steps should be aimed at simplifying both the chiroptical measurement and enhancement schemes [36]. In this regard, apart from investigating other designs of chiral structures simpler to fabricate [58,82], we also suggest exploring the recently introduced full-reconfigurable silicon-based on-chip wireless photonic systems [83], as a promising alternative platform for realizing chiral applications, such as sensing, spectroscopy, and enantioselectivity, from a lab-on-a-chip perspective.

D.VI Numerical Methods

All the numerical simulations and calculations were performed with the aid of the commercial software packages CST Microwave Studio and MATLAB. In particular, for

the simulations, the 3D full-wave solver was used to implement the finite-integration technique in the time domain. The whole model (waveguides and nanohelix) was meshed using a hexahedral grid with 16 cells per wavelength, except near the metallic helix where additional refinement was necessary to properly resolve the small inclusions. Open boundary conditions (perfectly matched layers) were chosen for all external facets, noticing that the background medium is the vacuum. The input excitation was provided by means of standard waveguide ports. In order to obtain the transmission as well as the mode conversion spectra at the output port, both the TE and TM modes were sequentially stimulated, recording their corresponding S-parameters. Then, applying the superposition principle, these signals were translated to the circular polarization basis, allowing the calculation of the corresponding dissymmetry factor for each case. On the other side, the dispersion relation of the fundamental TE and TM guided modes was obtained by simulating the guided modes only at the ports, for each central frequency. This calculation provides useful information about several waveguide port characteristics, in particular, the effective dielectric constant.

Acknowledgments

The authors thank S. Lechago for valuable comments and technical support with the numerical simulations. This work was partially supported by funding from the European Commission Project THOR H2020-EU-829067. A.M. also acknowledges funding from Generalitat Valenciana (Grant No. PROMETEO/2019/123) and Spanish Ministry of Science, Innovation and Universities (Grant No. PRX18/00126).

References

[1] U.S. Food and Drug Administration (FDA), *FDA's policy statement for the development of new stereoisomeric drugs*, Chirality **4**, 338 (1992).

[2] A. J. Hutt and S. C. Tan, *Drug chirality and its clinical significance*, Drugs **52**, 1 (1996).

[3] S. W. Smith, *Chiral toxicology: It's the same thing...only different*, Toxicol. Sci. **110**, 4 (2009).

[4] R. Naaman, Y. Paltiel, and D. H. Waldeck, *Chiral molecules and the electron spin*, Nat. Rev. Chem. **3**, 250 (2019).

[5] P. Lodahl, S. Mahmoodian, S. Stobbe, A. Rauschenbeutel, P. Schneeweiss, J. Volz, H. Pichler, and P. Zoller, *Chiral quantum optics*, Nature (London) **541**, 473 (2017).

[6] B. Göhler, V. Hamelbeck, T. Z. Markus, M. Kettner, G. F. Hanne, Z. Vager, R. Naaman, and H. Zacharias, *Spin selectivity in electron transmission through self-assembled monolayers of double-stranded DNA*, Science **331**, 894 (2011).

[7] H. Zhu, J. Yi, M.-Y. Li, J. Xiao, L. Zhang, C.-W. Yang, R. A. Kaindl, L.-J. Li, Y. Wang, and X. Zhang, *Observation of chiral phonons*, Science **359**, 579 (2018).

[8] R. P. Cameron, S. M. Barnett, and A. M. Yao, *Optical helicity, optical spin and related quantities in electromagnetic theory*, New J. Phys. **14**, 053050 (2012).

[9] F. Alpeggiani, K. Y. Bliokh, F. Nori, and L. Kuipers, *Electromagnetic helicity in complex media*, Phys. Rev. Lett. **120**, 243605 (2018).

[10] Y. Tang and A. E. Cohen, *Optical chirality and its interaction with matter*, Phys. Rev. Lett. **104**, 163901 (2010).

[11] K. Y. Bliokh and F. Nori, *Characterizing optical chirality*, Phys. Rev. A **83**, 021803 (2011).

[12] Y. Tang and A. E. Cohen, *Enhanced enantioselectivity in excitation of chiral molecules by superchiral light*, Science **332**, 333 (2011).

[13] N. Berova, K. Nakanishi, and R. W. Woody, *Circular Dichroism: Principles and Applications* (Wiley-VCH, New York, USA, 2000).

[14] L. D. Barron, *Molecular Light Scattering and Optical Activity* (Cambridge University Press, Cambridge, England, 2004).

[15] R. Hassey, E. J. Swain, N. I. Hammer, D. Venkataraman, and M. D. Barnes, *Probing the chiroptical response of a single molecule*, Science **314**, 1437 (2006).

[16] E. Hendry, T. Carpy, J. Johnston, M. Popland, R. V. Mikhaylovskiy, A. J. Lapthorn, S. M. Kelly, L. D. Barron, N. Gadegaard, and M. Kadodwala, *Ultrasensitive detection and characterization of biomolecules using superchiral fields*, Nat. Nanotechnol. **5**, 783 (2010).

[17] H. Rhee, J. S. Choi, D. J. Starling, J. C. Howell, and M. Cho, *Amplifications in chiroptical spectroscopy, optical enantioselectivity, and weak value measurement*, Chem. Sci. **4**, 4107 (2013).

[18] C.-S. Ho, A. García-Etxarri, Y. Zhao, and J. Dionne, *Enhancing enantioselective absorption using dielectric nanospheres*, ACS Photonics **4**, 197 (2017).

[19] J. E. Vázquez-Lozano and A. Martínez, *Optical chirality in dispersive and lossy media*, Phys. Rev. Lett. **121**, 043901 (2018).

[20] M. Schäferling, *Chiral Nanophotonics: Chiral Optical Properties of Plasmonic Systems* (Springer, Berlin, 2017).

[21] M. Schäferling, D. Dregely, M. Hentschel, and H. Giessen, *Tailoring enhanced optical chirality: Design principles for chiral plasmonic nanostructures*, Phys. Rev. X **2**, 031010 (2012).

[22] S. Lee, S. J. Yoo, and Q.-Han Park, *Microscopic origin of surface-enhanced circular dichroism*, ACS Photonics **4**, 2047 (2017).

[23] L. E. Barr, S. A. R. Horsley, I. R. Hooper, J. K. Eager, C. P. Gallagher, S. M. Hornett, A. P. Hibbins, and E. Hendry, *Investigating the nature of chiral near-field interactions*, Phys. Rev. B **97**, 155418 (2018).

[24] J. T. Collins, C. Kuppe, D. C. Hooper, C. Sibilia, M. Centini, and V. K. Valev, *Chirality and chiroptical effects in metal nanostructures: Fundamentals and current trends*, Adv. Opt. Mater. **5**, 1700182 (2017).

[25] M. Hentschel, M. Schäferling, X. Duan, H. Giessen, and N. Liu, *Chiral plasmonics*, Sci. Adv. **3**, e1602735 (2017).

[26] A. O. Govorov, Z. Fan, P. Hernandez, J. M. Slocik, and R. R. Naik, *Theory of circular dichroism of nanomaterials comprising chiral molecules and nanocrystals: Plasmon enhancement, dipole interactions, and dielectric effects*, Nano Lett. **10**, 1374 (2010).

[27] Y. Zhao, A. N. Askarpour, L. Sun, J. Shi, X. Li, and A. Alù, *Chirality detection of enantiomers using twisted optical metamaterials*, Nat. Commun. **8**, 14180 (2017).

[28] L. Kang, Q. Ren, and D. H. Werner, *Leveraging superchiral light for manipulation of optical chirality in the near-field of plasmonic metamaterials*, ACS Photonics **4**, 1298 (2017).

[29] A. García-Etxarri and J. A. Dionne, *Surface-enhanced circular dichroism spectroscopy mediated by nonchiral nanoantennas*, Phys. Rev. B **87**, 235409 (2013).

[30] E. Hendry, R. V. Mikhaylovskiy, L. D. Barron, M. Kadodwala, and T. J. Davis, *Chiral electromagnetic fields generated by arrays of nanoslits*, Nano Lett. **12**, 3640 (2012).

[31] N. Meinzer, E. Hendry, and W. L. Barnes, *Probing the chiral nature of electromagnetic fields surrounding plasmonic nanostructures*, Phys. Rev. B **88**, 041407 (2013).

[32] M. L. Nesterov, X. Yin, M. Schäferling, H. Giessen, and T. Weiss, *The role of plasmon-generated near fields for enhanced circular dichroism spectroscopy*, ACS Photonics **3**, 578 (2016).

[33] J. Lasa-Alonso, D. R. Abujetas, A. Nodar, J. A. Dionne, J. J. Sáenz, G. Molina-Terriza, J. Aizpurua, and A. García-Etxarri, *Surface-enhanced circular dichroism spectroscopy on periodic dual nanostructures*, ACS Photonics **7**, 2978 (2020).

[34] M. L. Solomon, J. Hu, M. Lawrence, A. García-Etxarri, and J. A. Dionne, *Enantiospecific optical enhancement of chiral sensing and separation with dielectric metasurfaces*, ACS Photonics **6**, 43 (2019).

[35] F. Graf, J. Feis, X. Garcia-Santiago, M. Wegener, C. Rockstuhl, and I. Fernandez-Corbaton, *Achiral, helicity preserving, and resonant structures for enhanced sensing of chiral molecules*, ACS Photonics **6**, 482 (2019).

[36] J. Hu, M. Lawrence, and J. A. Dionne, *High quality factor dielectric metasurfaces for ultraviolet circular dichroism spectroscopy*, ACS Photonics **7**, 36 (2020).

[37] X. Zhao and B. M. Reinhard, *Switchable chiroptical hot-spots in silicon nanodisk dimers*, ACS Photonics **6**, 1981 (2019).

[38] F. R. Gómez, O. N. Oliveira, Jr., P. Albella, and J. R. Mejía-Salazar, *Enhanced chiroptical activity with slotted high refractive index dielectric nanodisks*, Phys. Rev. B **101**, 155403 (2020).

[39] F. R. Gómez, J. R. Mejía-Salazar, and P. Albella, *All-dielectric chiral metasurfaces based on crossed-bowtie nanoantennas*, ACS Omega **4**, 21041 (2019).

[40] E. Mohammadi, K. L. Tsakmakidis, A. N. Askarpour, P. Dehkhoda, A. Tavakoli, and H. Altug, *Nanophotonic platforms for enhanced chiral sensing*, ACS Photonics **5**, 2669 (2018).

[41] E. Mohammadi, A. Tavakoli, P. Dehkhoda, Y. Jahani, K. L. Tsakmakidis, A. Tittl, and H. Altug, *Accessible superchiral near-fields driven by tailored electric and magnetic resonances in all-dielectric nanostructures*, ACS Photonics **6**, 1939 (2019).

[42] G. Pellegrini, M. Finazzi, M. Celebrano, L. Duò, and P. Biagioni, *Chiral surface waves for enhanced circular dichroism*, Phys. Rev. B **95**, 241402 (2017).

[43] M. C. Estevez, M. Alvarez, and L. M. Lechuga, *Integrated optical devices for lab-on-a-chip biosensing applications*, Laser Photonics Rev. **6**, 463 (2012).

[44] X. Nie, E. Ryckeboer, G. Roelkens, and R. Baets, *CMOS-compatible broadband co-propagative stationary Fourier transform spectrometer integrated on a silicon nitride photonics platform*, Opt. Express **25**, A409 (2017).

[45] J. Petersen, J. Volz, and A. Rauschenbeutel, *Chiral nanophotonic waveguide interface based on spin-orbit interaction of light*, Science **346**, 67 (2014).

[46] R. J. Coles, D. M. Price, J. E. Dixon, B. Royall, E. Clarke, P. Kok, M. S. Skolnick, A. M. Fox, and M. N. Makhonin, *Chirality of nanophotonic waveguide with embedded quantum emitter for unidirectional spin transfer*, Nat. Commun. **7**, 11183 (2016).

[47] S.-H. Gong, F. Alpeggiani, B. Sciacca, E. C. Garnett, and L. Kuipers, *Nanoscale chiral valley-photon interface through optical spin-orbit coupling*, Science **359**, 443 (2018).

[48] F. Le Kien, T. Busch, V. G. Truong, and S. Nic Chormaic, *Higher-order modes of vacuum-clad ultrathin optical fibers*, Phys. Rev. A **96**, 023835 (2017).

[49] M. F. Picardi, K. Y. Bliokh, F. J. Rodríguez-Fortuño, F. Alpeggiani, and F. Nori, *Angular momenta, helicity, and other properties of dielectric-fiber and metallic-wire modes*, Optica **5**, 1016 (2018).

[50] D. R. Abujetas and J. A. Sánchez-Gil, *Spin angular momentum of guided light induced by transverse confinement and intrinsic helicity*, ACS Photonics **7**, 534 (2020).

[51] B. E. A. Saleh and M. C. Teich, *Fundamentals of Photonics* (Wiley-Interscience, New York, USA, 2007).

[52] K. Y. Bliokh and F. Nori, *Transverse spin of a surface polariton*, Phys. Rev. A **85**, 061801 (2012).

[53] M. H. Alizadeh and B. M. Reinhard, *Enhanced optical chirality through locally excited surface plasmon polaritons*, ACS Photonics **2**, 942 (2015).

[54] S. Nechayev, R. Barczyk, U. Mick, and P. Banzer, *Substrate-induced chirality in an individual nanostructure*, ACS Photonics **6**, 1876 (2019).

[55] E. Petronijevic and C. Sibilia, *Enhanced near-field chirality in periodic arrays of Si nanowires for chiral sensing*, Molecules **24**, 853 (2019).

[56] S. Romero-García, F. Merget, F. Zhong, H. Finkelstein, and J. Witzens, *Silicon nitride CMOS-compatible platform for integrated photonics applications at visible wavelengths*, Opt. Express **21**, 14036 (2013).

[57] A. Espinosa-Soria and A. Martínez, *Transverse spin and spin-orbit coupling in silicon waveguides*, IEEE Photonics Technol. Lett. **28**, 1561 (2016).

[58] L. V. Poulikakos, P. Thureja, A. Stollmann, E. De Leo, and D. J. Norris, *Chiral light design and detection inspired by optical antenna theory*, Nano Lett. **18**, 4633 (2018).

[59] M. H. P. Pfeiffer, C. Herkommer, J. Liu, T. Morais, M. Zervas, M. Geiselmann, T. J. Kippenberg, *Photonic damascene process for low-loss, high-confinement silicon nitride waveguides*, IEEE J. Sel. Top. Quantum Electron. **24**, 6101411 (2018).

[60] V. R. Almeida, Q. Xu, C. A. Barrios, and M. Lipson, *Guiding and confining light in void nanostructure*, Opt. Lett. **29**, 1209 (2004).

[61] C. A. Barrios, K. B. Gylfason, B. Sánchez, A. Griol, H. Sohlström, M. Holgado, and R. Casquel, *Slot-waveguide biochemical sensor*, Opt. Lett. **32**, 3080 (2007).

[62] J. S. Choi and M. Cho, *Limitations of a superchiral field*, Phys. Rev. A **86**, 063834 (2012).

[63] C. Kramer, M. Schäferling, T. Weiss, H. Giessen, and T. Brixner, *Analytic optimization of near-field optical chirality enhancement*, ACS Photonics **4**, 396 (2017).

[64] J. K. Gansel, M. Thiel, M. S. Rill, M. Decker, K. Bade, V. Saile, G. von Freymann, S. Linden, and M. Wegener, *Gold helix photonic metamaterial as broadband circular polarizer*, Science **325**, 1513 (2009).

[65] J. K. Gansel, M. Wegener, S. Burger, and S. Linden, *Gold helix photonic metamaterials: A numerical parameter study*, Opt. Express **18**, 1059 (2010).

[66] Z. Yang, M. Zhao, and P. Lu, *How to improve the signal-to-noise ratio for circular polarizers consisting of helical metamaterials?*, Opt. Express **19**, 4255 (2011).

[67] M. Schäferling, X. Yin, N. Engheta, and H. Giessen, *Helical plasmonic nanostructures as prototypical chiral near-field sources*, ACS Photonics **1**, 530 (2014).

[68] M. Esposito, V. Tasco, M. Cuscunà, F. Todisco, A. Benedetti, I. Tarantini, M. De Giorgi, D. Sanvitto, and A. Passaseo, *Nanoscale 3D chiral plasmonic helices with circular dichroism at visible frequencies*, ACS Photonics **2**, 105 (2015).

[69] R. Ji, S.-W. Wang, X. Liu, H. Guo, and W. Lu, *Hybrid helix metamaterials for giant and ultrawide circular dichroism*, ACS Photonics **3**, 2368 (2016).

[70] D. Kosters, A. de Hoogh, H. Zeijlemaker, H. Acar, N. Rotenberg, and L. Kuipers, *Core-shell plasmonic nanohelices*, ACS Photonics **4**, 1858 (2017).

[71] P. Woźniak, I. De Leon, K. Höflich, C. Haverkamp, S. Christiansen, G. Leuchs, and P. Banzer, *Chiroptical response of a single plasmonic nanohelix*, Opt. Express **26**, 19275 (2018).

[72] K. Höflich, T. Feichtner, E. Hansjürgen, C. Haverkamp, H. Kollmann, C. Lienau, and M. Silies, *Resonant behavior of a single plasmonic helix*, Optica **6**, 1098 (2019).

[73] P. B. Johnson and R. W. Christy, *Optical constants of the noble metals*, Phys. Rev. B **6**, 4370 (1972).

[74] M. Thiel, M. Decker, M. Deubel, M. Wegener, S. Linden, and G. von Freymann, *Polarization stop bands in chiral polymeric three-dimensional photonic crystals*, Adv. Mater. **19**, 207 (2007).

[75] M. Thiel, G. von Freymann, and M. Wegener, *Layer-by-layer three-dimensional chiral photonic crystals*, Opt. Lett. **32**, 2547 (2007).

[76] H. J. Singh and A. Ghosh, *Large and tunable chiro-optical response with all dielectric helical nanomaterials*, ACS Photonics **5**, 1977 (2018).

[77] A. Espinosa-Soria, A. Griol, and A. Martínez, *Experimental measurement of plasmonic nanostructures embedded in silicon waveguide gaps*, Opt. Express **24**, 9592 (2016).

[78] A. Espinosa-Soria, E. Pinilla-Cienfuegos, F. J. Díaz-Fernández, A. Griol, J. Martí, and A. Martínez, *Coherent control of a plasmonic nanoantenna integrated on a silicon chip*, ACS Photonics **5**, 2712 (2018).

[79] X. Yin, M. Schäferling, B. Metzger, and H. Giessen, *Interpreting chiral nanophotonic spectra: The plasmonic Born-Kuhn model*, Nano Lett. **13**, 6238 (2013).

[80] V. N. Filippov, O. I. Kotov, and V. M. Nikolayev, *Measurement of polarisation beat length in single-mode optical fibres with a polarisation modulator*, Electron. Lett. **26**, 658 (1990).

[81] Q. Zhang, T. Hernandez, K. W. Smith, S. A. H. Jebeli, A. X. Dai, L. Warning, R. Baiyasi, L. A. McCarthy, H. Guo, D.-H. Chen, J. A. Dionne, C. F. Landes, and S. Link, *Unraveling the origin of chirality from plasmonic nanoparticle-protein complexes*, Science **365**, 1475 (2019).

[82] M. Schäferling, N. Engheta, H. Giessen, and T. Weiss, *Reducing the complexity: Enantioselective chiral near-fields by diagonal slit and mirror configuration*, ACS Photonics **3**, 1076 (2016).

[83] C. García-Meca, S. Lechago, A. Brimont, A. Griol, S. Mas, L. Sánchez, L. Bellieres, N. S. Losilla, and J. Martí, *On-chip wireless silicon photonics: from reconfigurable interconnects to lab-on-chip devices*, Light Sci. Appl. **6**, e17053 (2017).

Part III

Discussions & Conclusions

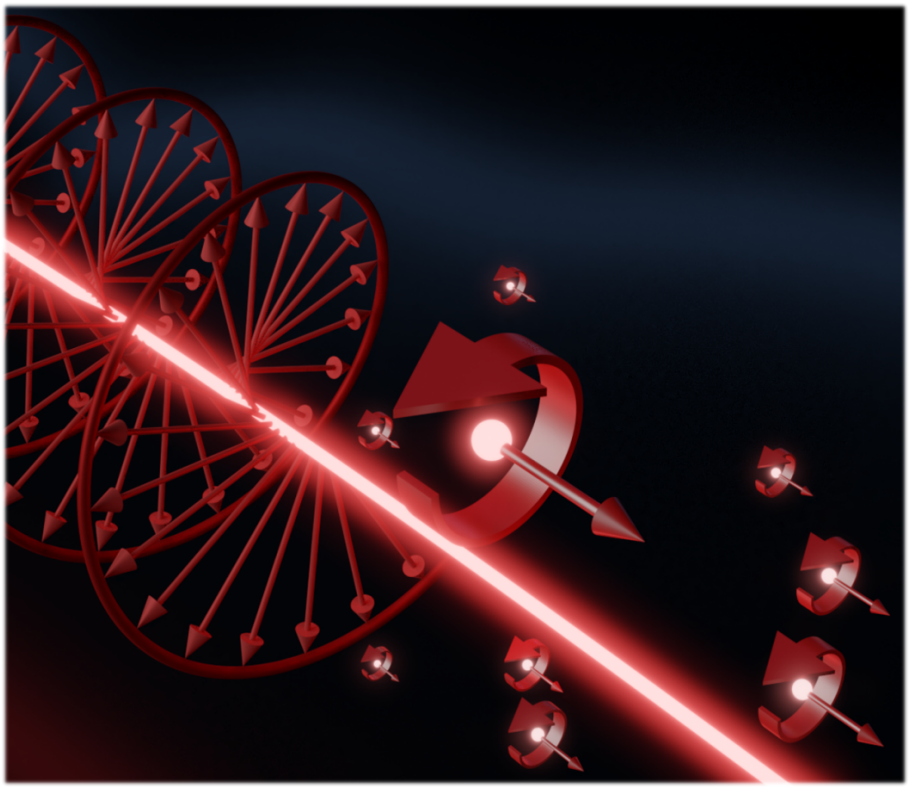

Chapter 7

General Discussion of Results

In science, it is not speed that is the most important.
It is the dedication, the commitment, the interest
and the will to know something and to understand it.
These are the things that come first.

Eugene Wigner

In this chapter we provide a brief discussion and synthesis on the main results presented throughout this thesis. We will consider separately the contributions concerning the spin-orbit interaction of light and the near-field directionality (Part I), from those addressing the optical chirality and its applications in integrated photonics (Part II). By way of a final summary, two original papers are included at the end of each discussion.

7.I SOI of Light & Near-Field Directionality

The first part of this thesis has been essentially devoted to the theoretical study of spin-orbit interaction (SOI) of light. Although this is a topic quite well understood in the context of quantum mechanics (as can be found all over the main textbooks on this matter), its extension to optics and photonics has been introduced only very recently. Since the seminal paper put forward by V. S. Liberman and B. Y. Zel'dovich in 1992 [63], the optical SOI has grown into a subject of extensive research activity. In fact, in a much broader sense, nanophotonics and quantum optics communities have recently witnessed a special interest in the emergence of new optical phenomena enabled by the spin of light. By looking at the evolution and latest breakthroughs in nanoelectronics, which finally led to quantum electronics and spintronics, it is no wonder that, likewise, the spin of photons has been brought in to the photonics realm. Indeed, it can be thought of as a natural consequence of its own development, tending toward structures and devices with sizes getting increasingly smaller. Largely spurred by the recent advances in nanofabrication and the deployment of an entire photonic technology (including plasmonics and metamaterials, resulting, e.g., in point-like optical sources, novel materials, and artificially designed structures), new venues are being opened up for experimentally exploring dynamical properties and optical phenomena occurring at the nanoscale, among which there are the spin of light and, of course, the optical SOI.

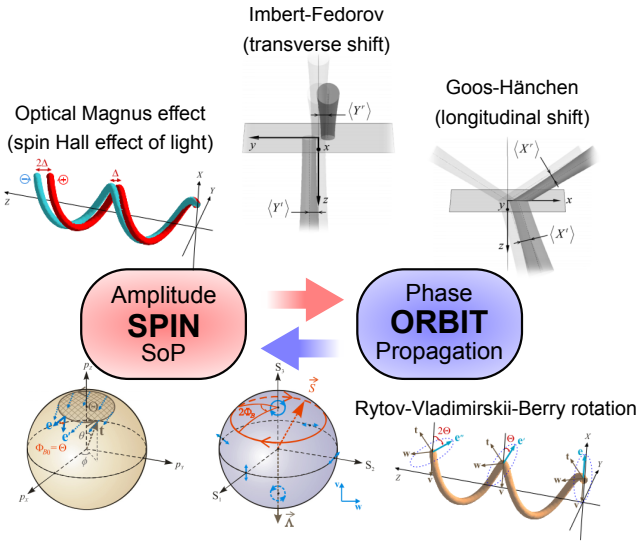

Figure 7.1: Depiction of some important SOI-based effects [302, 303]. From a fundamental point of view, SOI of light can be regarded as the mutual influence between the amplitude and the phase.

It should be noted that, until recently, these features were only accessible by theoretical means, thus limiting, to a great extent, the scope of the researches that could be conducted out. Be that as it may, nowadays the surge of interest in SOI-based optical phenomena is giving rise to a wide variety of novel effects (Figure 7.1), thereby affording us a higher control over the main characteristics of electromagnetic (EM) waves, improving and extending the ways for generating, manipulating, and detecting light properties, and providing us a better understanding of light-matter interactions at the subwavelength scale.

In the middle of the maelstrom of works addressing the SOI of light, regardless of whether they are performed from a theoretical or an experimental standpoint (either from a fundamental or an applied approach), it can be found the following set of common features associated with such a phenomenon: it originates naturally from fundamental properties of **Maxwell's equations**, appears necessarily at the **nanoscale**, and gives rise to **very weak effects**. On this basis, and with the only premise of just building upon the analytical formalism of Maxwell's equations (as indicated in the first prescription), PAPER A is aimed at explaining away how, from where, and why does the subwavelength character of the optical SOI emerge naturally and necessarily. Besides its own fundamental interest from a theoretical point of view, finding out an analytical solution to this seemingly naive question may be useful to unveil the optimal conditions for enhancing the response of SOI-based effects (whose contribution is very small, and even negligible at the macroscopic scale), and, consequently, for properly engineering the experimental setups that may be used to improve and/or facilitate its observation as well as its potential functionalities. In this regard, PAPER B is basically conceived to explicitly disclose such evidences. For that, we focused on the spin-controlled unidirectional excitation of guided modes, considered as one of the most insightful

examples of SOI-based effect occurring in nanophotonic systems. Specifically, taking into account the conclusions drawn from the prior fundamental analysis, we show that, sure enough, the higher is the multipole order of the EM field under consideration, the wider is the spatial range of its corresponding near-field region, and thus, the zone wherein the SOI of light comes into play. In this sense, this work constitutes a generalization of the near-field directionality beyond the dipole approximation, extending it so as to include EM multipole fields of arbitrary order (as well as their possible linear combinations). This allows us to confirm that successively higher-order multipole fields provide the advantages previously predicted; essentially, facilitating the experimental observation and upgrading the functionalities of the spin-dependent near-field directional coupling. For a better depiction of all of this, and by way of a complement to the original contributions set out in the above chapters, here below we elaborate a little more in-depth discussion of these matters, for which turns out to be convenient refreshing some basics of EM waves.

It is well known that, in a simple and general manner, EM waves can be characterized in terms of an amplitude and a phase. This is a commonplace for any kind of wave. It is also well known that one of the main particularities of EM waves relies on its vectorial nature, so that the amplitude is not a scalar quantity, but a vector, and then, it is said that they possess a certain polarization, indicating the direction in which the electric (and the magnetic) field oscillates along the wave propagation. Then, the whole EM wave field, i.e., the state of polarization (SoP) as well as the direction of propagation (encoded into the phase), can be algebraically characterized by a set of three complex numbers, actually resulting in a set of six real numbers, accounting for the amplitude and the relative phase of each component with respect to each other. For the particular case of EM plane waves, there is a more meaningful picture that allows us to identify each of these six numbers with the following wave characteristics: two for the direction of propagation, and the remaining four — often referred to as the *Stokes parameters* — for the SoP (actually describing the polarization ellipse traced out in the plane perpendicular to the direction of propagation). It should be noted that this characterization for the SoP turns out to be particularly effective and simple when assuming a fixed propagation direction. Indeed, in such a case, the evolution of the SoP, and thus that of the whole EM plane wave, can be mapped into points on the so-called *Poincaré sphere*. Notwithstanding, it is worth remarking that, in a more general situation in which the propagation direction is also considered as a variable, this representation is no longer valid, and one should resort to the so-called *Majorana sphere* — a geometrical construction inherited from the quantum formalism that is typically used for describing spin systems [304]. In this way, this wave property, i.e., the SoP, is actually regarded as a macroscopic manifestation of the photon spin. In fact, from a quantum approach, the correspondence principle states that left (L) and right (R) circularly polarized light (CPL), are associated to photons with spin $\pm\hbar$*.

*The choice of this association between L- and R-CPL with the signs + and − for the photon spin is completely arbitrary, and is indeed a matter of convention. In fact, whereas physicists, specifically those working on classical optics, usually consider the so-called *detector's view* convention, in engineering and quantum optics it is widely used the *source's view* convention, both opposed to each other.

According to this fundamental consideration, the most natural polarization basis should be related to the states of circular polarization, though for simplicity (or perhaps by inertia), the basis most often used is commonly referred to states of linear polarization.

Based on the foregoing, and taking into account the transversality condition naturally stemmed from Maxwell's equations, amplitude and phase appear to be separated properties of the optical fields described in terms of single plane waves. Notice that, besides in plane waves — which may be seen as the simplest mathematical idealization of EM waves — this feature (i.e., the amplitude-phase separability) is regularly encountered in standard paraxial optics as well, that is, in macroscopic geometrical optics wherein light can be characterized by means of propagating rays. Bearing these considerations in mind and using a rather prosaic terminology, the optical SOI would arise when the SoP may affect to the propagation properties of light, and vice versa, when the propagation process can modify the polarization properties of the optical field (Figure 7.1)[†]. Namely, there may eventually be certain circumstances in which it would be possible to observe a mutual influence between the amplitude and the phase of light[‡]. This necessarily would break the aforementioned *amplitude-phase separability condition* (mathematically encoded in terms of the so-called *factorizability condition*), and hence, the occurrence of optical SOI is impossible in plane-like waves, as they always present such a factorized form (i.e., they are always expressible as a product of an amplitude and a global phase factor).

Then, as pointed out in all the current literature, SOI of light only takes place in nontrivially structured optical fields as well as in evanescent waves, typically supported either by surface waves (e.g., in surface plasmon polaritons) or guided modes (e.g., those propagating through dielectric photonic waveguides). This assertion is closely related with the prescription, up to now assumed, though confirmed (both experimentally and numerically), that intrinsic optical SOI should naturally and necessarily emerge at the near-field region. In this respect, some attempts to provide demonstrations of this fact have proven to be rather pragmatic, and have been largely relied upon the interplay and mutual exchange between the different types of angular momentum, i.e., the spin angular momentum (SAM) and the orbital angular momentum (OAM) — this latter, in turn, splitted into the intrinsic (IOAM) and extrinsic (EOAM) contributions (Figure 7.2). However, such explanations only emphasizes into the effects, neglecting the fundamental appearance, and even leading to a certain controversy about the manner in which should be properly performed such a separation between the spin and orbital terms [76]. Apart from that, the identification of optical SOI with the nanoscale by means of its resulting effects would be, in a way, equivalent to say that the ultimate reason why SOI does happen in the hydrogen atom is because of the appearance

[†]Notice that, in order to follow the terminology employed throughout this thesis, the amplitude actually refers to the SoP, and this, in turn, to the *spin* of light. On the other side, the phase is related to the spatial structure or the wave propagation features, which, in a way, can be simply termed as the *orbit*.

[‡]It should be noted that, from a layman approach, this interlinked behavior should be the normality, whereas the amplitude-phase separability, should be the exceptionality. Indeed, a priori, just by looking at the Maxwell's equations, the SoP and the spatial degrees of freedom appear to be coupled to each other.

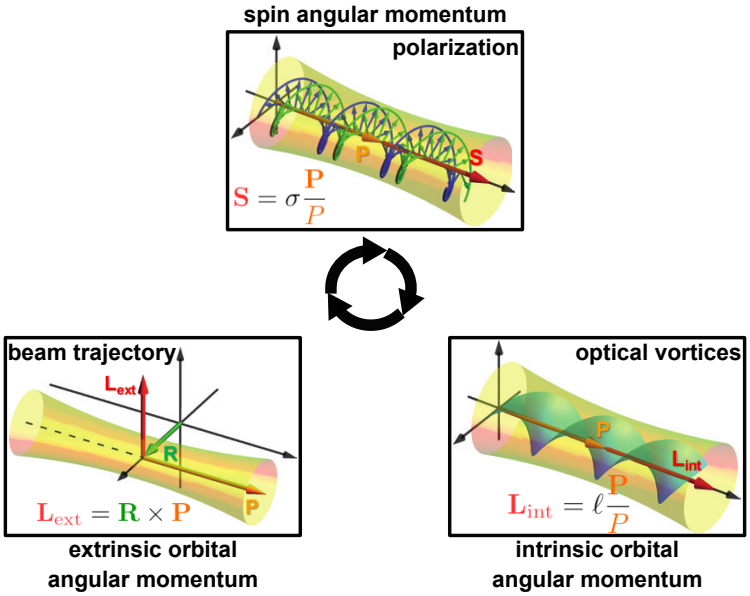

Figure 7.2: Depiction of the different contributions to the angular momentum of light [94]. From a pragmatic viewpoint, SOI of light is commonly understood as their interplay and mutual exchange.

of a splitting in the energy levels (explaining the fine-structure energy corrections). Namely, this would be an argument that simply relates the cause with the effect, and the effect as an unavoidable consequence of the cause. Yet, concerning the homonymous phenomenon occurring in the framework of quantum mechanics, also referred to as *spin-orbit coupling*, we know that it is actually an effective phenomenon of relativistic nature wherein the movement of a charged particle is coupled with its spin. Without going into further details, we will only say that its fundamentals can be understood through the Lorentz transformations, whereby electric and magnetic fields are different representations of the same entity, and whose physical manifestation will only depend on the relative motion between the reference frame of the moving electric charge and the observer. So, the electric field generated by the atomic nucleus is viewed by the orbiting electron as an effective magnetic field, which, according to the Schrödinger equation (considering also the Pauli's correction), is the one that couples with the electron spin, here readily interpreted as a *magnetic dipole moment*. Of course, a deeper comprehension can be found out by means of the celebrated Dirac equation, comprising the most precise formalism we have for describing electrons, accounting for both the spin features and their relativistic behavior. Therein, SOI emerges as an intrinsic consequence from the own structure of the Dirac formalism. Hence, it might be surmised that, on account of the similarities between the Dirac and Maxwell's equations [305], the optical SOI should also naturally arise from the fundamental spin (or polarization-like) properties of Maxwell's equations, thereby setting down a rigorous and analytical framework within which one may explicitly show the inherent link that there exists between the intrinsic SOI of light with the nanoscale. These were, therefore, the preliminary thoughts that led us to conceive the work undertaken in PAPER A.

The analytical core of this study has relied on the formalism of the vector spherical wave functions (VSWFs) and the vector spherical harmonics (VSH). Building on this, we firstly performed a general analysis of the overall properties of full-vector waves, disclosing its derivation and their explicit expressions. In this regard we thought that, for our purposes of dealing with optical processes occurring at the subwavelength scale, this was the most suitable theoretical framework, and, consequently, it should be highly advantageous to unveil the occurrence of optical SOI. So, once these basics were established, we turned to the main claim of the work, namely, the classical emergence of intrinsic SOI of light at the nanoscale. For that, we focused on several aspects aiming to capture analytically its main features, i.e., showing that there exists a mutual influence between the propagation features and the SoP of light. The first insight we realized was that, unlike for plane-like waves, the SoP of the multipole fields turns out to be spatially inhomogeneous, even in homogeneous media. Specifically, we observed that their longitudinal field component, i.e., the field contribution pointing along the radial direction, naturally vanishes as it gets far away from the source. This, together with the dynamical behavior of the relative phase with respect to the transverse component, yields an intrinsic evolution of the SoP along the wave propagation that suggests the occurrence of intrinsic SOI. Furthermore, it is worth noticing that all the inner features underlying such evolution fulfill the main prescriptions tied to this phenomenon. In order to find out the analytical signature proving such an occurrence of optical SOI, we then proceeded with the analysis of the factorizability (or separability) condition. To this aim, we looked into the mathematical properties of the Bessel-like functions (i.e., the functions that describe the radial distribution of the EM multipole field amplitudes). After a judicious analytical procedure, we identify a single term encompassing the main features of SOI, i.e., a term with an additional relative phase that prevents the amplitude-phase separability (or factorizability), but solely in the near-field region. Besides enclosing the nonseparability of the spin-orbit degrees of freedom, this SOI-term would also serve as an universal criterion to define the near-field region, so far characterized in terms of a rather arbitrary condition based on the dependence of the distance from the point-like optical source[§]. Even though this is only carried out in an explicit way for the electric dipole, such an identification shall be specially useful for higher-order multipole fields, where the arbitrariness becomes even more evident because of the appearance of more and more terms that depend on higher order powers of r. This essentially concludes the analytical demonstration showing the universality of the optical SOI as a phenomenon occurring at the subwavelength scale, and specifically, in the so-called near-field region of multipole fields. Yet, as a final discussion, we addressed qualitatively the influence of the SOI-term on the wave propagation process by looking into the behavior of a set of local dynamical properties in the near-field region. In this respect, we pointed out the existence

[§]For the particular case of an oscillating electric dipole, the spatial regions associated with the near-, intermediate- and far-field contributions, are determined by the corresponding terms proportional to $1/r^3$, $1/r^2$, and $1/r$, respectively. This distinction is often useful in the theory of radiating systems, providing a notable simplification in the analysis of the fields, so it would be advisable to have a definition as accurate as possible to identify each of them.

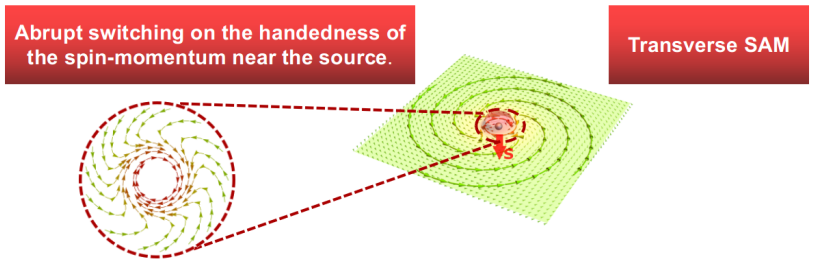

Figure 7.3: Spin-momentum and transverse SAM are independent to each other. Yet, for modes with transverse SAM, there is an abrupt switching on the handedness of the spin-momentum.

of a switching on the handedness of the spin-momentum near the source (Figure 7.3), and an azimuthal deviation of the orbital-momentum. These intriguing features are, ultimately, a consequence of the nonseparability between the spin-orbit degrees of freedom. Finally, we also found out an interesting relationship between the complex Poynting vector and the transverse SAM resembling somehow that of the spin-momentum locking. Remarkably, this finding, which also relies upon the spin-orbit nonseparability, suggests that the phenomenon of spin-momentum locking, which thus far has proven to be an inherent property of evanescent waves, could also be extended to propagating modes.

A full understanding of the role played by the factorizability condition on the dynamical properties would deserve further efforts beyond the scope of this incipient work. Despite that and the seemingly trivial standpoint, our approach is able to capture analytically most of the relevant physics involved in the SOI of light, showing that the factorizability condition is certainly the key ingredient to unveil its classical emergence. In this regard, our contribution demonstrates that the optical SOI naturally arises from the fundamental spin properties of Maxwell's equations and that necessarily appears at the nanoscale. Moreover, as for practical applications, the main conclusion that can be drawn is that the higher is the multipole order, the wider is the corresponding near-field region, and thus, the spatial range susceptible of presenting SOI features, thereby opening up a pathway to facilitate and enhance both the observation and the occurrence of SOI-based effects. This will be in fact the starting point of the next work, wherein we address the spin-dependent near-field directional coupling (as a particular example of SOI-based effect) beyond the dipole approximation. Here below we will outline the main insights on it.

As a paramount manifestation of the optical SOI there stands out the intrinsic quantum spin Hall effect (QSHE) of light [103]. This was the last remaining member of the Hall effects' family in finding its corresponding optical (or photonic) analogue. Regarded as a topological spin-dependent phenomenon of photonic transport, it has led to a general and unified theoretical framework able to explain the existence of exotic dynamical properties of light fields, such as the "extraordinary" momentum (also known as the *Belinfante's spin momentum*) and the transverse spin arising in evanescent waves (e.g., in that formed by surface plasmon-polariton modes at a metal-dielectric interface) [99],

as well as the occurrence of photonic topological insulators [100]. Furthermore, the QSHE can also be seen as an essential tool for disclosing significant analogies between spin-dependent electronic properties and their photonic counterparts, thereby establishing a direct correspondence between quantum and classical features of waves. Notice that, as aforementioned, these analogies are ultimately underpinned by the overall resemblance between the Maxwell's equations (in particular, when expressed in the *Riemann-Silberstein representation* [306]) and the Dirac equation. All in all, for our purposes, the most distinct signature of QSHE is the universal occurrence of strong *spin-momentum locking* and its incontrovertible relationship with the transverse SAM of surface or guided modes [101]. According to this picture, the direction of propagation of guided waves can be directly controlled by the spin of an oscillating optical source placed in close proximity to waveguiding systems (e.g., dielectric waveguides or metallic surfaces); a phenomenon that has been termed as *spin-controlled unidirectional excitation* [102]. Even though it has been explored in a wide variety of platforms and spectral ranges, so far, the focus has been mostly placed on dipolar sources, either electric or magnetic (or a linear combination of them), leaving aside the higher-order multipoles. Besides being highly relevant at the nanoscale[¶], a full description of near-field directionality induced by higher-order multipoles may lead to an unprecedented degree of control over the near-field source-waveguide interactions, thus enabling a wide applicability in many fields of physics (even beyond the photonics), as well as furthering the design of new spin-based optical devices.

On account of this background, the aim of PAPER B was to work out a general, systematic, and, in a way, ready-to-use formulation for addressing the near-field directionality beyond the dipole approximation, thus accounting for higher-order multipole optical sources (i.e., quadrupole, octupole, and so on). This is carried out by taking advantage of the *angular spectrum representation*, also called the spatial spectrum, or simply as the momentum representation. According to this formalism, any arbitrarily shaped optical field defined over a homogeneous medium (e.g., that emanating from a point-like optical source in free space, or scattering by an arbitrary-shaped nanoparticle) can be simply expressed as a series expansion of elementary plane waves with components that can be either propagating or evanescent (Figure 7.4). The procedure essentially consists in calculating the Fourier transform in the 2D partial momentum space perpendicular to an arbitrarily chosen axis. Once the angular spectrum at a given plane has been gotten, let us say the plane $z = z_0$, the field over the whole space can be simply calculated just by multiplying such a solution by the propagator $e^{\pm ik\kappa_z z}$. Notice that we are assuming a wave vector defined as $\mathbf{k}^{\pm} = k(\kappa_x, \kappa_y, \pm\kappa_z)$, where the $\pm$ signs stand for the EM fields propagating into the upper ($z > z_0$) or the lower ($z < z_0$) half-spaces. Importantly, to produce consistent results, the medium is to be homogeneous and source-free, so that the corresponding refractive index stays real and positive.

[¶]Notice that, in realistic situations, optical sources are actually bulky emitters or scatterers, for which the multipole expansion provides for a complete description of the EM fields emanating from or coupling to such optical systems, regardless of their material, shape, or size. This is crucial in nanophotonics, whose strongly confined fields may lead to steep field gradients that largely overcome the first dipolar order.

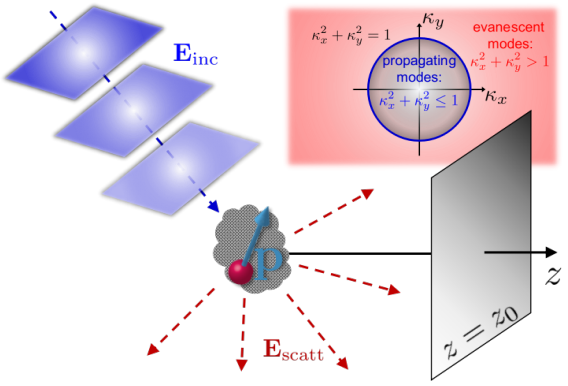

Figure 7.4: Depiction of a generic situation wherein to apply the angular spectrum representation. The scattered field by an arbitrary-shaped object is expressed as a superposition of elementary plane waves (either propagating or evanescent) projected onto planes perpendicular to a given axis.

Thus, propagating and evanescent modes will be related to wave vectors being purely real or imaginary, respectively, and then, the propagator will display either an oscillatory or exponentially decaying behavior. Yet, the strongest mathematical restrictions of this procedure set that the time-independent complex amplitudes (regardless of whether they are either scalar or vector fields) must satisfy the Helmholtz wave equation and ought to show a divergence-free behavior, i.e., they must fulfill the transversality condition.

Besides being very useful for describing far-field features of EM waves (e.g., in laser-beam propagation and light focusing), the angular spectrum representation has found to be extremely practical in the context of near-field directionality [102]. In this regard, it is worth mentioning that there are several other routes for understanding the near-field coupling between a point-like optical source and a directional mode [132]. Likely, the most straightforward way of doing this, takes directly into consideration the local dynamical properties of light, in particular the SAM, from which the coupling is simply understood as a matching between the longitudinal component of the external spinning source (typically regarded as a dipole), and the transverse spin associated with the evanescent tail of the corresponding surface or guided mode. On the other side, there is an approach, somehow inherited from quantum mechanics, which is based on the *Fermi's Golden Rule*[‖] [133]. Under this picture, the coupling relies on the matching condition of the local EM field distribution, whose efficiency depends on the degree of similarity between the dipole moment ($\mathbf{p}$ and/or $\mathbf{m}$) and the EM field ($\mathbf{E}$ and/or $\mathbf{H}$) of either the guided or the surface mode at the same location than the source, i.e., it is proportional to a formula resembling the Fermi's Golden Rule: $|\mathbf{p} \cdot \mathbf{E}^* + \mathbf{m} \cdot \mu \mathbf{H}^*|^2$. Although having the virtue of being very general, these two schemes have a clear drawback; they require a prior knowledge

[‖]Within the quantum context, Fermi's Golden Rule describes the spontaneous emission (or transition) rate between two quantum states. The probability of such events will depend on the density of final states. On account of its relationship to the Purcell effect, it might be reasonable to think in the search of configurations or environments that could enhance further the near-field optical coupling.

$$\tilde{\mathbf{E}}(\kappa_x, \kappa_y; 0) = \frac{ik^3}{8\pi^2\varepsilon}\frac{1}{\kappa_z}\left\{[\mathbf{e}_s \cdot \mathbf{p}_{\text{eff}}]\,\mathbf{e}_s + [\mathbf{e}_p^{\pm} \cdot \mathbf{p}_{\text{eff}}]\,\mathbf{e}_p^{\pm}\right\}$$

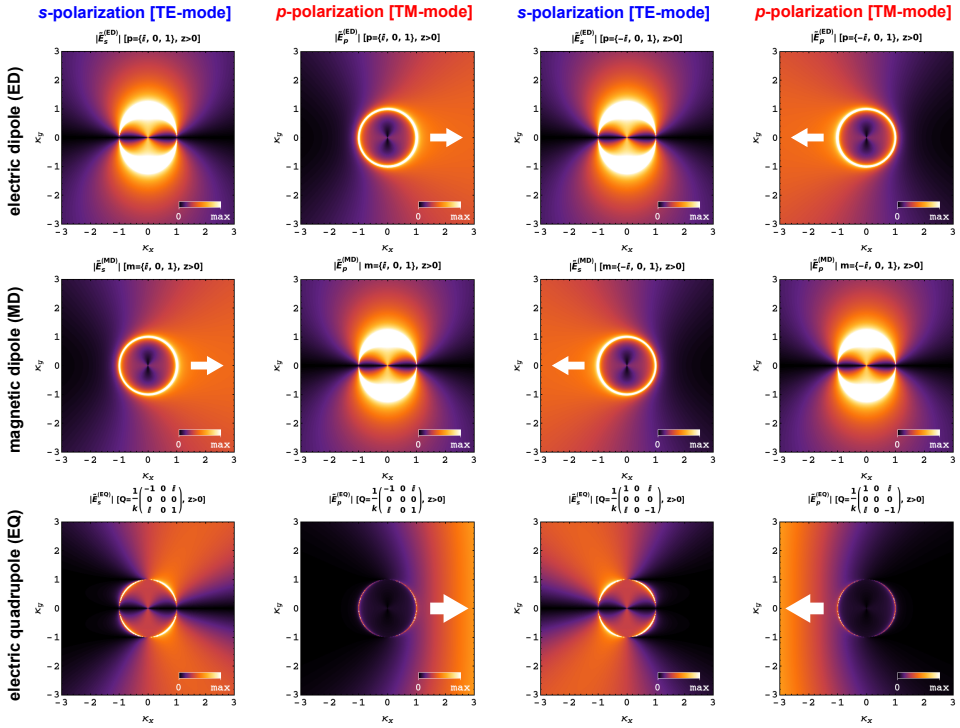

Figure 7.5: Angular spectrum of s- and p-polarized electric fields of different optical sources.

of the whole vector field structure of the EM modes. The treatment based on the angular spectrum representation, though, provides with an alternative approach that does solely involve the source in itself. Roughly speaking, it consists in calculating and analyzing the spatial frequency (or the angular) spectrum of the optical source, and looking into the symmetry features (if any), concretely, at the near-field region, i.e., the part of the spectrum corresponding to the evanescent modes (Figure 7.4). Within this framework, the coupling efficiency (i.e., the fraction of power generated by the source that is coupled to a specific mode) is proportional to the amplitude of the angular spectrum of the source at the transverse wave vector of the specific mode to be excited. Therefore, this leads to a sort of phase-matching condition, according to which the coupling does result from the overlapping between the angular spectra of the source and that of the guided mode. Thus, the unidirectionality will be achieved on account of the presence of asymmetries in the evanescent components of the angular spectrum of the source, becoming sharper as higher is the contrast ratio between light coupled into opposite directions (Figure 7.5). Strikingly, as can be shown, for instance, in the case of circularly polarized dipoles (either electric or magnetic), this asymmetry at the near-field region might lead to a symmetric behavior at the far-field region. This allows us then to confirm that the asymmetric coupling that yields the unidirectional excitation is a characteristic property entirely underpinned by the evanescent part of the angular spectrum associated to spinning sources.

Noteworthily, by means of the angular spectrum representation one can deal analytically, and even exactly, with the EM field radiation in the presence of nearby structures with planar geometries, namely, structures exhibiting a translational symmetry along two directions of a given plane (e.g., slabs, interfaces, or layered media). Specifically, this can be performed by applying the *transfer matrix method*, a procedure equivalent to the *Green's function* approach that permits to transit from a homogeneous medium to the inhomogeneous case (e.g., that in which one consider the presence of N slabs). The core of this method lies in the calculation of the transfer function, that is, a complex function behaving just like the previously introduced propagator, i.e., so that the angular spectrum of the EM field in any arbitrary plane (*image plane*) is directly related to that at a given plane (*object plane*), thereby letting an analytical extension to the whole space including the planar structure. To obtain such a transfer function one should first calculate the angular spectrum of the total optical field at a given plane to then, by considering individually both the propagating and the evanescent components, propagate each of those contributions through every plane. This is to be performed by considering the corresponding reflection and transmission Fresnel coefficients, conveying the characteristics of the medium. Finally one only has to add all the contributions up together, and retrieve the fields to the real space just by evaluating the corresponding numerical inverse fast Fourier transform on each plane. Importantly, in our particular case, in which we are considering planar structures, this approach leads to results identical (or at least equivalent) to those obtained through the mode coupling description (i.e., the approach based on the Fermi's Golden Rule), but with the advantage of gaining in some physical intuition and mathematical simplicity. Furthermore, it should be noted that, even though not giving exact results, the same treatment could be carried out for nonplanar structures, provided that they are translationally invariant along a given direction. This is possible on account of the conservation of the wave vector component along the direction of propagation (i.e., that of the symmetry axis), and thus, it is ultimately a consequence of the momentum conservation. Hence, besides endowing this formalism with a more fundamental sense, all the above considerations allow us to suggest that the near-field directionality is actually an universal phenomenon, as it is only determined by the source.

Since the initial demonstration of the near-field unidirectional excitation by circularly polarized electric dipoles [102], several efforts have been undertaken to extend it beyond this particular case. In this respect, the first steps were aimed at the development of their magnetic counterpart [132], whose contribution becomes really important when considering high-index dielectric nanoparticles. Magnetic dipoles introduce an additional degree of freedom, and, importantly, enable the near-field directionality through s-polarized modes, being strictly forbidden in the case of electric-like sources (Figure 7.5). This extension, along with the insights gained from the angular spectrum representation, were arguably the seeds that fostered the exploration of the simultaneous excitation of electric and magnetic dipoles to get near-field directional effects. One of the major achievements resulting from a linear combination of both dipoles was the unveiling of the so-called *Janus dipole* [133], a topologically protected source in which the electric and the magnetic dipoles

oscillate out of phase, thus producing a side-dependent near-field coupling. This gave way to a novel optical source with two faces (hence its namesake with the ancient Roman god Janus): one producing near-field coupling to both directions while the opposite one being absolutely non-coupling. Together with the *Huygens' dipole* (a source satisfying the *Kerker's condition* and then exhibiting a full directional behavior both in the near- and the far-field regimes), and the circularly polarized dipoles, these three sources have been proven to form a complete set of directional sources in planar geometries, thereby pushing the near-field directionality beyond the spin-momentum locking. At any rate, in all these extensions the focus has only been placed on dipolar sources and, hence, there was still plenty of room for exploring the behavior of higher-order contributions.

Following this enticing trend toward a widening generalization of near-field directionality, our work was aimed to extend the available theoretical toolbox surrounding this phenomenon by including multipole fields of arbitrary order and their combinations. To be constructive in our analysis, we provided a step-by-step derivation starting from the immediately higher order, i.e., the electric quadrupole. Just as for the electric dipole, the first step for the quadrupole was to calculate its angular spectrum. However, whereas this is a trivial task for the dipole, as it essentially relies on the *Weyl's identity*, in the case of quadrupoles the situation becomes slightly trickier. In this sense, calculating its corresponding angular spectrum, and being able of expressing it in a closed form, might be regarded as a main achievement in its own right. In fact, just with this partial result one could appreciate the sought feature on how to enlarge the spatial range in which the near-field directional coupling might occur. It should be noted that, at the very beginning of this research, the purpose was to explicitly show evidence of the main conclusions drawn in the previous work, an endeavor for which quadrupolar sources were more than enough. Despite this, given the similarities of the quadrupole angular spectrum with that of the dipole, and the relative easiness of the procedure, it turned out to be quite tempting going ahead "a little further" to look into the possibility of addressing a general approach including any multipolar order. After a hard and lengthy struggle with the calculations (see the step-by-step derivations carried out in Chapter 3), we finally reached a general, analytical, and closed expression for the angular spectrum of any higher-order multipole field. This was the second main result of this work, and actually the most important outcome, since it also encompasses the previous one. Furthermore, it is worth noticing that, likewise the angular spectrum of the dipole relied upon the Weyl's identity, since our result is general for all the multipolar orders, it might be somehow envisaged as a generalization of such an identity. Hence, with our formula one have a ready-to-use treatment that can be directly applied to the analytical design of optical sources for engineering the near-field directional scattering and coupling. Indeed, once the angular spectrum has been determined, we only have to follow the procedure outlined above to get the unidirectional excitation of EM guided modes. That is why we built up a calculator (Figure 7.6) that performs all the necessary calculations and substitution to provide the angular spectra of EM multipole fields of arbitrary order (this resource is available at https://doi.org/10.5281/zenodo.2677908). Moreover, as for the applications,

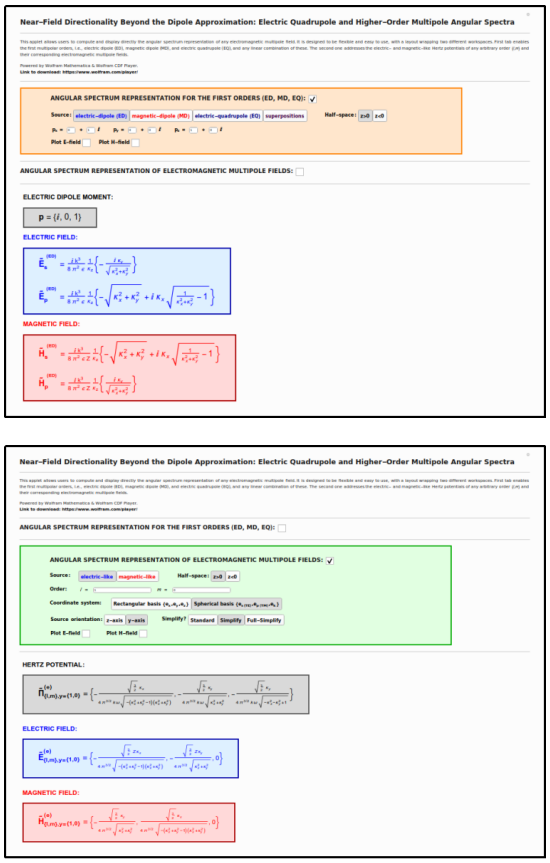

Figure 7.6: Calculator of angular spectra of arbitrary EM multipole sources (powered by *Wolfram Mathematica* & *Wolfram CDF Player*). This applet allows users to compute and display directly the angular spectrum representation of any electromagnetic multipole field. It is designed to be flexible and easy to use, with a layout having two different workspaces. First tab enables the first multipolar orders, i.e., electric dipole (ED), magnetic dipole (MD), and electric quadrupole (EQ), and any linear combination. The second one addresses the electric- and magnetic-like Hertz potentials of any arbitrary order $\{l, m\}$ and their corresponding electromagnetic multipole fields.

it should also be noted that, as previously anticipated for the quadrupole, successively higher-order multipole fields provide with several advantages: increasing the available degrees of freedom, broadening the spatial range for near-field directional coupling, and leading to a spatially broadband enhancement of the contrast ratio. All these features translate directly into a higher versatility, ease, effectiveness, and efficiency in the occurrence of this phenomenon. Thus, our results enable a considerable upgrade toward a full control on spin-dependent directionality at the nanoscale, and should be enormously relevant for dealing with light-matter interactions in nanophotonics and quantum optics.

The following paper highlights the main insights concerning the first part of this thesis. In particular, it focuses on this latter contribution along with other works carried out in parallel by the group of Dr. F.J. Rodríguez-Fortuño at *King's College London*.

PAPER E

Optics in 2019: Near-Field Unidirectional Excitation...and Beyond

Opt. Photonics News 30, 58 (2019)

Near-Field Unidirectional Excitation...and Beyond

J. Enrique Vázquez-Lozano,[1,2] Michela F. Picardi,[2] Anatoly V. Zayats,[2]
Francisco J. Rodríguez-Fortuño,[2] and Alejandro Martínez[1]

[1]*Nanophotonics Technology Center, Universitat Politècnica de València, Camino de Vera s/n, 46022 Valencia, Spain*
[2]*Department of Physics, King's College London, Strand, London WC2R 2LS, United Kingdom*

As with a waterwheel over a channel, in which the sense of rotation determines the flow direction, the circular motion of charges close to waveguiding structures may result in unidirectional excitation of surface or guided electromagnetic modes [1]. This topological phenomenon offers a clear evidence of spin–momentum locking, underscoring the incontrovertible relationship between the transverse spin of evanescent waves and the propagation direction of guided modes. It is generally interpreted as a manifestation of the photonic counterpart to the quantum spin Hall effect [2].

This universal and robust feature has enabled the observation of near-field directionality for circularly polarized dipolar sources in a wide variety of photonic platforms and spectral ranges. Yet, in work published recently, we showed that by considering linear combinations of electric and magnetic dipolar sources, the near-field directionality can be extended beyond spin-momentum locking [3]. This generalization led to the theoretical prediction of a new type of local source: the Janus dipole. Together with circularly polarized and Huygens dipoles, Janus dipoles form a complete set of directional sources, thus simplifying the analytical description and broadening the possibilities for engineering the near-field coupling.

Beyond their scientific interest, these dipolar sources are intended to be exploited in practical applications. This year, Janus dipoles were experimentally demonstrated using high-index dielectric nanoparticles with spectrally overlapping electric and magnetic resonances of comparable strengths [4]. This showed that the apparently exotic amplitude and phase relations between electric and magnetic moments required for these theoretical dipoles are indeed experimentally feasible in simple illumination configurations.

This year, we also explored near-field directionality beyond the dipolar approximation, by considering higher-order electric and magnetic multipoles and their combinations [5]. This increases the available degrees of freedom, enhances the directional contrast and spatial frequency bandwidth, and enlarges the accessible spatial range, thus providing versatility for engineering directional scattering and coupling.

We believe that superposition of electric and magnetic dipoles that experimentally achieve near-field directionality, and the theoretical possibility of combining them with higher-order multipoles, promise new avenues for miniaturized light switching and nanorouting, photonic logical circuits, light polarimetry and novel optical forces, among other applications.

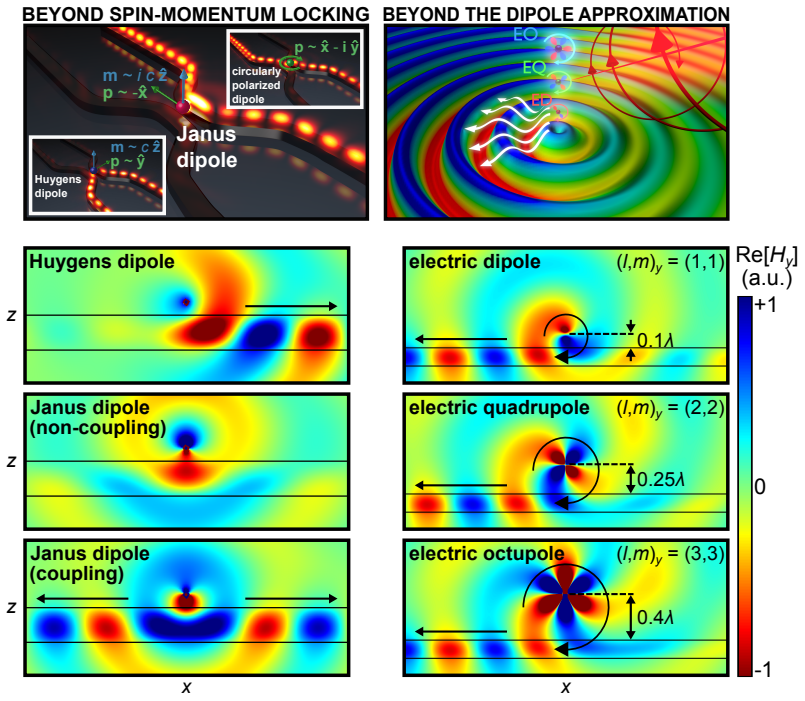

Figure E.1: Top left: Simulation showing the directionality of dipolar sources. Top right: Artistic representation of directional multipoles. Bottom left: Near-field behavior of Huygens and Janus sources placed over a dielectric slab waveguide. Bottom right: Near-field directional excitation of guided modes from higher-order multipolar sources.

References

[1] F. J. Rodríguez-Fortuño, G. Marino, P. Ginzburg, D. O'Connor, A. Martínez, G. A. Wurtz, and A. V. Zayats, *Near-field interference for the unidirectional excitation of electromagnetic guided modes*, Science **340**, 328 (2013).

[2] K. Y. Bliokh, D. Smirnova, and F. Nori, *Quantum spin Hall effect of light*, Science **348**, 1448 (2015).

[3] M. F. Picardi, A. V. Zayats, and F. J. Rodríguez-Fortuño, *Janus and Huygens dipoles: Near-field directionality beyond spin-momentum locking*, Phys. Rev. Lett. **120**, 117402 (2018).

[4] M. F. Picardi, M. Neugebauer, J. S. Eismann, G. Leuchs, P. Banzer, F. J. Rodríguez-Fortuño, and A. V. Zayats, *Experimental demonstration of linear and spinning Janus dipoles for polarisation- and wavelength-selective near-field coupling*, Light Sci. Appl. **8**, 52 (2019).

[5] J. E. Vázquez-Lozano, A. Martínez, and F. J. Rodríguez-Fortuño, *Near-field directionality beyond the dipole approximation: Electric quadrupole and higher-order multipole angular spectra*, Phys. Rev. Applied **12**, 024065 (2019).

7.II Optical Chirality & Chiral Light-Matter Interactions

The second part of this thesis has been devoted to the study of optical chirality and its interactions with matter in integrated photonic platforms. The optical chirality is a property useful for describing experiments of circular dichroism (CD) spectroscopy, in which one evaluates the differential signal, either in transmission or absorption, of a chiral medium — this may be an artificial structure, or simply a single object, e.g., a molecule — when is being sequentially illuminated by light with opposite handednesses (or chiralities). Provided that the object under analysis is chiral, the absorption (or the transmission) of one handedness will be different from that of the opposite one, so that the higher is the chirality (of either the object or that of the light), the greater will be this effect**. Since the physical object is generally regarded as a fixed piece of the system, all the available degrees of freedom shall depend on the chirality of the input light. This directly leads us to the notion of optical chirality, which, roughly speaking, assigns a numerical value to the optical field that quantifies how twisted it is. For the particular case of EM plane waves, the paradigmatic example of chiral light is related to states of circular polarization, so that left- and right-handed circular polarizations will display opposite chiralities. Although at a first glance the chirality can be thought as a dichotomic feature (namely, it might be either left or right, i.e., positive or negative), when it is related with optical fields, it adopts a continuous character, thus quantifying not only the handedness, but also its magnitude. In this manner, whereas states of linear polarization have a null optical chirality (indicating that it is absolutely nonchiral), all the elliptical states, till reach the circular polarization, will exhibit an increasingly higher chirality, in absolute value. Hence, for EM plane waves, the highest chirality is reached for circularly polarized light, i.e., the states located at the poles of the *Poincaré sphere*.

Beyond its practical interest as an useful tool for describing optical effects as the aforementioned, the most remarkable feature of optical chirality relies on its fundamental character. Indeed, this dynamical property is in turn a conserved quantity, and as such, it encloses a symmetry of the system. This identification was originally realized in 1964 by D. M. Lipkin [164], who demonstrated the existence of this and nine other independent quantities that appeared to be preserved for any given EM field in free space. Unfortunately, this finding was considered merely as an interesting mathematical exercise of limited usefulness in physics, so that it was widely dismissed for a long time. This lack of physical meaning was lifted only very recently, in 2010, in a seminal work authored by Y. Tang and A. E. Cohen [64], where they proposed this quantity as a measure of the handedness (or knottedness) of the streamlines describing highly contorted optical fields.

**Notice that, although CD spectroscopy requires both the analyte and the light to be chiral, it should not be misinterpreted to mean that the chiral response is only attained in such a particular situation. In fact, near-field chiroptical responses can be found in each of the four possible situations categorized in terms of the chiral symmetry of both the light and the matter, i.e., it can occur either when both or neither the light and matter are chiral, or when only one of them (either light or matter) it is. Whatever the combination chosen, all of these schemes are being customarily exploited to search for ways to enhance chiral light-matter interactions [184].

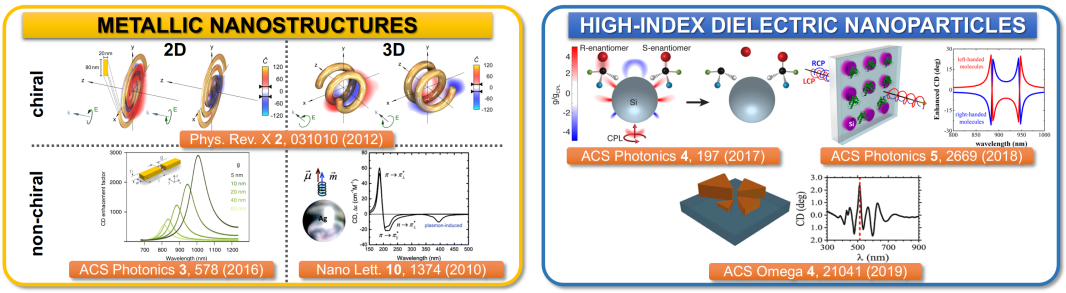

Figure 7.7: Metallic and high-index dielectric nanostructures used to enhance the chiral responses.

Just by taking a glance at the current literature on optics and nanophotonics, one can realize that optical chirality is an active research topic that very often goes hand in hand with plasmonics and metamaterials [184]. These kind of systems are actually being regarded as the best-suited platforms for strengthening, and thus for investigating, chiral light-matter interactions. Indeed, the surroundings of complex-shaped metallic nanostructures allow for a strong light concentration at subwavelength scales (owing to their plasmonic character), and, importantly, enable the possibility to achieve a great spatiotemporal control of light-matter interactions (by properly engineering their geometrical features, e.g., the size, the shape, or the orientation). This may lead to sculpted and highly contorted three-dimensional EM field distributions, which, ultimately, has been proven to be the main requirement for the occurrence of strong optical chirality, and, consequently, for enhancing the chiroptical interactions. With this in mind, multiple enhancement schemes have been proposed; from twisted structures, such as spirals or helices, arrays of chiral and even achiral plasmonic nanostructures, to stacked planar metasurfaces (Figure 7.7). Furthermore, more recently, there is a steadily growing trend in using assemblies of high-index dielectric nanostructures in very distinct arrangements and geometries (e.g., nanospheres, nanodisks, or bowtie-like structures), which are actually revealing promising results in terms of the enhancement of near-field chiroptical effects. Ultimately, all these approaches, either based on metallic or dielectric nanostructures, have been strongly spurred on account of the early proposal of getting superchiral fields in spatially accessible regions, in order to get high levels of resolution and sensitivity for checking and characterizing the chirality of matter. In this regard, it should be noted that, akin to the case of the SOI-based effects, the chiroptical responses resulting from the interactions between chiral light and chiral matter (typically biomolecules such as sugars or proteins, or artificial metamolecules at the micro or even nanoscale) are in general extremely weak. Indeed, leaving aside the complexity that the experimental arrangements might entail in themselves (thereby weakening the efficiency), this smallness is generally attributed to the large scale difference (and the subsequent mismatch) between the operational wavelength of the input light and the typical size of the chiral analyte.

Notwithstanding the foregoing, whatever the type of the medium or the material is, it is very well known that the effects of dispersion and, consequently (in compliance with

the *Kramers-Kronig relations*), the absorption losses, need to be accounted for, with the only exception of the vacuum. These considerations are often neglected, presuming media with an ideal lossless and/or dispersionless behavior. However, when matter is nanostructured to achieve more complex behaviors, as for the case of metamaterials or plasmonic nanostructures, the effects of dispersion and losses should not be disregarded at all (even more by noticing that they are often regarded as the paradigmatic examples of dispersive and lossy media). Hence, as with the energy, the optical chirality should also be generalized to the case of arbitrary dispersive and lossy optical media, and this precisely has been the matter of PAPER C; namely, a thorough derivation of the optical chirality, extending it so as to include both dispersive and dissipative effects. Noteworthily, for simplicity, as well as for constructiveness, the theoretical basis of this work has been relied upon the most complete form of the conservation law for the optical chirality.

Thus far, most of the previous studies addressing the optical chirality and its interaction with matter have been using the earliest definition originally derived for monochromatic optical fields in free space. Despite having proved its usefulness in the experimental assessment of CD spectroscopic measurements for the detection and characterization of chiral biomolecules, its applicability can be certainly questionable beyond the simplest case of the vacuum; even further when used for looking into chiral effects either in metallic nanostructures or metamaterials. That in itself may be regarded as a sufficient reason for wanting to address a generalization of such a quantity. Furthermore, recent advances in nanofabrication are opening up new interesting possibilities for the experimental measurement and investigation of dynamical properties such as the EM energy-momentum, the optical orbital and spin angular momentum, and the EM helicity, so far only accessible theoretically[††]. This fact has likely led to reexamine both the theoretical treatment and the formulation of these dynamical properties taking into account their dispersive features. Concerning the optical chirality, it should be noted that there have also been few attempts to extend its original definition, for instance, to arbitrarily defined linear media, to gyrotropic systems, or even to dispersive materials. Regardless of the debatable accurateness in the realization of such endeavors (particularly as for the latter one, which precisely dwells on dispersion features), one of the major remaining issues lies on the existing loophole for including the contributions associated to the absorption losses. In this respect, it is worth highlighting the following annotation pointed out in Ref. [190]:

> «*We have derived the electromagnetic helicity operator and density [...] This quantity completes the set of dynamical properties of light in optical media, including the Brillouin energy density, canonical momentum, and spin [...] Our results can also be applied to systems with small losses or gain, by considering only the real part of the permittivities and permeabilities, similarly to the case of the Brillouin energy density. However,* ***the extension of the present formalism to highly lossy systems is an open task*** *because of the ambiguity in defining cycle averages with nonoscillatory fields*».

[††]In this regard, it is noteworthy to draw attention on the aforementioned *Abraham-Minkowski dilemma*.

Although this comment actually refers to the EM helicity, the fact is that such a dynamical property is closely related with the optical chirality, and hence, it is also applicable to it. In such a sense, this need for extending the formalism to highly dispersive systems considering dissipative effects as well, is perfectly accomplished in our work. By the way of an off-the-record note, it is worth pointing out that this paper concerning the helicity was published just before than ours (though such a mention claiming for the inclusion of losses were already appearing in a second submission of its preprint version posted in arXiv), when we were already working out the formulation for the optical chirality considering the inclusion of lossy media. Certainly, and despite the own theoretical interest that our work may have, this statement coming from widely recognized authors in the field could have been quite relevant for catching the eye and proceed with the rapid acceptation of our manuscript. Further, from a purely objective point of view, our outcomes show that there are important differences in the optical chirality when comparing both the lossless and the lossy approaches. Such deviations mainly occur at the anomalous dispersion region, i.e., the spectral range where the real part of the permittivity decreases abruptly (or, to put it simply, near the resonance frequencies), and result into a strong enhancement of the optical chirality density. This therefore underscores the important role played by the absorption losses of a given medium in the analysis of the optical behavior by a dispersive material, in particular, as far as the chiral light-matter interactions are concerned; for instance, by suggesting the possibility of *lossy-induced optical chirality enhancements*. Hence, a full description of optical chirality in dispersive media, extending it to account for the medium's dissipative effects as well would be highly valuable and enlightening (from both fundamental and applied perspectives), and should be carefully considered.

There are many different ways in which one might want to conduct such a generalization, either from phenomenological aspects (just by fitting experimental outcomes or via arguments stemming from the chiroptical responses), or directly through an entirely theoretical analysis. The latter was the approach we followed out, specifically, by taking advantage of the underlying mathematical structure of the corresponding continuity equation (or conservation law) for the optical chirality. Notice that just as much the energy, the linear momentum, the angular momentum, or the helicity, optical chirality is also a conserved quantity for free-space EM fields. Upon this basis, we worked out on the most complete form of the continuity equation for the optical chirality, without any restrictions on the nature of the medium. From this, and building on previous approaches addressing the EM energy density considering dispersion as well as dissipation, we put forward an alternative derivation for the optical chirality density in dispersive media, distinguishing between the lossless and lossy cases. Remarkably, our description is completely general (it is valid for arbitrarily varying radiation fields, and could be applicable to any kind of medium) and perfectly consistent with that originally introduced for EM fields in free space.

In order to avoid misleading outcomes when including the dissipation, the analysis of the local dynamical properties (in this case the optical chirality) is to be carefully carried

out from a material standpoint. This should be made out by means of the corresponding dynamic equations characterizing the polarization and the magnetization fields, that ultimately lead to additional terms which must be explicitly accounted for. Thus, even though our goal was an approach as general as possible, just like with the EM energy, the general expression for the optical chirality density in lossy media will crucially depend on the specific features of the model characterizing such a medium. For practical purposes, we focused on the treatment originally outlined by Loudon for the energy [231] (considering an absorbing classical medium with a single resonance frequency), which was afterward extended by many other authors to account for dispersive magnetic permeabilities [232], as well as for the possibility of multiple resonance frequencies describing interband transition effects [212]. Hence, the only restriction we need to impose relies on the characterization of the material parameters, which must be fitted by Lorentzian line shapes (i.e., it should be able to be described as a combination of Drude and Lorentz oscillators).

As pointed out in the original work, the possibility for such a characterization (along with the mathematical structure of the continuity equation), turned out to be key point to derive the most general expression of the optical chirality density in dispersive and lossy media. Still, we would like to remark that, regarding the EM energy in dispersive and lossy media, non-Lorentz-type dispersions have also been considered [197]:

> «*It has been pointed out,* ***if the medium has finite power loss, it is impossible to define the energy density uniquely if we do not have a microstructure model of the material****. With the microscopic models of the electric and magnetic constituents of the medium, the dynamical behaviors of the corresponding electric and magnetic dipoles can be predicted, and the energy stored in the medium can be correctly evaluated. In the literature, several dispersive media with different microscopic dipole models have been considered.* ***The simplest one is an absorptive classical dielectric (Lorentz dispersion)*** *with a single resonant frequency. This can be generalized to the case that both the permittivity and the permeability have Lorentz-type dispersions.* ***Non-Lorentz-type dispersions have also been considered. For example, in the wire-split-ring resonator (SRR) metamaterial medium*** *[...]*».

Something similar was also claimed by Tretyakov [195]:

> «***If the material has considerable losses near the frequency of interest, it is not possible to define the stored energy density in a general way*** *(more precisely, it is not possible to express that in terms of the material permittivity and permeability functions).* ***Knowledge about the material microstructure is necessary to find the energy density****, and this problem is far from trivial. Attempts to derive a general expression in terms of the effective parameters may give negative values of*

> *the stored energy.* ***In the literature, the energy density expressions for lossy dispersive media have been derived only for some special cases: for an absorbing classical dielectric (Lorentz dispersion) with a single resonant frequency and for the case where also the permeability obeys the same dispersion law as the permittivity*** *[...] the energy density in lossy dispersive media are different for media with different microstructures, which means that* ***specific derivations must be done for each specific material****».*

Furthermore, as pointed out by Semchenko *et al.* [308]:

> *«[...] For artificial materials based on metal or dielectric inclusions of various shapes, called metamaterials, absorption can be neglected when the operational frequency is far from the resonant frequencies of the inclusions and from the lattice resonance if the material is periodic [...]* ***If the material exhibits considerable losses near the frequency of interest, it is not possible to define the stored energy density in a general way****, i.e., to express that in terms of the material permittivity and permeability functions.* ***Only if the internal structure of the medium is known and a specific dispersion model (like the Lorentz or Drude dispersion) is applicable is it possible to define and find the stored reactive energy*** *in terms of the dispersion model parameters (the resonant frequency or the plasma frequency as well as the damping factor) even if losses are significant [...]»*

Of course, all these arguments would also be applicable to our approach dealing with the optical chirality density. Nonetheless, it is worth noticing that, although our analysis is indeed limited to the particular case of materials that can be characterized by Lorentzian line shapes, such a multi-resonant Drude-Lorentz model has been proved to fit very well with experiments, and so, it can be regarded as a generic approach for characterizing the electric (and the magnetic) response of any arbitrary optical medium. Accordingly, the analytical and closed expression derived in our original contribution provides the most general definition for the optical chirality density in lossless and lossy dispersive media, thus being applicable to any frequency, bandwidth, and material system, including dielectrics, semiconductors, as well as highly dispersive material systems such as metals (or plasmonic nanostructures) and metamaterials. It is in this sense that it may be regarded as completely general, as it may provide a description as accurate and reliable as needed.

All along the whole exposure of this work, we have always kept in mind the classical development for the EM energy, whose conservation is dictated by the very well-known Poynting's theorem. For our purposes, it has served as a guideline for mathematics and also for the interpretation when addressing the optical chirality density, specially with regard to the source-like contributions, since its physical meaning in such a case may not

be so obvious (in comparison with the energy). Notice that, even though this matter may seem somewhat trivial at a first glance, simply the fact of considering EM waves propagating through a dispersive medium poses a challenge, making the mathematical treatment much more complicated, and, at the same time, tremendously enriching the physics. Good evidence of this is the considerable number of papers on this issue that still continue being published nowadays in renowned journals, wherein it is discussed and reexamined both the fundamentals and the interpretation of the EM energy density in dispersive media. This renewed interest in such seemingly basic aspects has likely been fostered by recent progresses on left-handed materials, and metamaterial photonics in general. Furthermore, by including the presence of a material system, the analysis of the continuity equation reveals the appearance of additional source-like terms describing the loss (or gain) rates. Remarkably, whatever the dynamical property is concerned, these contributions are important because enable one to get deeper insights into fundamental aspects of light-matter interaction [219, 220]. For example, in the familiar case of EM energy, the term $\boldsymbol{\mathcal{J}} \cdot \boldsymbol{\mathcal{E}}$ is directly related to the power lost (or the work exerted) by the EM fields on the sources. However, in the optical chirality case, the physical significance of its associated source-like terms is not so obvious, thereby limiting to some extent the concept of source (or sink) of optical chirality and thus hindering a proper interpretation. An in-depth understanding of the meaning and the physical implications of these contributions remain as yet unclear and would deserve further efforts. Finally, it is also worth to be mentioned the controversial debate currently existing around the meaningfulness and the differences between the EM helicity and the optical chirality [187, 309–311]. It is quite possible that a complete approach relying upon the role played by the material absorption losses may shed some light on the solution of this and many other intriguing questions.

Undoubtedly, the research area concerning the optical chirality and chiroptical light-matter interactions is currently attracting a great deal of attention, from both fundamental and applied viewpoints, and even beyond the optics and nanophotonics. Yet, in contrast to well-established techniques for sensing or spectroscopy, such as the SPP-based sensors or the Raman spectroscopy, there have not been previous attempts (or at least, to be more precise, if any, they have been very scarce) for carrying out chiral spectroscopy in a photonic integrated platform, being so far most of the chiroptical experiments and applications performed by means of free-space excitation and detection arrangements. Motivated by the current trend toward a full-integration of multiple optical devices and instruments, in PAPER D we explored the possibility to generate and convey (enhanced) optical chirality through EM guided modes supported by all-dielectric integrated photonic waveguides. Ultimately, the main goal was to assess its potential for conventional chiroptical functionalities, such as sensing, spectroscopy, or enantioselectivity, from a lab-on-a-chip perspective. While essentially keeping the same working principle as the prevailing free-space approaches, besides the miniaturization, the integrated-like proposal brings forth many practical advantages, mainly if realized onto silicon-based platforms compatible with standard CMOS technology: low-cost and large-volume production, massive parallel detection, repeatability, portability, or integration with

electronics, among others. Thus, in addition to expand the portfolio of spectroscopic techniques in integrated photonic platforms, the presented approach holds the promise for a more robust and simpler fabrication and implementation, displaying a performance (given via the dissymmetry factor) comparable to (and even better than) those already reported from free-space schemes.

Unlike all the previous works conducted throughout this thesis, mostly based on analytical models, in this case the study to test the feasibility of chiroptical applications in integrated platforms has had to be necessarily carried out by means of numerical simulations, for which, we have made use of the commercial 3D full-wave solver CST Microwave Studio. Despite the large amount of options that are available, unfortunately CST does not allow to model a chiral medium, namely, it does not enable the implementation of constitutive relations such as those enclosed by the *Born-Kuhn model*. To settle this issue, we chose to consider a metallic nanohelix. All along this work such a structure has served as the chiral sample to probe the chiroptical interactions. As can be found all over the literature, such a consideration is helpful and customarily embraced in order to mimic the enantiomeric behavior of the sensing target (typically chiral biomolecules). In this regard, it should be noted that the fact that the probing sample has been modeled as a metal is merely for simplicity, so as to enhance the outcomes. Indeed, due to its opacity (in comparison with a dielectric scatterer), the chiral scattering and/or absorption (notice that the absorption should be taken into account only when considering a lossy material) by a metallic structure provides a clearer differential response from left- and right-handed circularly polarized guided modes (CPGMs). In a real chiral spectroscopy system, though, one may have to deal with a bunch of chiral molecules placed in the active region (i.e., the region in which the chiroptical interaction takes place). At any rate, they will show different absorption for each handedness, which would also result ultimately in a different transmission of the optical power. In this sense, the chiroptical behavior of the system should be essentially the same no matter which kind of object we place in the sensing region (either dielectric or metallic structures, or just chiral molecules), as long as it has a chiral response (for further details on this issue see, e.g., Refs. [292–294]). So, even though metals exhibit radically different properties when compared with dielectrics or biomolecules, in this work we are only concerned about the differential response for each handedness, which is what we want to show in our guided system. In this respect, notice that, in order to perform an accurate comparison with a realistic situation, one would have to consider not a dielectric single helix, but a chiral medium (with the corresponding constitutive relations), so that the chirality of the matter accounts for the averaged response over many molecules randomly orientated.

Continuing on the discussion about the modeling of the helix it is worth remarking that, by all the means, all the particular considerations has been aimed at providing an approach attempting to achieve a good trade-off between simplicity and generality. In this vein, the election of a helix has been simply based on the fact that it is often regarded as the prototypical example of chiral object (in fact, resembling the shape traced out by the

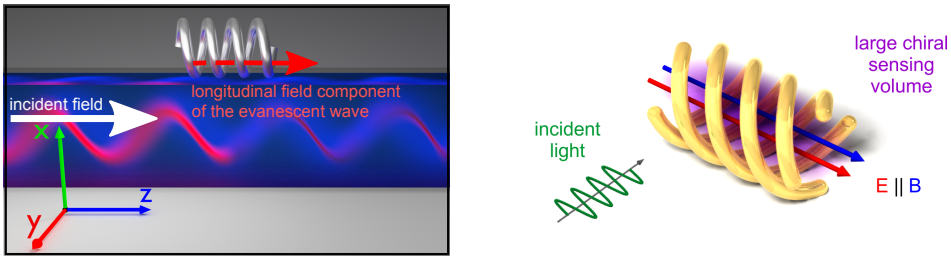

Figure 7.8: Analogy between the integrated approach showing optical chirality induced by evanescent fields neighboring waveguiding structures (*on-top configuration*), and the free-space scheme proposed in Ref. [285], exhibiting high optical chirality over a large volume within the helix.

circularly polarized light when evolving over time). Likewise, to be constructive in our analysis, this structure has been first modeled as a perfect electric conductor, so that the chiral interaction is only due to the geometrical aspects and the influence of dispersion or absorption effects can be neglected. As it is pointed out in previous works, on which we actually inspire this working strategy (see, e.g., Ref. [300]), this prior consideration allows us to gain general insights for understanding the chiral behavior of the helix in itself, wherein the dominant response should be just due to the chiral-shape dependent scattering. Furthermore, with regard to the helix structure, it is important to note that it merely acts as a chiral sample. Still, in view of the corresponding chirality maps obtained, the nanohelix could also be considered as a kind of chiral enhancer[‡‡]. In fact, it can be observed a clear similarity between the EM field distribution associated with the «*on-top configuration*» (in particular by looking at the longitudinal field component of the evanescent tail of the CPGMs), and that resulting from the arrangement proposed in Ref. [285], in which the optical chirality is longitudinally confined in the center of the helical structure (Figure 7.8). In this manner, along with the improved and simpler version of this helical structure outlined in Ref. [300], the integrated approach might lead to a more straightforward way to get large areas of enhanced chirality for practical applications.

Regarding this «*on-top configuration*», in which the optical chirality is induced by the evanescent field neighboring the waveguide, it should be noticed that the fact that the guided modes have an evanescent tail (as a result of the evanescent decay of the optical field in the waveguide core surroundings) does not translate into energy losses at all. On the contrary, the dielectric waveguides we use are theoretically assumed to be lossless. A small amount of losses may arise in real waveguides as a result of etching-induced roughness in the lateral sidewalls. However, in silicon nitride technology, actual fabrication processes enable propagation losses as low as 5.5 dB/m at telecom wavelengths [279]. Indeed, the strong current interest in SiN waveguides for multiple purposes (ranging from Brillouin lasers to micro-combs for LiDAR applications) will surely lead even to lower propagation losses as a result of the improvement of the fabrication processes. This means that we can ensure on-chip propagation distances above several cm with negligible

[‡‡]Notice that we are not taking into account the feasibility neither of its fabrication nor the realization.

losses, with the corresponding chiroptical interaction taking place over the whole distance. Perhaps the losses can be a little bit higher at smaller wavelengths, but still cm-scale propagation with negligible losses is completely realistic in SiN chips.

An important consideration that is in a way related to this work concerns the relationship between the circular dichroism (CD) and the dissymmetry factor (g). In this regard there exists a very common misunderstanding which was likely introduced in the field of chiral light-matter interactions by Tang and Cohen in their seminal article [64][§§]. As far as the circular dichroism is concerned, it should be noted that it is strictly defined as $CD = A^+ - A^-$ [170]. On the other side, the dissymmetry factor usually reads as $g = (A^+ - A^-)/(A^+ + A^-)$. In the case of a pure plane wave excitation (and assuming a non-structured environment), $(A^+ + A^-)$ is a constant, and so, CD can be considered to be proportional to g. In any other case, both A^+ and A^- are quantities depending on the position, and thus, $(A^+ + A^-)$ ceases to be a constant, thereby breaking the aforementioned proportionality between CD and g. Nevertheless, it can be proved that the CD signal of small molecules in the presence of structured environments is proportional to the local density of optical chirality C[¶¶]. In those scenarios, it can be shown that g, when modified by the structured environment, may be used to quantify some other interesting properties such as the efficiency of enantiomeric separation for photolysis or photoionization processes [252].

Despite their undeniable importance and interest, a more in-depth analysis of these issues lies beyond the scope of our work. We have merely introduced the dissymmetry factor in order to provide a standard metric with which to perform a quantitative analysis and a fair comparison between the different scenarios that we have proposed for chiroptical applications in integrated photonic platforms. Likewise, the expression of the optical chirality has been simply used for mapping such a local dynamical property in the different configurations, thus allowing for a more intuitive description illustrating the strong enhancement in the chiral excitation of the nanohelix when its chirality coincides with that of the input CPGM. Hence, our work is simply focused on the numerical computation of the differential transmission of left (L-) and right (R-) CPGM, for a given handedness of the chiral probe, to the subsequent evaluation of g, and the mapping of C for each of the proposed schemes. Importantly, the characterization of the dissymmetry factor that we did, was made via the transmissions through the output waveguides (instead of the absorption rate), as they are the easiest signals to be obtained both in integrated

[§§]Indeed, apart from this, it is noticeable that there exists a generalized set of misconceptions (or perhaps, more precisely, a lack of common agreements) surrounding many chiroptical-like issues; in particular, those related with the more convenient way for performing such measurements, about the corresponding definitions involved on it, or even on account of their right physical meaning (e.g., when comparing the optical chirality with the electromagnetic helicity).

[¶¶]As shown in Ref. [252], owing to the electric field enhancements at resonance, the local enhancement peaks of C/C_{CPL} (and consequently that of CD signal, $CD/CD_{\mathrm{CPL}} = C/C_{\mathrm{CPL}}$) are slightly wavelength-shifted from those of g/g_{CPL}. This prevents the, up to now assumed, universal proportionality between g and CD, via C; at least in structured environments.

optics experimental setups, as well as from our numerical solver. This is the manner in which we show of the possibility to get chiroptical responses enabled by all-dielectric waveguides in integrated photonic systems.

With regard to the controversial definition of the dissymmetry factor, as pointed out above, it is worth stressing that there exists a generalized lack of agreement. Indeed, apart from the original derivation by Tang and Cohen [64], going from the familiar *Kuhn's dissymmetry factor*, $g \equiv 2\,(A^+ - A^-)\,/\,(A^+ + A^-)$ (yet canonically expressed through the decadic molar extinction coefficient), to that relating it to the optical chirality density,

$$g = -\left(\frac{G''}{\alpha''}\right)\left(\frac{2C}{\omega U_e}\right), \tag{7.1}$$

in their famous experiment to probe superchiral light (certainly argued by many), they also proposed a relationship between g and the reflectivity R (in units of g_{CPL}):

$$g/g_{\mathrm{CPL}} = \frac{1+\sqrt{R}}{1-\sqrt{R}}. \tag{7.2}$$

In addition to this, Hendry and coworkers [171] "*evaluate the strength of the chiral interaction with the adsorbed molecular layers by estimating the dissymmetry in the effective refractive indices of the chiral layers*", using:

$$g = \frac{n_{\mathrm{R}} - n_{\mathrm{L}}}{n_{\mathrm{R}} + n_{\mathrm{L}}}. \tag{7.3}$$

Still, though not canonical, much more common is the characterization of g in terms of the differential transmission of both polarizations, R- and L-CPL. In this regard, Schäferling *et al.* [177] stated that:

> «*[...] By now, the most common method to detect the handedness of chiral molecules is a* ***circular dichroism measurement****. With this method, one illuminates the sample with left- and right-handed circularly polarized light and detects the* ***difference signal of transmission or absorption*** *[...]*».

Furthermore, according to Yin *et al.* [297], this consideration might also be applicable to the definition of CD (in such a case is often referred to as the *circular dichroism in transmission* CDT):

> «*[...] The CD spectra for D- and L-enantiomer are exactly mirror symmetric to each other. It is clear how the signs of the CD peaks are determined. Evaluating the expression* $\Delta T = T_{\mathrm{R}} - T_{\mathrm{L}}$ *for the D-enantiomer, one obtains a negative sign of the CD peak at* 1250 *nm and a positive sign for the peak at* 1350 *nm with a zero crossing at* 1300 *nm. Similarly, the L-enantiomer exhibits the opposite behavior due to its switched modes [...]*»

Therefore, as can be seen, there exists a large list of references using indistinctly both g and CD (expressed either in terms of absorption, $A^{\pm}$, or transmission, $T^{\pm}$, and in several functional forms), for describing the asymmetric chiroptical response of chiral matter.

All in all, none of the above expressions are absolute, and all of them are susceptible to critics. For instance, Eq. (7.1), which is the main finding of the celebrated paper by Tang and Cohen (setting down a proportionality between the chirality of the matter and that of the optical field), has been widely questioned by many (see, e.g., Ref. [173]). On the other side, Höflich *et al.* [290], put into question the usual definition,

$$g_{\mathrm{T}} = \frac{2\,(T_{\mathrm{RCP}} - T_{\mathrm{LCP}})}{T_{\mathrm{RCP}} + T_{\mathrm{LCP}}}, \tag{7.4}$$

on account of a "contradictory physical meaning". Rather, they propose the following:

$$g_{1-\mathrm{T}} = \frac{2\,(T_{\mathrm{RCP}} - T_{\mathrm{LCP}})}{2 - T_{\mathrm{RCP}} - T_{\mathrm{LCP}}}, \tag{7.5}$$

claiming that

> «*A generally strongly absorbing material with a small difference in transmission for LCP and RCP incidence provides larger values of* g_{T} *than a material with the same asymmetry* $(T_{\mathrm{LCP}} - T_{\mathrm{RCP}})$ *but weaker polarization independent absorption. As a consequence, the definition* g_{T} *achieves its maximum value of* 2 *not only for maximally EM chiral objects but also for objects with a strong achiral absorption background and/or polarization conversion (e.g.,* $T_{\mathrm{LCP}} = 0.1$ *and* $T_{\mathrm{RCP}} = 0$*)*».

However, this issue can be easily rebutted going to the opposed situation (which is indeed much closer to our case), considering objects with weak achiral absorption background and/or polarization conversion (e.g., $T_{\mathrm{LCP}} = 1$ and $T_{\mathrm{RCP}} = 0.9$).

Regardless of the discrepancies for setting a unified definition of the dissymmetry factor, there should not be any problem on it (once an appropriate criterion is set and specified), since all of them, ultimately, attempt to provide the same meaning, i.e., establishing a metric (absolute or relative) to quantify the efficiency of the asymmetrical response (expressed in terms of differential absorption, transmission, or extinction) due to the chiroptical behavior of the system. In this regard, it turns out to be interesting the insightful perspective offered by Kramer and coworkers [176]:

> «*[...] the local optical chirality* $C(\mathbf{r}, \omega)$ *is proportional to the absolute chirality-induced signal in a spectroscopy experiment, that is,* C *is responsible for the absolute signal difference between measurements of systems with opposite chirality [...]* ***In some cases, one may be interested in the relative, rather than the absolute, signal difference****, in which case one*

> *has to normalize the obtained signal difference with respect to the absolute (chirality-independent) absorption signal. The resulting quantity, often called* ***dissymmetry factor*** g***, is responsible for the signal contrast*** *[...]*»;

> «*[...] For practical reasons, one has to decide carefully whether the absolute or the relative signal is the relevant quantity. Hence,* ***for applications of molecular chiral sensing or spectroscopy, one should analyze*** *in addition signal-to-noise ratios to find "optimal" external driving fields, and very likely one should be interested in* ***the right balance between absolute chiral signal strength and contrast*** *[...]*».

Reaching a general consensus would be certainly important in order to make fair, reliable, and straightforward, the comparisons among different results, e.g., as done by Höflich *et al.* (see the Supplementary Material of Ref. [290]). Notwithstanding that, this would only be possible for systems under the same conditions. For instance, free-space and waveguide excitation (and read-out) are extremely different techniques, so a comparison between them may result meaningless. Remarkably, the efficiency of excitation in a free-space approach is directly related to the ratio between the beam waist and the nanostructure size. In other words, the total amount of chiral absorption induced on a CPL beam will depend on how much light are we able to focus on the nanoparticle. In this sense, our «*in-gap configuration*» could be understood as identical to a free-space approach in which both illumination and read-out of the response of a single nanostructure is performed using very-high NA objectives placed in the near-field. In such a case, the input objective would produce a diffraction-limited hot-spot to illuminate the nanostructure, as our SiN waveguide end does. Yet, on the other hand, it is difficult to relate the «*on-top configuration*» with a free-space system, since it is not possible that light propagates with a waist around $\lambda/2$ over great distances so that the evanescent tails can be put in contact with the chiral nanostructures (or molecules).

Finally, it is worth remarking that the structure considered all along the manuscript (i.e., the metallic nanohelix) is merely regarded as a chiral probe. We do not attempt to provide a thorough analysis of its chiroptical behavior nor finding its optimal performance for the present integrated approach, which would deserve further efforts far beyond the aims of the present work (and may be the topic of future research). Nonetheless, for our purpose of showing the viability of this integrated approach, the choice of the helix has two significant advantages related to each other. The first is that, according to Woźniak and coworkers [289], analyzing the chiroptical response of a single plasmonic nanohelix from a multipolar decomposition, it can be observed that:

> «*[...] the optical response of the fundamental resonance has contributions from dipole and quadrupole moments, but* ***it is dominated by the dipolar response*** *[...]*»

> «*[...]* ***the optical response of the nanohelix is dominated by the two dipoles.*** *Our multipolar analysis indicates also the presence of electric and magnetic quadrupoles. However, their contribution and the* ***contribution of other higher order multipoles can be neglected*** *because their strength is several orders of magnitude smaller than the dipoles. A similar dipole-dominated chiroptical response of a two-loop helix was recently reported by Fruhnert et al. [...]*»

This means that the familiar definition of the dissymmetry factor provided by Tang and Cohen, i.e., Eq. (7.1), whose derivation relies upon the dipole approximation, turns out to be applicable to our chiral sample. This allows us to make a fair comparison with many other examples of chiral structures studied elsewhere. Secondly, and more importantly, since there are a large number of studies devoted to analyze the chiroptical behavior of metallic nanohelices excited with circularly polarized plane waves, it is quite straightforward to compare our results with those found in the existing literature (see, e.g., Refs. [282–289]). Of course, it should be noted that, so as to get unbiased results, special care is to be taken in considering the same definition for the dissymmetry factor. In this regard, there is a very complete and updated overview table of the achieved values of the dissymmetry factors in the Supplementary Material of Ref. [290]. There, it is presented a wide set of both theoretical and experimental values of the dissymmetry factor (considering different definitions) for either dielectric or metallic helices found out by many authors.

Thus far, many of the topical works on optical chirality have striven to enhance the chiroptical responses locally through scattering by either metal or high-index dielectric nanoparticles. In such cases, the enhancement of the optical chirality density (and/or the CD signal), is achieved by considering the so-called surface-enhanced approaches [240,312], which essentially rely on the interference between the incident and the scattered EM fields. This leads to enhancements of the electric and magnetic fields that increase the optical chirality density, but only within relative small active regions. In most of these cases (if not all), the external source of excitation are generally considered to be freely propagating plane waves. Our two contributions on this matter ultimately show that it is possible to achieve a global enhancement of the chiroptical interactions by directly engineering the optical behavior of materials (setting the operational bandwidth around the anomalous dispersion region), and that this could be perfectly attainable in integrated platforms.

The following original contribution highlights the main insights concerning the second part of this thesis. In particular, it mainly focuses on results from the former work (PAPER C), referring to a theoretical generalization of the optical chirality for any arbitrary optical medium.

PAPER F

Optics in 2018: Generalizing Optical Chirality to an Arbitrary Medium

Opt. Photonics News 29, 39 (2018)

Generalizing Optical Chirality to an Arbitrary Medium

J. Enrique Vázquez-Lozano and Alejandro Martínez

Nanophotonics Technology Center, Universitat Politècnica de València, Camino de Vera s/n, 46022 Valencia, Spain

Chirality, the "handedness" or sense of twist seen in natural systems, is everywhere–from organic molecules such as sugars or proteins, to the shapes traced out by spiral galaxies. Not only physical objects but also electromagnetic waves can exhibit chirality; this fundamental property of light was originally proposed in 2010 as a measure of the handedness, or knottedness, of the streamlines describing optical fields in free space [1]. Shortly thereafter, chirality was used in circular-dichroism spectroscopic measurements for the experimental detection and characterization of chiral biomolecules [2], thus confirming its physical significance and feasibility for practical applications such as drug development.

The occurrence of strong optical chirality relies on the complexity of the electromagnetic-field distribution. Metallic nanostructures have been regarded as the best-suited platforms for investigating chiroptical effects, and recent advances in nanofabrication have resulted in nanostructured metamaterials and plasmonic system that tremendously boost chiral light-matter interactions. Surprisingly, however, the chiral medium's contributions to dispersion and dissipation have mostly been ignored. Instead, the original definition derived for vacuum is commonly applied [1], even when its applicability is highly questionable.

Motivated by recent theoretical results regarding the conservation laws of several dynamic properties in dispersive and lossless media [3,4], we have generalized optical chirality, extending it to include the medium's dissipative effects as well [5]. We first examined the most complete form of the conservation law for the optical chirality, without any restrictions on the nature of the medium. Then, taking into account the underlying mathematical structure of the continuity equation, we were able to identify a general expression for the optical chirality density both in lossless and lossy dispersive media.

We found that both approaches yield similar results, but that they differ significantly in spectral regions with high absorption and anomalous dispersion. This fact should be carefully accounted for and examined in experiments considering chiroptical interaction between light and metamaterials or plasmonic systems.

Chirality occupies increasing importance not only in optics and nanophotonics, but also for the much broader world of physics, chemistry and biology. We believe that our findings may pave the way for the development of advanced chiroptical applications, such as enhanced enantioselectivity and the detection and characterization of chiral biomolecules in lossy dispersive media.

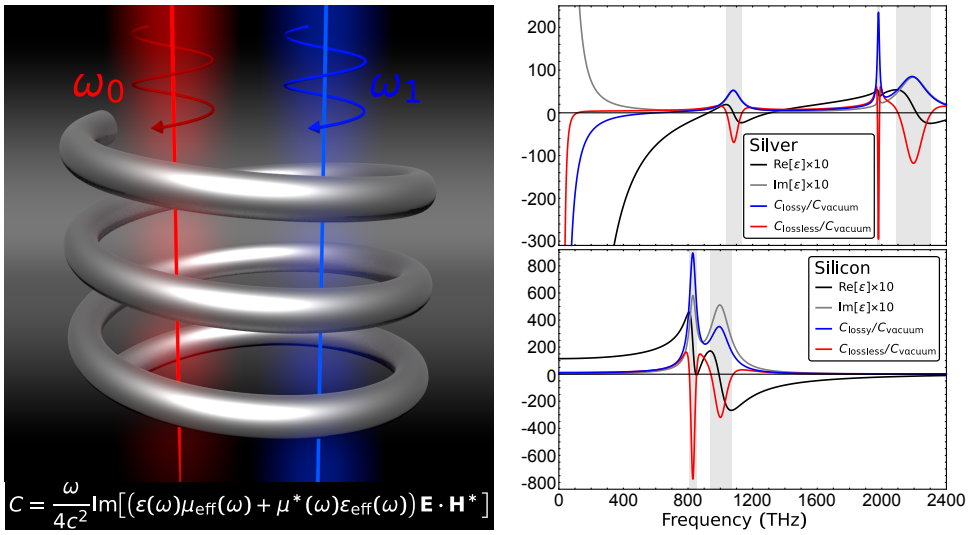

Figure F.1: Left: Conceptual illustration of optical chirality through a lossy dispersive medium. Right: Comparison of dispersion-dependent optical chirality density for silver and silicon, assuming lossless and lossy dispersive media. Anomalous dispersion spectral ranges are shaded for clarity.

References

[1] Y. Tang and A. E. Cohen, *Optical chirality and its interaction with matter*, Phys. Rev. Lett. **104**, 163901 (2010).

[2] E. Hendry, T. Carpy, J. Johnston, M. Popland, R. V. Mikhaylovskiy, A. J. Lapthorn, S. M. Kelly, L. D. Barron, N. Gadegaard, and M. Kadodwala, *Ultrasensitive detection and characterization of biomolecules using superchiral fields*, Nat. Nanotechnol. **5**, 783 (2010).

[3] K. Y. Bliokh, A. Y. Bekshaev, and F. Nori, *Optical momentum, spin, and angular momentum in dispersive media*, Phys. Rev. Lett. **119**, 073901 (2017).

[4] F. Alpeggiani, K. Y. Bliokh, F. Nori, and L. Kuipers, *Electromagnetic helicity in complex media*, Phys. Rev. Lett. **120**, 243605 (2018).

[5] J. E. Vázquez-Lozano and A. Martínez, *Optical chirality in dispersive and lossy media*, Phys. Rev. Lett. **121**, 043901 (2018).

Chapter 8

Conclusions and Outlook

Yes, yes, I see it; a huge social activity, a powerful civilization, a lot of science, a lot of art, a lot of industry, a lot of morality, and then, when we have filled the world with industrial wonders, with large factories, with paths, with museums, with libraries, we will fall down exhausted near all this, and it will be, for whom? Was man made for science or science made for man?

Miguel de Unamuno – Tragic Sense of Life

8.I Main Conclusions

First and foremost, this thesis comes to stand out the high value of wondering over and over again about the very basic fundamentals, thereby putting the emphasis into the suitability of the posited questions in addition on the own outcomes*. This is somehow in line with the insights outlined at the beginning of the introduction chapter, spotlighting the importance of looking further into the bottom. Besides being enlightening and enrichening, such a stance is highly appropriate at the very beginning stages of a research career (such as they actually are the doctoral studies), as it also confers to it an additional pedagogical value. Indeed, regardless of the specific matter that one may have in hand (and irrespective of whether it could be either theoretical or experimental), an approach focusing on the very basics would allow one to set down a solid and self-consistent background on which to underpin, build up, and inspire further research in future stages.

Customarily, reaching a comprehensive understanding of a given matter, whatever it is, sometimes does require to reconsider it again and again. Eventually, a more in-depth analysis might also involve a thorough and careful review of early works, which frequently include some assumptions or key details that, by any reason, might have been unnoticed. Even so, it very often happens that the most basic foundations turn out

*In order not to be misunderstood on this consideration, let me clarify that, of course, and in any case, the outcomes are really the pursued goal. However, by this statement, the intention is to underline the high value that in themselves may have the "well-formulated" questions, and the hard task of searching for and finding them. This is indeed something that, although sometimes appears to be somewhat underrated, is really essential when aiming to undergo a sound research work.

to be either disregarded or simply obviated, as if they really were an absolute truth. Obviously, this reflection goes beyond the routinely prospecting task aiming to find out the precise way to conduct a specific calculation, development, or realization, that may rely upon certain fundamentals to address a particular issue. By this, I actually mean to refer to the search of general and far-reaching responses to original groundbreaking questions, so that they may lead to the introduction of new paradigms, approaches, or even to an integral overhaul of a given matter. In this regard, I would venture to claim that, broadly, and only with few exceptions, there seems to be a sort of generalized reticence to dig deeper into the ground of the very basic fundamentals. Almost in all likelihood, these misgivings may be due to one (or a linear combination) of the following lingering hesitations, namely, about whether the matter under consideration could has already been undertaken, whether it actually has actual relevance on the current scientific landscape, whether it could lead to enough satisfactory conclusions, and very especially, as for the possible applications to which it could give rise in short term. Indeed, quite often one tends to think that if a matter looks either too basic or evident (as might be thought to be the fundamentals), it should be something that either it has already been solved (or, at least, addressed), it is irrelevant (or rather trivial), meaningless, or is simply useless from a practical standpoint[†]. Yet, it does not need to look far to find examples underscoring that this does not have to be necessarily so at all (at least not always). In fact, already within the context of nanophotonics there is a considerable number of cases showing it. In a very clear manner (but not limiting to these), one can find the daring proposal by Veselago of considering media with negative refractive index (something that *a priori* should be a nonsense); the *Abraham-Minkowski dilemma*, illustrating that there may still be a controversial discussion around a longstanding concept such as the linear momentum (something that might seem quite trivial); or the own revisitation of the Lipkin's work by Tang and Cohen, that finally led to endow the *zilches* of the electromagnetic field with a worthwhile physical meaning (something that at first was regarded as futile), thus giving rise to what we now know as the optical chirality.

From a humbler perspective and pursuing much more modest goals than those just sketched out in the above examples, throughout this thesis, and very especially in the works dealing with fundamental aspects, we have embraced this approach of raising basic issues such that may bring forth general outcomes; in this case, as far as the spin-dependent optical phenomena are concerned. Specifically, regarding the SOI of light, from the simple question of why it is a phenomenon that may only occur at the nanoscale (a feature that has been widely obviated), we have generalized completely one of the most insightful examples of SOI-based effects: the spin-controlled unidirectional excitation. On the other hand, the subtle realization that the optical chirality was being systematically considered improperly, or at least, incompletely (disregarding dispersion and absorption), led us to work out a theoretical generalization so that it could be applied to any arbitrary medium. On this basis, we were able to adequately investigate the feasibility of generating and conveying chiral light through integrated photonic platforms as well as its potential for applications.

[†]These have certainly been the major internal struggles I have had to face all these years of research.

In a little more detailed manner, and by way of a final overview, here below we recapitulate the main results of this dissertation (paper by paper), in connection with the objectives outlined at the end of the introduction chapter:

- The aim of PAPER A has consisted in linking analytically the optical SOI with the nanoscale. In the light of what can be found in the existing literature on this topic, such a link is a characteristic feature that, even though has been widely assumed, it has not been rigorously demonstrated[‡]. In this respect, our work provides a suitable theoretical framework able to explain the main features of intrinsic SOI of light. This is essentially performed just by taking into account the so-called *factorizability* (or *separability*) *condition*, which accounts for the mutual influence between the state of polarization (*spin*) and the propagation (*orbit*) of light[§]. In accordance with such a condition, and building upon an analytical approach based on the formalism of the vector spherical wave functions, we unravel the existence of a term, referred to as the *SOI-term*, that prevents such a factorization and bears out a number of dynamical characteristics underlying the occurrence of SOI of light at the nanoscale. Despite its simplicity, our analytical treatment gathers together the overall prescriptions of optical SOI, showing that it is a phenomenon that naturally arises from the fundamental properties of Maxwell's equations and that necessarily appears at subwavelength distances. Besides allowing us to gain further insights about the mechanism that leads to its classical emergence at the nanoscale, the acquired knowledge can be used to unveil how to enhance its occurrence and facilitate the observation of its stemming effects, which, inherently, turn out very weak. Concretely, our study suggests that the manifestation of SOI-based effects will become easier and sharper the higher is the multipolar order of the optical field.

- On the basis of the outcomes drawn from the above work, the purpose of PAPER B (and its Supplemental Material) has been twofold. The first and most evident was to show explicitly both the validity and the soundness of the conclusion described just above, i.e., the ease for yielding and/or observing SOI-based effects. To this end, we focused on the *spin-controlled unidirectional excitation*, an effect that, in turn, relies on the *spin-momentum locking*[¶]. Thus far, most of the contributions (either theoretical or experimental) on these matters have been limited to deal with dipolar sources (electric, magnetic, or a linear combination of them), so just by considering the quadrupole would have been sufficient to accomplish our goal. Notwithstanding the foregoing, and for the sake of completeness, we decided to go a step further raising a second aim: to develop a general and systematic theoretical formulation to extend the near-field directionality beyond the dipole approximation, namely, to electromagnetic multipole fields of arbitrary order.

[‡]At most, we found out some qualitative arguments claiming to identify and explain the emergence of SOI of light from its effects (e.g., by means of an interplay between the angular momenta contributions).

[§]It is worth pointing out that such a factorizability condition was indeed the key point to carry out this work, and, strikingly, it was already brought up in the seminal paper [63] (right at the second paragraph!).

[¶]Therefore, it can ultimately be interpreted as a manifestation of the *quantum spin Hall effect of light*.

This was carried out from an approach based on the *angular spectrum* (or *momentum*) *representation*, which combines a relative mathematical simplicity with a valuable physical intuition. Specifically, we derive an analytical and closed expression for the angular spectra of multipole fields of any higher order, which, in a way, can be regarded as a generalization of *Weyl's identity*. From this main result, we look into the spin-dependent near-field directional coupling (or excitation), and show that, indeed, higher-order multipoles bring forward the following advantages:

- Longer spatial range for the near-field directional coupling;
- Enhanced contrast ratio between guided modes coupled to opposite directions;
- Increased number of degrees of freedom.

Hence, besides relaxing the proximity condition, the full consideration of higher-order multipole moments gives flexibility and robustness, which ultimately translates into a higher coupling efficiency. Noteworthily, all these features are considerably enhanced as higher multipole orders are considered. Furthermore, the final results are presented in a ready-to-use form[‖], thus allowing for a direct and easy way to analytically design nanoscale optical sources. This enables a considerable advance toward a full control of spin-dependent near-field directionality, and opens up interesting perspectives for engineering light-matter interactions in nanophotonics and quantum optics.

- On another front, the aim of PAPER C (and its Supplemental Material) has been to provide a generalization of the optical chirality that accounts for both the effects of material dispersion as well as the absorption losses. Such considerations have mostly been disregarded, and it is indeed a common practice to apply the definition originally introduced for optical fields in vacuum to any kind of medium, even when its applicability can be highly questionable. This is the case of plasmonic structures and metamaterials (often regarded as the paradigmatic examples of dispersive and lossy media), which are customarily being used as the mainstream platforms for enhancing the chiroptical interactions[**]. Motivated by this practical need, and inspired by the latest theoretical generalizations of other dynamical properties to dispersive and lossless media, we carry out the corresponding re-derivation for the optical chirality, extending it so as to include dissipative effects as well. For simplicity, as well as for constructiveness, we elaborate our treatment upon the basis of the most complete form of the corresponding conservation law for the optical chirality. Specifically, in order to obtain the general expression for the optical chirality density, both in lossless and lossy dispersive media, we simply look into the underlying mathematical structure of the continuity equation. Likewise, for the lossy case, the analysis is to be carefully performed considering the dynamic equation of the polarization and the magnetization fields, which are given by the Drude-Lorentz model. Despite being a

[‖] We provide an applet to compute and display directly the angular spectra of arbitrary multipole fields. It is available online at https://doi.org/10.5281/zenodo.2677908.

[**] More recently, assemblies of high-index dielectric nanoparticles (or nanostructures), in very distinct geometries (or arrangements), are also being suggested as suitable systems to boost the near-field chirality.

particular characterization, such a multi-resonant model has proved to fit very well with experiments, being applicable to any frequency, bandwidth, and medium. Thus, it can be considered as completely general, and, consequently, the resulting expression for the optical chirality density too. Besides the inherent theoretical interest that in itself may have a general and closed formulation of a fundamental property (as it is a conserved quantity), this full description allows us to disclose the following features appearing in spectral regions with high absorption and anomalous dispersion:

  - There are important deviations between the optical chirality density obtained from the lossless (Brillouin's approach) and the lossy (Loudon's approach) cases;
  - The optical chirality density obtained from the lossy approach stays positive, while that obtained from the lossless approach may also draw negative values;
  - Peaks in the lossy approach coincide with the dips in the lossless one.

  According to this, there are additional aspects that, from now on, should be explicitly accounted for and carefully examined when analyzing chiral light-matter interactions.

- Finally, and completely independently from the above work, the goal of PAPER D has been to investigate the existence of enhanced optical chirality in integrated photonic platforms, as well as assessing its potential to perform chiroptical applications such as chiral sensing and spectroscopy. Despite the enormous attention that is lately engaging the research on this matter, thus far, most of the practical approaches are being conducted by means of free-space illumination and detection schemes, involving very sophisticated and sensitive arrangements. In this respect, our integrated proposal has a twofold purpose: to show the feasibility of realizing chiroptical applications in integrated platforms, so as to follow the trend toward the miniaturization and integration of photonic devices, and pursue setups more robust and simpler to fabricate. In contrast to all our previous works, this study has been carried out by numerical means. Specifically, by considering common guiding structures used in nanophotonics (the strip and slot waveguides), and, for simplicity, a single metallic nanohelix acting as a chiral sample (which, for constructiveness, is first modeled as a PEC, so that the interaction is only due to the geometrical aspects), we simulated two configurations, referred to as the *in-gap* and the *on-top configurations*. After that, we moved on to explore further considerations toward more realistic and/or improved scenarios: considering a silver made helix; looking into the *slotted configuration*; and examining the consequences of breaking the C_4 rotational symmetry of the waveguide. For each configuration, we obtained the transmission spectra, which display a very well localized chiral-like resonance, that, in turn, translates into a peak in the dissymmetry factor. According to the results, the performance of the integrated approach is comparable (and even better) to that of free-space setups, retaining many important features for practical purposes (enantiopure enhancement, tunability, switchability, and spatial accessibility), along with the following benefits: low-cost and mass-volume production, portability, and CMOS compatibility, among others. Therefore, this work allows us to suggest the

possibility of expanding the current palette of applications in integrated platforms by implementing chiroptical interactions, thus providing a good starting point that lays the groundwork for further research in this direction.

8.II Future Work

In a direct manner, this thesis has merely allowed us to respond to a few issues (in a way, it could be said that they are exactly four, one for each original contribution) whose main implications has just been summarized above. Notwithstanding, given the generality of the global approach, the accomplishments presented in this dissertation leave open the door for further interesting research directions, not only for going forward, but also for reconsidering and reexamining previously well-established statements in order to check their validity as well as their accuracy. Here below we provide a short list briefly describing some of the matters that might (and should) be undertaken in short (or mid) term:

- It is well known that, both in electronics and photonics, SOI of light is underpinned by the geometric (*Pancharatnam-Berry*) phases [93, 94]. In fact, such a formalism has been proven to be very useful for controlling the spin dynamics and, therefore, for guiding light [313]. In this regard, it would be insightful to identify such a geometric phase contribution within the analytical framework developed for understanding the classical emergence of intrinsic SOI of light, and explore its possibilities, e.g., toward an optical analogue to the spin-dependent topological phase transitions [314, 315].

- It has been demonstrated that the spin-momentum locking is a phenomenon universal to evanescent waves [101, 103]. From Eq. (A.15), it could be envisaged an extension for propagating waves. Thus, looking further into this outcome may be quite enlightening, and shed new light upon the physics underlying this intriguing feature.

- Regarding the spin-dependent near-field directionality, the use of circularly polarized dipoles affords two possibilities for coupling: to the right or to the left [102, 132, 133]. In the light of the extra versatility provided by the consideration of higher-order multipole moments, it could be foreseen a rather straight upgrade of such a phenomenon so as to achieve a kind of spin-controlled (coherent) multidirectional excitation (coupling), which could be very useful toward the realization of all-optical SOI-based logic gates. In this same line, it would still remain to numerically (and/or experimentally) check our analytical results by considering realistic bulky scatterers, as well as to extend the recently introduced approach for engineering the near-field directionality to higher-order multipole fields [316].

- Overall, it should be convenient to reconsider many of the previous works on optical chirality to account for (and/or identify) the contribution due to dispersion and/or absorption losses. In this respect, it could be found, e.g., statements claiming that «*the optical chirality for a plane wave SPP is strictly zero*» since $\mathbf{H}^* \cdot \mathbf{E} = 0$ [82, 274]. Yet, the new general expression [Eq. (C.17)] predicts that it is possible a nonzero value (due to the material dispersion). This deserves further and careful investigation.

- The fundamental result of the original paper by Tang and Cohen [64] concerns the analytical relationship between optical chirality density (an abstract concept) with the dissymmetry factor (a measurable quantity). According to their treatment, such a proportionality (by the way, very contested on account of its unbounded character [173]) relies on a derivation constrained to the dipole approximation. It could be quite enlightening to extend such a treatment to higher-order multipole moments in order to check whether such a relation still holds, or conversely, there appear other terms (that, at any rate, would lead to enrich the underlying physics).

- There is a controversial debate around the meaningfulness and the differences between the helicity and the optical chirality [187, 309–311]. In this regard, it is certainly striking to note that the optical chirality is a local dynamical property defined in terms of the fields, whereas its underlying symmetry lies on the potentials. Conversely, the helicity is given in terms of the potentials, and its symmetry (referred to as the duality symmetry [317, 318]) involves the fields [190, 319]. Likely, this cross-correlation may entail and/or disclose fundamental features regarding such a distinction, and it is quite possible that a complete approach relying upon the role played by the material absorption losses may shed some light on its resolution[††].

- Concerning the numerical research toward the realization of chiroptical applications in integrated platforms, next steps should be aimed at optimizing the arrangement and the dimensions, as well as at simplifying the measurement and enhancement schemes. In this vein, a configuration that is currently being investigated consists in a kind of integrated optical analog to the *Stern-Gerlach* [320, 321], in which the chirality under study is that of a sample which is illuminated by a linearly polarized light beam. In this case, the enantio-discrimination would be spatial-like (by means of a set of antennas placed in front at right and left sides), thus having the benefit of not requiring circular polarization; the chiral absorption of the circular component matching the chirality of the sample should produce an unbalanced angular momentum that would deflect the beam toward the corresponding side [322].

- For the sake of completeness, it would be worthwhile to extend this numerical study from the simple consideration of a single metallic chiral scatterer to a chiral medium (i.e., by implementing a chiral medium through the corresponding constitutive relations, e.g., those given by the *Born-Kuhn model* [260]). In this way, one could get a better assessment of its actual relevance in a more realistic experimental situation.

Even though it has not been mentioned, given that the entire work performed has been theoretical, a remaining background task is, of course, that relative to the experimental verification of each and every one of the matters discussed throughout this thesis.

[††]I admit that perhaps it may seem a nonsense but my conjecture at this respect is that, in the same way that in the Dirac formalism the chirality and the helicity are distinct quantities only for massive particles, their optical counterparts should be able to be distinguished only when including the presence of absorption losses (which would act as a sort of mass, or resistance, that yield dissipative effects).

8.III Concluding Remarks

Roughly speaking, the main contributions of this thesis can be summarized as follows: an analytical demonstration showing the universality of SOI of light as a phenomenon occurring at the nanoscale, two generalizations, concerning the spin-dependent near-field directionality (beyond the dipole approximation) and the optical chirality (for dispersive and lossy media), and the ascertainment of the viability for realizing chiroptical applications in integrated photonic platforms.

There is no contribution more important than another. Even if it is true that the fundamental work in PAPER A has been published in a rather modest journal (in comparison with the rest of the contributions), and it was quite contested on account of its seemingly triviality (as was pointed out by the reviewers), it was actually the work that paved the way to move on toward the interesting possibilities successfully accomplished in PAPER B, followed later by the highlight given in PAPER E. On the other side, with regard to the contributions on optical chirality the situation is quite similar, but with nuances. Once again, the fundamental contribution resulting in PAPER C was published in a journal with, objectively, lower impact factor than the applied-like study provided in PAPER D. Nonetheless, in this case it should be taken into account the extra allure of publishing in a journal of long-established prestige as it is *Physical Review Letters*, to what it should also be added the two acknowledgments by the Editors of APS and those of OSA, this latter finally resulting in PAPER F.

Besides the generality, it is also worth mentioning the analytical character of the obtained results (being also present throughout most of the developments carried out). In this regard, apart from the fact that generality and analyticity are notions closely tied to each other (in fact, it could be said that every general result is to be analytic, though not necessarily so the reverse), it is also important to underline that, except in the last study (performed by means of numerical simulations), by virtue of the analyticity, the entire work of this thesis would have been possible without needing to use any computational resource. Of course, and for obvious reasons (given the huge amount of derivatives and integrals to solve), we made use of computers and software of symbolic calculations (particularly, *Wolfram Mathematica*), but, in any case, the main resource has simply been the own reasoning; along with a blackboard (unfortunately, it was actually a whiteboard), and some (centi)liters of ink (which hopefully it would have been chalks).

Together with the generality and the analyticity, there is another last point that should not be disregarded: the importance that have had the focus on the subtleties; even though they may seem very trivial, or going against (or not following) the mainstream current. Indeed, each of these two stances has been, in a way, embraced in this thesis (mainly in the works about the fundamentals), and can essentially be regarded as the seeds that have fueled the aforementioned generalizations. In this respect, I cannot refrain from noticing the importance of a thorough reading task (without obviating the earliest

works) for building a solid background. This is a triviality, I know, but still I would like to emphasize once again that a comprehensive reading procedure has been crucial for the realization of this thesis. Certainly, it was thank to this that we could readily find the factorizability condition (set out at the beginning of the seminal paper on optical SOI), and realize that a generalization of the optical chirality was a must (as may be indirectly guessed from the original work putting forward this quantity). Likewise, it should be noted that justly the only attempt with a view to minimizing this endeavor of reading turned out to be a failure. I am referring to the work concerning the generalization of the Weyl's identity, wherein we realized that such a formula had already been found out, but practically at the end of the investigation, so we had to restructure the original aim of the work. This fact straightforwardly reflects the enormous benefit (regarding the time expended vs. the quality of the work) that actually provides an intensive and extensive reading process, and even more at the first stages of a research career. In this sense, it comes to my mind the following quotation by Zeno of Citium: «*We have two ears and one mouth, therefore we should listen twice as much as we speak*», what it could (and should) be readily adapted to the scientific reading/writing process.

Finally, and to wrap up, one final remark. We are currently living in a time of exacerbated production, consumerism, and hurry. Unfortunately, this is also impinging on science. In fact, the scientific activity is lately being enveloped by the lush backdrop of publishing as much and as rapid as possible, by all means in journals with impact as high as possible, and, to a great extent, focusing on values such as the usefulness and the applicability. Certainly, and this is purely a personal opinion, such stances (which, by the way, seem to be on the increase) are, in my view, rather detrimental, both at individual level and (perhaps even more importantly) for the overall scientific advancement; undermining the creativity and jeopardizing (at long-term) the strengthening of an analytical and critical thinking. This is merely an observation referred to a general trend that I have been noticing for some time now, and, ultimately, herein serves to me to reinforce the claim as for the importance of working out a general, sound, and far-reaching research work, without having to be worried beforehand about what will be the applications that may arise, or the specific journal at which to aspire. Definitely, science can be undertaken in many ways, but, I believe that, in these accelerated times, it would be very healthy to halt, take perspective, and reconsider stances such as the ones encouraged by Feynman at the end of his lecture 'Plenty of Room':

> «*Now, you might say, "Who should do this and why should they do it?" Well, I pointed out a few of the economic applications, but I know that the reason that you would do it might be just for fun. But have some fun!*».

Author's Merits

Journal Papers

Main Contributions:

[PAPER A] **J. E. Vázquez-Lozano** and A. Martínez, "Classical emergence of intrinsic spin-orbit interaction of light at the nanoscale," Physical Review A **97**(3), 033804 (2018).

[PAPER B] **J. E. Vázquez-Lozano**, A. Martínez, and F. J. Rodríguez-Fortuño, "Near-Field Directionality Beyond the Dipole Approximation: Electric Quadrupole and Higher-Order Multipole Angular Spectra," Physical Review Applied **12**(2), 024065 (2019).

[PAPER C] **J. E. Vázquez-Lozano** and A. Martínez, "Optical Chirality in Dispersive and Lossy Media," Physical Review Letters **121**(4), 043901 (2018).
[*Highlighted as Editors' Suggestion*]

[PAPER D] **J. E. Vázquez-Lozano** and A. Martínez, "Toward Chiral Sensing and Spectroscopy Enabled by All-Dielectric Integrated Photonic Waveguides," Laser & Photonics Reviews **14**(9), 1900422 (2020).
[*Featured on the Back Cover, September 2020*]

Highlights:

[PAPER E] **J. E. Vázquez-Lozano**, M. F. Picardi, A. V. Zayats, F. J. Rodríguez-Fortuño, and A. Martínez, "Optics in 2019: Near-Field Unidirectional Excitation . . . and Beyond," Optics & Photonics News **30**(12), 58 (2019).

[PAPER F] **J. E. Vázquez-Lozano** and A. Martínez, "Optics in 2018: Generalizing Optical Chirality to an Arbitrary Medium," Optics & Photonics News **29**(12), 39 (2018).

Other Contributions:

[PAPER 7] **J. E. Vázquez-Lozano**, A. Cordero, and J. R. Torregrosa, "Dynamical analysis on cubic polynomials of Damped Traub's method for approximating multiple roots," Applied Mathematics and Computation **328**, 82 (2018).

[PAPER 8] **J. E. Vázquez-Lozano** and A. Martínez, "Enhanced Excitation and Readout of Plasmonic Cavity Modes in NPoM via SiN Waveguides for On-Chip SERS." (To be submitted, 2021).

Book chapters

[BOOK 1] **J. E. Vázquez-Lozano** and A. Martínez, "Chapter 13: Theoretical Generalization of the Optical Chirality to Arbitrary Optical Media," *Chirality, Magnetism and Magnetoelectricity: Separate Phenomena and Joint Effects in Metamaterial Structures*, (Springer, 2021). Editor: E.O. Kamenetskii; ISBN: 978-3-030-62843-7.

Conferences

Poster Contributions:

[POSTER 1] **J. E. Vázquez-Lozano** and A. Martínez, "Spin-dependent light interference," in *Conferencia Española de Nanofotónica* (2016) [CEN-2016]. Valencia, Spain.

[POSTER 2] **J. E. Vázquez-Lozano** and A. Martínez, "Intrinsic emergence of optical spin-orbit interaction at the nanoscale," in *Nanophotonics and Micro/Nano Optics International Conference* (2017) [NANOP-2017]. Barcelona, Spain.

[POSTER 3] **J. E. Vázquez-Lozano** and A. Martínez, "Chiroptical applications enabled by integrated photonic waveguides," in *22nd European Conference on Integrated Optics* (2020) [ECIO'2020]. Paris, France [ONLINE].

Oral Contributions:

[ORAL 1] **J. E. Vázquez-Lozano** and A. Martínez, "Intrinsic spin-orbit coupling of light at the nanoscale in free space," in *11th International Congress on Engineered Material Platforms for Novel Wave Phenomena* (2017) [Metamaterials'2017]. Marseille, France.

[ORAL 2] **J. E. Vázquez-Lozano** and A. Martínez, "Optical chirality in dispersive media," in *Conferencia Española de Nanofotónica* (2018) [CEN-2018]. Donostia-San Sebastián, Spain.

[ORAL 3] **J. E. Vázquez-Lozano** and A. Martínez, "Chiral properties of light in dispersive media," in *27th Annual International Conference on Composites/Nano Engineering* (2019) [ICCE-27]. Granada, Spain.

[ORAL 4] **J. E. Vázquez-Lozano** and A. Martínez, "Towards integrated chiroptical applications," in *14th International Congress on Artificial Materials for Novel Wave Phenomena* (2020) [Metamaterials'2020]. New York, USA [ONLINE].

Invited Contributions:

[INVITED 1] **J. E. Vázquez-Lozano** and A. Martínez, "Generalization of the optical chirality to arbitrary media," in *10th International Conference on Metamaterials, Photonic Crystals and Plasmonics* (2019) [META-2019]. Lisbon, Portugal.
[*Special Symposium IV: Chirality, magnetism, and magnetoelectricity*]

[INVITED 2] **J. E. Vázquez-Lozano** and A. Martínez, "Chiral properties of light in material systems," in *13th International Congress on Artificial Materials for Novel Wave Phenomena* (2019) [Metamaterials'2019]. Rome, Italy.
[*Special Session: Physical Review Journals Symposium*]

Other Contributions:

[OTHER 1] **J. E. Vázquez-Lozano**, "Optical chirality in dispersive media," in *Physics at the Nanoscale Seminars, Department of Physics, King's College London* (2018). London, UK.

[OTHER 2] **J. E. Vázquez-Lozano**, "Recent progress in spin-based photonic effects occurring at the nanoscale: spin-orbit interaction of light, near-field directionality and optical chirality in arbitrary media," in *Workshop on Geometric Resources for Quantum Engineering* (2020). Sevilla, Spain.

[OTHER 3] A. Martínez and **J. E. Vázquez-Lozano**, "Chiroptical applications enabled by all-dielectric integrated photonic waveguides," in *Photonics Online Meetup* (2020) [#POM20ju]. [ONLINE].

Other Research Activities:

Research Stays:

[STAY 1] King's College London, London, UK. Photonics & Nanotechnology Group (Department of Physics). Theoretical research on *spin-orbit coupling of light* (supervised by Dr Francisco J. Rodríguez-Fortuño). [01/10/2018 – 15/01/2019].

Reviewer:

[JOURNAL 1] Photonics Research;

[JOURNAL 2] Optics Letters;

[JOURNAL 3] Physics Letters A;

[JOURNAL 4] ACS Photonics;

[JOURNAL 5] Optics Express;

[JOURNAL 6] Nanomaterials (Reviewer Board Member).

Scientific Artwork:

[ARTWORK 1] Table-of-Contents (ToC) figure of PAPER B:

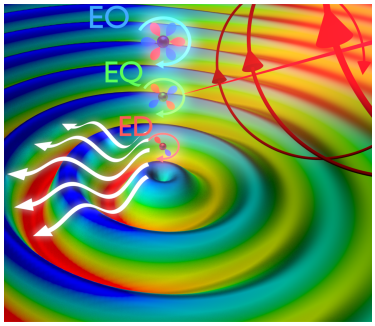

[ARTWORK 2] Table-of-Contents (ToC) figure of PAPER C:

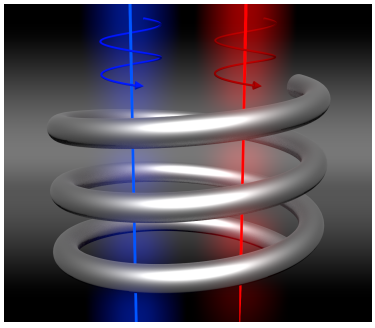

[ARTWORK 3] Table-of-Contents (ToC) figure of PAPER D:

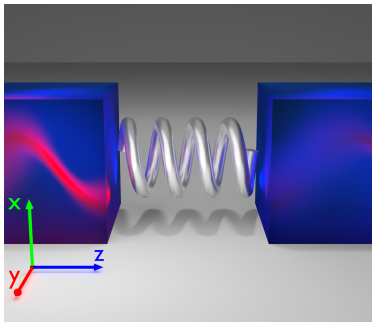

[ARTWORK 4] Outside Back Cover of the September 2020 issue of Laser & Photonics Reviews (Laser Photonics Rev. 14(9)/2020) highlighting PAPER D:

Bibliography

[1] G. Adesso, R. Lo Franco, and V. Parigi, *Foundations of quantum mechanics and their impact on contemporary society*, Phil. Trans. R. Soc. A **376**, 20180112 (2018).

[2] J. P. Dowling and G. J. Milburn, *Quantum technology: the second quantum revolution*, Phil. Trans. R. Soc. Lond. A **361**, 1655 (2003).

[3] R. P. Feynman, *There's plenty of room at the bottom*, Eng. Sci. **23**, 22 (1960).

[4] Editorial: *'Plenty of room' revisited*, Nat. Nanotechnol. **4**, 781 (2009).

[5] R. Jones, *Feynman's unfinished business*, Nat. Nanotechnol. **4**, 785 (2009).

[6] C. Toumey, *Plenty of room, plenty of history*, Nat. Nanotechnol. **4**, 783 (2009).

[7] P. Daukantas, *Still plenty of room at the bottom*, Opt. Photonics News **30**, 24 (2019).

[8] M. Segal, *Surely you're happy, Mr Feynman!*, Nat. Nanotechnol. **4**, 786 (2009).

[9] List of IEEE Milestones.

[10] K. v. Klitzing, G. Dorda, and M. Pepper, *New method for high-accuracy determination of the fine-structure constant based on quantized Hall resistance*, Phys. Rev. Lett. **45**, 494 (1980).

[11] G. E. Moore, *Cramming more components onto integrated circuits*, Proc. IEEE **86**, 82 (1998).

[12] M. M. Waldrop, *The chips are down for Moore's law*, Nature (London) **530**, 144 (2016).

[13] C. E. Leiserson, N. C. Thompson, J. S. Emer, B. C. Kuszmaul, B. W. Lampson, D. Sanchez, and T. B. Schardl, *There's plenty of room at the Top: What will drive computer performance after Moore's law?*, Science **368**, eaam9744 (2020).

[14] E. Gerstner, *Information in a spin*, Nat. Phys. **4**, S18 (2008).

[15] F. Pulizzi, *The rise of semiconductor spintronics*, Nat. Phys. **4**, S20 (2008).

[16] J. Heber, *A giant leap for electronics*, Nat. Phys. **4**, S16 (2008).

[17] S. Datta and B. Das, *Electronic analog of the electro-optic modulator*, Appl. Phys. Lett. **56**, 665 (1990).

[18] S. Datta, *How we proposed the spin transistor*, Nat. Electron. **1**, 604 (2018).

[19] D. D. Awschalom and M. E.. Flatté, *Challenges for semiconductor spintronics*, Nat. Phys. **3**, 153 (2007).

[20] B. Dieny, I. L. Prejbeanu, K. Garello, P. Gambardella, P. Freitas, R. Lehndorff, W. Raberg, U. Ebels, S. O. Demokritov, J. Akerman, A. Deac, P. Pirro, C. Adelmann, A. Anane, A. V. Chumak, A. Hirohata, S. Mangin, S. O. Valenzuela, M. C. Onbasli, M. d'Aquino, G. Prenat, G. Finocchio, L. Lopez-Diaz, R. Chantrell, O. Chubykalo-Fesenko, and P. Bortolotti, *Opportunities and challenges for spintronics in the microelectronics industry*, Nat. Electron. **3**, 446 (2020).

[21] A. Manchon, H. C. Koo, J. Nitta, S. M. Frolov, and R. A. Duine, *New perspectives for Rashba spin-orbit coupling*, Nat. Mater. **14**, 871 (2015).

[22] R. Kirchain and L. Kimerling, *A roadmap for nanophotonics*, Nat. Photonics **1**, 303 (2007).

[23] D. Thomson, A. Zilkie, J. E. Bowers, T. Komljenovic, G. T. Reed, L. Vivien, D. Marris-Morini, E. Cassan, L. Virot, J.-M. Fédéli, J.-M. Hartmann, J. H. Schmid, D.-X. Xu, F. Boeuf, P. O'Brien, G. Z. Mashanovich, and M. Nedeljkovic, *Roadmap on silicon photonics*, J. Opt. **18**, 073003 (2016).

[24] R. A. Soref and J. P. Lorenzo, *Single-crystal silicon: a new material for 1.3 and 1.6 μm integrated-optical components*, Electron. Lett. **21**, 953 (1985).

[25] E. Ozbay, *Plasmonics: Merging photonics and electronics at nanoscale dimensions*, Science **311**, 189 (2006).

[26] D. Pile, *Small and beautiful*, Nat. Mater. **9**, S18 (2010).

[27] W. L. Barnes, A. Dereux, and T. W. Ebbesen, *Surface plasmon subwavelength optics*, Nature (London) **424**, 824 (2003).

[28] D. K. Gramotnev and S. I. Bozhevolnyi, *Plasmonics beyond the diffraction limit*, Nat. Photonics **4**, 83 (2010).

[29] J. A. Schuller, E. S. Barnard, W. Cai, Y. C. Jun, J. S. White, and M. L. Brongersma, *Plasmonics for extreme light concentration and manipulation*, Nat. Mater. **9**, 193 (2010).

[30] T. J. Davis, D. E. Gómez, and A. Roberts, *Plasmonic circuits for manipulating optical information*, Nanophotonics **6**, 543 (2017).

[31] M. L. Brongersma and V. M. Shalaev, *The case for plasmonics*, Science **328**, 440 (2010).

[32] F. J. Rodríguez-Fortuño, A. Espinosa-Soria, and A. Martínez, *Exploiting metamaterials, plasmonics and nanoantennas concepts in silicon photonics*, J. Opt. **18**, 123001 (2016).

[33] S. V. Boriskina, T. A. Cooper, L. Zeng, G. Ni, J. K. Tong, Y. Tsurimaki, Y. Huang, L. Meroueh, G. Mahan, and G. Chen, *Losses in plasmonics: from mitigating energy dissipation to embracing loss-enabled functionalities*, Adv. Opt. Photon. **9**, 775 (2017).

[34] J. B. Khurgin, *How to deal with the loss in plasmonics and metamaterials*, Nat. Nanotechnol. **10**, 2 (2015).

[35] C. Caloz, A. Alù, S. Tretyakov, D. Sounas, K. Achouri, and Z.-L. Deck-Léger, *Electromagnetic nonreciprocity*, Phys. Rev. Applied **10**, 047001 (2018).

[36] A. B. Khanikaev, N. Arju, Z. Fan, D. Purtseladze, F. Lu, J. Lee, P. Sarriugarte, M. Schnell, R. Hillenbrand, M. A. Belkin, and G. Shvets, *Experimental demonstration of the microscopic origin of circular dichroism in two-dimensional metamaterials*, Nat. Commun. **7**, 12045 (2016).

[37] N. I. Zheludev, *The road ahead for metamaterials*, Science **328**, 582 (2010).

[38] J. Heber, *The masters of light*, Nat. Mater. **9**, S19 (2010).

[39] A. Sihvola, *Metamaterials in electromagnetics*, Metamaterials **1**, 2 (2007).

[40] N. I. Zheludev, *Obtaining optical properties on demand*, Science **348**, 973 (2015).

[41] V. G. Veselago, *The electrodynamics of substances with simultaneously negative values of ϵ and μ*, Sov. Phys. Usp. **10**, 509 (1968).

[42] V. G. Veselago and E. E. Narimanov, *The left hand of brightness: past, present and future of negative index materials*, Nat. Mater. **5**, 759 (2006).

[43] K. L. Tsakmakidis, A. D. Boardman, and O. Hess, *'Trapped rainbow' storage of light in metamaterials*, Nature (London) **450**, 397 (2007).

[44] U. Leonhardt and T. G. Philbin, *Quantum levitation by left-handed metamaterials*, New J. Phys. **9**, 254 (2007).

[45] J. B. Pendry, *Negative refraction makes a perfect lens*, Phys. Rev. Lett. **85**, 3966 (2000).

[46] R. A. Shelby, D. R. Smith, and S. Schultz, *Experimental verification of a negative index of refraction*, Science **292**, 77 (2001).

[47] C. M. Soukoulis, S. Linden, M. Wegener, *Negative refractive index at optical wavelengths*, Science **315**, 47 (2007).

[48] C. M. Soukoulis and M. Wegener, *Past achievements and future challenges in the development of three-dimensional photonic metamaterials*, Nat. Photonics **5**, 523 (2011).

[49] N. Meinzer, W. L. Barnes, and I. R. Hooper, *Plasmonic meta-atoms and metasurfaces*, Nat. Photonics **8**, 889 (2014).

[50] M. Choi, S. H. Lee, Y. Kim, S. B.Kang, J. Shin, M. H. Kwak, K.-Y. Kang, Y.-H. Lee, N. Park, and B. Min, *A terahertz metamaterial with unnaturally high refractive index*, Nature (London) **470**, 369 (2011).

[51] I. Liberal and N. Engheta, *The rise of near-zero-index technologies*, Science **358**, 1540 (2017).

[52] U. Leonhardt, *Optical conformal mapping*, Science **312**, 1777 (2006).

[53] J. B. Pendry, D. Schurig, D. R. Smith, *Controlling electromagnetic fields*, Science **312**, 1780 (2006).

[54] A. Poddubny, I. Iorsh, P. Belov, and Y. S. Kivshar, *Hyperbolic metamaterials*, Nat. Photonics **7**, 948 (2013).

[55] N. Liu, H. Liu, S. Zhu, and H. Giessen, *Stereometamaterials*, Nat. Photonics **3**, 157 (2009).

[56] C. É. Kriegler, M. S. Rill, S. Linden, and M. Wegener, *Bianisotropic photonic metamaterials*, IEEE J. Sel. Top. Quantum Electron. **16**, 367 (2010).

[57] N. M. Litchinitse, *Structured light meets structured matter*, Science **337**, 1054 (2012).

[58] G. Yoon, I. Kim, and J. Rho, *Challenges in fabrication towards realization of practical metamaterials*, Microelectron. Eng. **163**, 7 (2016).

[59] N. I. Zheludev and Y. S. Kivshar, *From metamaterials to metadevices*, Nat. Mater. **11**, 917 (2012).

[60] R. Loudon, *The Quantum Theory of Light*, (Oxford University Press, Oxford, England, 2000).

[61] W. Vogel and D.-G. Welsch, *Quantum Optics*, (Wiley-VCH, Weinheim, 2006).

[62] A. Trabesinger, *Quantum light*, Nat. Mater. **9**, S12 (2010).

[63] V. S. Liberman and B. Y. Zel'dovich, *Spin-orbit interaction of a photon in an inhomogeneous medium*, Phys. Rev. A **46**, 5199 (1992).

[64] Y. Tang and A. E. Cohen, *Optical chirality and its interaction with matter*, Phys. Rev. Lett. **104**, 163901 (2010).

[65] A. Y. Elezzabi, *The dawn of spinplasmonics*, Nano Today **2**, 48 (2007).

[66] Y. Gorodetski, A. Niv, V. Kleiner, and E. Hasman, *Observation of the spin-based plasmonic effect in nanoscale structures*, Phys. Rev. Lett. **101**, 043903 (2008).

[67] T. V. Shahbazyan and M. I. Stockman, *Plasmonics: Theory and Applications* (Springer Netherlands, Dordrecht, 2013), Chap. 13.

[68] N. Shitrit, I. Yulevich, E. Maguid, D. Ozeri, D. Veksler, V. Kleiner, and E. Hasman, *Spin-optical metamaterial route to spin-controlled photonics*, Science **340**, 724 (2013).

[69] N. Shitrit, I. Yulevich, E. Maguid, D. Ozeri, D. Veksler, V. Kleiner, and E. Hasman, *Spinoptical metamaterials: A novel class of metasurfaces*, Opt. Photonics News **24**, 53 (2013).

[70] H. Mathur, *Thomas precession, spin-orbit interaction, and Berry's phase*, Phys. Rev. Lett. **67**, 3325 (1991).

[71] E. I. Rashba, *Spin-orbit coupling and spin transport*, Physica E **34**, 31 (2006).

[72] A. I. Akhiezer and V. B. Berestetskii, *Quantum Electrodynamics* (Interscience, New York, USA, 1965).

[73] S. A. Wolf, D. D. Awschalom, R. A. Buhrman, J. M. Daughton, S. von Molnár, M. L. Roukes, A. Y. Chtchelkanova, and D. M. Treger, *Spintronics: A spin-based electronics vision for the future*, Science **294**, 1488 (2001).

[74] F. J. Belinfante, *On the current and the density of the electric charge, the energy, the linear momentum and the angular momentum of arbitrary fields*, Physica (Utrecht) **7**, 449 (1940).

[75] D. L. Andrews and M. Babiker, *The Angular Momentum of Light* (Cambridge University Press, Cambridge, England, 2013).

[76] I. Bialynicki-Birula and Z. Bialynicka-Birula, *Canonical separation of angular momentum of light into its orbital and spin parts*, J. Opt. **13**, 064014 (2011).

[77] J. H. Poynting, *The wave motion of a revolving shaft, and a suggestion as to the angular momentum in a beam of circularly polarised light*, Proc. R. Soc. London A **82**, 560 (1909).

[78] L. Allen, M. W. Beijersbergen, R. J. C. Spreeuw, and J. P. Woerdman, *Orbital angular momentum of light and the transformation of Laguerre-Gaussian laser modes*, Phys. Rev. A **45**, 8185 (1992).

[79] K. Y. Bliokh, A. Y. Bekshaev, and F. Nori, *Dual electromagnetism: helicity, spin, momentum and angular momentum*, New J. Phys. **15**, 033026 (2013).

[80] S. M. Barnett, L. Allen, R. P. Cameron, C. R. Gilson, M. J. Padgett, F. C. Speirits, and A. M. Yao, *On the natures of the spin and orbital parts of optical angular momentum*, J. Opt. **18**, 064004 (2016).

[81] A. Aiello, P. Banzer, M. Neugebauer, and G. Leuchs, *From transverse angular momentum to photonic wheels*, Nat. Photonics **9**, 789 (2015).

[82] K. Y. Bliokh and F. Nori, *Transverse spin of a surface polariton*, Phys. Rev. A **85**, 061801 (2012).

[83] A. Y. Bekshaev, K. Y. Bliokh, and F. Nori, *Transverse spin and momentum in two-wave interference*, Phys. Rev. X **5**, 011039 (2015).

[84] M. Nieto-Vesperinas, *Optical torque: Electromagnetic spin and orbital-angular-momentum conservation laws and their significance*, Phys. Rev. A **92**, 043843 (2015).

[85] S. Abdulkareem and N. Kundikova, *Joint effect of polarization and the propagation path of a light beam on its intrinsic structure*, Opt. Express **24**, 19157 (2016).

[86] T. A. Nieminen, A. B. Stilgoe, N. R. Heckenberg, and H. Rubinsztein-Dunlop, *Angular momentum of a strongly focused Gaussian beam*, J. Opt. A **10**, 115005 (2008).

[87] E. Leader and C. Lorcé, *The angular momentum controversy: What's it all about and does it matter?*, Phys. Rep. **541**, 163 (2014).

[88] D. F. Nelson, *Momentum, pseudomomentum, and wave momentum: Toward resolving the Minkowski-Abraham controversy*, Phys. Rev. A **44**, 3985 (1991).

[89] S. M. Barnett, *Resolution of the Abraham-Minkowski dilemma*, Phys. Rev. Lett. **104**, 070401 (2010).

[90] K. Y. Bliokh, A. Y. Bekshaev, and F. Nori, *Optical momentum and angular momentum in complex media: from the Abraham-Minkowski debate to unusual properties of surface plasmon-polaritons*, New J. Phys. **19**, 123014 (2017).

[91] K. Y. Bliokh, A. Y. Bekshaev, and F. Nori, *Optical momentum, spin, and angular momentum in dispersive media*, Phys. Rev. Lett. **119**, 073901 (2017).

[92] M. G. Silveirinha, *Reexamination of the Abraham-Minkowski dilemma*, Phys. Rev. A **96**, 033831 (2017).

[93] F. Cardano and L. Marrucci, *Spin-orbit photonics*, Nat. Photonics **9**, 776 (2015).

[94] K. Y. Bliokh, F. J. Rodríguez-Fortuño, F. Nori, and A. V. Zayats, *Spin-orbit interactions of light*, Nat. Photonics **9**, 796 (2015).

[95] K. Y. Bliokh, M. A. Alonso, E. A. Ostrovskaya, and A. Aiello, *Angular momenta and spin-orbit interaction of nonparaxial light in free space*, Phys. Rev. A **82**, 063825 (2010).

[96] K. Y. Bliokh, *Geometrodynamics of polarized light: Berry phase and spin Hall effect in a gradient-index medium*, J. Opt. A **11**, 094009 (2009).

[97] M. Onoda, S. Murakami, and N. Nagaosa, *Hall effect of light*, Phys. Rev. Lett. **93**, 083901 (2004).

[98] D. Haefner, S. Sukhov, and A. Dogariu, *Spin Hall effect of light in spherical geometry*, Phys. Rev. Lett. **102**, 123903 (2009).

[99] K. Y. Bliokh, A. Y. Bekshaev, and F. Nori, *Extraordinary momentum and spin in evanescent waves*, Nat. Commun. **5**, 3300 (2014).

[100] A. B. Khanikaev, S. H. Mousavi, W.-K. Tse, M. Kargarian, A. H. MacDonald, and G. Shvets, *Photonic topological insulators*, Nat. Mater. **12**, 233 (2013).

[101] T. Van Mechelen and Z. Jacob, *Universal spin-momentum locking of evanescent waves*, Optica **3**, 118 (2016).

[102] F. J. Rodríguez-Fortuño, G. Marino, P. Ginzburg, D. O'Connor, A. Martínez, G. A. Wurtz, and A. V. Zayats, *Near-field interference for the unidirectional excitation of electromagnetic guided modes*, Science **340**, 328 (2013).

[103] K. Y. Bliokh, D. Smirnova, and F. Nori, *Quantum spin Hall effect of light*, Science **348**, 1448 (2015).

[104] L. Novotny and B. Hecht, *Principles of Nano-Optics* (Cambridge University Press, Cambridge, England, 2012).

[105] J. D. Jackson, *Classical Electrodynamics* (Wiley, New York, USA, 1998).

[106] M. Born and E. Wolf, *Principles of Optics* (Pergamon, New York, USA, 2005).

[107] I. Fernandez-Corbaton, X. Zambrana-Puyalto, N. Bonod, and C. Rockstuhl, *Transverse multipolar light-matter couplings in evanescent waves*, Phys. Rev. A **94**, 053822 (2016).

[108] O. G. Rodríguez-Herrera, D. Lara, K. Y. Bliokh, E. A. Ostrovskaya, and C. Dainty, *Optical nanoprobing via spin-orbit interaction of light*, Phys. Rev. Lett. **104**, 253601 (2010).

[109] K. Y. Bliokh, E. A. Ostrovskaya, M. A. Alonso, O. G. Rodríguez-Herrera, D. Lara, and C. Dainty, *Spin-to-orbital angular momentum conversion in focusing, scattering, and imaging systems*, Opt. Express **19**, 26132 (2011).

[110] R. G. Barrera, G. A. Estévez, and J. Giraldo, *Vector spherical harmonics and their application to magnetostatics*, Eur. J. Phys. **6**, 287 (1985).

[111] A. G. Curto, T. H. Taminiau, G. Volpe, M. P. Kreuzer, R. Quidant, and N. F. van Hulst, *Multipolar radiation of quantum emitters with nanowire optical antennas*, Nat. Commun. **4**, 1750 (2013).

[112] L. J. Pereira, A. Z. Khoury, and K. Dechoum, *Quantum and classical separability of spin-orbit laser modes*, Phys. Rev. A **90**, 053842 (2014).

[113] R. J. C. Spreeuw, *A classical analogy of entanglement*, Found. Phys. **28**, 361 (1998).

[114] A. Aiello, F. Töppel, C. Marquardt, E. Giacobino, and G. Leuchs, *Quantum-like nonseparable structures in optical beams*, New J. Phys. **17**, 043024 (2015).

[115] A. Aiello and M. Ornigotti, *Near field of an oscillating electric dipole and cross-polarization of a collimated beam of light: Two sides of the same coin*, Am. J. Phys. **82**, 860 (2014).

[116] A. Y. Bekshaev, K. Y. Bliokh, and M. Soskin, *Internal flows and energy circulation in light beams*, J. Opt. **13**, 053001 (2011).

[117] K. Y. Bliokh, A. Y. Bekshaev, A. G. Kofman, and F. Nori, *Photon trajectories, anomalous velocities and weak measurements: a classical interpretation*, New J. Phys. **15**, 073022 (2013).

[118] A. Espinosa-Soria, F. J. Rodríguez-Fortuño, A. Griol, and A. Martínez, *On-chip optimal Stokes nanopolarimetry based on spin-orbit interaction of light*, Nano Lett. **17**, 3139 (2017).

[119] B. le Feber, N. Rotenberg, and L. Kuipers, *Nanophotonic control of circular dipole emission*, Nat. Commun. **6**, 6695 (2015).

[120] I. Söllner, S. Mahmoodian, S. L. Hansen, L. Midolo, A. Javadi, G. Kiršanskė, T. Pregnolato, H. El-Ella, E. H. Lee, J. D. Song, S. Stobbe, and P. Lodahl, *Deterministic photon-emitter coupling in chiral photonic circuits*, Nat. Nanotechnol. **10**, 775 (2015).

[121] F. J. Rodríguez-Fortuño, D. Puerto, A. Griol, L. Bellieres, J. Martí, and A. Martínez, *Universal method for the synthesis of arbitrary polarization states radiated by a nanoantenna*, Laser Photonics Rev. **8**, L27 (2014).

[122] F. J. Rodríguez-Fortuño, I. Barber-Sanz, D. Puerto, A. Griol, and A. Martínez, *Resolving light handedness with an on-chip silicon microdisk*, ACS Photonics **1**, 762 (2014).

[123] F. J. Rodríguez-Fortuño, D. Puerto, A. Griol, L. Bellieres, J. Martí, and A. Martínez, *Sorting linearly polarized photons with a single scatterer*, Opt. Lett. **39**, 1394 (2014).

[124] D. O'Connor, P. Ginzburg, F. J. Rodríguez-Fortuño, G. A. Wurtz, and A. V. Zayats, *Spin-orbit coupling in surface plasmon scattering by nanostructures*, Nat. Commun. **5**, 5327 (2014).

[125] P. V. Kapitanova, P. Ginzburg, F. J. Rodríguez-Fortuño, D. S. Filonov, P. M. Voroshilov, P. A. Belov, A. N. Poddubny, Y. S. Kivshar, G. A. Wurtz, and A. V. Zayats, *Photonic spin Hall effect in hyperbolic metamaterials for polarization-controlled routing of subwavelength modes*, Nat. Commun. **5**, 3226 (2014).

[126] J. Carbonell, F. J. Rodríguez-Fortuño, A. Díaz-Rubio, A. Martínez, F. Cervera, and J. Sánchez-Dehesa, *Directive excitation of guided electromagnetic waves through polarization control*, Phys. Rev. B **89**, 155121 (2014).

[127] J. Petersen, J. Volz, and A. Rauschenbeutel, *Chiral nanophotonic waveguide interface based on spin-orbit interaction of light*, Science **346**, 67 (2014).

[128] M. F. Picardi, K. Y. Bliokh, F. J. Rodríguez-Fortuño, F. Alpeggiani, and F. Nori, *Angular momenta, helicity, and other properties of dielectric-fiber and metallic-wire modes*, Optica **5**, 1016 (2018).

[129] M. Wang, H. Zhang, T. Kovalevich, R. Salut, M.-S. Kim, M. A. Suarez, M.-P. Bernal, H.-P. Herzig, H. Lu, and T. Grosjean, *Magnetic spin-orbit interaction of light*, Light Sci. Appl. **7**, 24 (2018).

[130] L. Marrucci, *Spin gives direction*, Nat. Phys. **11**, 9 (2015).

[131] A. Espinosa-Soria and A. Martínez, *Transverse spin and spin-orbit coupling in silicon waveguides*, IEEE Photonics Technol. Lett. **28**, 1561 (2016).

[132] M. F. Picardi, A. Manjavacas, A. V. Zayats, and F. J. Rodríguez-Fortuño, *Unidirectional evanescent-wave coupling from circularly polarized electric and magnetic dipoles: An angular spectrum approach*, Phys. Rev. B **95**, 245416 (2017).

[133] M. F. Picardi, A. V. Zayats, and F. J. Rodríguez-Fortuño, *Janus and Huygens dipoles: Near-field directionality beyond spin-momentum locking*, Phys. Rev. Lett. **120**, 117402 (2018).

[134] M. Neugebauer, T. Bauer, P. Banzer, and G. Leuchs, *Polarization tailored light driven directional optical nanobeacon*, Nano Lett. **14**, 2546 (2014).

[135] M. Neugebauer, P. Woźniak, A. Bag, G. Leuchs, and P. Banzer, *Polarization-controlled directional scattering for nanoscopic position sensing*, Nat. Commun. **7**, 11286 (2016).

[136] M. F. Picardi, M. Neugebauer, J. S. Eismann, G. Leuchs, P. Banzer, F. J. Rodríguez-Fortuño, and A. V. Zayats, *Experimental demonstration of linear and spinning Janus dipoles for polarisation- and wavelength-selective near-field coupling*, Light Sci. Appl. **8**, 52 (2019).

[137] L. Wei, M. F. Picardi, J. J. Kingsley-Smith, A. V. Zayats, and F. J. Rodríguez-Fortuño, *Directional scattering from particles under evanescent wave illumination: the role of reactive power*, Opt. Lett. **43**, 3393 (2018).

[138] O. Keller, *Quantum Theory of Near-Field Electrodynamics* (Springer, Berlin, Heidelberg, 2012).

[139] A. B. Evlyukhin, C. Reinhardt, E. Evlyukhin, and B. N. Chichkov, *Multipole analysis of light scattering by arbitrary-shaped nanoparticles on a plane surface*, J. Opt. Soc. Am. B **30**, 2589 (2013).

[140] A. B. Evlyukhin, T. Fischer, C. Reinhardt, and B. N. Chichkov, *Optical theorem and multipole scattering of light by arbitrarily shaped nanoparticles*, Phys. Rev. B **94**, 205434 (2016).

[141] R. Alaee, C. Rockstuhl, and I. Fernandez-Corbaton, *An electromagnetic multipole expansion beyond the long-wavelength approximation*, Opt. Commun. **407**, 17 (2018).

[142] R. Alaee, C. Rockstuhl, and I. Fernandez-Corbaton, *Exact multipolar decompositions with applications in nanophotonics*, Adv. Opt. Mater. **7**, 1800783 (2019).

[143] A. J. Devaney and E. Wolf, *Multipole expansions and plane wave representations of the electromagnetic field*, J. Math. Phys. **15**, 234 (1974).

[144] L. Mandel and E. Wolf, *Optical Coherence and Quantum Optics* (Cambridge University Press, Cambridge, UK, 1995).

[145] G. C. Sherman, J. J. Stamnes, and E. Lalor, *Asymptotic approximations to angular-spectrum representations*, J. Math. Phys. **17**, 760 (1976).

[146] A. T. Friberg and E. Wolf, *Angular spectrum representation of scattered electromagnetic fields*, J. Opt. Soc. Am. **73**, 26 (1983).

[147] E. Wolf and M. Nieto-Vesperinas, *Analyticity of the angular spectrum amplitude of scattered fields and some of its consequences*, J. Opt. Soc. Am. A **2**, 886 (1985).

[148] T. Inoue and H. Hori, *Theoretical treatment of electric and magnetic multipole radiation near a planar dielectric surface based on angular spectrum representation of vector field*, Opt. Rev. **5**, 295 (1998).

[149] H. F. Arnoldus, *Angular spectrum representation of the electromagnetic multipole fields, and their reflection at a perfect conductor*, Surf. Sci. **590**, 101 (2005).

[150] J. W. Goodman, *Introduction to Fourier Optics* (McGraw-Hill, New York, USA, 1988).

[151] T. Setälä, M. Kaivola, and A. T. Friberg, *Decomposition of the point-dipole field into homogeneous and evanescent parts*, Phys. Rev. E **59**, 1200 (1999).

[152] H. Weyl, *Ausbreitung elektromagnetischer Wellen über einem ebenen Leiter* [*Propagation of electromagnetic waves on an even conductor*], Ann. Phys. **365**, 481 (1919).

[153] G. N. Watson, *A Treatise on the Theory of Bessel Functions* (Cambridge University Press, New York, USA, 1995).

[154] A. Ishimaru, *Electromagnetic Wave Propagation, Radiation, and Scattering* (Prentice-Hall, Englewood Cliffs, NJ, 1991).

[155] E. A. Essex, *Hertz vector potentials of electromagnetic theory*, Am. J. Phys. **45**, 1099 (1977).

[156] M. Ornigotti and A. Aiello, *The Hertz vector revisited: a simple physical picture*, J. Opt. **16**, 105705 (2014).

[157] M. Abramowitz and I. A. Stegun, *Handbook of Mathematical Functions* (Dover, New York, USA, 1972).

[158] P. A. Bobbert and J. Vlieger, *Light scattering by a sphere on a substrate*, Physica A **137**, 209 (1986).

[159] R. Borghi, *On the angular-spectrum representation of multipole wave fields*, J. Opt. Soc. Am. A **21**, 1805 (2004).

[160] F. J. Rodríguez-Fortuño, N. Engheta, A. Martínez, and A. V. Zayats, *Lateral forces on circularly polarizable particles near a surface*, Nat. Commun. **6**, 8799 (2015).

[161] D. Smirnova and Y. S. Kivshar, *Multipolar nonlinear nanophotonics*, Optica **3**, 1241 (2016).

[162] T. W. B. Kibble, *Conservation laws for free fields*, J. Math. Phys. **6**, 1022 (1965).

[163] W. I. Fushchich and A. G. Nikitin, *The complete sets of conservation laws for the electromagnetic field*, J. Phys. A **25**, L231 (1992).

[164] D. M. Lipkin, *Existence of a new conservation law in electromagnetic theory*, J. Math. Phys. **5**, 696 (1964).

[165] T. A. Morgan, *Two classes of new conservation laws for the electromagnetic field and for other massless fields*, J. Math. Phys. **5**, 1659 (1964).

[166] M. G. Calkin, *An invariance property of the free electromagnetic field*, Am. J. Phys. **33**, 958 (1965).

[167] D. J. Candlin, *Analysis of the new conservation law in electromagnetic theory*, Nuovo Cimento **37**, 1390 (1965).

[168] T. Brixner, F. J. García de Abajo, J. Schneider, and W. Pfeiffer, *Nanoscopic ultrafast space-time-resolved spectroscopy*, Phys. Rev. Lett. **95**, 093901 (2005).

[169] N. Yang, Y. Tang, and A. E. Cohen, *Spectroscopy in sculpted fields*, Nano Today **4**, 269 (2009).

[170] L. D. Barron, *Molecular Light Scattering and Optical Activity* (Cambridge University Press, Cambridge, England, 2004).

[171] E. Hendry, T. Carpy, J. Johnston, M. Popland, R. V. Mikhaylovskiy, A. J. Lapthorn, S. M. Kelly, L. D. Barron, N. Gadegaard, and M. Kadodwala, *Ultrasensitive detection and characterization of biomolecules using superchiral fields*, Nat. Nanotechnol. **5**, 783 (2010).

[172] Y. Tang and A. E. Cohen, *Enhanced enantioselectivity in excitation of chiral molecules by superchiral light*, Science **332**, 333 (2011).

[173] J. S. Choi and M. Cho, *Limitations of a superchiral field*, Phys. Rev. A **86**, 063834 (2012).

[174] K. Y. Bliokh and F. Nori, *Characterizing optical chirality*, Phys. Rev. A **83**, 021803 (2011).

[175] L. E. Barr, S. A. R. Horsley, I. R. Hooper, J. K. Eager, C. P. Gallagher, S. M. Hornett, A. P. Hibbins, and E. Hendry, *Investigating the nature of chiral near-field interactions*, Phys. Rev. B **97**, 155418 (2018).

[176] C. Kramer, M. Schäferling, T. Weiss, H. Giessen, and T. Brixner, *Analytic optimization of near-field optical chirality enhancement*, ACS Photonics **4**, 396 (2017).

[177] M. Schäferling, D. Dregely, M. Hentschel, and H. Giessen, *Tailoring enhanced optical chirality: Design principles for chiral plasmonic nanostructures*, Phys. Rev. X **2**, 031010 (2012).

[178] N. Meinzer, E. Hendry, and W. L. Barnes, *Probing the chiral nature of electromagnetic fields surrounding plasmonic nanostructures*, Phys. Rev. B **88**, 041407 (2013).

[179] V. K. Valev, J. J. Baumberg, C. Sibilia, and T. Verbiest, *Chirality and chiroptical effects in plasmonic nanostructures: Fundamentals, recent progress, and outlook*, Adv. Mater. **25**, 2517 (2013).

[180] M. L. Nesterov, X. Yin, M. Schäferling, H. Giessen, and T. Weiss, *The role of plasmon-generated near fields for enhanced circular dichroism spectroscopy*, ACS Photonics **3**, 578 (2016).

[181] J. T. Collins, C. Kuppe, D. C. Hooper, C. Sibilia, M. Centini, and V. K. Valev, *Chirality and chiroptical effects in metal nanostructures: Fundamentals and current trends*, Adv. Opt. Mater. **5**, 1700182 (2017).

[182] Y. Luo, C. Chi, M. Jiang, R. Li, S. Zu, Y. Li, and Z. Fang, *Plasmonic chiral nanostructures: Chiroptical effects and applications*, Adv. Opt. Mater. **5**, 1700040 (2017).

[183] M. Hentschel, M. Schäferling, X. Duan, H. Giessen, and N. Liu, *Chiral plasmonics*, Sci. Adv. **3**, e1602735 (2017).

[184] M. Schäferling, *Chiral Nanophotonics: Chiral Optical Properties of Plasmonic Systems* (Springer, Berlin, 2017).

[185] M. M. Coles and D. L. Andrews, *Chirality and angular momentum in optical radiation*, Phys. Rev. A **85**, 063810 (2012).

[186] I. Proskurin, A. S. Ovchinnikov, P. Nosov, and J. Kishine, *Optical chirality in gyrotropic media: symmetry approach*, New J. Phys. **19**, 063021 (2017).

[187] T. G. Philbin, *Lipkin's conservation law, Noether's theorem, and the relation to optical helicity*, Phys. Rev. A **87**, 043843 (2013).

[188] T. G. Philbin, *Electromagnetic energy momentum in dispersive media*, Phys. Rev. A **83**, 013823 (2011); Erratum, Phys. Rev. A **85**, 059902 (2012).

[189] T. G. Philbin and O. Allanson, *Optical angular momentum in dispersive media*, Phys. Rev. A **86**, 055802 (2012).

[190] F. Alpeggiani, K. Y. Bliokh, F. Nori, and L. Kuipers, *Electromagnetic helicity in complex media*, Phys. Rev. Lett. **120**, 243605 (2018).

[191] H. J. Lezec, J. A. Dionne, and H. A. Atwater, *Negative refraction at visible frequencies*, Science **316**, 430 (2007).

[192] N. Engheta, *Circuits with light at nanoscales: Optical nanocircuits inspired by metamaterials*, Science **317**, 1698 (2007).

[193] J. Valentine, S. Zhang, T. Zentgraf, E. Ulin-Avila, D. A. Genov, G. Bartal, and X. Zhang, *Three-dimensional optical metamaterial with a negative refractive index*, Nature (London) **455**, 376 (2008).

[194] T. J. Cui and J. A. Kong, *Time-domain electromagnetic energy in a frequency-dispersive left-handed medium*, Phys. Rev. B **70**, 205106 (2004).

[195] S. A. Tretyakov, *Electromagnetic field energy density in artificial microwave materials with strong dispersion and loss*, Phys. Lett. A **343**, 231 (2005).

[196] A. D. Boardman and K. Marinov, *Electromagnetic energy in a dispersive metamaterial*, Phys. Rev. B **73**, 165110 (2006).

[197] P.-G. Luan, *Power loss and electromagnetic energy density in a dispersive metamaterial medium*, Phys. Rev. E **80**, 046601 (2009).

[198] A. Raman and S. Fan, *Photonic band structure of dispersive metamaterials formulated as a Hermitian eigenvalue problem*, Phys. Rev. Lett. **104**, 087401 (2010).

[199] W. Shin, A. Raman, and S. Fan, *Instantaneous electric energy and electric power dissipation in dispersive media*, J. Opt. Soc. Am. B **29**, 1048 (2012).

[200] F. S. S. Rosa, D. A. R. Dalvit, and P. W. Milonni, *Electromagnetic energy, absorption, and Casimir forces: Uniform dielectric media in thermal equilibrium*, Phys. Rev. A **81**, 033812 (2010).

[201] K. J. Webb and Shivanand, *Electromagnetic field energy in dispersive materials*, J. Opt. Soc. Am. B **27**, 1215 (2010).

[202] F. D. Nunes, T. C. Vasconcelos, M. Bezerra, and J. Weiner, *Electromagnetic energy density in dispersive and dissipative media*, J. Opt. Soc. Am. B **28**, 1544 (2011).

[203] J. Askne and B. Lind, *Energy of electromagnetic waves in the presence of absorption and dispersion*, Phys. Rev. A **2**, 2335 (1970).

[204] C.-G. Huang and Y.-Z. Zhang, *Poynting vector, energy density, and energy velocity in an anomalous dispersion medium*, Phys. Rev. A **65**, 015802 (2001).

[205] R. W. Ziolkowski, *Superluminal transmission of information through an electromagnetic metamaterial*, Phys. Rev. E **63**, 046604 (2001).

[206] L. J. Wang, A. Kuzmich, and A. Dogariu, *Gain-assisted superluminal light propagation*, Nature (London) **406**, 277 (2000).

[207] S. Glasgow, M. Ware, and J. Peatross, *Poynting's theorem and luminal total energy transport in passive dielectric media*, Phys. Rev. E **64**, 046610 (2001).

[208] G. Dolling, C. Enkrich, M. Wegener, C. M. Soukoulis, and S. Linden, *Simultaneous negative phase and group velocity of light in a metamaterial*, Science **312**, 892 (2006).

[209] E. Feigenbaum, N. Kaminski, and M. Orenstein, *Negative dispersion: a backward wave or fast light? Nanoplasmonic examples*, Opt. Express **17**, 18934 (2009).

[210] S. M. Barnett and R. Loudon, *The enigma of optical momentum in a medium*, Phil. Trans. R. Soc. A **368**, 927 (2010).

[211] K. E. Oughstun and S. Shen, *Velocity of energy transport for a time-harmonic field in a multiple-resonance Lorentz medium*, J. Opt. Soc. Am. B **5**, 2395 (1988).

[212] F. D. Nunes, B.-H. V. Borges, and J. Weiner, *Analysis of dispersive and dissipative media with optical resonances*, Opt. Express **20**, 15679 (2012).

[213] H. S. Sehmi, W. Langbein, and E. A. Muljarov, *Optimizing the Drude-Lorentz model for material permittivity: Method, program, and examples for gold, silver, and copper*, Phys. Rev. B **95**, 115444 (2017).

[214] W. I. Fushchich and A. G. Nikitin, *Symmetries of Maxwell's Equations. Mathematics and its Applications* (Springer, Amsterdam, 1987).

[215] E. Noether, *Invariant variation problems*, Gott. Nachr. **1918**, 235 (1918) [Transp. Theory Stat. Phys. **1**, 186 (1971)].

[216] W.-K Tung, *Group Theory in Physics* (World Scientific, Singapore, 1985).

[217] R. P. Cameron, J. B. Götte, S. M. Barnett, and A. M. Yao, *Chirality and the angular momentum of light*, Phil. Trans. R. Soc. A **375**, 20150433 (2017).

[218] S. Weinberg, *The Quantum Theory of Fields* (Cambridge University Press, Cambridge, UK, 1995).

[219] G. Nienhuis, *Conservation laws and symmetry transformations of the electromagnetic field with sources*, Phys. Rev. A **93**, 023840 (2016).

[220] I. Fernandez-Corbaton and C. Rockstuhl, *Unified theory to describe and engineer conservation laws in light-matter interactions*, Phys. Rev. A **95**, 053829 (2017).

[221] J. H. Poynting, *On the transfer of energy in the electromagnetic field*, Phil. Trans. R. Soc. London **175**, 343 (1884).

[222] L. V. Poulikakos, P. Gutsche, K. M. McPeak, S. Burger, J. Niegemann, C. Hafner, and D. J. Norris, *Optical chirality flux as a useful far-field probe of chiral near fields*, ACS Photonics **3**, 1619 (2016).

[223] H. Rhee, J. S. Choi, D. J. Starling, J. C. Howell, and M. Cho, *Amplifications in chiroptical spectroscopy, optical enantioselectivity, and weak value measurement*, Chem. Sci. **4**, 4107 (2013).

[224] C. Rosales-Guzmán, K. Volke-Sepulveda, and J. P. Torres, *Light with enhanced optical chirality*, Opt. Lett. **37**, 3486 (2012).

[225] I. Fernandez-Corbaton, M. Fruhnert, and C. Rockstuhl, *Objects of maximum electromagnetic chirality*, Phys. Rev. X **6**, 031013 (2016).

[226] M. V. Gorkunov, V. E. Dmitrienko, A. A. Ezhov, V. V. Artemov, and O. Y. Rogov, *Implications of the causality principle for ultra chiral metamaterials*, Sci. Rep. **5**, 9273 (2015).

[227] L. Brillouin, *Wave Propagation and Group Velocity* (Academic, New York, USA, 1960).

[228] L. D. Landau, E. M. Lifshitz, and L. P. Pitaevskii, *Electrodynamics of Continuous Media* (Pergamon, New York, USA, 1984).

[229] R. W. Boyd and D. J. Gauthier, *Controlling the velocity of light pulses*, Science **326**, 1074 (2009).

[230] V. Gerasik and M. Stastna, *Complex group velocity and energy transport in absorbing media*, Phys. Rev. E **81**, 056602 (2010).

[231] R. Loudon, *The propagation of electromagnetic energy through an absorbing dielectric*, J. Phys. A: Gen. Phys. **3**, 233 (1970).

[232] R. Ruppin, *Electromagnetic energy density in a dispersive and absorptive material*, Phys. Lett. A **299**, 309 (2002).

[233] S. A. Maier, *Plasmonics: Fundamentals and Applications* (Springer, New York, USA, 2007).

[234] A. D. Rakić, A. B. Djurišić, J. M. Elazar, and M. L. Majewski, *Optical properties of metallic films for vertical-cavity optoelectronic devices*, Appl. Opt. **37**, 5271 (1998).

[235] E. D. Palik, *Handbook of Optical Constants of Solids* (Academic Press, New York, USA, 1985).

[236] D. R. Smith, W. J. Padilla, D. C. Vier, S. C. Nemat-Nasser, and S. Schultz, *Composite medium with simultaneously negative permeability and permittivity*, Phys. Rev. Lett. **84**, 4184 (2000).

[237] C. García-Meca, J. Hurtado, J. Martí, A. Martínez, W. Dickson, and A. V. Zayats, *Low-loss multilayered metamaterial exhibiting a negative index of refraction at visible wavelengths*, Phys. Rev. Lett. **106**, 067402 (2011).

[238] S. J. Yoo, M. Cho, and Q.-Han Park, *Globally enhanced chiral field generation by negative-index metamaterials*, Phys. Rev. B **89**, 161405 (2014).

[239] S. J. Yoo and Q.-Han Park, *Chiral light-matter interaction in optical resonators*, Phys. Rev. Lett. **114**, 203003 (2015).

[240] A. García-Etxarri and J. A. Dionne, *Surface-enhanced circular dichroism spectroscopy mediated by nonchiral nanoantennas*, Phys. Rev. B **87**, 235409 (2013).

[241] G. Pellegrini, M. Finazzi, M. Celebrano, L. Duò, and P. Biagioni, *Chiral surface waves for enhanced circular dichroism*, Phys. Rev. B **95**, 241402 (2017).

[242] U.S. Food and Drug Administration (FDA), *FDA's policy statement for the development of new stereoisomeric drugs*, Chirality **4**, 338 (1992).

[243] A. J. Hutt and S. C. Tan, *Drug chirality and its clinical significance*, Drugs **52**, 1 (1996).

[244] S. W. Smith, *Chiral toxicology: It's the same thing...only different*, Toxicol. Sci. **110**, 4 (2009).

[245] R. Naaman, Y. Paltiel, and D. H. Waldeck, *Chiral molecules and the electron spin*, Nat. Rev. Chem. **3**, 250 (2019).

[246] P. Lodahl, S. Mahmoodian, S. Stobbe, A. Rauschenbeutel, P. Schneeweiss, J. Volz, H. Pichler, and P. Zoller, *Chiral quantum optics*, Nature (London) **541**, 473 (2017).

[247] B. Göhler, V. Hamelbeck, T. Z. Markus, M. Kettner, G. F. Hanne, Z. Vager, R. Naaman, and H. Zacharias, *Spin selectivity in electron transmission through self-assembled monolayers of double-stranded DNA*, Science **331**, 894 (2011).

[248] H. Zhu, J. Yi, M.-Y. Li, J. Xiao, L. Zhang, C.-W. Yang, R. A. Kaindl, L.-J. Li, Y. Wang, and X. Zhang, *Observation of chiral phonons*, Science **359**, 579 (2018).

[249] R. P. Cameron, S. M. Barnett, and A. M. Yao, *Optical helicity, optical spin and related quantities in electromagnetic theory*, New J. Phys. **14**, 053050 (2012).

[250] N. Berova, K. Nakanishi, and R. W. Woody, *Circular Dichroism: Principles and Applications* (Wiley-VCH, New York, USA, 2000).

[251] R. Hassey, E. J. Swain, N. I. Hammer, D. Venkataraman, and M. D. Barnes, *Probing the chiroptical response of a single molecule*, Science **314**, 1437 (2006).

[252] C.-S. Ho, A. García-Etxarri, Y. Zhao, and J. Dionne, *Enhancing enantioselective absorption using dielectric nanospheres*, ACS Photonics **4**, 197 (2017).

[253] S. Lee, S. J. Yoo, and Q.-Han Park, *Microscopic origin of surface-enhanced circular dichroism*, ACS Photonics **4**, 2047 (2017).

[254] A. O. Govorov, Z. Fan, P. Hernandez, J. M. Slocik, and R. R. Naik, *Theory of circular dichroism of nanomaterials comprising chiral molecules and nanocrystals: Plasmon enhancement, dipole interactions, and dielectric effects*, Nano Lett. **10**, 1374 (2010).

[255] Y. Zhao, A. N. Askarpour, L. Sun, J. Shi, X. Li, and A. Alù, *Chirality detection of enantiomers using twisted optical metamaterials*, Nat. Commun. **8**, 14180 (2017).

[256] L. Kang, Q. Ren, and D. H. Werner, *Leveraging superchiral light for manipulation of optical chirality in the near-field of plasmonic metamaterials*, ACS Photonics **4**, 1298 (2017).

[257] E. Hendry, R. V. Mikhaylovskiy, L. D. Barron, M. Kadodwala, and T. J. Davis, *Chiral electromagnetic fields generated by arrays of nanoslits*, Nano Lett. **12**, 3640 (2012).

[258] J. Lasa-Alonso, D. R. Abujetas, A. Nodar, J. A. Dionne, J. J. Sáenz, G. Molina-Terriza, J. Aizpurua, and A. García-Etxarri, *Surface-enhanced circular dichroism spectroscopy on periodic dual nanostructures*, ACS Photonics **7**, 2978 (2020).

[259] M. L. Solomon, J. Hu, M. Lawrence, A. García-Etxarri, and J. A. Dionne, *Enantiospecific optical enhancement of chiral sensing and separation with dielectric metasurfaces*, ACS Photonics **6**, 43 (2019).

[260] F. Graf, J. Feis, X. Garcia-Santiago, M. Wegener, C. Rockstuhl, and I. Fernandez-Corbaton, *Achiral, helicity preserving, and resonant structures for enhanced sensing of chiral molecules*, ACS Photonics **6**, 482 (2019).

[261] J. Hu, M. Lawrence, and J. A. Dionne, *High quality factor dielectric metasurfaces for ultraviolet circular dichroism spectroscopy*, ACS Photonics **7**, 36 (2020).

[262] X. Zhao and B. M. Reinhard, *Switchable chiroptical hot-spots in silicon nanodisk dimers*, ACS Photonics **6**, 1981 (2019).

[263] F. R. Gómez, O. N. Oliveira, Jr., P. Albella, and J. R. Mejía-Salazar, *Enhanced chiroptical activity with slotted high refractive index dielectric nanodisks*, Phys. Rev. B **101**, 155403 (2020).

[264] F. R. Gómez, J. R. Mejía-Salazar, and P. Albella, *All-dielectric chiral metasurfaces based on crossed-bowtie nanoantennas*, ACS Omega **4**, 21041 (2019).

[265] E. Mohammadi, K. L. Tsakmakidis, A. N. Askarpour, P. Dehkhoda, A. Tavakoli, and H. Altug, *Nanophotonic platforms for enhanced chiral sensing*, ACS Photonics **5**, 2669 (2018).

[266] E. Mohammadi, A. Tavakoli, P. Dehkhoda, Y. Jahani, K. L. Tsakmakidis, A. Tittl, and H. Altug, *Accessible superchiral near-fields driven by tailored electric and magnetic resonances in all-dielectric nanostructures*, ACS Photonics **6**, 1939 (2019).

[267] M. C. Estevez, M. Alvarez, and L. M. Lechuga, *Integrated optical devices for lab-on-a-chip biosensing applications*, Laser Photonics Rev. **6**, 463 (2012).

[268] X. Nie, E. Ryckeboer, G. Roelkens, and R. Baets, *CMOS-compatible broadband co-propagative stationary Fourier transform spectrometer integrated on a silicon nitride photonics platform*, Opt. Express **25**, A409 (2017).

[269] R. J. Coles, D. M. Price, J. E. Dixon, B. Royall, E. Clarke, P. Kok, M. S. Skolnick, A. M. Fox, and M. N. Makhonin, *Chirality of nanophotonic waveguide with embedded quantum emitter for unidirectional spin transfer*, Nat. Commun. **7**, 11183 (2016).

[270] S.-H. Gong, F. Alpeggiani, B. Sciacca, E. C. Garnett, and L. Kuipers, *Nanoscale chiral valley-photon interface through optical spin-orbit coupling*, Science **359**, 443 (2018).

[271] F. Le Kien, T. Busch, V. G. Truong, and S. Nic Chormaic, *Higher-order modes of vacuum-clad ultrathin optical fibers*, Phys. Rev. A **96**, 023835 (2017).

[272] D. R. Abujetas and J. A. Sánchez-Gil, *Spin angular momentum of guided light induced by transverse confinement and intrinsic helicity*, ACS Photonics **7**, 534 (2020).

[273] B. E. A. Saleh and M. C. Teich, *Fundamentals of Photonics* (Wiley-Interscience, New York, USA, 2007).

[274] M. H. Alizadeh and B. M. Reinhard, *Enhanced optical chirality through locally excited surface plasmon polaritons*, ACS Photonics **2**, 942 (2015).

[275] S. Nechayev, R. Barczyk, U. Mick, and P. Banzer, *Substrate-induced chirality in an individual nanostructure*, ACS Photonics **6**, 1876 (2019).

[276] E. Petronijevic and C. Sibilia, *Enhanced near-field chirality in periodic arrays of Si nanowires for chiral sensing*, Molecules **24**, 853 (2019).

[277] S. Romero-García, F. Merget, F. Zhong, H. Finkelstein, and J. Witzens, *Silicon nitride CMOS-compatible platform for integrated photonics applications at visible wavelengths*, Opt. Express **21**, 14036 (2013).

[278] L. V. Poulikakos, P. Thureja, A. Stollmann, E. De Leo, and D. J. Norris, *Chiral light design and detection inspired by optical antenna theory*, Nano Lett. **18**, 4633 (2018).

[279] M. H. P. Pfeiffer, C. Herkommer, J. Liu, T. Morais, M. Zervas, M. Geiselmann, T. J. Kippenberg, *Photonic damascene process for low-loss, high-confinement silicon nitride waveguides*, IEEE J. Sel. Top. Quantum Electron. **24**, 6101411 (2018).

[280] V. R. Almeida, Q. Xu, C. A. Barrios, and M. Lipson, *Guiding and confining light in void nanostructure*, Opt. Lett. **29**, 1209 (2004).

[281] C. A. Barrios, K. B. Gylfason, B. Sánchez, A. Griol, H. Sohlström, M. Holgado, and R. Casquel, *Slot-waveguide biochemical sensor*, Opt. Lett. **32**, 3080 (2007).

[282] J. K. Gansel, M. Thiel, M. S. Rill, M. Decker, K. Bade, V. Saile, G. von Freymann, S. Linden, and M. Wegener, *Gold helix photonic metamaterial as broadband circular polarizer*, Science **325**, 1513 (2009).

[283] J. K. Gansel, M. Wegener, S. Burger, and S. Linden, *Gold helix photonic metamaterials: A numerical parameter study*, Opt. Express **18**, 1059 (2010).

[284] Z. Yang, M. Zhao, and P. Lu, *How to improve the signal-to-noise ratio for circular polarizers consisting of helical metamaterials?*, Opt. Express **19**, 4255 (2011).

[285] M. Schäferling, X. Yin, N. Engheta, and H. Giessen, *Helical plasmonic nanostructures as prototypical chiral near-field sources*, ACS Photonics **1**, 530 (2014).

[286] M. Esposito, V. Tasco, M. Cuscunà, F. Todisco, A. Benedetti, I. Tarantini, M. De Giorgi, D. Sanvitto, and A. Passaseo, *Nanoscale 3D chiral plasmonic helices with circular dichroism at visible frequencies*, ACS Photonics **2**, 105 (2015).

[287] R. Ji, S.-W. Wang, X. Liu, H. Guo, and W. Lu, *Hybrid helix metamaterials for giant and ultrawide circular dichroism*, ACS Photonics **3**, 2368 (2016).

[288] D. Kosters, A. de Hoogh, H. Zeijlemaker, H. Acar, N. Rotenberg, and L. Kuipers, *Core-shell plasmonic nanohelices*, ACS Photonics **4**, 1858 (2017).

[289] P. Woźniak, I. De Leon, K. Höflich, C. Haverkamp, S. Christiansen, G. Leuchs, and P. Banzer, *Chiroptical response of a single plasmonic nanohelix*, Opt. Express **26**, 19275 (2018).

[290] K. Höflich, T. Feichtner, E. Hansjürgen, C. Haverkamp, H. Kollmann, C. Lienau, and M. Silies, *Resonant behavior of a single plasmonic helix*, Optica **6**, 1098 (2019).

[291] P. B. Johnson and R. W. Christy, *Optical constants of the noble metals*, Phys. Rev. B **6**, 4370 (1972).

[292] M. Thiel, M. Decker, M. Deubel, M. Wegener, S. Linden, and G. von Freymann, *Polarization stop bands in chiral polymeric three-dimensional photonic crystals*, Adv. Mater. **19**, 207 (2007).

[293] M. Thiel, G. von Freymann, and M. Wegener, *Layer-by-layer three-dimensional chiral photonic crystals*, Opt. Lett. **32**, 2547 (2007).

[294] H. J. Singh and A. Ghosh, *Large and tunable chiro-optical response with all dielectric helical nanomaterials*, ACS Photonics **5**, 1977 (2018).

[295] A. Espinosa-Soria, A. Griol, and A. Martínez, *Experimental measurement of plasmonic nanostructures embedded in silicon waveguide gaps*, Opt. Express **24**, 9592 (2016).

[296] A. Espinosa-Soria, E. Pinilla-Cienfuegos, F. J. Díaz-Fernández, A. Griol, J. Martí, and A. Martínez, *Coherent control of a plasmonic nanoantenna integrated on a silicon chip*, ACS Photonics **5**, 2712 (2018).

[297] X. Yin, M. Schäferling, B. Metzger, and H. Giessen, *Interpreting chiral nanophotonic spectra: The plasmonic Born-Kuhn model*, Nano Lett. **13**, 6238 (2013).

[298] V. N. Filippov, O. I. Kotov, and V. M. Nikolayev, *Measurement of polarisation beat length in single-mode optical fibres with a polarisation modulator*, Electron. Lett. **26**, 658 (1990).

[299] Q. Zhang, T. Hernandez, K. W. Smith, S. A. H. Jebeli, A. X. Dai, L. Warning, R. Baiyasi, L. A. McCarthy, H. Guo, D.-H. Chen, J. A. Dionne, C. F. Landes, and S. Link, *Unraveling the origin of chirality from plasmonic nanoparticle-protein complexes*, Science **365**, 1475 (2019).

[300] M. Schäferling, N. Engheta, H. Giessen, and T. Weiss, *Reducing the complexity: Enantioselective chiral near-fields by diagonal slit and mirror configuration*, ACS Photonics **3**, 1076 (2016).

[301] C. García-Meca, S. Lechago, A. Brimont, A. Griol, S. Mas, L. Sánchez, L. Bellieres, N. S. Losilla, and J. Martí, *On-chip wireless silicon photonics: from reconfigurable interconnects to lab-on-chip devices*, Light Sci. Appl. **6**, e17053 (2017).

[302] K. Y. Bliokh, A. Niv, V. Kleiner, and E. Hasman, *Geometrodynamics of spinning light*, Nat. Photonics **2**, 748 (2008).

[303] K. Y. Bliokh and A. Aiello, *Goos-Hänchen and Imbert-Fedorov beam shifts: an overview*, J. Opt. **15**, 014001 (2013).

[304] J. H. Hannay, *The Majorana representation of polarization, and the Berry phase of light*, J. Mod. Opt. **45**, 1001 (1998).

[305] S. M. Barnett, *Optical Dirac equation*, New J. Phys. **16**, 093008 (2014).

[306] I. Bialynicki-Birula and Z. Bialynicka-Birula, *The role of the Riemann-Silberstein vector in classical and quantum theories of electromagnetism*, J. Phys. A: Math. Theor. **46**, 053001 (2013).

[307] W. T. Kelvin, *Baltimore Lectures on Molecular Dynamics and the Wave Theory of Light* (CJ Clay and Sons, London, 1904).

[308] I. Semchenko, A. Balmakou, S. Khakhomov, and S. Tretyakov, *Stored and absorbed energy of fields in lossy chiral single-component metamaterials*, Phys. Rev. B **97**, 014432 (2018).

[309] F. Crimin, N. Mackinnon, J. B. Götte, and S. M. Barnett, *Optical helicity and chirality: Conservation and sources*, Appl. Sci. **9**, 828 (2019).

[310] N. Mackinnon, *On the differences between helicity and chirality*, J. Opt. **21**, 125402 (2019).

[311] L. V. Poulikakos, J. A. Dionne, and A. García-Etxarri, *Optical helicity and optical chirality in free space and in the presence of matter*, Symmetry **11**, 1113 (2019).

[312] T. V. Raziman, R. H. Godiksen, M. A. Müller, and A. G. Curto, *Conditions for enhancing chiral nanophotonics near achiral nanoparticles*, ACS Photonics **6**, 2583 (2019).

[313] S. Slussarenko, A. Alberucci, C. P. Jisha, B. Piccirillo, E. Santamato, G. Assanto, and L. Marrucci, *Guiding light via geometric phases*, Nat. Photonics **10**, 571 (2016).

[314] I. A. Shelykh, G. Pavlovic, D. D. Solnyshkov, and G. Malpuech, *Proposal for a mesoscopic optical Berry-phase interferometer*, Phys. Rev. Lett. **102**, 046407 (2009).

[315] H. Saarikoski, J. E. Vázquez-Lozano, J. P. Baltanás, F. Nagasawa, J. Nitta, and D. Frustaglia, *Topological transitions in spin interferometers*, Phys. Rev. B **91**, 241406 (2015).

[316] M. F. Picardi, A. V. Zayats, and F. J. Rodríguez-Fortuño, *Amplitude and phase control of guided modes excitation from a single dipole source: Engineering far- and near-field directionality*, Laser Photonics Rev. **13**, 1900250 (2019).

[317] I. Fernandez-Corbaton, X. Zambrana-Puyalto, and G. Molina-Terriza, *Helicity and angular momentum: A symmetry-based framework for the study of light-matter interactions*, Phys. Rev. A **86**, 042103 (2012).

[318] I. Fernandez-Corbaton, X. Zambrana-Puyalto, N. Tischler, X. Vidal, M. L. Juan, and G. Molina-Terriza, *Electromagnetic duality symmetry and helicity conservation for the macroscopic Maxwell's equations*, Phys. Rev. Lett. **111**, 060401 (2013).

[319] I. Fernandez-Corbaton, *Total helicity of electromagnetic fields and matter*, Phys. Rev. B **103**, 054406 (2021).

[320] N. Kravets, A. Aleksanyan, and E. Brasselet, *Chiral optical Stern-Gerlach Newtonian experiment*, Phys. Rev. Lett. **122**, 024301 (2019).

[321] O. Arteaga, E. Garcia-Caurel, and R. Ossikovski, *Stern-Gerlach experiment with light: separating photons by spin with the method of A. Fresnel*, Opt. Express **27**, 4758 (2019).

[322] Y.-Y. Chen, C. Ye, Q. Zhang, and Y. Li, *Enantio-discrimination via light deflection effect*, J. Chem. Phys. **152**, 204305 (2020).

List of Acronyms

AFM . . . . . Atomic-Force Microscope
CD . . . . . Circular Dichroism
CMOS . . . . . Complementary Metal-Oxide-Semiconductor
CPGM . . . . . Circularly Polarized Guided Mode
CPL . . . . . Circularly Polarized Light
ED . . . . . Electric Dipole
EM . . . . . Electromagnetic
EOAM . . . . . Extrinsic Orbital Angular Momentum
EQ . . . . . Electric Quadrupole
FET . . . . . Field-Effect Transistor
GMR . . . . . Giant Magnetoresistance
IOAM . . . . . Intrinsic Orbital Angular Momentum
L-CPGM . . . . . Left-Handed CPGM
L-CPL . . . . . Left-Handed CPL
MD . . . . . Magnetic Dipole
MOS . . . . . Metal-Oxide-Semiconductor
MOSFET . . . . . Metal-Oxide-Semiconductor Field-Effect Transistor
NIR . . . . . Near-Infrared
OAM . . . . . Orbital Angular Momentum
PBL . . . . . Polarization Beat Length
QSHE . . . . . Quantum Spin Hall Effect
PEC . . . . . Perfect Electric Conductor
PIC . . . . . Photonic Integrated Circuit
R-CPGM . . . . . Right-Handed CPGM
R-CPL . . . . . Right-Handed CPL
SAM . . . . . Spin Angular Momentum

SoI . . . . . Silicon-on-Insulator
SOI . . . . . Spin-Orbit Interaction
SoP . . . . . State of Polarization
SPP . . . . . Surface Plasmon Polariton
SP . . . . . Surface Plasmon
STM . . . . . Scanning Tunneling Microscope
TE . . . . . Transverse Electric
TM . . . . . Transverse Magnetic
UV . . . . . Ultraviolet
VSH . . . . . Vector Spherical Harmonics
VSWF . . . . . Vector Spherical Wave Function

List of Figures

Figure 1 Timeline of major milestones and breakthroughs in nanoscience and nanotechnology. . . . 3

Figure 2 Schematic of the spin Field-Effect Transistor (spin-FET) proposed by Datta and Das. . . . 5

Figure 3 Spin-dependent electron transport phenomena in solid-state systems. 6

Figure 4 Evolution and future forecast of different technological approaches and materials in terms of working performance along the time and as a function of the critical device size. . . . 9

Figure 5 Plasmonics Kübler-Ross Grief Cycle. Lighthearted diagram showing gradually the different attitudes when examining the role played by absorption losses in plasmonic systems. . . . 10

Figure 6 Conceptualization of naturally occurring materials formed by atoms, against metamaterials, built upon meta-atoms that are in turn made of atoms. The effective parameters of metamaterials (ε_{eff} and μ_{eff}) will depend on that of the constituent matter (ε and μ) as well as on the shape, size, orientation, and the arrangement of the meta-atoms. . . . 11

Figure A.1 Amplitude ratio and phase delay between the longitudinal and transverse components for different propagating TM multipole fields. Normalized instantaneous intensity distribution of the $\mathbf{E}^{\text{TM}}_{4,4}$ mode. Evolution of the polarization ellipse along the x axis showing the transition from the near- to the far-field zone. . . . 30

Figure A.2 Main features of the SOI term $\Delta_l^{(\pm)}$ for different values of l. . . . 32

Figure A.3 Schematic representation of the near-field features (complex Poynting vector, the orbital and the spin momentum) for the $\mathbf{E}^{\text{TM}}_{4,4}$ mode. . . . 33

Figure A.4 Densities of the local dynamical properties (real part of the Poynting vector, the orbital and spin momentum, and the locally normalized electric field distribution) for different multipole fields of (l,m) order over the xy plane. . . . 35

Figure A.5 Separate contributions to the local orbital- and spin-momentum densities for the $\mathbf{E}^{\text{TM}}_{1,1}$ mode (circularly polarized oscillating electric dipole). . . . 37

Figure B.1 Schematic description for visualizing the near-field directionality of arbitrary multipole sources. 51
Figure B.2 The electromagnetic field calculation of electric multipolar sources in free space and near a dielectric slab waveguide, showing the directional excitation of TM guided modes. 52
Figure B.3 Electric field amplitude angular spectra of electriclike multipolar sources. Contrast ratio between guided modes coupled to opposite directions. Additional spatial range of higher-order multipoles, with respect to that of the electric dipole, to achieve the same coupling to the guided mode. 55

Figure C.1 Optical chirality density in lossless and lossy dispersive media. . . . 102
Figure C.2 Optical chirality density for silver and silicon; comparison between the lossless and the lossy approaches. 104

Figure C.S1 Separate contributions to the optical chirality density in lossless and lossy dispersive media. 130
Figure C.S2 Summary of mathematical expressions for the electromagnetic energy and the optical chirality densities derived by using different approaches. 131

Figure D.1 Cross-sectional maps of the normalized chirality density for L- and R-CPGM in silicon nitride strip and slot waveguides with square cross section at NIR frequencies. 145
Figure D.2 Effective refractive index of the fundamental TE and TM eigenmodes of a silicon nitride strip and slot waveguide with square cross section. 146
Figure D.3 Scheme of the arrangement for chiral excitation and read-out under normal incidence (in-gap configuration). Transmission, mode conversion spectra, and dissymmetry factor considering the chiral metallic structure modeled as a PEC. 148
Figure D.4 Scheme of the arrangement for the evanescent-induced chiral response in a dielectric strip waveguide (on-top configuration). Transmission, mode conversion spectra, and dissymmetry factor considering the chiral metallic structure modeled as a PEC. 150
Figure D.5 Cross-sectional maps of the optical chirality density for L- and R-CPGM in silicon nitride strip waveguides for the in-gap and the on-top configurations considering the chiral metallic structure modeled as a PEC. 151
Figure D.6 Transmission, mode conversion spectra, and dissymmetry factor for the in-gap and the on-top configurations considering the chiral metallic structure as made of silver. 152

Figure D.7 Cross-sectional maps of the optical chirality density for L- and R-CPGM in silicon nitride strip waveguides for the in-gap and the on-top configurations considering the chiral metallic structure as made of silver. . . . 153
Figure D.8 Scheme of the arrangement for chiral sensing and spectroscopy enabled by a dielectric slot waveguide (slotted configuration). Transmission, mode conversion spectra, and dissymmetry factor considering the chiral metallic structure as made of silver. . . . 154
Figure D.9 Polarization beat length (PBL) of a silicon nitride strip and slotted waveguide as a function of the wavelength. . . . 156

Figure 7.1 Depiction of some of the most important SOI-based effects. . . . 168
Figure 7.2 Depiction of the different contributions to the angular momentum of light. . . . 171
Figure 7.3 Abrupt switching on the handedness of the spin-momentum and its relation with the transverse SAM near the source. . . . 173
Figure 7.4 Depiction of a generic situation wherein to apply the angular spectrum representation. . . . 175
Figure 7.5 Angular spectrum of *s*- and *p*-polarized electric fields of different optical sources. . . . 176
Figure 7.6 Calculator of angular spectra of arbitrary EM multipole sources. . . . 179
Figure E.1 Near-field unidirectional excitation...and beyond. . . . 184
Figure 7.7 Metallic and high-index dielectric nanostructures used to enhance the chiral responses. . . . 186
Figure 7.8 Analogy between the integrated approach showing optical chirality induced by evanescent fields (*on-top configuration*), and the free-space scheme proposed in Ref. [285]. . . . 193
Figure F.1 Generalizing optical chirality to an arbitrary medium. . . . 202

List of Tables

Table B.SI Spectral amplitudes of the Hertz potential associated to the first four electric-like multipole moments. 80

Table C.SI Material parameters for the multi-resonant model characterizing the permittivity of silver. 133

Table C.SII Fitting parameters for the multi-resonant model characterizing the permittivity of silicon. 133

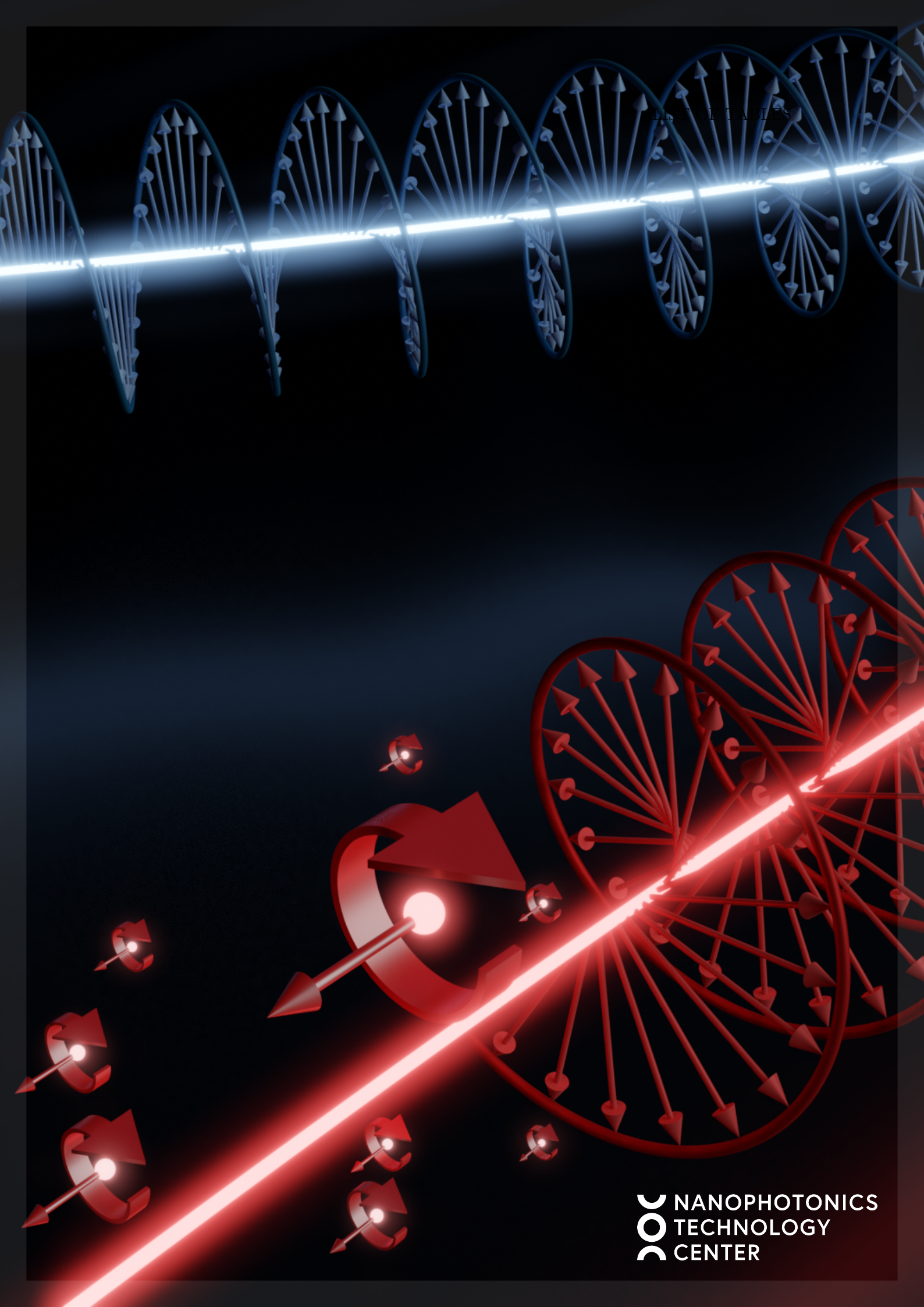
NANOPHOTONICS
TECHNOLOGY
CENTER